Energy Research and Development Division
FINAL PROJECT REPORT

TESTING COMPRESSED NATURAL GAS FUEL ECONOMY WITH DYNAMIC SKIP FIRE TECHNOLOGY

Prepared for: California Energy Commission
Prepared by: University of California, at Berkeley

JULY 2016
CEC-500-2016-050

PREPARED BY:

Primary Author(s):
Miguel Sierra Aznar

University of California, at Berkeley
72 Hesse Hall, MC 1740
Berkeley, CA 94720
Phone: 510-642-5573 | Fax: 510-642-1850
http://www.firebrand.me.berkeley.edu/~combustion/

Contract Number: PIR-12-014

Prepared for:

California Energy Commission

Matthew Fung
Contract Manager

Aleecia Gutierrez
Office Manager
Energy Generation Research Office

Laurie ten Hope
Deputy Director
ENERGY RESEARCH AND DEVELOPMENT DIVISION

Robert P. Oglesby
Executive Director

DISCLAIMER

This report was prepared as the result of work sponsored by the California Energy Commission. It does not necessarily represent the views of the Energy Commission, its employees or the State of California. The Energy Commission, the State of California, its employees, contractors and subcontractors make no warranty, express or implied, and assume no legal liability for the information in this report; nor does any party represent that the uses of this information will not infringe upon privately owned rights. This report has not been approved or disapproved by the California Energy Commission nor has the California Energy Commission passed upon the accuracy or adequacy of the information in this report.

ACKNOWLEDGEMENTS

This work was made possible thanks to the support of the California Energy Commission, through the Natural Gas Research and Development Program in the shape of a research grant.

Acknowledgment and thanks for the support provided by *Tula Technology, Inc.* who not only provided the engine and material needed but an immense amount of man hours support. Special mention to Chris Chandler and Ryan Kuhlenbeck. Thanks to Ricky Chien, Mark Wilcutts, Jackie Yuan and Matthew Younkins.

Thanks to *Westport Innovations Inc.* and its representative Mark Dunn for donating the engine CNG conversion kit.

Thanks to *Veriflo Division Parker Hannifin* and its representative Anil Raina for donating a considerable amount of high pressure fittings and instrumentation for the natural gas.

Sincere gratitude to Prof. R. W. Dibble who offered the great opportunity to work in such a challenging and equally enjoyable project. Thanks to Sebastian Thiem for partnering on this project.

Special thanks to Mary Anne Peters, Noriko Katagiri and Jean Lin-Wong, our laboratory administrators, and the technicians at the Hesse Hall shop: Mike Neufer, Scott McCormick, Pete Graham and Alex Jordan.

Acknowledgment also goes to the contributions of Tim Sennott, Ben Wolk, Johnathan Corvello, Christoph Berger, Eric Olsen, Russell LaBrie, Georg Muller and Eddisson Castano for the construction and setup of the test cell.

PREFACE

The California Energy Commission Energy Research and Development Division supports public interest energy research and development that will help improve the quality of life in California by bringing environmentally safe, affordable, and reliable energy services and products to the marketplace.

The Energy Research and Development Division conducts public interest research, development, and demonstration (RD&D) projects to benefit California.

The Energy Research and Development Division strives to conduct the most promising public interest energy research by partnering with RD&D entities, including individuals, businesses, utilities, and public or private research institutions.

Energy Research and Development Division funding efforts are focused on the following RD&D program areas:

- Buildings End-Use Energy Efficiency
- Energy Innovations Small Grants
- Energy-Related Environmental Research
- Energy Systems Integration
- Environmentally Preferred Advanced Generation
- Industrial/Agricultural/Water End-Use Energy Efficiency
- Renewable Energy Technologies
- Transportation

Testing CNG fuel economy with Dynamic Skip Fire (DSF) technology is the critical project report for the Benefits of Dynamic Skip Fire (DSF) for Improved Natural Gas Engine Performance project (contract number PIR-12-014) conducted by the University of California, at Berkeley. The information from this project contributes to Energy Research and Development Division's Transportation Program.

For more information about the Energy Research and Development Division, please visit the Energy Commission's website at www.energy.ca.gov/research/ or contact the Energy Commission at 916-327-1551.

ABSTRACT

Premixed spark ignited engines are most efficient when running at *wide open throttle*, or full power. Keeping each cylinder at full power while reducing the number of cylinders in operation allows the engine to achieve a wide, dynamic range of rotational speeds and loads while maintaining high efficiency. This condition is known as variable displacement or *dynamic skip fire*.

In this study, researchers investigated the feasibility of running an eight cylinder gasoline engine modified to use compressed natural gas under dynamic skip fire conditions. They compared engine performance while operating under both throttled and dynamic skip fire conditions. As part of the comparison, the researchers determined the most efficient points of operation for modes by measuring operating factors such as temperature, pressure, emissions, fuel flow, power, and torque. The comparison results show that running the modified engine under dynamic skip fire conditions leads to improvements in fuel economy by up to 40 percent with specific fuels, reduced carbon dioxide emissions, and brake thermal efficiency during steady state operation.

Results also show that using pure methane as a fuel source results in higher efficiency than when using gasoline due to the gasoline's susceptibility to knock limitations and methane's higher heating value.

Due to the lower energy density of compressed natural gas compared to gasoline, researchers also tested a turbocharge system on the modified engine. The turbocharge system improved the power output of the compressed natural gas fueled engine to match the gasoline fueled engine at the cost of efficiency.

When used with compressed natural gas, dynamic skip fire is a promising method for reducing the environmental impact and improving the fuel economy of large displacement engines while maintaining performance.

Keywords: Dynamic Skip Fire, fuel economy, emissions, efficiency improvement, dynamic, compressed natural gas, methane, part load.

Please use the following citation for this report:

M. Sierra Aznar, R. W. Dibble, (University of California, at Berkeley). 2014. ***Testing Compressed Natural Gas Fuel Economy with Dynamic Skip Fire Technology***. California Energy Commission. Publication number: CEC-500-2016-050.

TABLE OF CONTENTS

Acknowledgements i

PREFACE ii

ABSTRACT iii

TABLE OF CONTENTS iv

LIST OF FIGURES vi

LIST OF TABLES x

EXECUTIVE SUMMARY 1

Introduction 1

Project Purpose 1

Project Results 2

Project Benefits 3

CHAPTER 1: Introduction 5

1.1 Background 5

1.2 Energy and Environmental Impact of the Transportation Sector 7

CHAPTER 2: Experimental Setup 12

2.1 Engine Testing Facility 12

2.2 Experimental Approach and Test Matrix 13

CHAPTER 3: CNG-Throttled Engine Operation 15

3.1 Effect of Spark Timing on Performance 15

3.1.1 Early Ignition Timing 16

3.1.2 Late Ignition Timing 19

3.1.3 Ignition Timing Effect on Emissions 19

3.1.4 Ignition Timing Variation with Engine Load and Speed 20

3.2 Effect of CAM Phasing on Performance 22

3.3 Effect of Engine Speed on Performance 28

3.4 Optimum Conditions for Standard Engine Operation 29

3.5 Conclusions 33

CHAPTER 4: CNG-DSF Engine Operation **34**
4.1 Firing Cylinder Characteristics 35
4.2 Deactivated Cylinder Characteristics 35
4.3 Dynamic Skip Fire Performance 38
4.3.1 Discrete Cylinder Management 42
4.3.2 DSF and Gasoline 44
4.4 Conclusions 45
CHAPTER 5: Turbocharging Spark Ignited Engines **48**
CHAPTER 6: Major Conclusions and Recommendations **56**
GLOSSARY **59**
NOMENCLATURE **63**
REFERENCES **67**
APPENDIX A: The Engine Test Facility **A-1**
A.1 General Overview A-1
A.2 Fuel Supply System A-3
A.3 Engine and Air Intake System A-7
A.4 Cooling System A-11
A.4.1 Engine Cooling A-13
A.4.2 Oil Cooling A-14
A.4.3 Dynamometer Cooling A-16
A.5 Dynamometer A-16
A.5 Exhaust System A-20
A.6 Control System A-20
A.6.1 Engine Control Module A-21
A.6.2 Power Supply Control Module A-22
A.7 Data Acquisition A-26
APPENDIX B: IC Engine Fundamentals **B-1**
B.1 Engine Geometry B-1

B.2 Engine Brake Parameters B-3
B.2.1 Brake Power and Torque B-3
B.2.2 Brake Specific Fuel Consumption B-4
B.2.3 Brake Specific Emissions B-4
B.3 Internal Combustion Engine Efficiency B-5
B.3.1 Mean Effective Pressure B-5
B.3.2 Combustion Efficiency B-7
B.3.3 Thermodynamic Efficiency B-9
B.3.4 Gas Exchange Efficiency B-12
B.3.5 Mechanical Efficiency B-15
B.3.6 Engine Brake Efficiency B-17
B.4 The Combustion Analysis System B-19
B.4.1 In-Cylinder Pressure B-20
B.4.2 Heat Release and Combustion Timing Characterization B-22
APPENDIX C: Benefits and Drawbacks of CNG for Automobiles C-1
C.1 Compressed Natural Gas C-4
C.2 Compressed Natural Gas and the Three-Way Catalyst C-8
APPENDIX D: Dynamic Skip Fire Technology D-1
D.1 Variable Volume Displacement D-1
D.2 Dynamic Skip Fire Hardware D-2
D.3 Dynamic Skip Fire Control D-8
D.4 Drive Pulse Generator Concept D-10

LIST OF FIGURES

Figure 1: Evolution of the World's Gross Domestic Product (GDP), CO_2 Emissions, Energy Supply, and Consumption Since 1975 5
Figure 2: Evolution of the World's Crude Oil Price and Associated Events 7
Figure 3: U.S. Energy Consumption By Sector Since 1949. 8
Figure 4: Light Vehicle Technology Penetration After First Significant Use 9

Figure 5: United States Fuel Prices and Crude Oil Reserves Estimations Since 1976 10

Figure 6: Production Share by Vehicle Type For 1975-2014 Period 11

Figure 7: The Finished Testing Facility as of 01/12/2013 after the Cell Was Designed and Constructed 13

Figure 8: Effect of Ignition Timing on the In-Cylinder Pressure while Running at Engine Speed 16

Figure 9: Effect of Ignition Timing on the Engine Gross Indicated Cumulative Work, at Engine Speed 17

Figure 10: Normalized Gross Cumulative Heat Release over Crank Angle Degrees after Ignition (CAD AIT). 18

Figure 11: Emissions of Main Compounds on Exhaust (THC, O_2, CO_2, CO and NO_x) 19

Figure 12: Brake Thermal Efficiency or Brake Efficiency Variation with Load and Ignition Timing 20

Figure 13: Ignition Timing for Maximum Brake Torque Plotted against Engine Load 21

Figure 14: In-Cylinder Pressure Trace Evolution for the Engine 23

Figure 15: Evolution of PMEP, PMEPpump, and PMEPvalves at Different Valve Timings 24

Figure 16: Effect of Valve Timing on Brake Specific Fuel Consumption 25

Figure 17: Emissions of Main Exhaust Compounds for Different Valve Timing Conditions 27

Figure 18: Evolution with Load of the Characteristic Angles of Combustion SOC and EOC for CAM 0, CAM 20, CAM 40, and CAM 50. 28

Figure 19: Brake Specific Fuel Consumption for Different Engine Speeds at Different Loads 29

Figure 20: Overall Efficiency Trends for the Optimal Engine Configuration 31

Figure 21: Overall Emissions Behavior for the Optimal Engine Configuration 32

Figure 22: In-Cylinder Pressure for DSF 34

Figure 23: Gross Instant and Cumulative Indicated Work During a DSF Mode Fire at (a) Actual Values and (b) Normalized Values Over Maximum 36

Figure 24: Gross Cumulative and Instant Indicated Work for a Deactivated Cylinder 37

Figure 25: Pressure Trace for a Momentarily Deactivated Cylinder and a Constant Deactivated Cylinder Operating at Engine Speed 1500 RPM 37

Figure 26: BSFC Values at Different Loads During the Operation of the Engine 38

Figure 27: Emissions Records During DSF Mode at Different Engine Loads 39

Figure 28: Emissions Records During DSF Mode at Different Engine Loads for CNG and Gasoline Operating at 1500 RPM 41

Figure 29: Normalized Emissions at Different Engine Loads for CNG and Gasoline 42

Figure 30: Comparison of Efficiency Trends for Throttled (Dashed Line) and DSF Modes (Solid Line) 44

Figure 31: Fuel Economy Approximated Gains Caused by DSF and AFM Compared to a Normal Throttled Operation 46

Figure 32: Engine Parametric Curve for BSFC (g/kWh), BMEP, and Mean Piston Velocity (sp) under Throttled and DSF Operation 47

Figure 33: Pressure Conditions Upstream of the Turbine During the Exhaust Stroke of the Cylinders 48

Figure 34: GT Power Model of a Naturally Aspirated GM L94 6.2 L Engine 50

Figure 35: Comparison of Experimental and Simulation Results on BSFC as a Function of BMEP at 1250 RPM and 1500 RPM 51

Figure 36: GT Power Model of a Virtually Turbocharged GM L94 6.2 L Engine 52

Figure 37: Engine Brake Power Output at WOT for Different Turbocharge Models at Different Engine Speeds 53

Figure 38: Naturally Aspirated Engine Brake Power and Turbocharged Engine Brake Power vs. Speed at Different Engine Loads 54

Figure 39: Naturally Aspirated Engine Brake Efficiency and Turbocharged Engine Brake Efficiency vs. Speed at Different Engine Loads 55

Figure A.1: General Overview of the Engine Test Cell At UC Berkeley A-2

Figure A.2: Generic Scheme of the Engine CNG Fuel Supply System at UC Berkeley A-3

Figure A.3: Methane Gas Expansion From 165 Bar to 18 Bar through a Single Stage Regulator Followed by a Heating Process from 230 K to Ambient Temperature 300 K A-5

Figure A.4: GM Engine Block with Enumerated Cylinders A-8

Figure A.5: Air Intake System Diagram A-9

Figure A.6: An Approximate Scheme of Both Shell-Tube Heat Exchangers with One-Shell Pass and Two-Tube Pass A-12

Figure A.7: Cooling System's Generic Scheme of the Engine Test Cell at UC Berkeley A-13

Figure A.8: Mid-West 1519 EC Dynamometer Cross Section Plane A-18

Figure A.9: Morse MORFLEX 1002-R And Its Properties to Withstand Torsional and Angular Deflection A-19

Figure A.10: Generic Scheme of the Engine Exhaust System at UC Berkeley A-21

Figure A.11: Illustration of the dSPACE Human Machine Interface (HMI) at the Engine Test Facility A-23

Figure A.12: Scheme of the Different Control Components at the Control Desk A-24

Figure A.13: Summary of the Data Acquisition System at UC Berkeley A-27

Figure B.1: Example of a Four Stroke SI Engine Cylinder-Pistion Geometry B-2

Figure B.2: Comparison of a Theoretical Air and an Air Fuel Otto Cycle with a Real Otto Cycle B-10

Figure B.3: Real Engine Operation B-12

Figure B.4: Concept of –MEP Values in Internal Combustion Engines B-14

Figure B.5: Striebeck Diagram B-16

Figure B.6: Multi-grade Lubricant Oil Sensitivty with Temperature B-17

Figure B.7: Summary of the Different Energy Flows, Losses, and Efficiency Terms B-18

Figure C.1: Effect of Lambda Ratio and Compression Ratio r_c on Efficiency C-1

Figure C.2: Effect of Mixture Strength on Laminar Flame Speed and Adiabatic Flame Temperature for Methane and Commercial Gasoline C-2

Figure C.3: Effect of Burning Temperature and Pressure in the Laminar Flame Speed of Methane-Air Mixtures C-3

Figure C.4: Mass Burnt Fraction Behavior of Methane and Gasoline C-7

Figure C.5: Different Conversion Levels for Different Air to Fuel Ratios of NO, CO, and HC C-8

Figure C.6: Catalytic Process Suffered by NO_x and CO Within a Three Way Catalytic Converter C-9

Figure C.7: Catalytic Process Suffered by CO Within a Three Way Catalytic Converter C-9

Figure C.8: Pt based TWC Methane Conversion Efficiency for Gasoline and CNG Combustion C-11

Figure D.1: Brake Thermodynamic Efficiency (η_T) at Full and Part Throttle Evaluation vs. Compression Ratio (r_c) D-2

Figure D.2: Example of a Deactivation Lifter and Lifter Oil Manifold Assembly Used in an LT1 GM Engine D-3

Figure D.3: Design of a Deactivation Lifter Used by GM for Their Cylinder Management Strategy AFM D-4

Figure D.4: Standard Valve Timing for the GM L94 Engine with Variable Valve Timing of up to 25 CAM Angle Degrees Retardation Shift (50 Crank Angle Degrees) D-6

Figure D.5: General Illustration on the Effect of Valve Timing on PMEP at Different Cylinder Loads D-7

Figure D.6: Example of a General Setup for a Fire Computer Unit D-9

Figure D.7: Example of a Sigma-Delta Module D-10

Figure D.8: Simplified Illustration of the Behavior of a Sigma-Delta Control for the Purpose of DSF D-12

Source: University of California, Berkeley D-12

Figure D.9: Approximate Behavior of DSF under Different Engine Loads D-13

LIST OF TABLES

Table 1: GM Gen IV L94 V8 VORTEC 6.2 VVT Engine Main Characteristics 12

Table 2: Test Matrix as Carried out for the Results Shown in This Report 14

Table 3: Engine Brake Parameter for Different Ignition Timings 15

Table 4: Engine Brake Parameter for Different CAM Phasing 22

Table 5: Result for the Two Possible Optimum Points on CNG-throttled Engine Operation 33

Table A.1: Methane Compressed Grade 2.0 composition as Supplied by Praxair. Gas Formula: CH4. Colorless, Odorless, and Flammable Gas. CAS Number: 74-82-8. ..... A-4

Table A.2: Fuel System Sensors and Property Measurements A-7

Table A.3: Engine Integrated and Installed Sensors for Engine Performance Assessment A-10

Table A.4: Modified GM Gen IV L94 V8 VORTEC 6.2 VVT Characteristic for Operation on CNG under DSF Mode A-11

Table A.5: Engine Coolant Circuit Operating Parameters A-14

Table A.6: Oil Cooling Circuit Operating Parameters A-15

Table A.7: Cooling System Sensors and Property Measurements Summary. A-17

Table A.8: Characteristics of the Eddy Current Dynamometer at UC Berkeley. A-17

Table A.9: Dynamometer Sensors and Property Measurements Summary. A-19

Table A.10: Exhaust System Sensors and Property Measurements. A-22

Table B.1: Lower Geating Value of CO, H2 and CH4 ..... B-9

Table C.1: Experimental Research Octant Numbers (RON) of Some Selected Fuels C-4

Table C.2: Specification of Natural Gas used for Emissions Certification and for General Vehicular Use C-5

Table C.3: Methane Physical Properties C-5

EXECUTIVE SUMMARY

Introduction

The United States transportation sector consumes 28.1 percent of the nation's energy (mostly in the form of fossil fuels) and produces 28 percent of greenhouse gas emissions. This problem is due to the limited penetration of renewable and alternative energy sources in the consumer market; however, the transition towards cleaner energy sources for transportation is slow because of obstacles such as the infrastructure cost, high dependency on infrastructure, and the high manufacturing cost of new transportation systems that use cleaner energy.

As of today, the internal combustion (IC) engine remains the only cost-effective option for commercial transportation needs. Light to heavy-duty vehicles alone produce 84 percent of the total GHG emitted by the transportation sector in 2014, with rail and air transport covering the remaining 16 percent. New solutions for improving the performance of IC engines combined with taxes and subsidies that encourage major energy consumers to transition to more energy-efficient methods have the greatest potential to reduce GHG emissions in the transportation.

Extensive research is being carried out to evaluate the benefits of new fuels and their combustion properties. Natural gas is a desirable fuel option due to its clean and efficient combustion, availability, and low cost compared to gasoline or diesel.

In the United States, many passenger vehicles are manufactured with large engines to meet consumer demand for low-cost engines that meet performance expectations. The low cost for large engines results from years of technological development and production scaling, which impedes American manufacturers from downsizing to more efficient engines. Large manufacturers, like General Motors, are looking into adaptive solutions that conserves their engine block sizes while improving fuel economy and emissions. Variable valve timing and cylinder management are more attractive solutions now that integral block modifications are not necessary for large volume displacement engines. These advancements will be noticeable steps towards sustainability, since freight in the United States is predominantly transported on large, gasoline and diesel trucks.

Project Purpose

For this project, researchers at the University of California ,Berkeley's Combustion Analysis Laboratory investigated the potential to save fuel and reduce emissions in light-duty trucks, pick ups, vans, minivans, and vehicles with large displacement light-duty engines by using compressed natural gas (CNG) engines combined with Dynamic Skip Fire (DSF) technology . DSF is an innovative approach to cylinder management for large spark-ignition (SI) engines that continually varies the number of firing cylinders to match engine load conditions.

The scope of work included setting up an engine cell with an eight cylinder gasoline engine retrofitted for CNG and evaluating its potential to replace current analog engines while meeting or exceeding standard fuel economy and GHG emissions levels. Key tasks of the performance evaluation include remapping the engine operational points to find the most efficient point at each operating condition for both throttled and DSF modes. During the evaluation, temperature,

pressure, emissions, fuel flow and performance parameters such as power and torque were measured as means of comparison between standard operation and DSF operation.

In expectation of a decrease in engine performance due to natural gas use, the project scope included an analysis of potential turbocharging strategies to reach gasoline engine performance levels. Turbocharging introduces extra air into the engine for combustion to increase power and efficiency. Natural gas with turbocharging strategies will take advantage of the low susceptibility of natural gas to knocking, a detrimental event caused when fuel combustion occurs before the desired point in the engine cycle. Natural gas engines require higher air to fuel ratios to combust natural gas compared to gasoline, which reduces the maximum amount of fuel that can be injected per cylinder, resulting in less power output. An engine model was built, validated with data provided by the experimental test, and ultimately fitted to simulate turbocharge systems commonly used in the automotive industry.

Researchers analyzed both the simulation and experimental data to determine the effectiveness of using DSF technology and CNG to improve fuel economy and reduce GHG emissions from SI engines.

Project Results

This project has proven that DSF improves the engine's fuel economy not only by reducing pumping losses, but also by reducing heat losses. DSF technology ultimately leads to more efficient fuel use by transmitting a higher percentage of the fuel energy to powering the engine. The major conclusions drawn from the experimental results are:

1. DSF technology reduces the fuel consumption of the engine by up to 40 percent compared to conventional natural gas engine operations.
2. DSF offers the benefits of cylinder deactivation for a larger load range compared to other cylinder management strategies. DSF extends the benefits of cylinder management by up to 14 percent compared to current cylinder management strategies.
3. DSF operation has not shown any effects on emissions of major pollutants such as carbon monoxide (CO), total hydrocarbons (THC), and oxides of nitrogen (NO_x). The test engine's emissions remained at levels typical for wide open throttle operation, which are generally lower than emission levels during idling operation.
4. DSF reduces carbon dioxide (CO_2) emissions and improves fuel economy due to a more efficient conversion of fuel to power.
5. CNG use improves the efficiency of the SI engine compared to gasoline use by allowing the engine to run at conditions not possible for gasoline engines due to knock. At 1500 revolutions per minute, the engine operates more efficiently with CNG than with gasoline. With increasing engine load, CNG further improves the efficiency of the SI engine compared to gasoline.
6. For the same load conditions, using CNG reduces the amount of CO_2 emitted by 27 percent compared to using gasoline.

7. CNG is less energy dense than gasoline. Using CNG reduces the power and torque delivered by approximately 25 percent and 10 percent, respectively, compared to using gasoline under the same engine operating conditions.
8. Turbocharging the CNG-fueled engine results in an increase in power delivered, matching that of the gasoline-fueled engine; however, the engine suffers a small loss in efficiency at the nominal operation range.
9. The influence of DSF on the turbocharge system could not be assessed in this project, but researchers predict it will have a strong influence in performance quality.
10. If the turbocharge system is used during full load operationwithout DSF, the performance is not expected to be affected.

The combination of DSF and CNG has been proven effective in improving fuel economy and reducing emissions. As much as 20 percent improvement in fuel economy and 41 percent reduction of carbon dioxide emissions can be attributed to the combination of DSF and CNG.

Project Benefits

The results of the project will have a huge impact on the transportation sector—particularly the light-duty truck population, which has grown 1.3 percent per year since 2002. Of the 251 million light-duty vehicles in the United States, 39 percent are within the truck category (trucks, pick-ups, and vans) with six or more engine cyclinders, a category ideal for DSF integration. This vehicle category has an average fuel economy of 20.1 miles per gallon and drives an average of 11,800 miles per year. Given the above numbers, if DSF follows technology integration patterns based on manufacturer market strategies, consumers can expect a 50 percent linear penetration of DSF in the sector by 2030. Considering a 20 percent improvement on fuel economy (25 miles per gallon), the introduction of DSF will save the sector from consuming 48 billion gallons of gasoline and, consequently, emitting of 434 mega tonnes of CO_2 in the coming 15 years. Natural gas ratepayers will save an average of 4 billion dollars per year along the next 15 years.

If CNG vehicles had the same market penetration as DSF technology, the transportation market would offset the oil consumption for CNG by three billion gallons per year average, increasing the saving of CO_2 emissions from 434 mega tonnes to 910 mega tonnes, an average of 61 mega tonnes per year.

Assuming the same rate of market penetration in California alone, all the above translates to a reduction of 5.30 billion gallons of gasoline over 15 years, a displacement of 353 million gallons of gasoline to CNG, and a total reduction of CO_2 emissions of 100 mega tonnes, an average of 7 mega tonnes per year.

Moreover, California can expect a reduction in the number imported crude oil by an average of 20 million barrels per year in the following 15 years, nearly 6 percent of the foreign current oil imports in 2014. With crude oil prices reaching an average of 60 dollars per barrel, this reduction in oil imports results in a reduction of California expenses of approximately 120 million dollars per year.

The above benefits could translate into a significant rate of job creation, especially if the aforementioned savings were to be reinvested in transportation technologies and facilitating market penetration of DSF and CNG. Specifically, 120 million dollars per year of state investment could translate to the direct creation of 1,300 jobs per year and the indirect creation of 730 jobs per year for a total of nearly 2,000 jobs per year. The state's tax incentive to use CNG can also influence California's job creation rate. While California pays a 30 cents per gallon gasoline fuel use tax, paying a 0.008 cents per gallon tax for CNG can save the state approximately 300 million dollars per year. Based on the American Recovery and Reinvestment Act, 300 million dollars per year could lead to the creation of up to 5,000 jobs per year, including indirectly created jobs. The developments in the CNG fuel supply and in DSF technology can translate into a huge change for transportation, economic development, energy, air quality, and climate policy in the coming years.

CHAPTER 1: Introduction

This report aims to collect and build understanding on the potential for fuel savings of cylinder management for medium-duty spark ignited (SI) engines. In an effort to help the energy transition towards cleaner modes of transportation, this report also assesses the benefits of using compressed natural gas (CNG) for road transportation.

1.1 Background

Over the course of the last decade, concerns regarding the environmental impacts resulting from non-sustainable practices have been raised (Bailey, 1995) (MacKay, 2009) Energy efficiency and emissions are now of serious concern for the energy sector. The concern is focused on the emissions of carbon dioxide (CO_2), which is believed by the majority of the scientific community to be the primary driving force of global climate change. Other gases, mainly hydrocarbons, also have major influences on the greenhouse gas effect (Blasing, 2009). Society emits CO_2 in the greatest quantities, owing in large part to the push for economic growth worldwide (Elkington, 1994) .

Considering the world's gross domestic product (GDP) as an overall indicator on economic growth helps identify the level of influence energy consumption has in the economic activity and vice-versa as illustrated in Figure 1.

Figure 1: Evolution of the World's Gross Domestic Product (GDP), CO_2 Emissions, Energy Supply, and Consumption Since 1975.

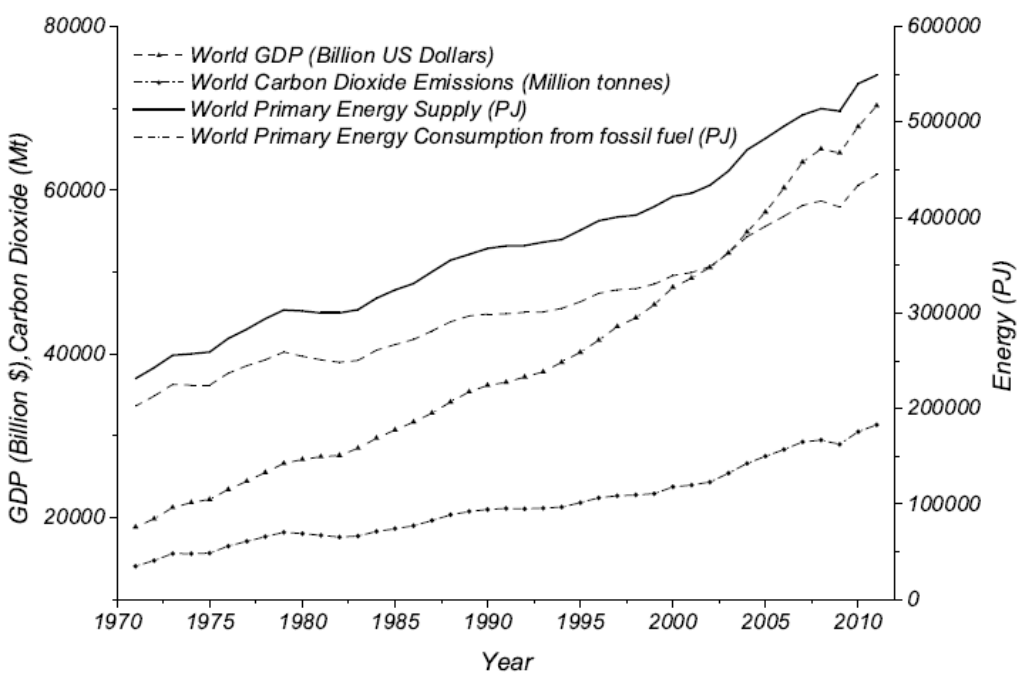

Source: International Energy Agency Organization (International Energy Agency, 2013) and the International Monetary Fund Organization (International Monetary Funds, 2013).

Since the oil embargo in 1973-74, use of energy and the influence of political instabilities on energy prices are seen from a completely different point of view (Pisarski & de Terra, 1975). Conflicts in the Middle East can easily lead to scarcity in fossil fuel supply and rising energy prices, as last seen in the Iraq war in 2003 or the Libyan civil war in 2011 (Isidore, 2013). The Middle East, according to British Petroleum, accounts for almost 50 percent of proven global fossil fuel reserves and still has the highest production rates in oil and among the highest in natural gas (British Petroleum, 2013).

Therefore conflicts in this region can easily lead to abrupt rises in energy prices. Fossil fuels such as coal and oil, which are easy to handle and have a high energy density (e.g. oil at 44 MJ/kg) (Droste-Franke et al., 2012), are demanded by developing countries to aid rapid economical growth. Fossil fuels have been produced for centuries, e.g. oil since 1859 (MacKay, 2009)(S. C. Davis, 2014)(U.S. Energy Information Agency, 2013). Although at present many fossil fuel resources exist (British Petroleum (BP), 2013), the planet will eventually run out of conventional fossil fuel. Reserves that are currently produced in an economical manner are at present still steadily replaced by either resources that become profitable to produce by developing and using new technologies and/or rising energy prices or by discovering new wells. (U.S. Energy Information Agency, 2013). However, new techniques also bring new challenges. Alternative methods of oil and gas production include a combination of horizontal drilling and hydraulic fracturing, also known as fracking, which allows production of large volumes of shale gases. Water, chemicals, and sand are pumped into a well, releasing hydrocarbons in shale formations by cracking the rock (Nemat-Nasser et al., 1982). Not every country is willing to explore the possibilities given by fracking due to concerns about ground water contamination and a lack of acceptance among the general populace. Secure access to and consumption of cheap fossil energy is somewhat linked to economical growth (S. C. Davis, 2014).

Assuming a continuous growth in the demand for fossil fuels in developing countries like China and India and persistent high demand in developed countries such as the U.S. and Europe, at some point fossil fuel production will most probably no longer be able to meet the demand for energy (Droste-Franke et al., 2012). As illustrated in Figure 2 prices for crude oil and natural gas increased over the past decade, interrupted or boosted by several events. However, this is not true for natural gas prices in North America, which almost continuously declined since 2005.

Fossil fuels are still the major source of energy. Tremendous efforts are being applied to transitioning to new sustainable energy sources. Nevertheless, fossil fuel combustion remains the most developed and reliable energy source, despite being the main agent responsible for the overall growth on CO_2 emissions. Governments are continuously developing laws and regulations to guide economies toward growth patterns which respect and maintain natural resources. Moreover, the highly fluctuating trend of fuel prices resulting from political instabilities, resource scarcity, and resource extraction costs uncovers a greater need for more efficient methods of energy conversion systems (Hawken, Lovins, & Lovins, 2008) (Porritt, 2007)

Figure 2: Evolution of the World's Crude Oil Price and Associated Events

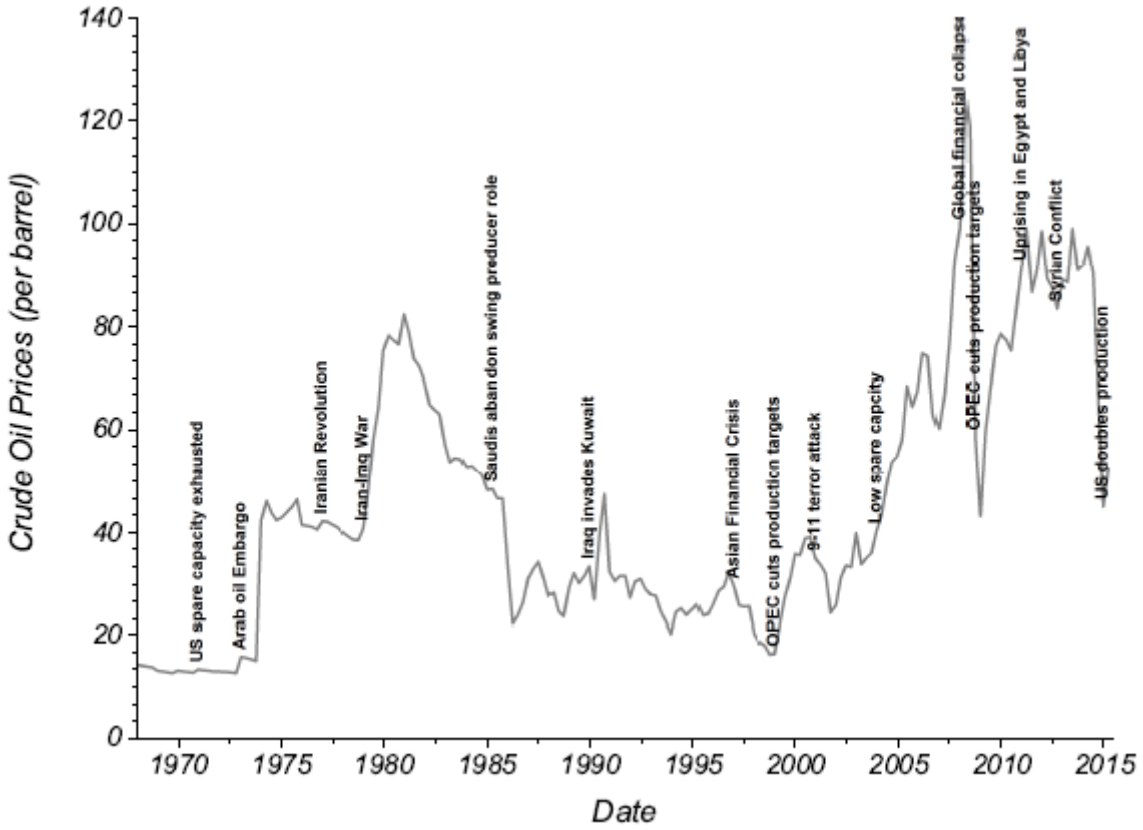

Source: (U.S. Energy Information Agency, 2013).

1.2 Energy and Environmental Impact of the Transportation Sector

The transportation sector is a major consumer of energy (28.1 percent) in the United States, as can be seen in Figure 3, mostly in the form of fossil fuels (92 percent) (S. C. Davis, Diegel, Boundy, & Moore, 2014). Due to the limited penetration of renewable and alternative energy sources, the percentage of greenhouse gas (GHG) emissions from transportation follows paired to the energy consumption and copes 28 percent of the total United States GHG emissions (U.S. Environmental Protection Agency, 2015). Electric cars and trains, and fuel cell vehicles appear in the market as an alternative to conventional transportation but yet they represent less than half a percentage of the total vehicles registered in the United States (U.S. Department of Transportation, 2014). The transition towards cleaner energy sources for transportation is slow due to large obstacles such as the cost of infrastructure, limited travel autonomy, and the high cost of manufacturing. The internal combustion engine (IC) remains the only affordable commercial option for our transportation needs and thus demands for strong research investment to reduce the share that transportation has on the GHG emissions. Light to heavy duty vehicles alone cover 84 percent of the total GHG emitted by the transportation sector in 2014 (S. C. Davis et al., 2014). Therefore, the potential impact of new solutions on how to improve

the performance of medium-large IC engines is greatest in terms of improving fuel economy, reducing greenhouse gases and ultimately reducing the share of transportation on the United States household expenditures, currently 18 percent of which 5 percent is used for fuel (S. C. Davis et al., 2014). Taxes and subsidies encourage, in one way or another, the major energy consumers to develop strategies which can accelerate the energy transition by balancing an economic regime which rewards the use of fossil fuel before any alternative energy source.

Figure 3: U.S. Energy Consumption By Sector Since 1949.

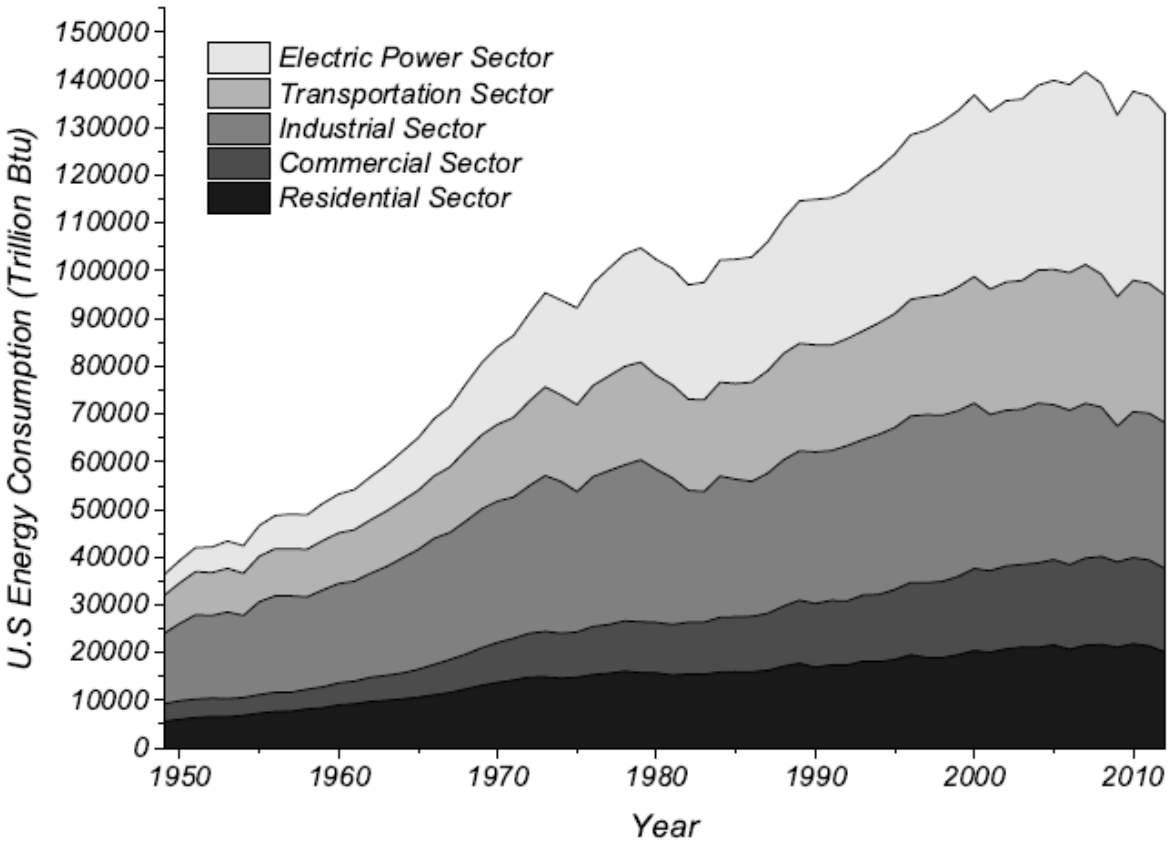

Transportation comprises nearly a fourth of the total energy consumed in the United States.
Source: U.S. Energy Information Administration (EIA) (U.S. Energy Information Agency, 2013)

With these new approaches, car manufacturers are motivated to develop technologies which improve fuel economy, both for environmental and economic reasons. Nevertheless, fuel economy is not car manufacturers' only problem. They have to find strategies which also address other challenging criteria such as comfort, reliability, performance, emissions, and cost. The broad amount of factors that influence a technological integration is the main reason why it takes in average 15 years for a technology to penetrate 50 percent in the market share as can be seen in Figure 4.

Figure 4: Light Vehicle Technology Penetration After First Significant Use

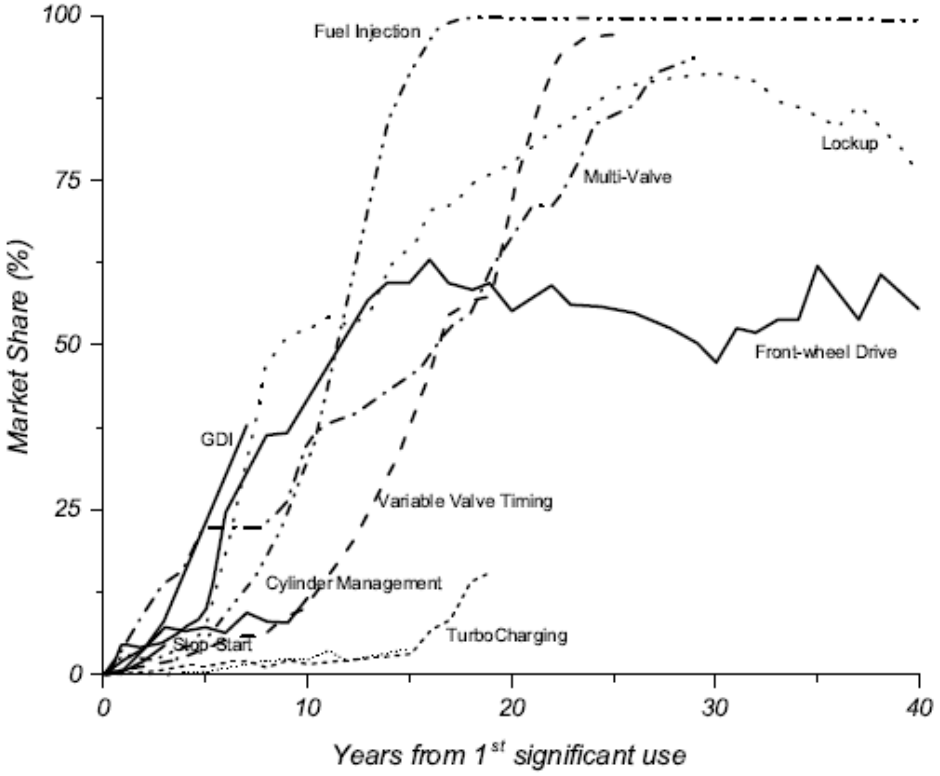

Source: U.S. EPA, 2014

The automotive industry has developed and implemented a variety of strategies for meeting emissions regulations while accomplishing client demands for comfort, performance, and cost. Today there are known mechanical strategies which are widely integrated in series produced SI engines, such as variable valve timing and actuation (Parvate-Patil, Hong, & Gordon, 2003), direct injection (Yang & Anderson, 1998), turbocharging (Arnold et al., 2005), cylinder management (Wilcutts, Switkes, Shost, & Tripathi, 2013) or smart start-stop (Hong, Zhang, Li, & Ouyang, 2008) and many others (Kutlar, Arslan, & Calik, 2005)(Wan & Du, 2013).

The use of biofuels is widely promoted (Wiesenthal et al., 2009). Extensive research is being carried out to develop and evaluate the benefits of new fuels and their combustion properties (Brown et al., 2011)(Maji, Ranjan, & Sharma, 2000)(Ceper, 2012). Natural gas, thanks to its low carbon to hydrogen ratio, is a chosen fuel for clean and efficient combustion. In addition, the availability of natural gas, and consequently its low cost compared to gasoline or diesel, makes it an attractive fuel in countries rich in natural gas such as the United States, shown in Figure 5. Furthermore, the high Research Octane Number (RON) value of methane extends the working conditions of the engine without knocking, allowing an efficient use of turbo groups or boosting (Blackmore, Thomas, & Affleck, 1977)(Owen & Coley, 1995).

The European automotive industry is leading the way towards downsizing engines while turbocharging in an effort to manufacture more efficient engines while maintaining performance

(Boye et al., 2009). However, for the United States automobile market, big engines are still foreseen to be demanded on passenger automobiles and the light truck demand is steadily increasing since 1980 starting at 20 percent and taking over 50 percent of the light duty vehicle production during 2014 as can be seen in Figure 6 (EPA, 2014)(Ramsey & Rogers, 2013)(Ramsey & Rogers, 2013).

Their low cost resulting from years of development and scale of production holds back American manufacturers from following their fellow Europeans. Large manufacturers, such as *General Motors* (GM), are looking into an adaptive approach by conserving their engine blocks while improving fuel economy and emissions through adaptive solutions. Variable valve timing and cylinder management become more attractive now that integral block modifications are not foreseen for big volume displacement engines. Large, heavy-duty V10s and V12s will potentially benefit more from such technologies. This approach is a noticeable step towards sustainability, since freight in the United States is predominantly transported on large, gasoline and diesel trucks (US Department of Transportation, 2007)(US Department of Transportation, 2012).

Figure 5: United States Fuel Prices and Crude Oil Reserves Estimations Since 1976

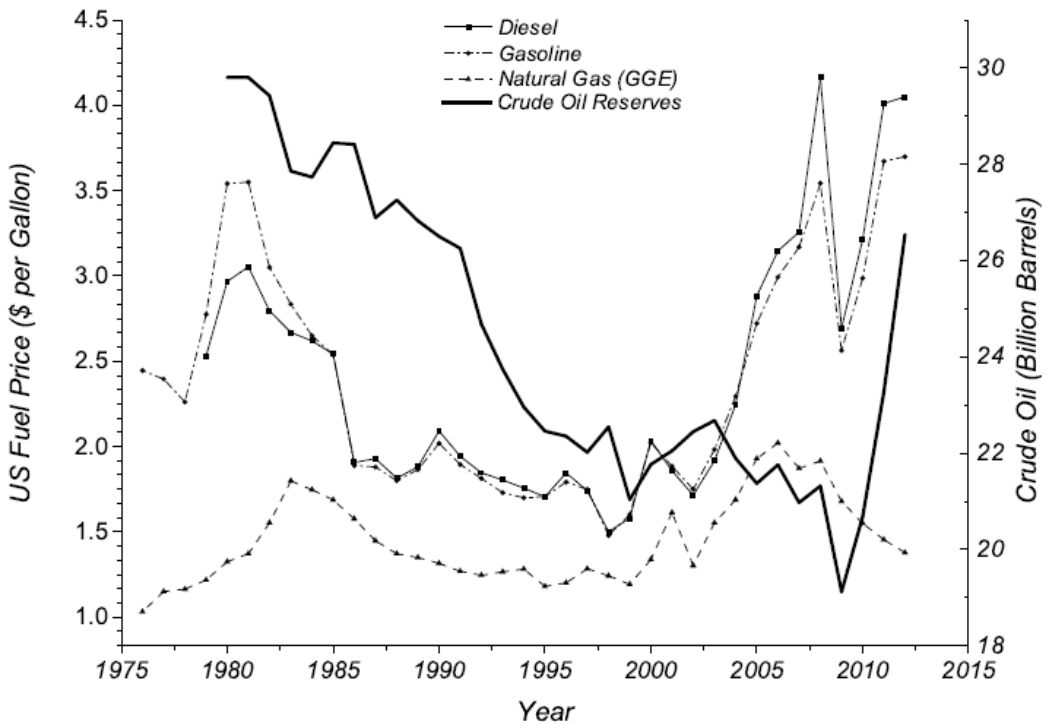

In 1970, the peak oil predicted by M. King Hubbert was reached and caused the price of conventional fuels to temporarily increase. Estimated reserves have decreased steadily until 2010 when fracking has been accepted as a possible source of crude oil, especially natural gas.

Source: U.S. Energy Information Administration (EIA) (U.S. Energy Information Agency, 2013)

Combination of technologies, such as turbocharging, cylinder management, and direct injection are promising for the future of large SI engines (Maji et al., 2000)(Ali, Kodoguchi, Oka, & Kaida, 2011)(Chiodi, Berner, & Bargende, 2006).

To the purpose of improving SI engine performance, this project studies the potential of Dynamic Skip Firing (DSF), an innovative approach to cylinder management combined with the use of CNG. Predicting the benefits of such combination should account for the ignition system limitations to ignite mixtures under high turbulence, high pressures and lean fuel conditions (Dale, 1997)(DeFilippo et al., 2011). Experimental data was obtained from a port injected GM V8 6.2 L94 SI engine with integrated *Tula Technology Inc.* DSF system (Wilcutts et al., 2013)(US, 2013).

Figure 6: Production Share by Vehicle Type For 1975-2014 Period

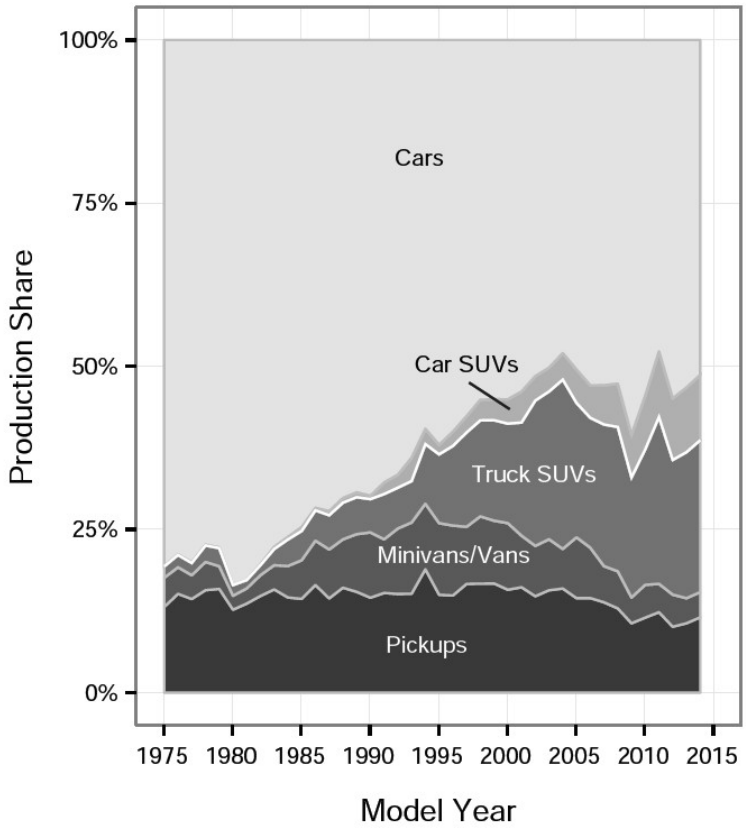

Source: (EPA, 2014)

CHAPTER 2:
Experimental Setup

In this chapter, the results of the experiments are presented. The chapter starts with Section 2.1, briefly introducing the engine testing facility. It is followed by a description of the experimental approach and some preliminary consideration in Section 2.2. The results are divided into throttled operation and dynamic skip fire operation conditions, and are presented separately in Chapters 3 and 4. The document ends with Chapter 6 where the comparison of both operating conditions is carried out and conclusions are drawn.

2.1 Engine Testing Facility

For the purpose of testing DSF, an engine test cell and the auxiliary systems had to be built. For simplicity and conciseness of this document, the experimental setup design and construction details are given in Appendix A. Figure 7 shows the finished test cell. A detailed scheme of the cell is found in Figures A.1 and A.14.

The engine tested on this work is a port injected GM Gen IV L94 V8 VORTEC 6.2 VVT whose main characteristics are listed in Table 1 The engine was converted to CNG through the replacement of the fuel injectors and the modification of the fuel rail. The engine was equipped with DSF (LOMA & deactivation lifters) and 16 proximity sensors to monitor the behavior of each valve. The engine was controlled from a main desk outside the cell and was carried out through *dSPACE* software and hardware. The data acquisition system and combustion analysis system were built on *Labview NI* software. The test cell was monitored through the allocation of different temperature, pressure, flow and emissions sensors listed in Tables A.2, A.3, A.7, A.9, and A.10.

Table 1: GM Gen IV L94 V8 VORTEC 6.2 VVT Engine Main Characteristics

Property	Unit	Value
Displacement	cc	6162
Compression ratio	-	10.4:1
Maximum power*	kW	301
Maximum torque*	Nm	565
Maximum speed	rpm	6000

*On Gasoline

Source: University of California, Berkeley

Figure 7: The Finished Testing Facility as of 01/12/2013 after the Cell Was Designed and Constructed

Photo Credit: University of California, Berkeley

2.2 Experimental Approach and Test Matrix

The goal of the experiments is to evaluate the potential fuel economy improvement that DSF can bring to a relatively large displacement engine fueled with CNG. This is achieved by an ultimate comparison between the engine in standard mode or throttled mode, with the engine running under dynamic skip fire mode. In order to do so, the engine is operated first on CNG and tuned to find its optimal performance. This is done by first finding the most efficient point on throttled mode, followed by a fine tuning of cam phasing and spark timing. Once the best conditions are determined, the optimum point for dynamic skip fire mode is determined as well. The engine is then operated on DSF under the same speed and load conditions used in throttled mode for a fair and accurate comparison. Moreover, the use of discrete variable displacement is also assessed through the operation of the engine under Active Fuel Management (AFM) introduced in Section D.1. Moreover, the expected reduction in power output and the effect of turbocharging is studies through software simulations (GT Power). Satisfying emission standard is achieved by comparing with current gasoline engine meeting California emission standards.

A summary of the test matrix is presented in Table 2.

Table 2: Test Matrix as Carried out for the Results Shown in This Report

Speed rpm	CAM phase CAD deg	MAP kPa	Firing pattern -	Spark timing CAD deg BTDC
1000	0, 20	40:10:100	Throttled V8	MBT
1000	0, 20	100	$\frac{7}{8}, \frac{3}{4}, \frac{2}{3}, \frac{5}{8}, \frac{1}{2}, \frac{1}{3}, \frac{1}{4}$	MBT
1500	20	40, 60	Throttled V8	+10, +5, MBT, −5, −10
1500	0, 20, 30, 40, 50	40:10:100	Throttled V8	MBT
1500	0, 20	90, 100	$\frac{7}{8}, \frac{3}{4}, \frac{2}{3}, \frac{5}{8}, \frac{1}{2}, \frac{1}{3}, \frac{1}{4}$	MBT
1500	0	40:10:100	AFM	MBT
2000	0	40:10:100	Throttled V8	MBT
2000	0	100	$\frac{7}{8}, \frac{3}{4}, \frac{2}{3}, \frac{5}{8}, \frac{1}{2}, \frac{1}{3}, \frac{1}{4}$	MBT
2500	0	40, 50, 60	Throttled V8	MBT
3000	0	40, 50	Throttled V8	MBT

MBT: maximum brake torque; CAM: valve train timing; CAD: crank angles of degree; MAP: manifold air pressure; BTDC: before TDC; kPa: kilopascal

Source: University of California, Berkeley

CHAPTER 3:
CNG-Throttled Engine Operation

In this chapter, the results regarding the throttled operation of the engine on CNG are introduced. The effect that spark timing, cam phasing and engine speed have on the engine performance are evaluated in Sections 3.1, 3.2 and 3.3. With this information, the optimum throttled mode performance is determined and presented in Section 3.4.

3.1 Effect of Spark Timing on Performance

The characteristics of the combustion event, normally described by the rate of heat release and the flame speed, are strongly dependent on temperature, pressure, fuel type and stoichiometry of the fuel-oxidizer mixture. During an engine cycle, as described in Appendix B, the aforementioned parameters change drastically as the piston moves along. The optimum position at which the combustion should be initiated is important to obtain the closest to an isochoric compression which reduces the thermodynamic losses. In a SI engine the combustion is triggered by a spark. The knock or auto-ignition phenomenom occurs when combustion starts independently of the spark event, which is not desired because no control over the process is possible. The spark occurs normally before the compression stroke has finished; therefore, the ignition timing (or spark timing) is referenced in values of crank angles of degree before top dead center (CAD BTDC). The reason for the advanced ignition timing relative to TDC is the finite burning velocity of the charge and the ignition delay observed in hydrocarbon air mixtures (Warnatz, Maas, & Dibble, 2006a).

Table 3: Engine Brake Parameter for Different Ignition Timings

Performance	Units	+10 CAD	+5 CAD	MBT	-5 CAD	-10 CAD
Brake efficiency	-	22.3	22.6	22.6	22.5	21.8
BT	Nm	88.108	89.252	89.674	89.532	87.167
BMEP	bar	1.797	1.820	1.829	1.826	1.778
BSFC	g/kWh	322.521	318.797	318.281	320.091	330.248
BSTHC	g/kWh	1.426	1.275	1.074	0.894	0.728
BSO_2	g/kWh	52.613	49.629	45.809	41.377	39.287
$BSCO_2$	g/kWh	793.907	785.913	787.512	797.131	825.333
BSCO	g/kWh	15.908	15.590	15.365	15.182	15.306
BS NO_x	g/kWh	8.968	7.714	6.382	5.262	3.811

Data acquired at 1500 rpm, 40 kPa MAP, 20 CAD CAM phasing.

Source: University of California, Berkeley

Figure 8: Effect of Ignition Timing on the In-Cylinder Pressure while Running at Engine Speed

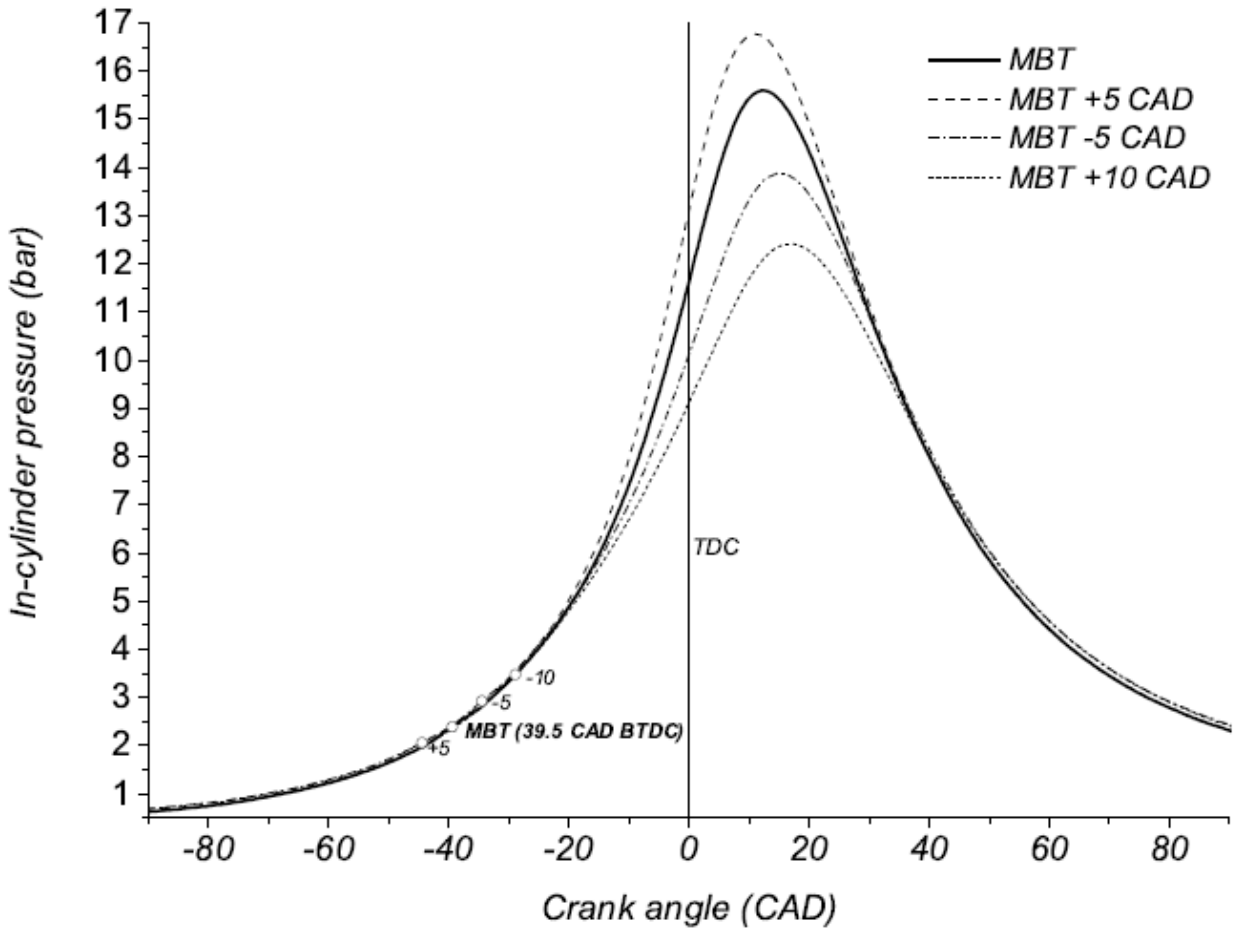

Data acquired at 1500 rpm, 40 kPa MAP, 20 CAD CAM, IT: MBT, +5 CAD, -5 CAD, -10 CAD. With ignition advance of +10 CAD, the proper pegging of the pressure signal could no longer be achieved.
Source: University of California, Berkeley

The pressure trace for four different ignition timings is shown in Figure 8 with their respective performance parameter listed in Table 3. The spark is triggered at four different timings: +5, MBT, -5, -10 CAD BTDC, where MBT stands for maximum brake torque or condition for maximum engine efficiency. This point is determined by carrying out a large swept of IT while monitoring engine torque. MBT is the ignition time at which maximum torque was generated.

3.1.1 Early Ignition Timing

In Figure 8, it can be seen that early ignition (MBT +5 CAD BTDC) results in the highest in-cylinder pressure of all of the traces presented. The reason lies on the added effect combustion has over pressure. Because combustion starts earlier, pressure increase is supported by both, the compression work exerted by the piston and the combustion reaction. Though higher pressures are achieved, and this is at first sight desired (explained in Appendix B.3), the optimal ignition timing is found few degrees later. This result can be better understood with the aid of Figure 9

where the cumulative indicated work is plotted against two engine revolutions in crank angles of degree (CAD). Figure 9 shows that the piston consumes work during the period enclosed within -180 CAD to 0 CAD or TDC because it needs to compress the charge. Because of the contribution combustion has on pressure, the piston must exert more work over the charge to reach TDC and thus the compression work consumed increases. Notice that the total indicated work generated by the piston is slightly higher for +5 than for MBT. The reason is that at certain IT range around MBT, performance is nearly constant and finding the optimum is based on the brake parameters which combine the performance of all eight cylinder of the engine.

Figure 9: Effect of Ignition Timing on the Engine Gross Indicated Cumulative Work, at Engine Speed

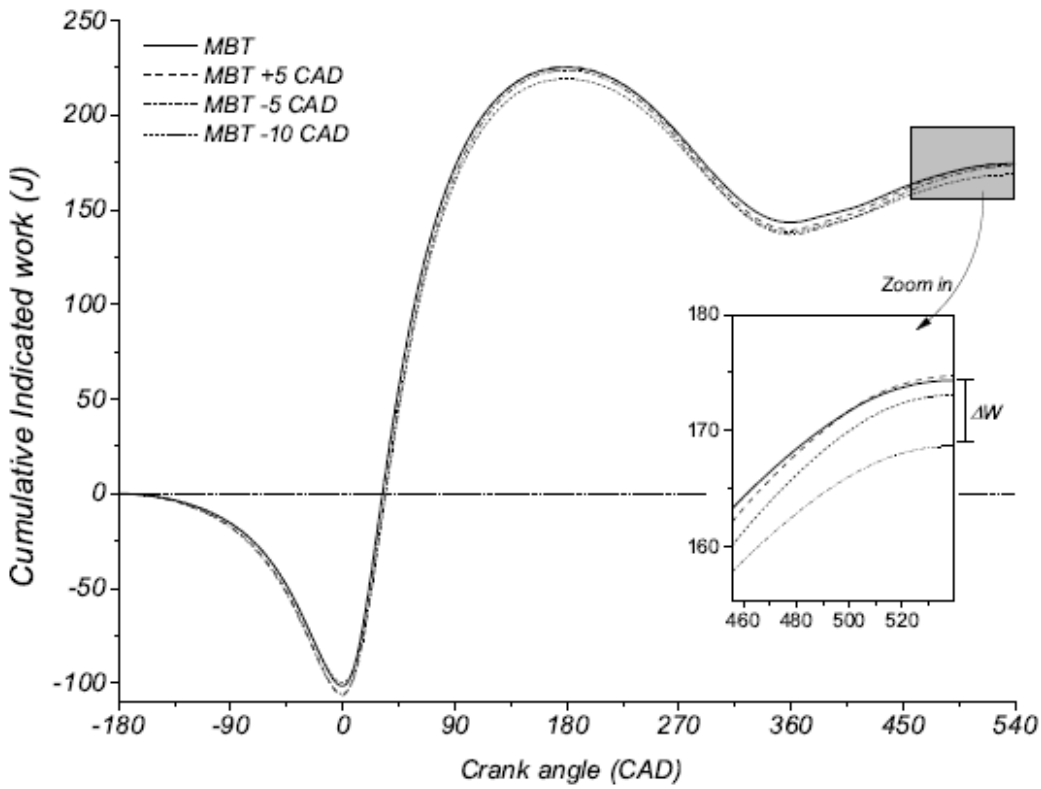

Data acquired at 1500 rpm, 40 kPa MAP, 20 CAM, IT: MBT, +5 CAD, -5 CAD, -10 CAD.
Source: University of California, Berkeley

Another consequence of early ignition is the higher combustion temperatures caused by both the higher peak pressure in the cylinder which increases temperature according to Equation B.68 and the higher heat release rate consequence of higher reaction rates parallel increasing with temperature. This effect can be seen in Figure 10, where the normalized heat released rate of combustion is plotted against the ignition timing (IT) at which the combustion was triggered. In this figure, the heat released increases at different rates (slopes) and timings for the different ignition timings. When combustion starts earlier, the pressure in the cylinder is lower and so is the initial temperature. This causes the reaction rate of the elementary reactions to be lower and

consequently the ignition delay to be longer (Warnatz et al., 2006a). Nevertheless, the initial low temperature effect is offset by a most rapidly increasing temperature caused by the compression. Ultimately, the reaction rates would be, on average, higher than in the other cases as can be observed by the stiffer slope of the MBT +5 CAD BTDC heat release trace.

Figure 10: Normalized Gross Cumulative Heat Release over Crank Angle Degrees after Ignition (CAD AIT).

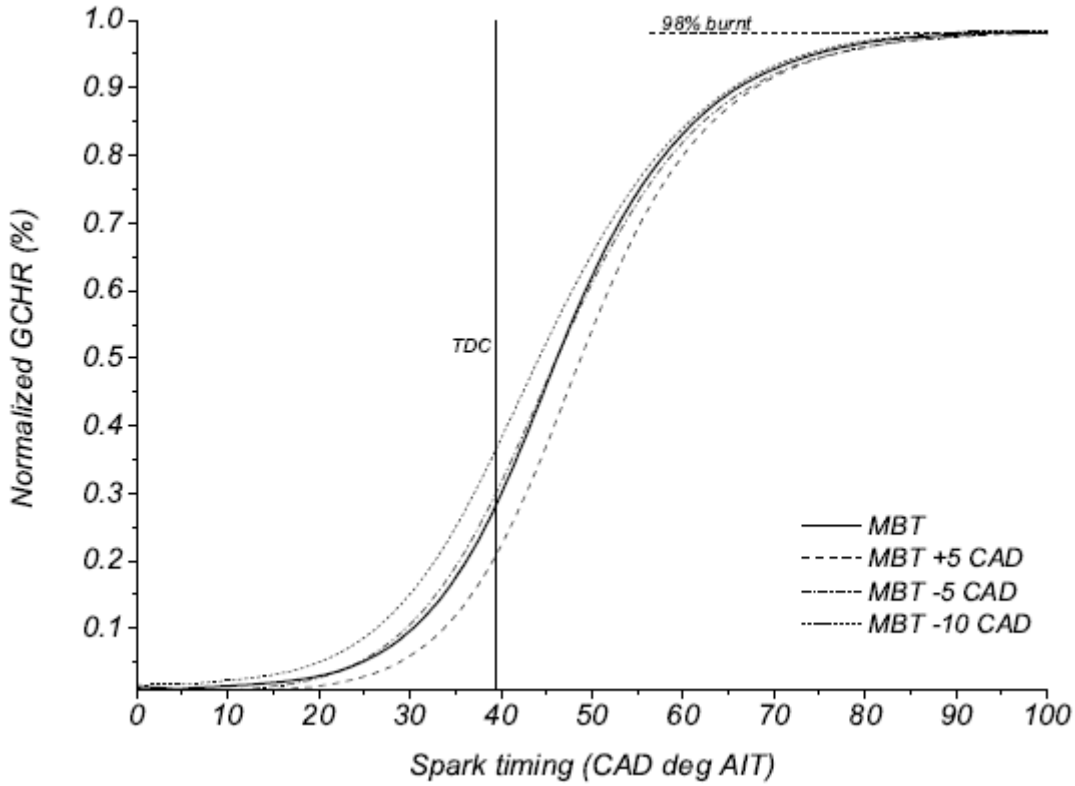

Data acquired at 1500 rpm, 40 kPa MAP, 20 CAM, IT: MBT, +5 CAD, -5 CAD, -10 CAD.
Source: University of California, Berkeley

Figure 11: Emissions of Main Compounds on Exhaust (THC, O_2, CO_2, CO and NO_x)

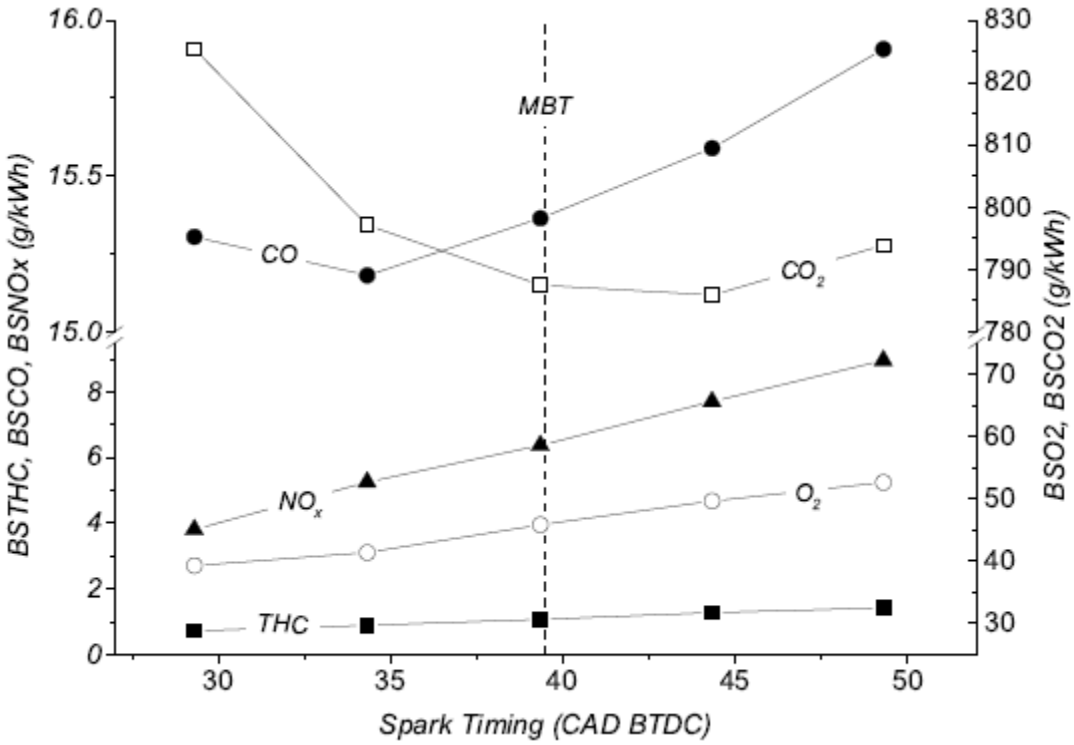

Engine speed 1500 rpm, 40 kPa MAP, 20 CAM, IT: MBT, +5 CAD, -5 CAD, -10 CAD.
Source: University of California, Berkeley

3.1.2 Late Ignition Timing

In the case of a later ignition (MBT -5 & -10 CAD BTDC), the effect on performance is similar to that of early ignition, but the reasons are opposite. Pressure when the spark is triggered is now higher (Figure 8, CAD -5 and -10) and the ignition delay is thus smaller due to induced higher temperature; however, the combustion event develops further along the expansion stroke and the temperature decreases, causing a consequent downgrade of the reaction rates of the elementary reactions. As a result, the combustion duration is longer and the power delivered lower.

3.1.3 Ignition Timing Effect on Emissions

Exhaust gas composition is also influenced by the spark timing. Although MBT is preferred regarding engine performance, from an environmental stand point, retarding or advancing spark timing may find a balance where emissions of CO_2 remain relatively low but the emissions of other undesired compounds are reduced. Results of spark timing effect on emissions are illustrated in Figure 11. From late to early ignition timing, emissions of major compounds such as carbon monoxide CO, nitrogen oxides NO_x and unburnt hydrocarbons THC grow linearly. The growth in THC is accompanied by an increase of O_2 concentrations in the exhaust. CO_2 on the other hand, increases when moving away from MBT. Notice that IT 40 CAD BTDC (MBT) and 45

CAD BTDC (+5) are nearly equal as the scale is rather large and the engine performance is nearly equal as explained in the previous paragraphs.

The growth in nitrogen oxides could be caused by the higher temperatures. This growth also explains the higher concentration of CO, caused by an equilibrium shift on the CO oxidation reaction which enhances CO_2 dissociation. The increase of carbon dioxide is directly related to the amount of fuel burnt, which decreases towards MBT IT as expected. The increase on unburnt charge with earlier IT may be caused by the quenching of the oxidation reaction during the expansion stroke. As the combustion starts earlier in time, burnt gases cool down quicker during the expansion stroke than in the case for later ignition, where the combustion duration is longer providing self-sufficient heat for the reaction to continue. Nevertheless, the variation in THC emissions is minimal.

Figure 12: Brake Thermal Efficiency or Brake Efficiency Variation with Load and Ignition Timing

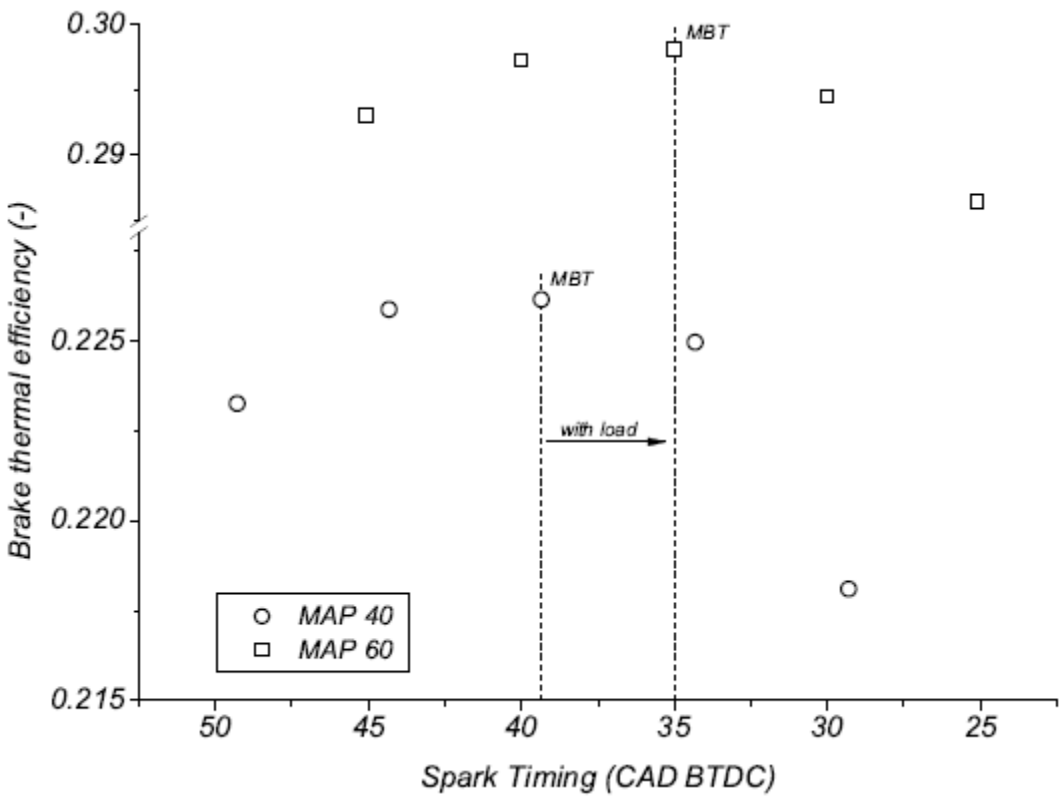

Data acquired at 1500 rpm, 40-60 kPa MAP, 20 CAM, IT: MBT, +5 CAD, -5 CAD, -10 CAD.
Source: University of California, Berkeley

3.1.4 Ignition Timing Variation with Engine Load and Speed

From the above stated, MBT is found within a small range before TDC, where burning velocities and pressure find the right balance. However, MBT shifts with engine conditions such as load and speed. Results for varying load are shown in Figure 12 with the engine operating at two different air manifold pressures: MAP 40 kPa and MAP 60 kPa. The IT for MBT shifts from

around 40 CAD BTDC at 40 kPa to around 34 CAD BTDC at 60 kPa. This change on ignition timing follows the reasoning given above. The charge at 60 kPa is denser than at 40 kPa. Consequently, pressure is higher in the cylinder due to a higher fuel-oxidizer charge and thus temperature rises faster, simultaneously with pressure, resulting on higher reaction rates and a shorter ignition delay.

The effect of speed is assessed in Figure 13. In the figure, results from the engine operated at speed 1000 rpm and 1500 rpm are illustrated. As explained above, load increase (BMEP in the chart) translates into later IT for MBT. On the contrary, earlier IT is needed with increasing speed to reach MBT. The reason being that at higher speeds, the time available for combustion is shorter and thus high reaction rates are needed to cope with lesser available time. Therefore, early ignition is desired because on one hand, it takes longer to initiate, which avoids consuming too much work from the piston before TDC and, on the other hand, early ignition relates to higher burning rates as seen before (Figure 10). Consequently, the combustion occurs closer to TDC and it is carried out in a shorter period of time. Notice that gasoline ignition timing changes more radically with load. The major reason for the radical ignition timing retardation of gasoline is the knock phenomena for which gasoline is more susceptible. At higher load, pressure and temperature reach values above which gasoline auto-ignites, even before any spark event has been triggered.

Figure 13: Ignition Timing for Maximum Brake Torque Plotted against Engine Load

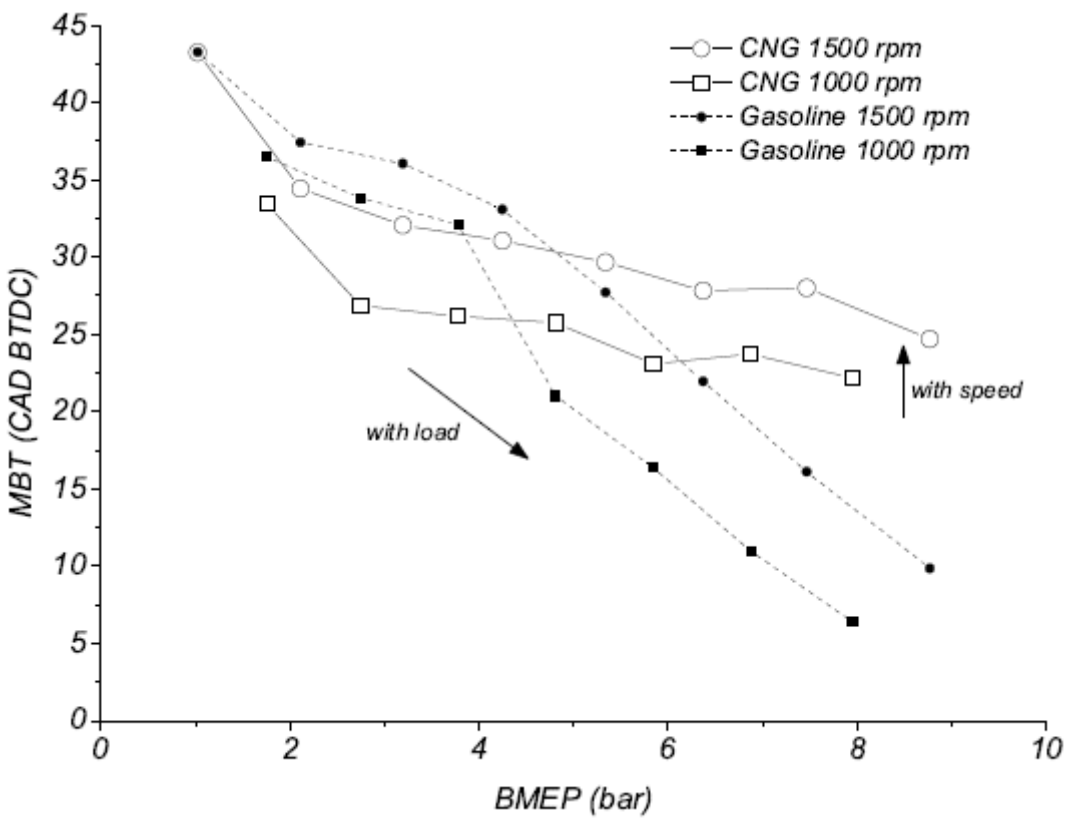

Data acquired at 1000 rpm & 1500 rpm, 0 CAM, IT: MBT

The main conclusions from this section can be summarized as follows:

1. Ignition timing has strong influence on the engine's work output.
2. Retarded ignition timing is needed at higher load to avoid excessive work from the piston during the compression stroke.
3. Advanced ignition timing is needed to cope with lesser time for combustion at higher engine's speed.
4. Emissions of undesired exhaust compounds could be finely tuned by means of ignition timing.
5. CNG, unlike gasoline, is not susceptible to knock at relatively small[1] compression ratios and stoichiometric conditions.

3.2 Effect of CAM Phasing on Performance

Although not every engine offers the possibility for variable valve train tuning or variable valve timing (VVT), the proper selection of valve timing is of extreme relevance for the overall engine performance. VVT is a fine tune option for variable displacement engines because it can partially control the cylinder load independently of throttle position. In order to evaluate the effect of valve timing, the engine, with VVT integrated (Figure D.4), has been operated at 5 different valve timing (also referred in this text as cam phasing) angles with the results shown in Table 4.

Table 4: Engine Brake Parameter for Different CAM Phasing

Performance parameters	Units	50 CAM	40 CAM	30 CAM	20 CAM	0 CAM
Brake efficiency	-	31.3 percent	32.4 percent	32.8 percent	34.1 percent	34.3 percent
BSFC	g/kWh	230.324	222.289	219.339	210.961	210.188
BMEP	bar	4.136	5.121	5.963	6.789	7.464
PMEP	bar	0.264	0.242	0.197	0.172	0.177
PMEPpump	bar	0.136	0.137	0.138	0.141	0.143
PMEPvalve	bar	0.127	0.105	0.059	0.031	0.034
Ignition timing (IT)	CAD	34.265	39.316	33.424	29.616	28.018

Data acquired at 1500 rpm, 90 kPa MAP, 0, 20, 30, 40, 50 CAD CAM phasing, IT: MBT

Source: University of California, Berkeley

The pressure traces for the points on Table 4 are shown in Figure 14. In the figure it can be seen that the peak pressure decreases gradually with the addition of cam retardation. At CAM 0 (fully advanced) the pressure is highest and is lowest at CAM 50 (fully retarded). The evolution of

[1] For methane, SI engines can reach up to r_c = 15 without incurring knock [66].

[2] At this pressure level, the sensor is not able to deliver a clean signal anymore and indicated values do not offer reliable information.

IVC, EVO and IT with cam phasing is also shown in the figure. It can be seen that IVC and IT get closer together with the retarding of the CAM. This effect is seen in the previous section. With cam retarding, the load is reduced and thus the IT needs to be advanced (Figure 13). This effect limits the possibilities for valve timing retardation because IT cannot go beyond IVC. The reason is that an open valve cannot withstand the pressure rise induced by the combustion event. As a result, the valve steam and possibly the rest of the valve train may break.

In Section B.3.4, the major sources of pumping losses (PMEP) on the breathing process of the engine were the pressure drop across the valves ($PMEP_{valve}$) and the pressure difference between inlet and exhaust manifolds ($PMEP_{pump}$). VVT plays an important role on reducing PMEP by balancing these terms.

$$PMEP = PMEP_{pump} + PMEP_{valves} \tag{1}$$

The first term on the right is more influenced by the throttle position than the second term. Nonetheless, though indirectly, valve timing can also alter the pressure at which the piston faces the inlet and exhaust manifolds. Moreover, by varying valve timing the pressure drop across the valve can be also modified. Figure 15 illustrates the effect a retard of 40 CAM has over the pumping losses. It can be seen that at standard valve timing (0 CAM) $PMEP_{pump}$ are higher than that at 40 CAM (+ 40 CAD shift towards TDC). On the other hand, with 40 CAM retarded valve timing the flow losses across the valves increase more accentuated than at 0 CAM valve timing.

Figure 14: In-Cylinder Pressure Trace Evolution for the Engine

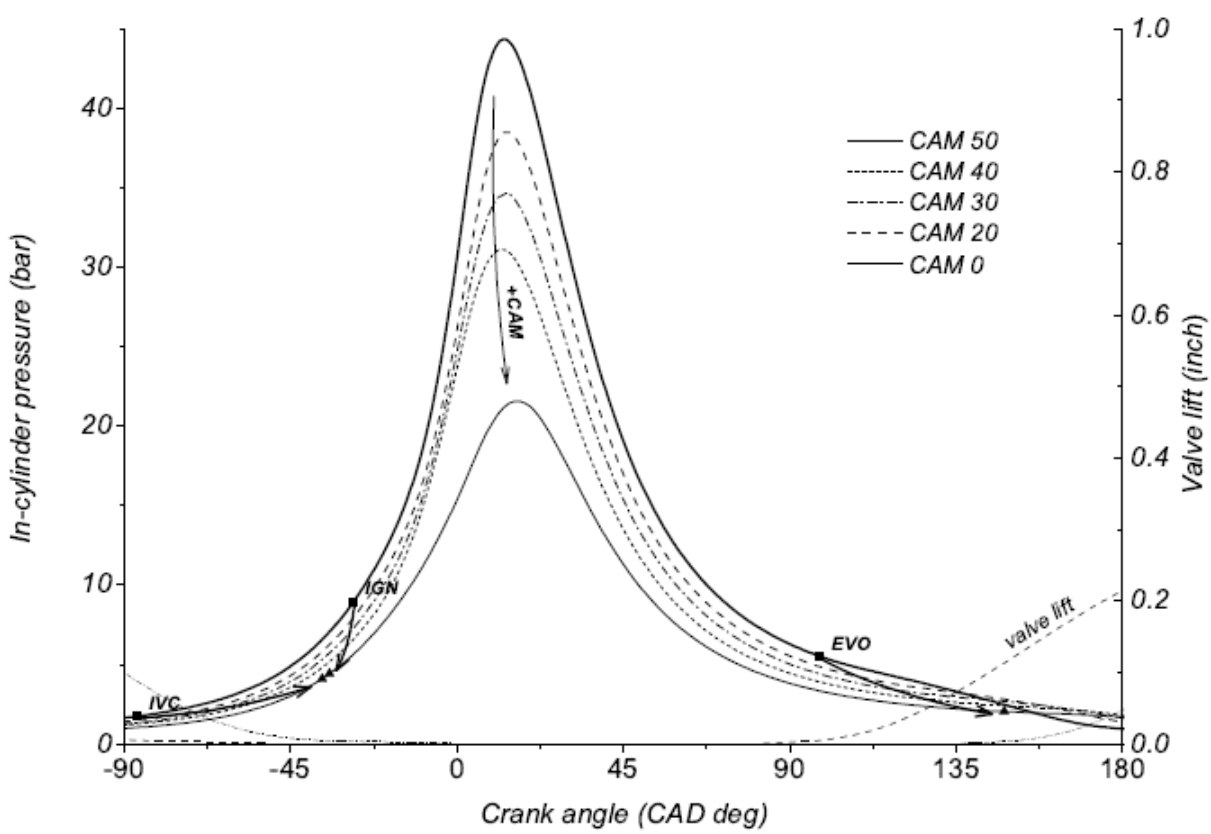

Data acquired at 1500 rpm, IT: MBT, and varying the valve timing from 0 CAD CAM up to 50 CAD CAM retard.

Source: University of California, Berkeley

Figure 15: Evolution of PMEP, PMEPpump, and PMEPvalves at Different Valve Timings

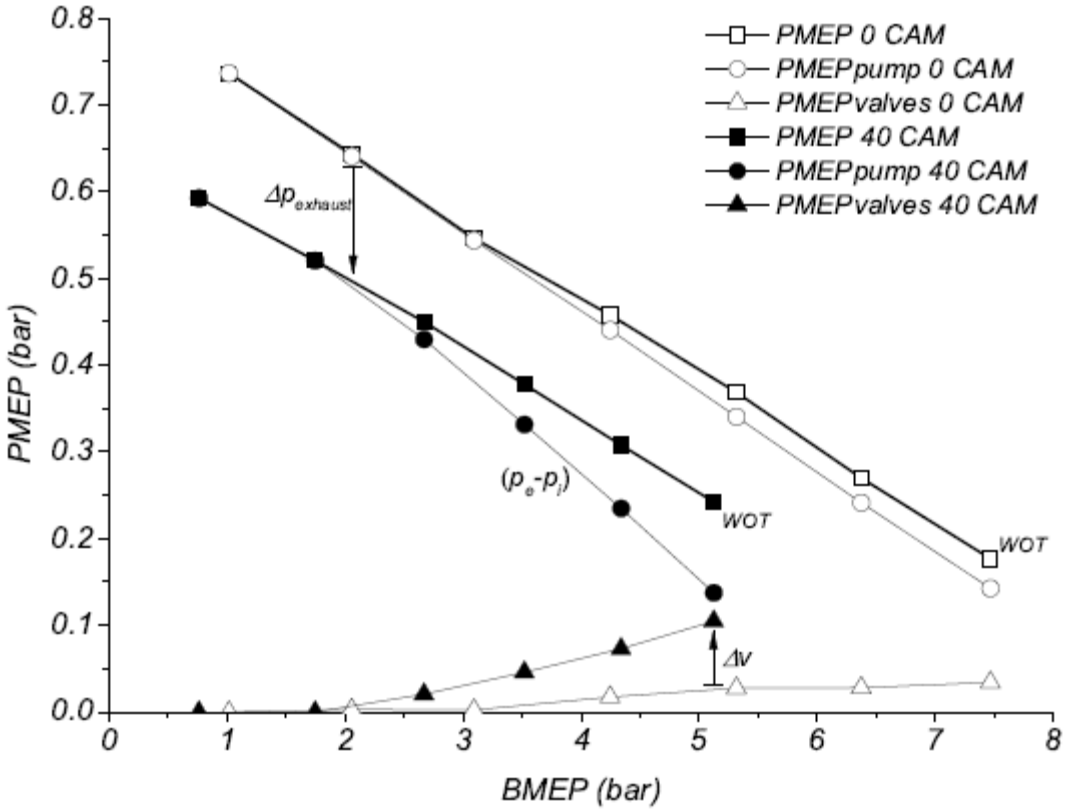

Data acquired at 1500 rpm, IT: MBT, valve timings at 0 & -40 CAD CAM.

Source: University of California, Berkeley

The reason for the reverse behavior lies in the flow velocity. When the inlet valve opens (IVO) early in time (0 CAM), a bigger amount of charge is drawn into the cylinders. Because the valve has opened before TDC, the piston has not yet created any suction, and during the intake stroke the air enters smoothly into the chamber. On the other hand, the exhaust valve also opens earlier and causes the burnt gas to face the outlet earlier, in the expansion stroke, and consequently at higher pressure. This increases the pressure of the exhaust bank. As a result, flow velocities are lower due to smaller pressure drops from intake manifold to cylinder, but the exhaust pressure is higher, increasing $PMEP_{pump}$.

By further retarding the inlet valve opening (IVO), even within the intake stroke (CAM 50), the piston generates suction before the inlet valve opens. The higher pressure drop between intake manifold and exhaust induces higher flow velocities and consequently more flow losses across the valves ($PMEP_{valves}$). Because the exhaust valve also opens later, exhaust pressure are lowered and thus pumping losses are reduced accordingly. Notice that because of the later inlet valve opening, less charge is drawn into the chamber and the generated power is therefore lower.

A balance shall be found among valve flow losses and pumping losses. Figure 16 illustrates the effect different valve timing has on the brake specific fuel consumption. As expected, early IVO results in higher BMEP while later exhaust valve opening EVO results on more efficient operation. Notice that the effect of valve timing nearly vanishes at low loads. The reason is that at this point flow velocity and charge are low enough to diminish the change in flow velocity and pressures across the cylinder intake and exhaust; therefore, the effect valves could have on reducing $PMEP_{valves}$ is not noticed because these losses are already low as can be seen in Figure 15, where at low BMEP and $PMEP_{valves}$ approaches 0 for both 40 and 0 CAM. Moreover, with low flow velocities the flow inertia is negligible and too late exhaust valve closure (EVC) may cause undesired exhaust gas recirculation (EGR).

Figure 16: Effect of Valve Timing on Brake Specific Fuel Consumption

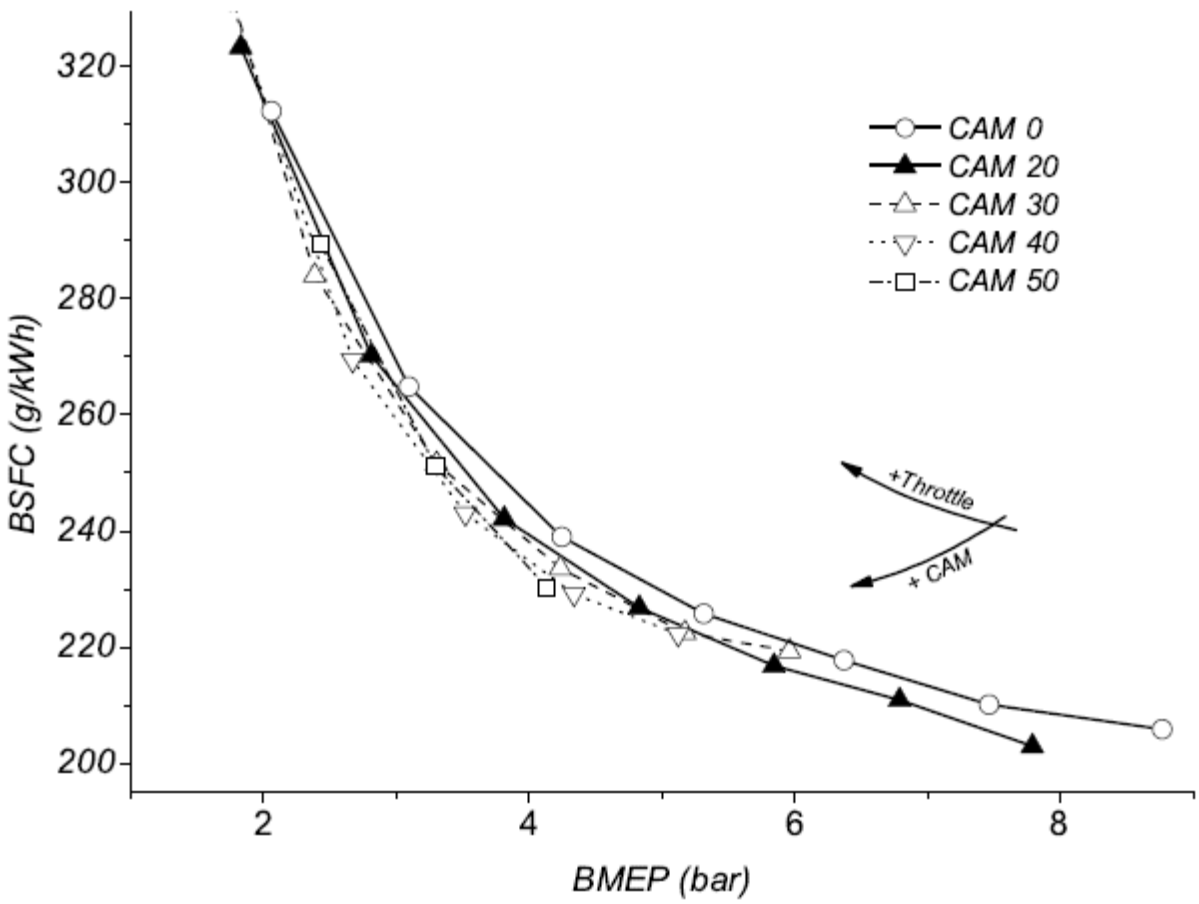

Data acquired at 1500 rpm, IT: MBT

Source: University of California, Berkeley

The effect of CAM phasing on emissions is shown in Figure 17. From top to bottom and left to right, the emissions of unburnt hydrocarbons, carbon dioxide, nitrogen oxides and carbon monoxide are illustrated. Values for oxygen are also plotted. We can see that emissions are not greatly influenced by valve timing and are rather similar at any cam phasing. At low loads the

concentration of total hydrocarbons (THC) in the exhaust increases together with O_2 levels for stoichiometric conditions. The reason for this a prolonged combustion reaction further in the expansion stroke and thus lower combustion temperatures. This could lead to a partial quench of the reaction near the wall due to insufficient heat release rates to maintain combustion near the end of the cycle.

Because of the reduction in engine load at later valve phasing (CAM 40) and the consequent improvement of BSFC, the emissions of CO_2 are reduced. On the other hand, the concentration of CO increases at lower loads. This could be a consequence of a worse oxidation as mentioned before for THC emissions. On the contrary, NO_x drastically decreases at late valve timing. The reason for such effect can be better understood with the aid of Figure 18. In this figure, the start of combustion SOC (3 percent mass burnt) and the end of combustion EOC (97 percent mass burnt) are plotted for different loads at different CAM timings. We can see that from 4 bar BMEP and higher, the combustion duration is constant for any CAM phasing configuration.

At low loads, however, the combustion duration slightly increases. This effect is more noticeable with late valve timing (i.e. at 40 CAM) where combustion duration increases from 50 CAD at 4 bar BMEP to nearly 100 CAD at 1 bar BMEP. At this point, the reaction rate is extremely low and the combustion duration increases radically. Because combustion takes longer, it extends further along the expansion stroke and temperatures are thus lower, preventing the formation of NO_x.

When the combustion event shifts too far within the expansion stroke, the decrease in temperature induced by the adiabatic expansion weakens the reaction rates to a point where combustion is no longer stable. This can be observed at later valve timing such as CAM 50. At this point manifold pressures below 60 kPa (BMEP < 2 bar) resulted in unstable engine operation. This can be seen in Figure 18 for CAM 50 for which no data is plotted below 2.5 bar BMEP.

The main conclusion for this section can be summarized as follows

1. Valve timing is fine tuning option for engine's volume displacement.
2. Valve timing strategies are limited by ignition timing, more if both inlet and exhaust are driven by the same camshaft.
3. Advanced valve timing increases load and also $PMEP_{pump}$.
4. Retarded valve timing reduces exhaust pressure but increases valve flow losses $PMEP_{valve}$ due to higher flow velocities.
5. Emissions are not strongly influenced by valve timing, but the ignition timing limitation may cause an overall increase at low loads.

Figure 17: Emissions of Main Exhaust Compounds for Different Valve Timing Conditions.

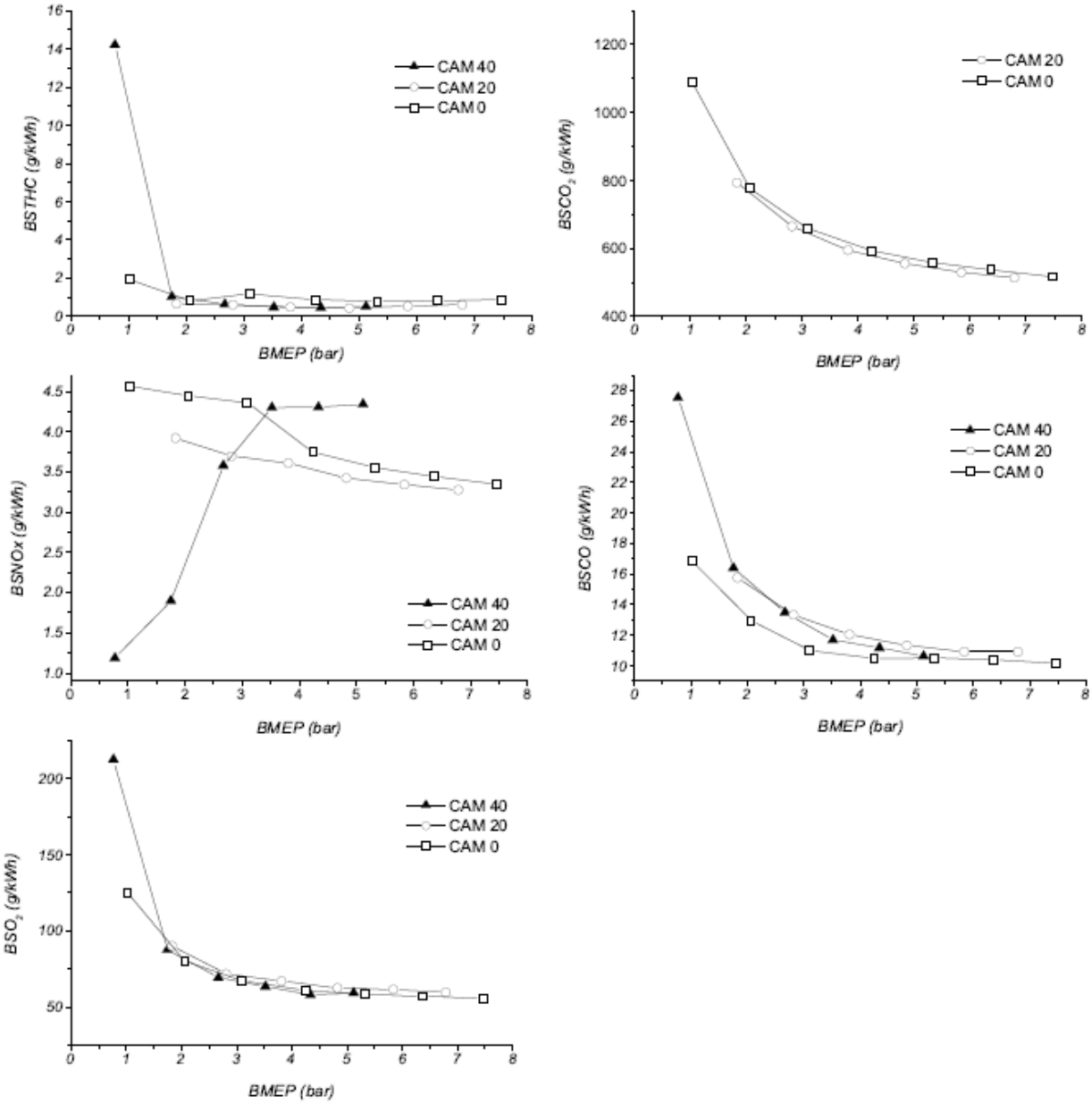

Data collected at engine speed 1500 rpm IT:MBT. Emissions of CO_2 at CAM 40 has not been plotted because of measurement irregularities. The range at which CO_2 emissions signal (0 – 5V) was being collected did not match the conversion function and the values were offset.

Source: University of California, Berkeley

Figure 18: Evolution with Load of the Characteristic Angles of Combustion SOC and EOC for CAM 0, CAM 20, CAM 40, and CAM 50.

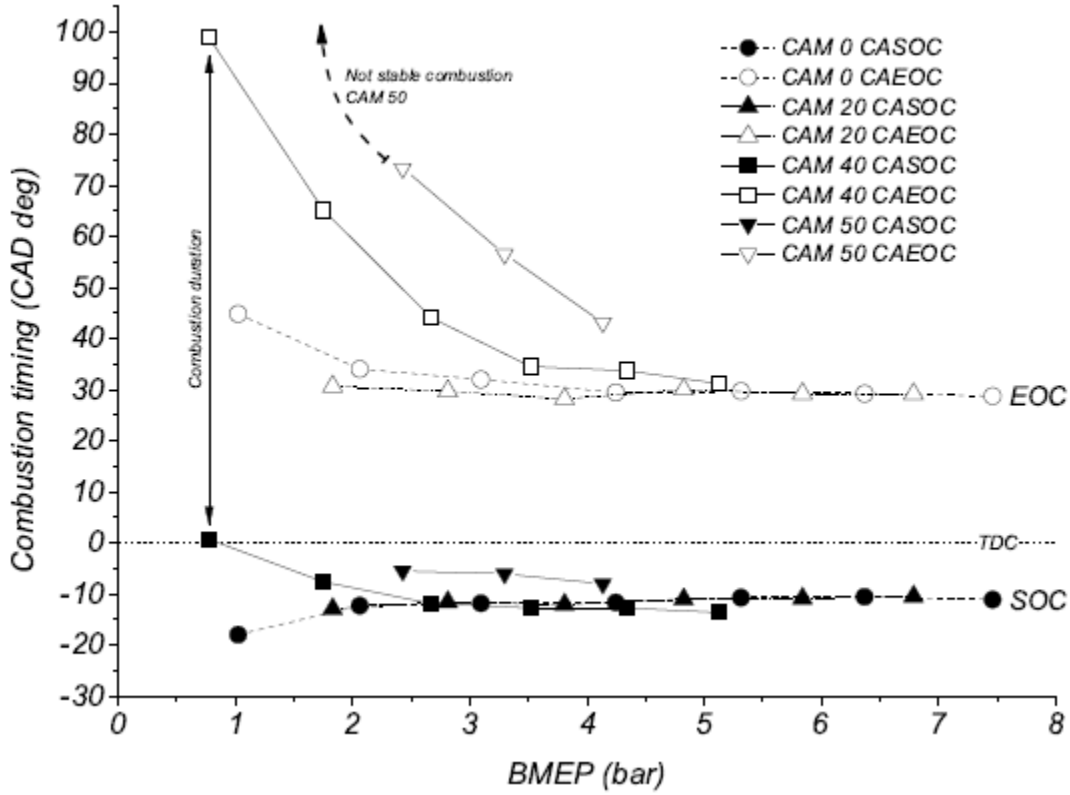

Data acquired at 1500 rpm and IT: MBT. Valve timings at CAM 0, 20, 40, 50

Source: University of California, Berkeley

3.3 Effect of Engine Speed on Performance

We have seen in Section 3.1 that engine speed has an effect on spark timing due to longer combustion duration. For the sake of comparison, it is desired to find the speed range at which the engine, under standard operation, is most efficient. In Figure 19, the brake specific fuel consumption of the engine is plotted within a speed range 1000:500:2500.

Figure 19: Brake Specific Fuel Consumption for Different Engine Speeds at Different Loads

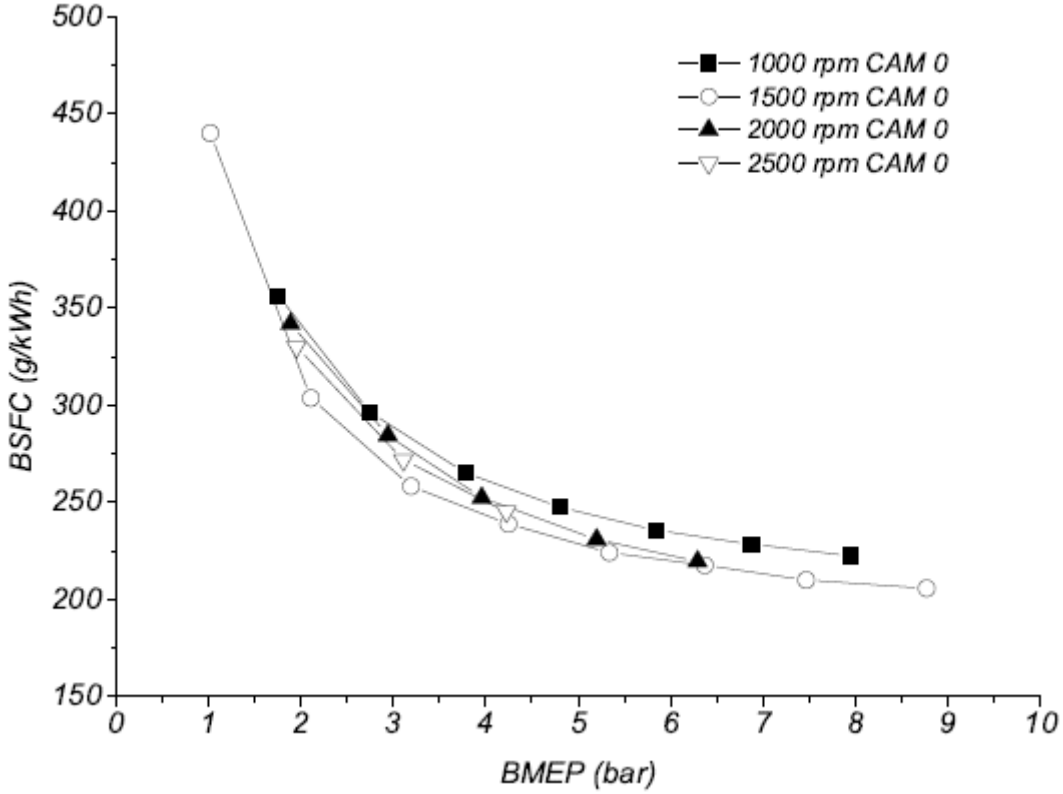

Data acquired at 0 CAM and IT: MBT.

Source: University of California, Berkeley

The results show that 1500 rpm is, within the samples, the optimum point of operation because the brake specific fuel consumption is lowest. Notice that the effect of speed vanishes at low load, where charge is small and time is not a constraint[4].

3.4 Optimum Conditions for Standard Engine Operation

From the previous sections, it has been determined that ignition timing, valve timing and engine regime are optimal for the best operation of the engine. The result of these points is shown in this section from maximum to minimum load. In Figure 20, the result for combustion efficiency (η_C), thermodynamic efficiency (η_T), gas exchange efficiency ($\eta_{G.E}$), mechanical efficiency (η_M), and brake efficiency (η_b) are shown. Also brake specific fuel consumption (BSFC) is illustrated.

Combustion efficiency η_C remains rather constant, around 98 percent and reduces under extreme low loads due to unstable combustion. A slight decrease is also found at WOT because valve timing is fully advanced (CAM 0). Thermodynamic efficiency η_T increases with load because the ratio between power produced to heat losses rises. The gas exchange efficiency $\eta_{G.E}$ peaks at highest load (WOT) and falls rapidly at part loads (below 5 bar BMEP). As in the case of the thermal efficiency, the friction losses vanish at high load because the ratio between energy consumed by friction is negligible compared to the engine power. Nevertheless, friction losses

actually increase linearly with load due to higher pressure over the piston rings at high loads. Finally, brake efficiency η_b, as combination of the previous four, shows a coupled increment of efficiency with increasing load. Consequently, BSFC peaks at lowest load and stabilizes at a minimum value under high loads.

Regarding engine emissions, the values for CO, CO_2, and THC follow a smooth increasing trend towards low loads as could be expected from the efficiency charts on Figure 20. Oxygen concentrations and unburnt hydrocarbons rise towards idle because combustion is not as stable due to ignition limitations, which cannot ignite before IVC. Carbon dioxide behaves inversely proportional to brake efficiency and grows towards low loads as the engine efficiency decreases. Finally, NO_x presents a more scattered data set but the values remain within range of 2-4 g/kWh.

Figure 20: Overall Efficiency Trends for the Optimal Engine Configuration

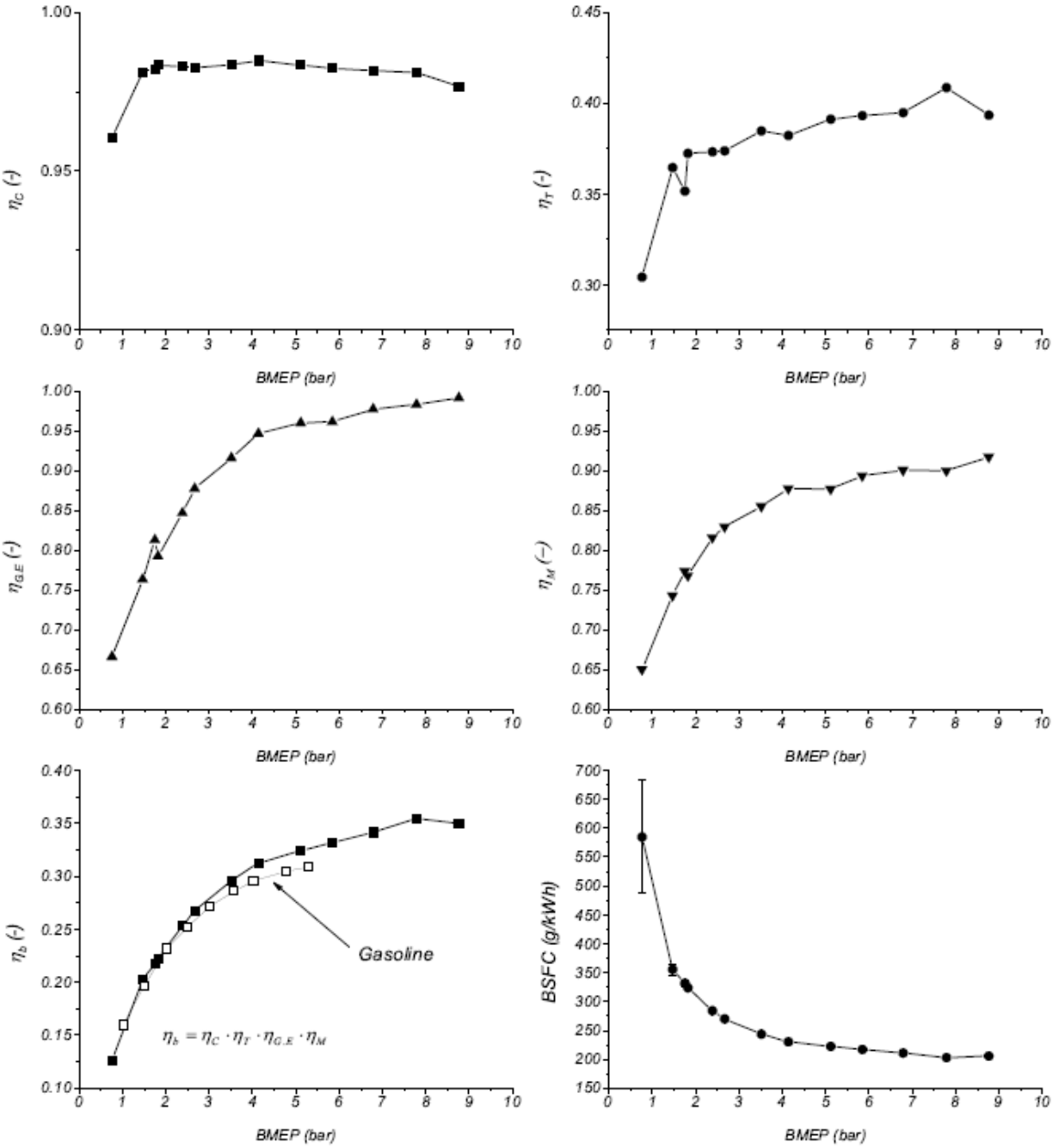

Data acquired at 1500 rpm, 0 CAM.

Source: University of California, Berkeley

Figure 21: Overall Emissions Behavior for the Optimal Engine Configuration

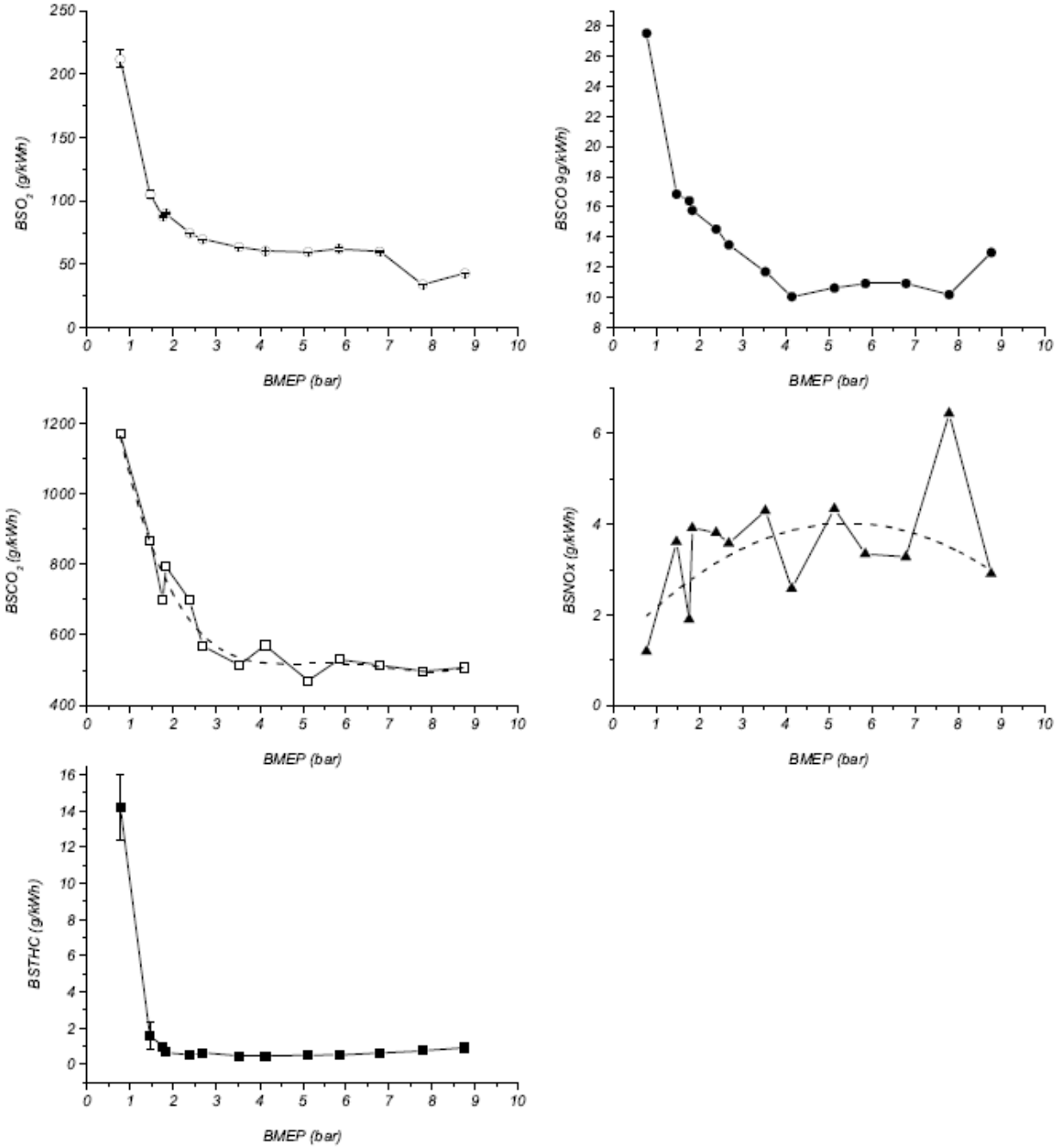

Data acquired at 1500 rpm.

Source: University of California, Berkeley

Table 5: Result for the Two Possible Optimum Points on CNG-throttled Engine Operation

Performance Parameters	Units	Point 1	Point 2
Manifold Air Pressure	kPa	100	100
Valve Timing Retard	CAD deg	0	20
Engine Speed	rpm	1500	1500
Brake Efficiency	-	34.95	35.45
Bmep	bar	8.76	7.78
Bsfc	g/kWh	205.93	202.98
Bsthc	g/kWh	0.922	0.778
Bso2	g/kWh	42.774	33.880
Bsco2	g/kWh	506.24	496.91
Bsco	g/kWh	12.99	10.20
Bsnox	g/kWh	2.90	6.45

Source: University of California, Berkeley

3.5 Conclusions

The goal of the previous experiments was to determine the best possible points at which the engine works most energy efficient. These two points have been found at wide open throttle (100 kPa manifold pressure) and least BSFC. The two points which accomplish the above conditions are:

1. Wide open throttle at 1500 rpm, and fully advance valve timing (CAM 0).
2. Wide open throttle at 1500 rpm, and retarded valve timing of 20 CAD degrees (CAM 20). The properties of these points are listed in Table 3.5.

The first point, at fully advance valve timing, generates a higher BMEP than point 2. Nevertheless, though point 2 generates less power, it does so in a more efficient manner. Higher cylinder loads will increase the number of skipped cylinders as lesser amount of cylinders would be sufficient to overcome driver's demand. On the other hand, a retardation of 20 CAM generates less power, thus less cylinders deactivation, which may lead to an overall higher heat losses within the entire engine. The best point can be found by comparing the increase in friction losses caused by the disabled cylinders and the heat losses reduction due to less active cylinders. Based on BSFC, at high firing fractions when maximum power is demanded, 0 CAM represents the optimum point. When power demand decreases (firing fraction decreases), valve retardation should be increased to maintain the maximum number of cylinders active in the most efficient manner as seen at 20 CAM in Figure 20.

For this project, both CAM 0, and CAM 20 have been sampled. Results are presented in the next sections.

CHAPTER 4:
CNG-DSF Engine Operation

DSF strategy profits from the best and optimum engine point to deliver the best performance at any time. Further data can be found in Appendix D. Ideally, the active cylinders will always operate at their best point obtained on the previously presented work. It is obvious that at high loads, DSF will not cause any benefit and could even harm the engine performance by an increase on friction losses to power ratio. At low loads, the benefit of DSF is expected to be maximum, where throttled operation suffers most from pumping losses.

Figure 22: In-Cylinder Pressure for DSF

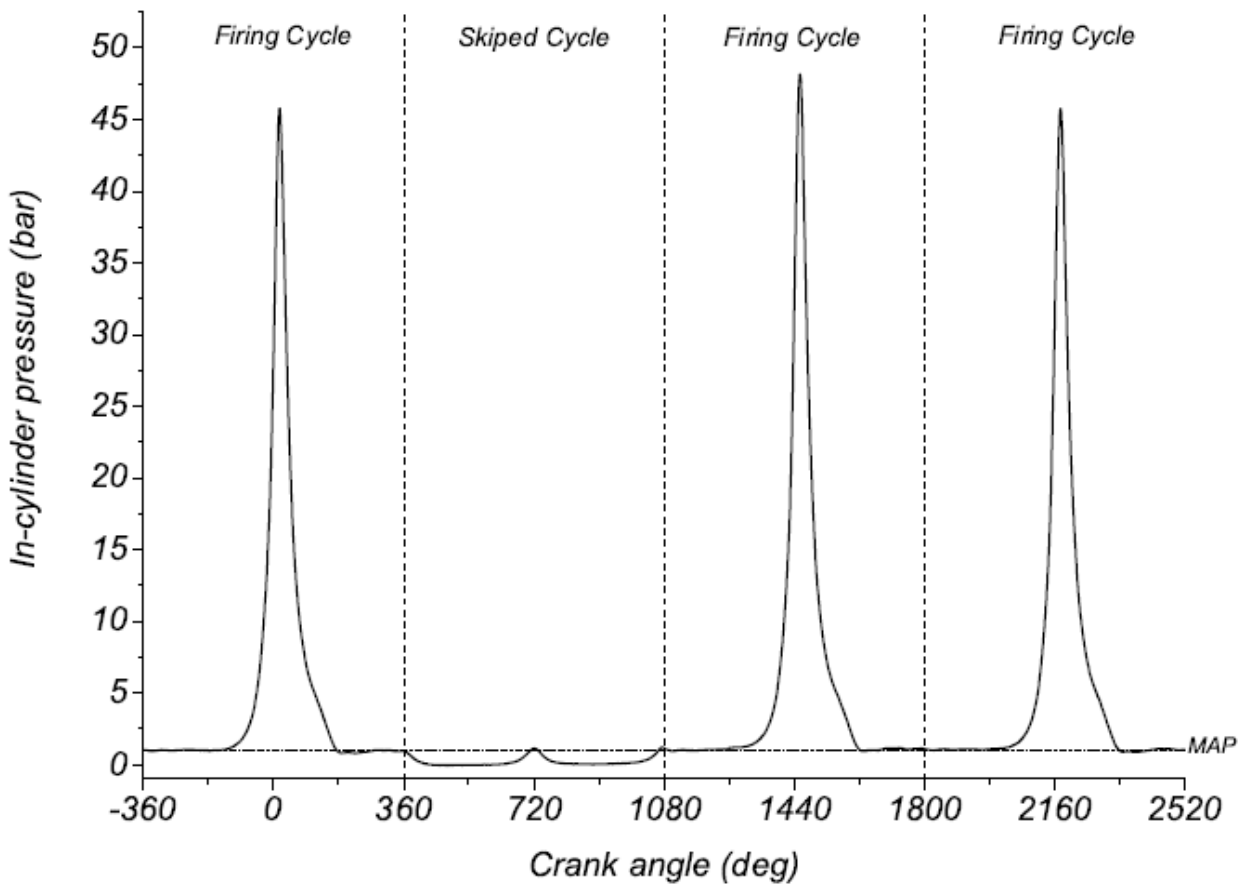

Data acquired at 2/3 1500 rpm, CAM 0.

Source: University of California, Berkeley

An overall 4 cycle long pressure trace for a single cylinder is plotted in Figure 22. On this figure the effective volume displacement of the engine is 4.13 liters which means that the engine fires twice every three fire opportunities. Following the original firing order of the engine 1-8-7-2-6-5-4-3, the behavior of the engine at these conditions follows: 1-8-2-6-4-3-1-7-2-5... In the following sections, the behavior of the firing cylinders as well as the disabled cylinders will be assessed.

4.1 Firing Cylinder Characteristics

The firing cylinder should work under the optimum conditions (MAP 100 kPa and CAM 0 or 20). For this example, samples at CAM 0 were chosen. The indicated net instant and cumulative work of the same cylinder under throttled and DSF operation are plotted in Figure 23, chart (a). The cylinder delivers nearly four times more power per cycle under DSF operation that under throttled conditions, though the engine delivers the same power.

A better comparison of the two is illustrated on the same figure, chart (b). In this graph, the cumulative and instant work has been normalized over its peak value. In both cases, maximum work is delivered at same CAD degree which means that in both cases the ignition timing was tuned appropriately to deliver MBT. Thanks to normalized values, the pumping losses due to the breathing process can be better identified. The gain per cylinder in this specific case stands around 18 percent. This improvement is further increased when considering the overall engine because thermodynamic losses η_T also decrease at full load as observed in Figure 20.

4.2 Deactivated Cylinder Characteristics

When the FCU orders the deactivation of a cylinder it waits until the cylinder has faced the EVC event, meaning that the cylinder is exhaust gas free during the skipped cycle. However, because the inlet valves is shot during the exhaust event, the cylinder does not benefit from the effect that valve overlap ($\Delta\theta$ in Figure D.4) has on the breathing process at high loads (Heywood, 1988). The volumetric efficiency of either the actual exhaust event or the next intake event may decrease as a consequence of the modified valve timing events.

The gross cumulative and instant indicated work for a deactivated cylinder is plot in Figure 24. In this figure, it can be seen that the cylinder behaves as a spring, releasing in the expansion strokes nearly all the energy consumed over the compression strokes. Nonetheless, though relatively low, the energy balance is negative. The reason being that the friction forces consume other's active cylinder power as can be seen by the cumulative indicated work profile at the end of the cycle (360 CAD).

Another noticeable factor influencing the behavior of a deactivated cylinder is the frequency at which it is deactivated. Figure 25 shows the effect that different skipping frequencies have over the pressure traces. Cylinders with high active-deactivate frequencies show lower peak pressures and an offset of nearly 1 bar in comparison with constantly skipped cylinders. The reason could be the appearance of negative blowby. Cylinders deactivated during a prolonged period of time would eventually suck air from the crankcase to the cylinder, slowly filling the cylinder.

Eventually, a balance between cylinder and crankcase pressure is reached and blowby effect vanishes. This can be seen in the pressure profile of the constantly skipped cylinder which presents pressures up to 1 bar higher than those alternatively deactivated. The effect can also be seen in the area enclosed within the pressure trace, lower for the constantly skipped cylinder.

Notice that the noisy pressure trace in the case of the temporarily skipped cylinder is caused by the extremely low pressure (< 0.1bar) which is near the sensing limits of the piezoelectric sensor.[2]

A further aspect for investigation is the possible oil suction caused by low pressure gas trapping which could lead to an increase on the undesired pollutants in the exhaust.

Figure 23: Gross Instant and Cumulative Indicated Work During a DSF Mode Fire at (a) Actual Values and (b) Normalized Values Over Maximum

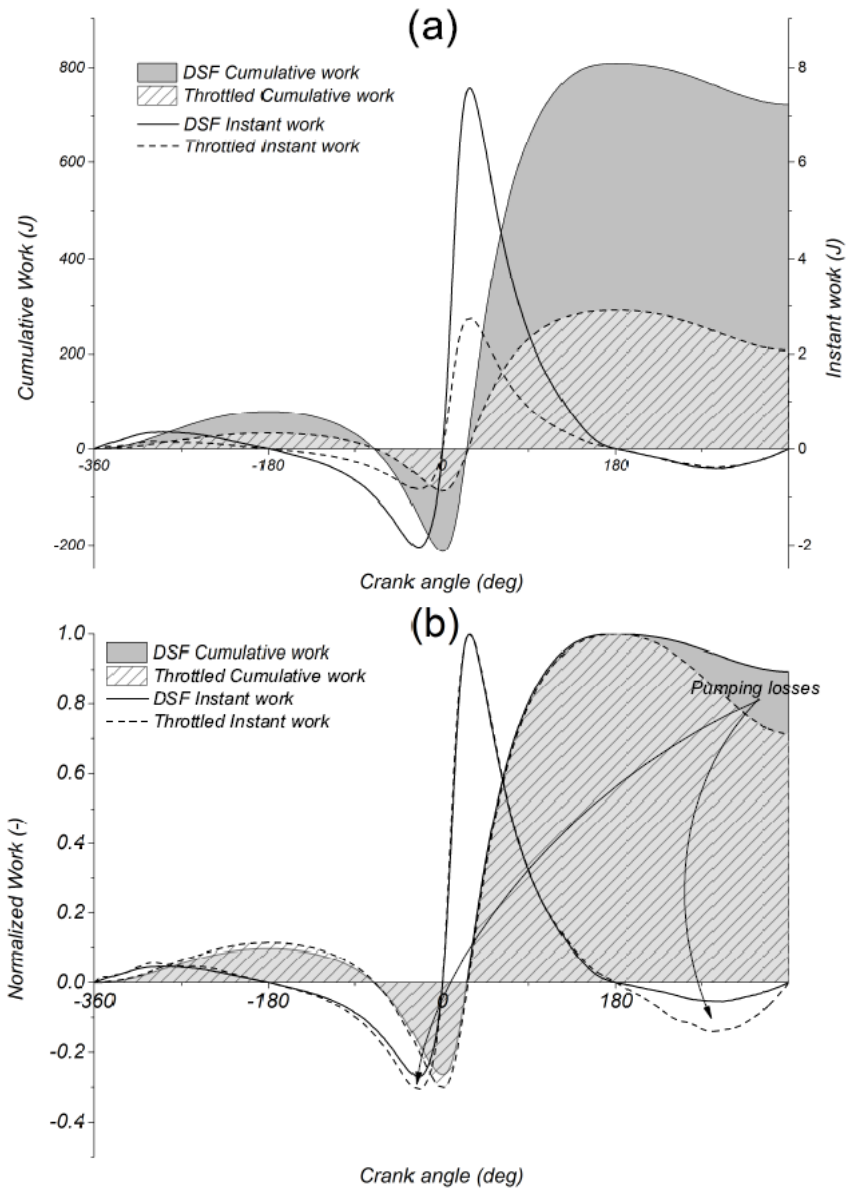

Engine speed 1500 rpm

Source: University of California, Berkeley

[2] At this pressure level, the sensor is not able to deliver a clean signal anymore and indicated values do not offer reliable information.

Figure 24: Gross Cumulative and Instant Indicated Work for a Deactivated Cylinder

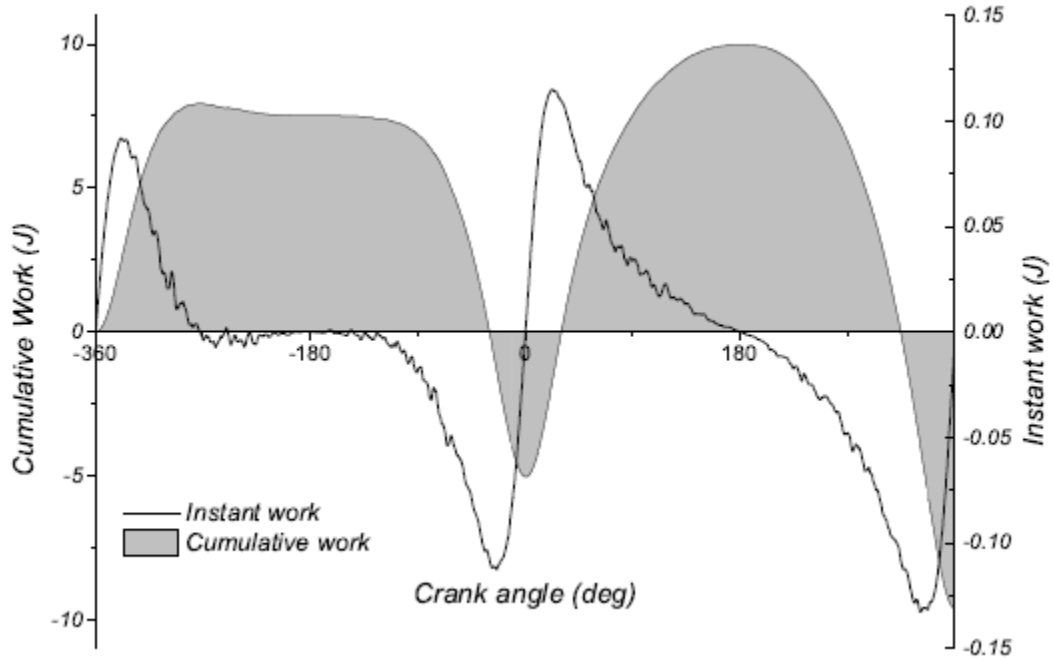

1500 rpm best mode V8, CAM 0 and 20

Source: University of California, Berkeley

Figure 25: Pressure Trace for a Momentarily Deactivated Cylinder and a Constant Deactivated Cylinder Operating at Engine Speed 1500 RPM

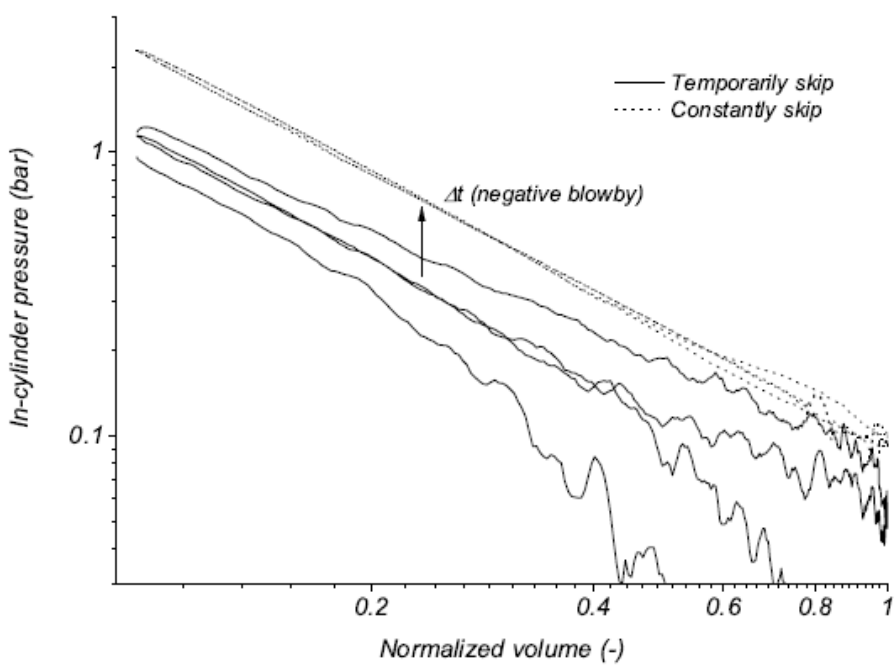

Source: University of California, Berkeley

4.3 Dynamic Skip Fire Performance

In this section, the overall performance of the engine under DSF is presented. The engine was run at different firing fraction as shown in Table 2. The data set for DSF operation is very disperse. While the standard deviation of the values acquired in every test is minimal (smaller than the points drawn), the results show strong variance from test to test. The change in the test cell conditions such as air humidity and ambient air temperature could have caused the variance in results. To that respect, a quadratic polynomial fit of BSFC has been computed and plotted in dashed style together with the tested points in Figure 26 in order to illustrate a good approximation of the overall behavior.

In this figure, a comparison on fuel consumption is made between throttled mode and DSF mode. It can be seen how at part and low loads (BMEP < 4 bar) the benefit of DSF mode is more noticeable and BSFC is up to around 100 g/kWh lower than in throttled mode; however, at high loads the DSF effects on fuel economy vanish as it would be expected.

Figure 26: BSFC Values at Different Loads During the Operation of the Engine

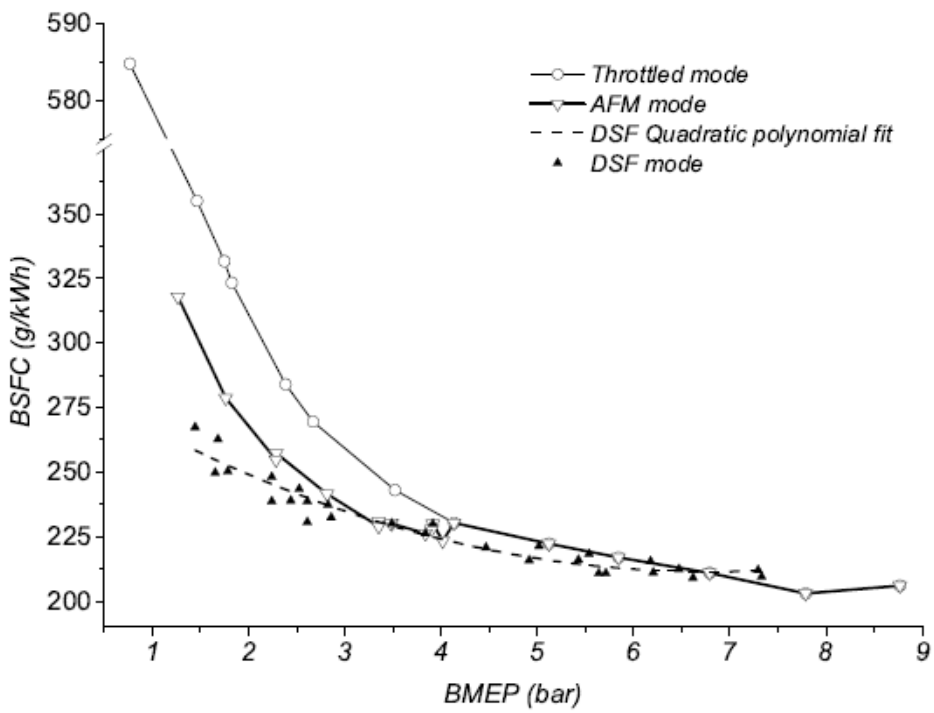

Throttled, AFM and DSF modes operating at engine speed 1500 rpm

Source: University of California, Berkeley

Figure 27: Emissions Records During DSF Mode at Different Engine Loads

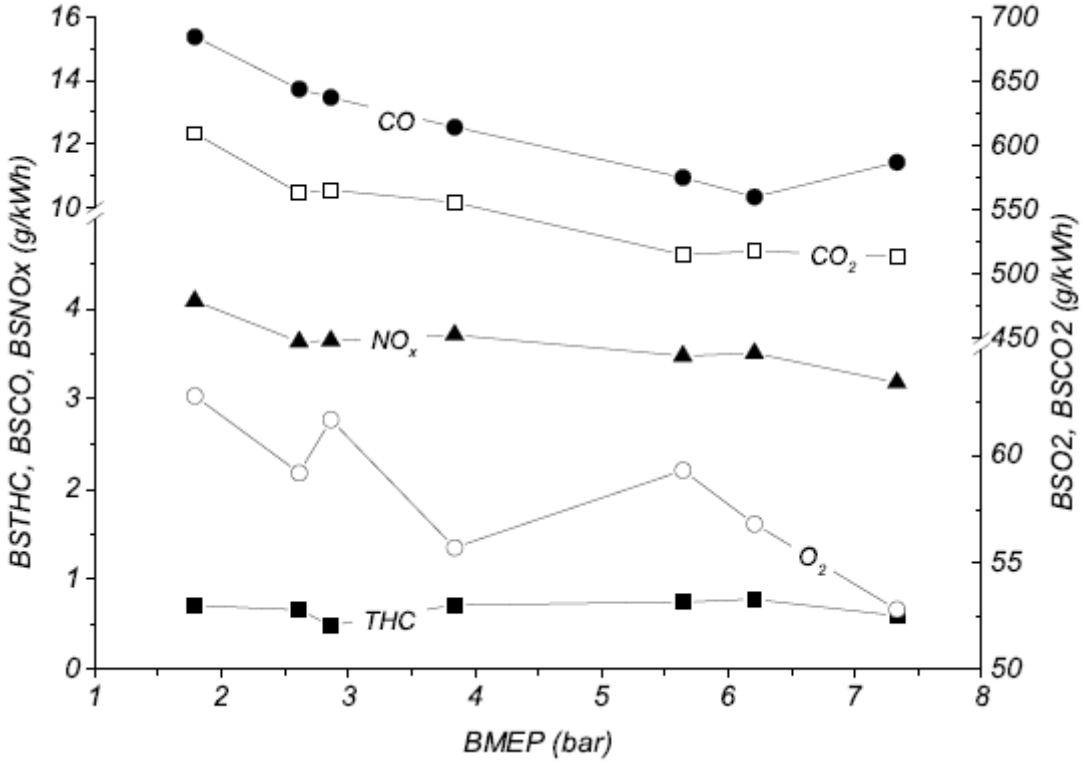

Operating at 1500 rpm

Source: University of California, Berkeley

The influence on emissions of DSF mode is illustrated in Figure 27. In this figure, the emissions of THC, CO, and NO_x are plotted respect to the left y-axis while emissions of CO_2 and values for O_2 are referenced in the right y-axis. Becaue these values are specific values regarding power, the emissions of CO_2 experiment a slight increase towards low loads when engine efficiency decreases. Unburnt hydrocarbons THC and consequently concentration of O_2 remain rather constant along the x-axis (BMEP), at levels similar to that of throttled mode at full load (Figure 21, bottom chart). As THC, NO_x also remains at same levels as full load throttled mode. The emissions of CO would be also expected to remain, as NO_x and THC, at levels of that of the throttled mode. Nevertheless, CO emissions experiment a slight increase toward low loads reaching levels seen in throttled mode at low loads (BMEP < 2). The author has not found an obvious reason for this phenomenon but a possible cause could be the parallel behavior of CO_2, which increases at low loads. If the rate of CO_2 dissociation is constant, the increment on CO_2 would directly cause an increase on CO emissions as well. In general, DSF mode seems not to have any remarkable effect on emissions apart from that of reducing the emissions of CO_2, a direct consequence of the reduction on fuel consumption (BSFC).

Moreover, we cannot directly state that the engine will overcome California emission standards with the above results only. It is important to notice that emission standard for light and medium duty system is defined in grams per mile which requires a vehicle test. Given our conditions, our experiments have been fixed based on an engine dyno for which mileage can not be derived.

Figure 28: Emissions Records During DSF Mode at Different Engine Loads for CNG and Gasoline Operating at 1500 RPM

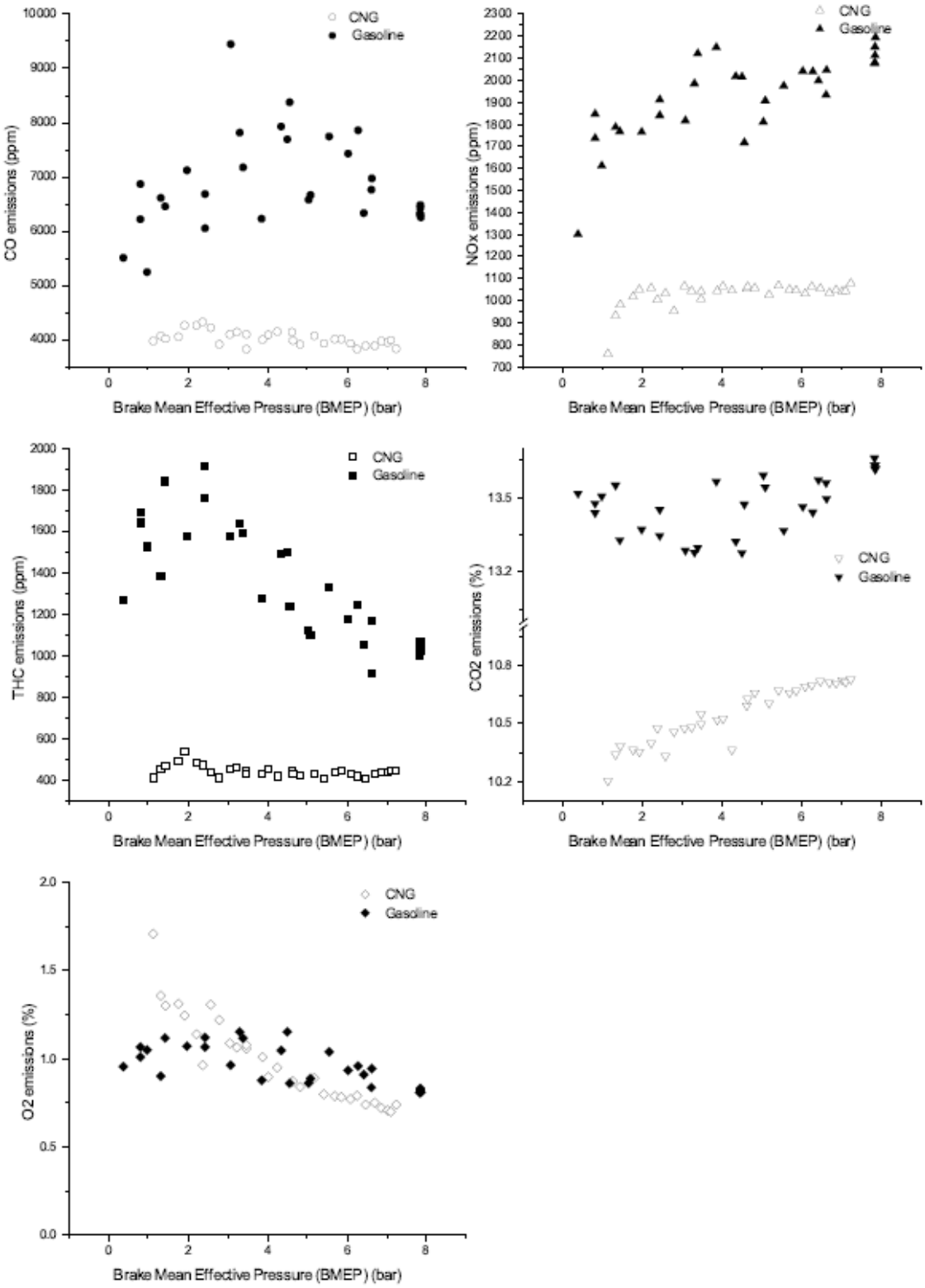

Source: University of California, Berkeley

Figure 29: Normalized Emissions at Different Engine Loads for CNG and Gasoline

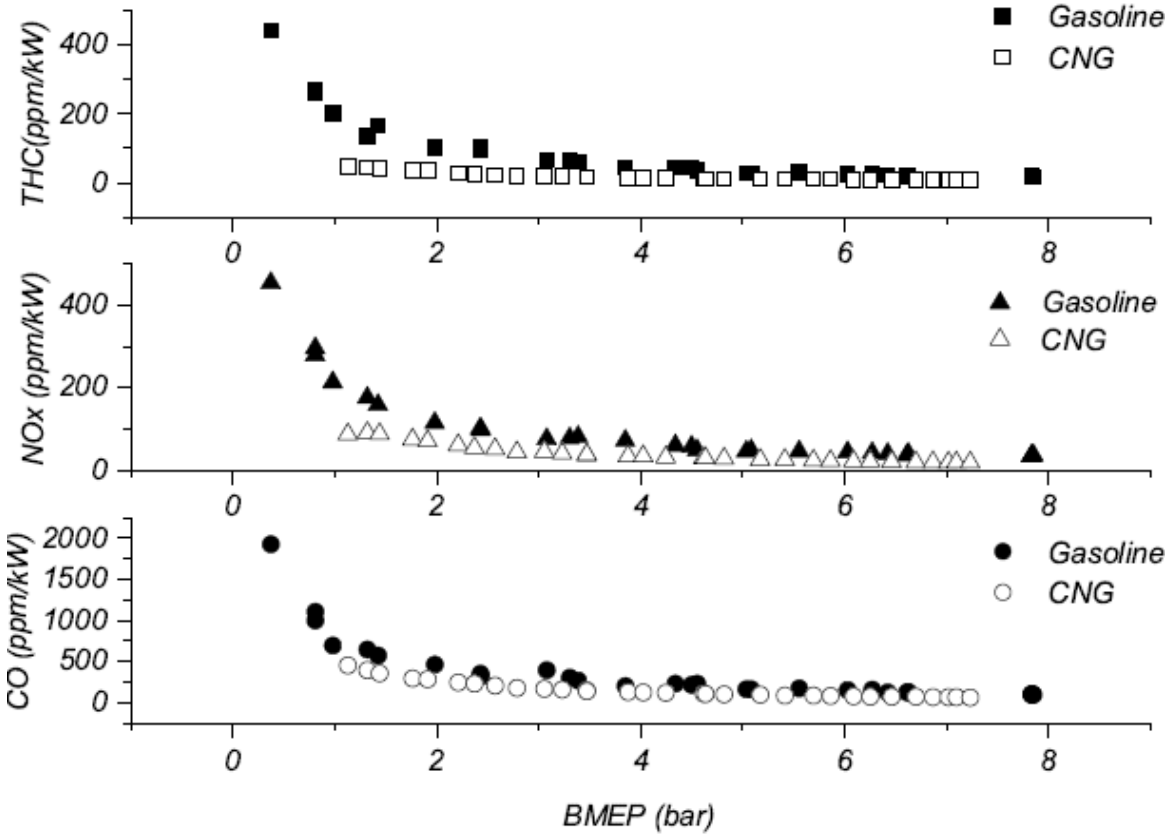

Operating at 1500 rpm

Source: University of California, Berkeley

Instead, the emissions results obtained from the CNG engine has been compared with its equivalent gasoline fueled one. The results of such test are presented in Figure 28. The results show that the CNG engine runs significantly cleaner, emitting less CO, NO_x and THC. In a per kW basis, the difference is not as noticeable as can be seen in Figure 29, but overall pollutant emissions from the CNG engine remains bellow that of the gasoline engine, which satisfies California emission standards.

An approximation of the general performance of DSF mode is given in Figure 30. Because there was wide test to test variation, values for tests ran during the same experiment session have been selected. In Figure 30, it can be seen that the combustion efficiency η_C, thermodynamic efficiency η_T and gas exchange efficiency $\eta_{G.E}$ remain at levels of that of throttled mode during full load. Mechanical efficiency, however, decreases with loads. This is caused by the deactivation of cylinders and consequently the increase on the ratio of friction losses to engine power.

4.3.1 Discrete Cylinder Management

For a better understanding of the benefits DSF brings to the concept of variable displacement engines, in this work it has also been tested discrete cylinder management strategies. Though the

results could be obvious to the reader, they can be seen in Figure 30 under the denomination AFM.

AFM stands for Active Fuel Management and is the technology already integrated on the engine prior to the addition of DSF. AFM strategy basically disables 4 cylinders at the time when power demand is sufficiently low that only 4 cylinders are necessary. As it can be seen in the plotted results, AFM only acts at loads bellow BMEP < 4 bar, nearly half of the maximum load that the engine can deliver. When AFM is activated (BMEP = 4 bar), the consumption immediately drops but increases when load decreases. This consumption trend results because throttling is still necessary for power control. AFM represents already a huge gain relative to throttled operation in terms of BSFC.

Figure 30: Comparison of Efficiency Trends for Throttled (Dashed Line) and DSF Modes (Solid Line)

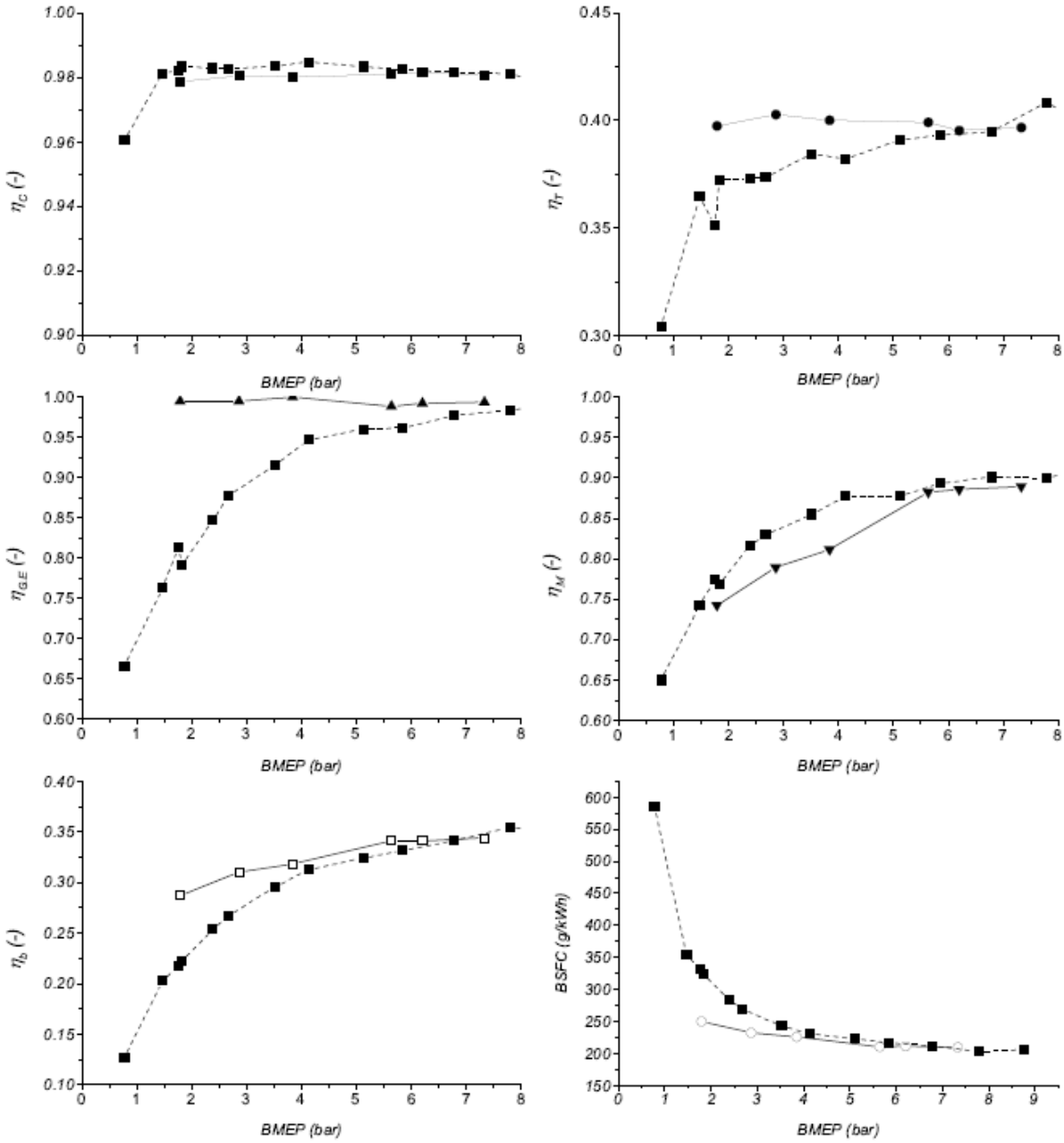

DSF data represents only test points taken during the same run of experiments. DSF engine conditions: 1500 rpm, 0 CAM, IT: MBT and WOT. Throttled data are brought from Figure 20.

Source: University of California, Berkeley

4.3.2 DSF and Gasoline

In Appendix C, the benefits derived from the use of CNG were presented. Comparison of brake efficiency η_b between gasoline and CNG show that the engine is slightly more efficient at higher loads running on CNG rather than gasoline (Figure 20). There are several reasons for this

phenomenon. Gasoline, due to its low research octane number (RON)[3], is limited by knock as previously explained, and at higher loads MBT cannot be reached. Natural gas instead does not present such limitation, and earlier ignition timings could be reached. Furthermore, in this work actual CNG was not used and instead, pure methane (grade 2.0)[4] was supplied, which, though less energy dense, presents a higher heating value (50 megajoules per kilogram [MJ/kg]) than gasoline (around 44 MJ/kg). Moreover, because the methane is not diluted in CO_2 and other inert gases, as is the case of CNG, the amount of fuel drawn into the cylinders is higher and the heat losses lower. As a result, the engine benefits with the use of methane, about 1 percent at part load (BEMP around 5) and could possibly increase at higher loads.

4.4 Conclusions

The fuel consumption gains brought by AFM and DSF are plotted in percentages relative to throttled mode. The results of this calculation are illustrated in Figure 31.

Improvement in fuel economy of up to 40 percent can be seen with DSF at low loads. DSF presents up to 14 percent more gain at lower loads than AFM. In general, it has been proved that DSF indeed improves the engine's fuel economy and does it by not only reducing pumping losses as was predicted but also heat losses as was shown in Figure 30. An approximation of the engine fuel consumption map is presented in Figure 32 to show what improvements DSF brings to the overall engine performance..

[3] Fuels with higher resistance to auto-ignition are thus desired. This propertyis defined as the research octane number of the fuel (RON)

[4] Grade 2.0: 99 percent methane content

Figure 31: Fuel Economy Approximated Gains Caused by DSF and AFM Compared to a Normal Throttled Operation

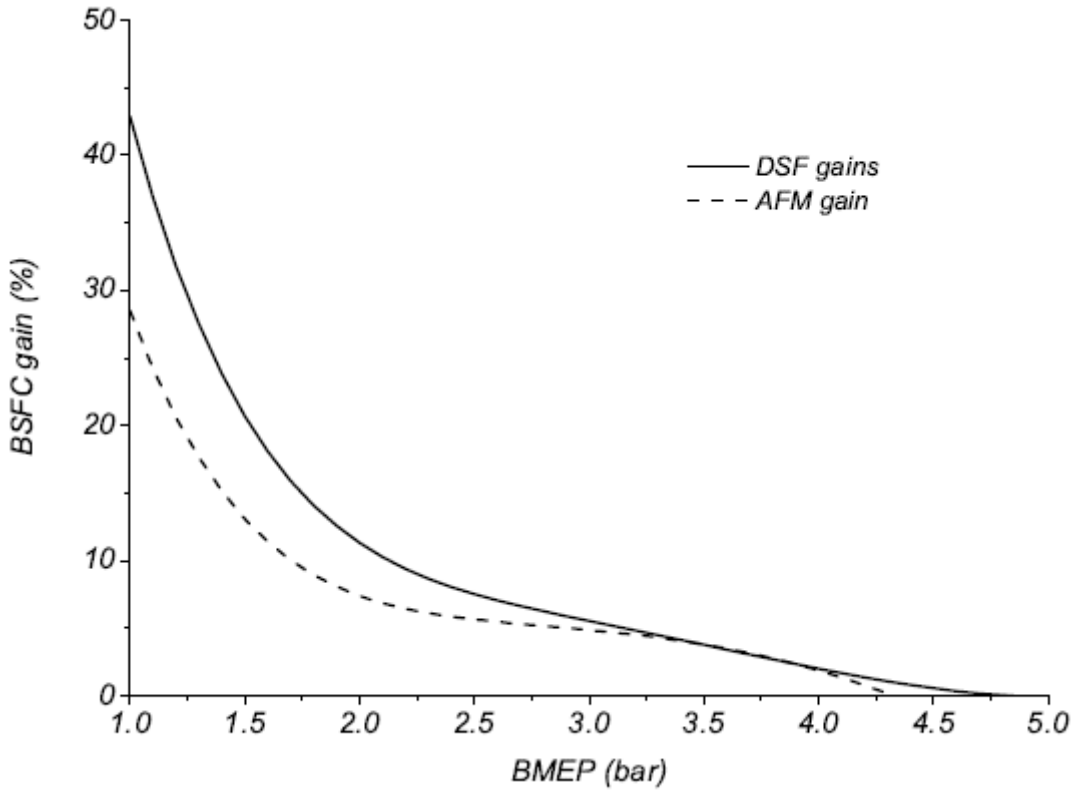

Results shown in this figure have been obtained by a polynomial fit of BSFC data for DSF, AFM, and Throttled operation with a polynomial order of 4, 4, and 6 respectively.

Source: University of California, Berkeley

Figure 32: Engine Parametric Curve for BSFC (g/kWh), BMEP, and Mean Piston Velocity (sp) under Throttled and DSF Operation

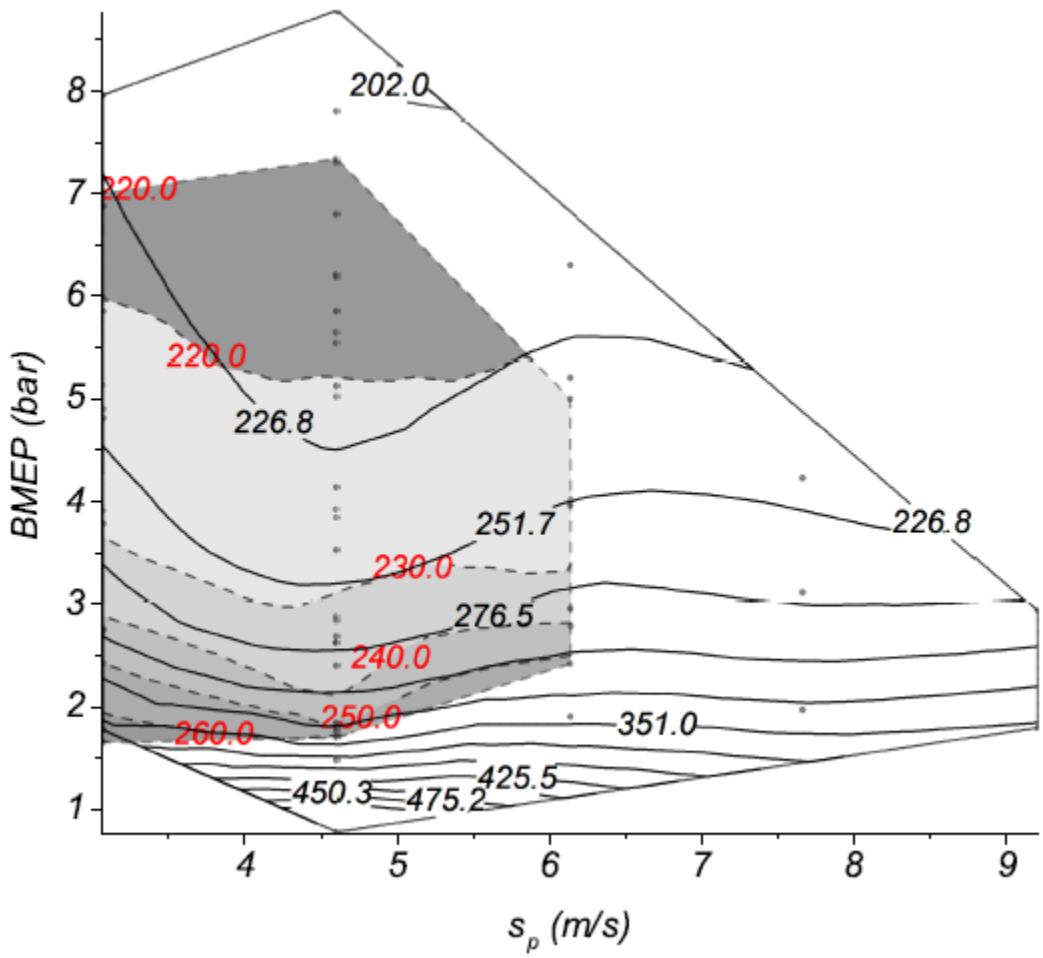

Source: University of California, Berkeley

CHAPTER 5:
Turbocharging Spark Ignited Engines

Turbocharging is often referred to as a fuel economy strategy, since it is a way of increasing engine maximum power by using wasted exhaust heat. The concept of turbocharging is similar to that of supercharging. Compressing the inlet air flow increases the inlet mass flow which is drawn into the engine, consequently allowing an increase on fuel flow. The direct consequence is an increase of the power output and fuel consumption. The peculiarity of turbocharging is the use of a turbine to power the compressor. The turbine is driven by the energy carried with the hot exhaust gases resulting from combustion, which would have been lost to the environment. The main allure of turbocharging with DSF is the ability to fit the demand for higher power outputs, such as heavy trucks, while improving substantially their fuel economy and representing a cost reduction, result of smaller and lighter engine blocks. CNG use does limit the power output of SI engines because of its lower energy density compared to gasoline; therefore, if CNG wants to be promoted to as an alternative fuel for freight transport, it has to overcome its lower power production capabilities, i.e. by turbocharging CNG engines (The California Energy Commission, n.d.)(Unnasch, Pont, & TIAX LLC, 2007).

Figure 33: Pressure Conditions Upstream of the Turbine During the Exhaust Stroke of the Cylinders

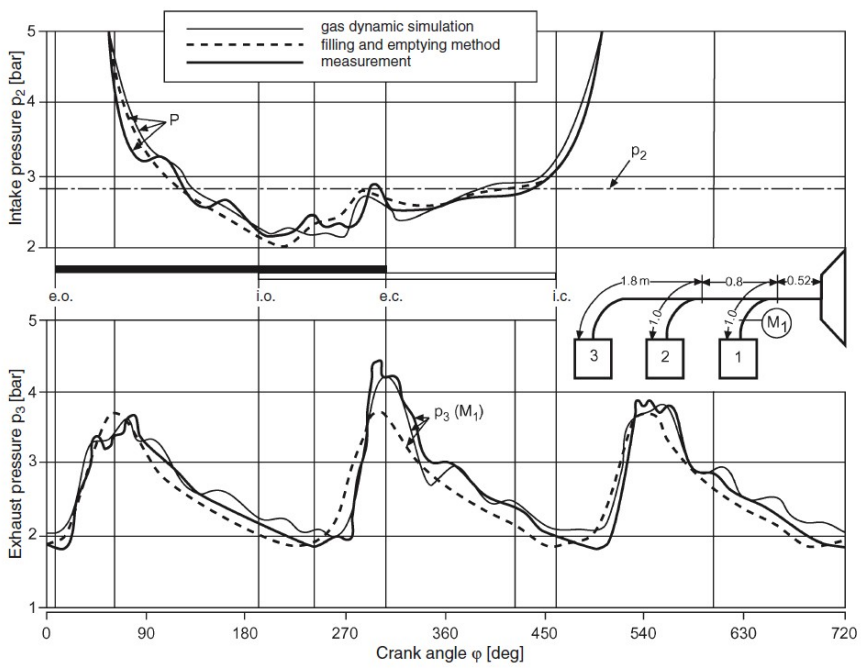

e.o = exhaust opens; i.o = inlet opens; e.c = exhaust closes; i.c = inlet closes (Hiereth & Prenninger, 2007)

Source: [159]

There is tendency to think that turbocharging inherently increases engine efficiency; however, turbocharging strongly depends on how precise the engineering and sizing of the turbo group is done for specific conditions. For automotive applications, radial turbocharges are the common choice due to its good performance at reasonably reduced sizes and wider flow ranges, due to the fact that they do not require stator blades, which are susceptible to relative inlet velocity of the fluid (Heywood, 1988)(Stone, 1999). Turbine and compressor efficiencies increase with size due to the potential increase in volume to area ratio of the machine. For radial compressors this effect is not as significant as for other mechanical systems given the .

Nevertheless, the work conditions of a turbocharge group coupled to a reciprocal displacement engine are not ideal. The reciprocal movement of cylinder pistons generates pulses, as can be seen in Figure 33, which result in unsteady exhaust flow and consequently a change in the air flow conditions that faces the turbo-group.

In conventional SI engines, power management is realized through the use of a throttle valve with support of variable valve timing, a technology widely spread nowadays. Moreover, current cylinder deactivation strategies still relay on such power management strategies but within a reduced cylinder sets. In other words, the volumetric displacement of the engine is cut by a set fraction of its maximum and load control is proportional to the active amount of cylinders. The modification may simply consist of a look up table that stablish the engine load based on the active number of cylinders. In DSF operation the number and sequence of firing cylinders is a continuously varying quantity, which means that the engine load is continuously changing and a cylinder event, either a skip or fire, influences the charge of its neighbors making harder for the power management system to regulate the engine load. The addition of a turbo group must have this into account to optimize the turbo group parameter to the continuously changing operating conditions.

Moreover, a known effect of turbocharging is the turbo-lag. When increasing power demand occurs, the energy available at the turbine is the remaining from previous lower power cycles, therefore not being able to supply the compressor with its actual power demand. To overcome the lack of energy, more fuel is injected bringing enthalpy up at the very end of the cycle.

Nonetheless, it is a slow process resulting in a lagged response. It is to be expected that the combination of turbocharging with DSF will lead to complex pulsing and variable exhaust flow phenomena, often unsteady, due to the dynamic deactivation of cylinders, therefore limiting the efficient use of the turbocharge.

When applying turbocharging to SI engines, special care has to be paid to combustion phenomena and load control since SI engines are throttle controlled and knock limited. Boosted intake translates into higher temperatures and pressures at the intake and over the rest of the process consequently. This may lead to pre-ignition of the mixture or even knocking. Avoiding so is commonly achieved by reducing the compression ratio of the engine and delaying the ignition timing, often to top dead center (TDC). As a consequence, efficiency is reduced which could lead to an overall cycle efficiency reduction (Stone, 1999)(Heywood, 1988). Furthermore, the wide flow range of SI engines and its low inertia make the increase of turbo lag even more obvious,

possibly enhanced by DSF. However, the use of CNG fuel for SI engine helps realizing more efficient turbocharged SI engines thanks to its higher research octane number, RON: 130. This allows compression ratios to remain considerably high while operating knock-free. Yet, another issue arises with the engine operation at such conditions. Misfires have been reported because the ignition system struggled to ignite fuel lean mixtures operating at relatively high pressures (H. C. Watson, Mehrani, & Brear, 2009)(Badr, Elsayed, & Karim, 1996). Summarizing, when turbocharging SI engines, efficiency increment is not guaranteed and major take cares arise. The turbocharging must be ensured to work in the proper regime, avoiding surge conditions, and be properly designed to reduce turbo lag, warrantying performance under transient operation (Stone, 1999).

Figure 34: GT Power Model of a Naturally Aspirated GM L94 6.2 L Engine

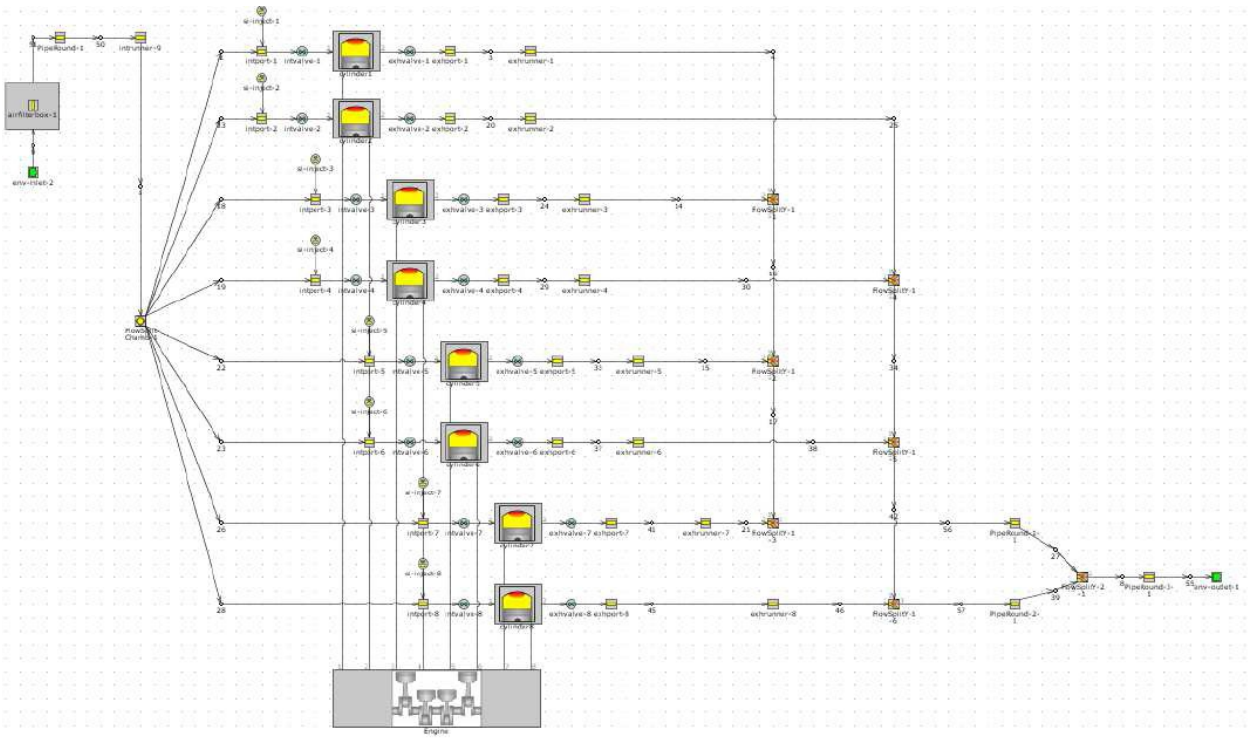

Source: University of California, Berkeley

Given the engine used in this project, experimental turbocharging of the engine could not be realized. Instead, a GT-Suite model of the engine was built. This way an estimate of the potential of turbocharging to balance the power loose due to Natural gas can be obtained. Figure 34 shows the top level diagram of a naturally aspirated engine GT Power model. This model was validated against experimental data and follows fairly the experimental data trends. An example of such validation results is shown in Figure 35. The simulation tends to under predict the fuel consumption at higher loads up to a 4 percent. Nevertheless, the results are within an acceptable margin of error for a qualitative study on the benefits of turbocharging. With the validated model, we proceeded to construct a turbocharged version of the engine by adding a radial compressor, inter-cooler and exhaust radial turbine as can be seen in Figure 36.Three different

turbocharge models were used to evaluate an ideal optimum device for the given engine conditions: Garret GT2052, Garret GT2056 and Garret GTX2860R. The compressor and turbine air flow to pressure ratio curved were introduce in the model and the results of the engine performance was evaluated. Results are depicted in Figure 37.

The turbocharge GT2052 fits best for the GM L94 engine which at normal operating conditions spins within 1,000 and 2,000 rpm. At this speed range, with the selected turbo, the engines perform best compared to the other models used. With the selected turbo, we proceed to compare the performance of the engine at different speed and loads. The integration of the turbo group increases substantially the power of the engine, to the level of the original gasoline engine as can be seen in Figure 38. A decrease in engine load influences the effectiveness of the turbo group and the power lose is substantial but the turbo still serves its purpose.

Figure 35: Comparison of Experimental and Simulation Results on BSFC as a Function of BMEP at 1250 RPM and 1500 RPM

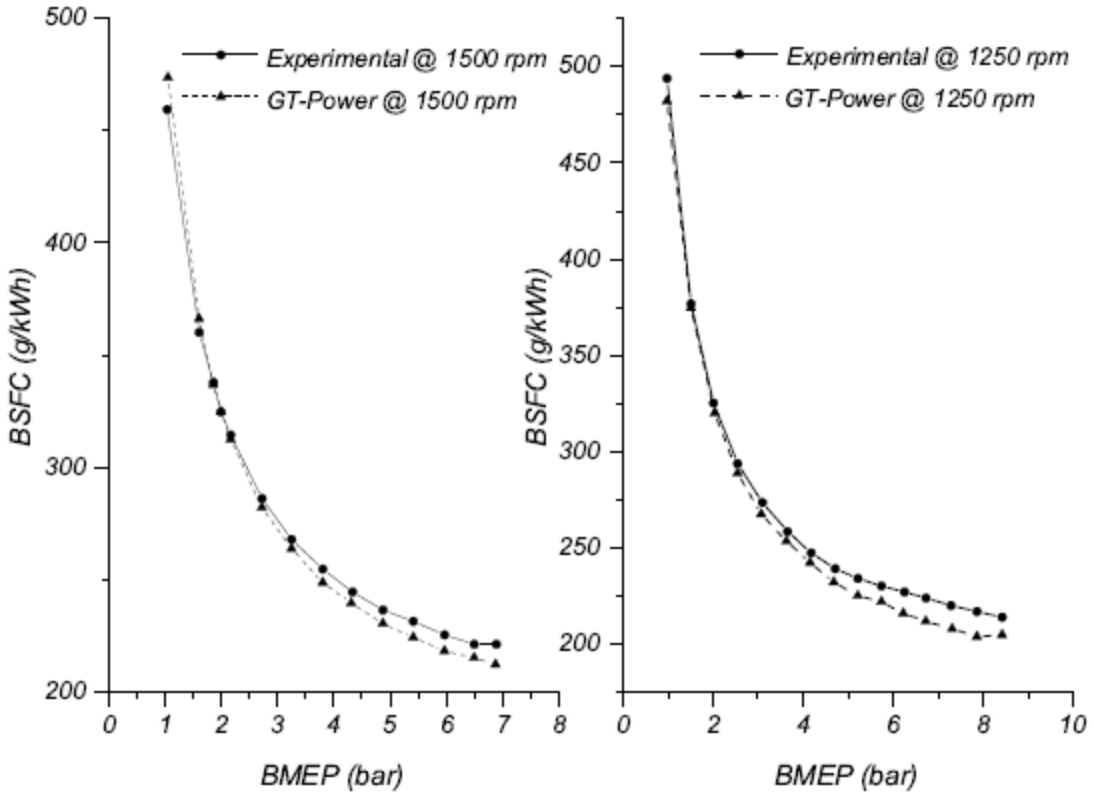

Source: University of California, Berkeley

It is necessary to evaluate the possible lose in efficiency due to the increase in back pressure at the exhaust. Efficiency versus load and speed can be seen in Figure 39. A slight loss occurred in efficiency compared to the naturally aspirated scheme but such difference remains in the range of 1 percent. In general, a more detailed analysis should be carried out to draw a definitive conclusion; however, the above case proves that an engine adaptation from gasoline to natural

gas is feasible and no major drawback is found with the addition of a turbo group. For the case of Dynamic Skip Fire a deeper study of the air-gas dynamic phenomena needs to be carried out.

With DSF, not only the turbo group may be influenced by the change in load, but by the appearance of unmatched pressure waves downstream the compressor and upstream the turbine due to deactivation of cylinders. The addition of a plenum may be recommended to reduce influence of these pressure waves on the turbo group performance, but overall, it will downgrade the efficiency of the overall engine. To this purpose, Tula Technology Inc is carrying out detailed studies on the influence of DSF on the intake gas dynamics (Chien, Younkins, & Wilcutts, 2015).

Final conclusions from the above described topics cannot be stated. An overview of the major concerns regarding turbocharging has been described and it has been shown that qualitatively, turbocharging current port injected engines is feasible if natural gas is used. Thanks to its higher octane number turbocharging can be done without incurring knock or substantial loss of efficiency while increasing the power output of the engine to a level comparable to a its current gasoline analogue.

Figure 36: GT Power Model of a Virtually Turbocharged GM L94 6.2 L Engine

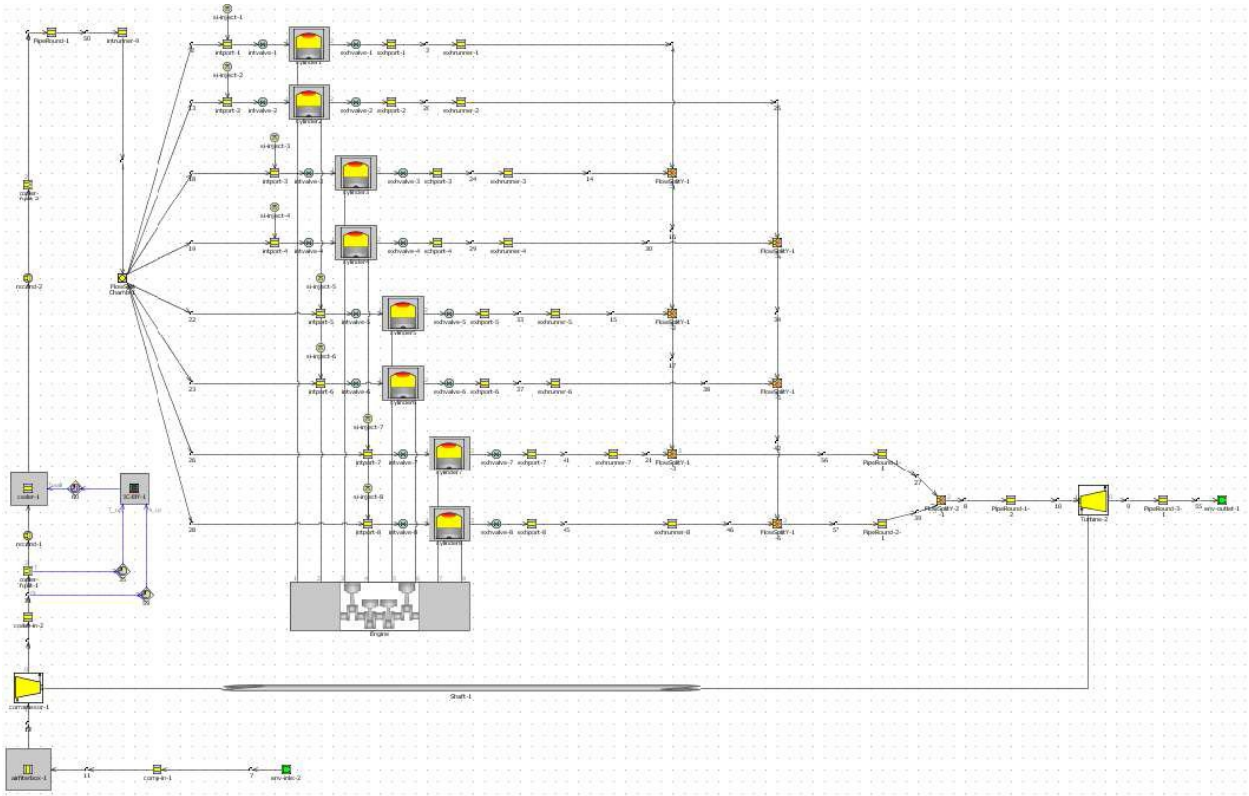

Source: University of California, Berkeley

Figure 37: Engine Brake Power Output at WOT for Different Turbocharge Models at Different Engine Speeds

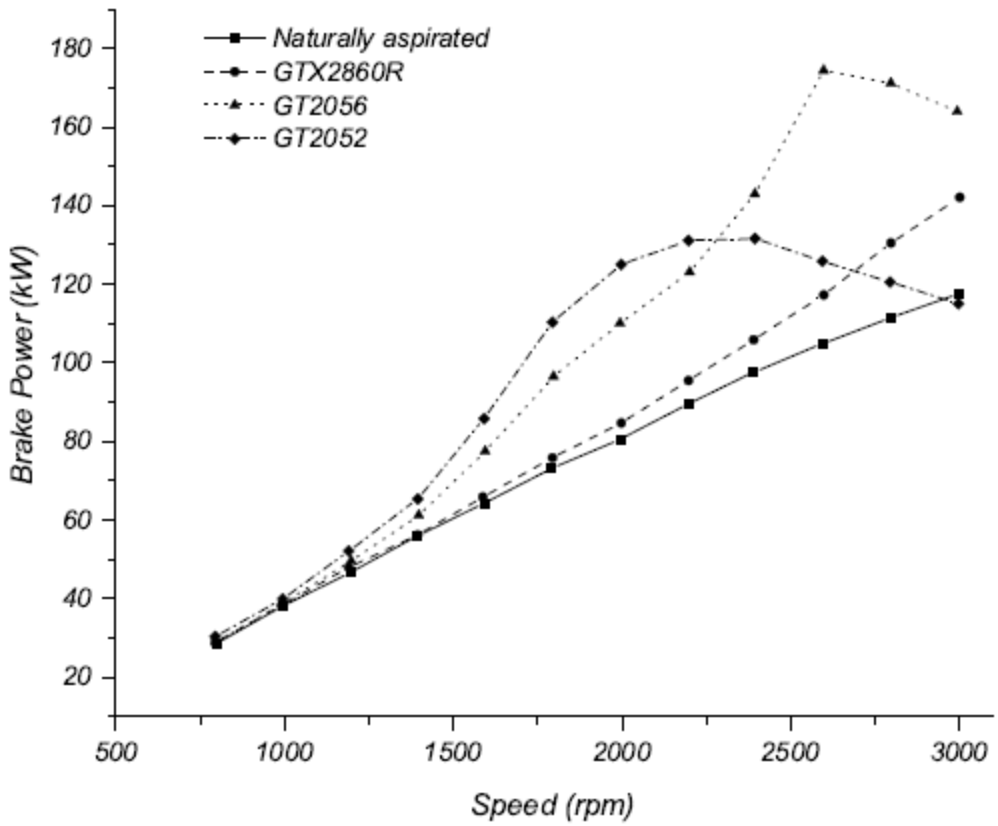

Source: University of California, Berkeley

Figure 38: Naturally Aspirated Engine Brake Power and Turbocharged Engine Brake Power vs. Speed at Different Engine Loads

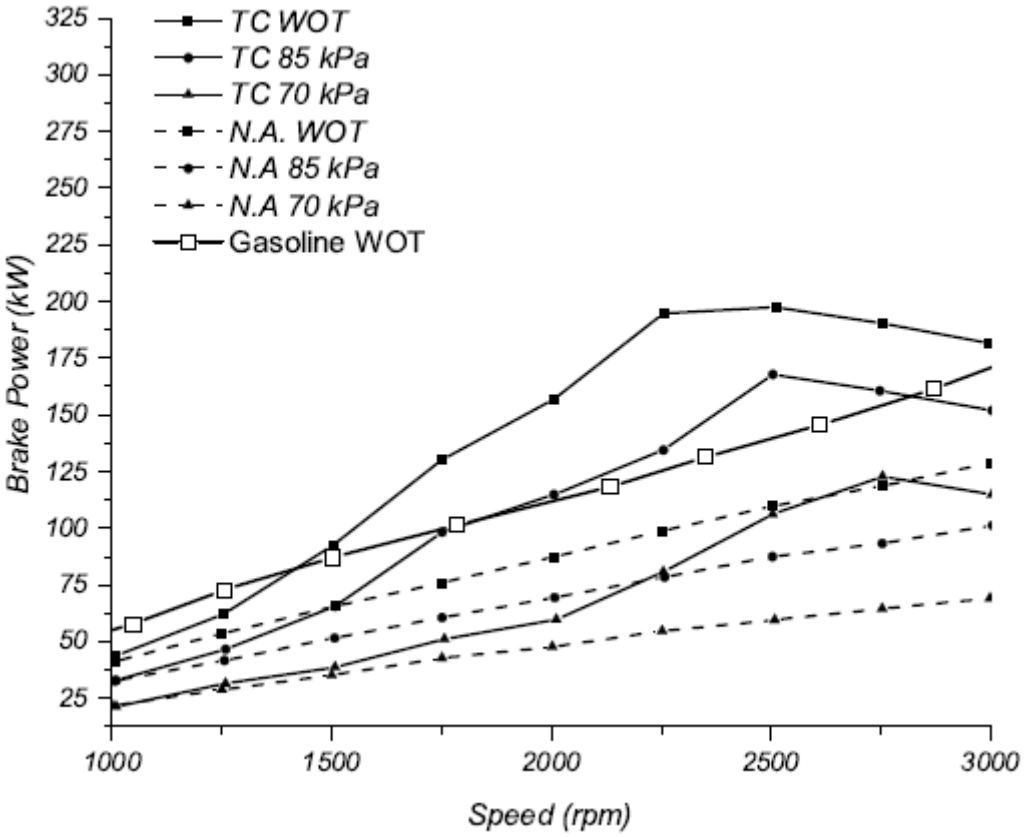

Source: University of California, Berkeley

Figure 39: Naturally Aspirated Engine Brake Efficiency and Turbocharged Engine Brake Efficiency vs. Speed at Different Engine Loads

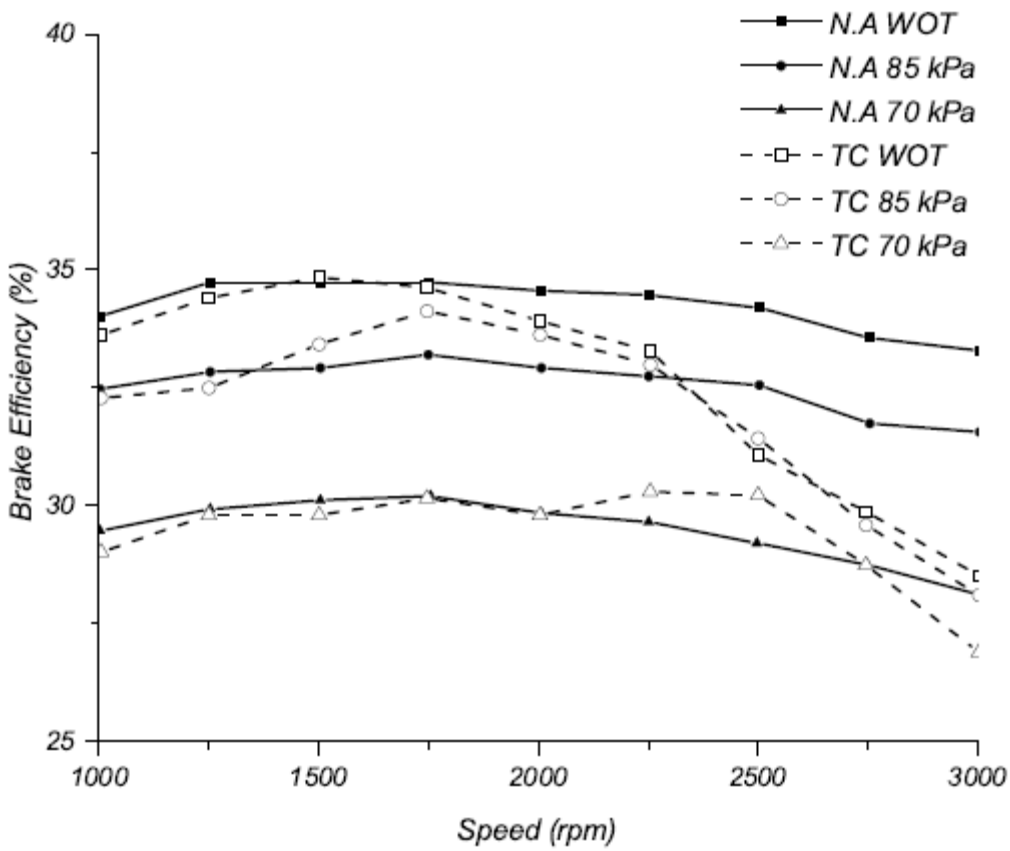

Source: University of California, Berkeley

CHAPTER 6:
Major Conclusions and Recommendations

In this report, a new concept of variable displacement engine, Dynamic Skip Fire, combined with the use of CNG has been investigated. The technology, developed by Tula Technology Inc., was deployed in a medium large displacement engine adapted to run in CNG. Normal volumetric displacement engine's strategies allow the discrete deactivation of cylinder to control the engine's load rather than throttling. Dynamic Skip Fire represents an innovative approach to variable volumetric displacement because it allows the dynamic deactivation of cylinders and allows a more accurate match of engine load and drivers demand without the need of throttling. This method eliminates the engine losses caused by the pressure drop across the throttle valve. The motivation for the use of CNG is its availability, mainly in the United States and in the State of California, where natural gas infrastructure is available and the price of CNG is low relative to that of comparable automobile fuels such as gasoline and diesel. In addition, CNG, due to its low carbon to hydrogen ratio and its higher heating value, burns cleaner and generates less CO_2 which would help the automotive industry to follow and accomplish with emissions policies and regulation.

To the purpose of testing DSF with CNG, an entire engine testing facility was built. Details on this part of the project have been given in the appendix of this report for sake of clarity. This information ensures that the test results presented in this work can be replicated in the future if needed or desired.

1. Dynamic Skip Fire technology reduces the fuel consumption of the engine by up to 40 percent compared to conventional throttled operation.
2. Dynamic Skip Fire extends the potential for fuel economy improvement that discrete cylinder management strategies already offer to SI engines. DSF has extended the benefits of cylinder management by up to 14 percent compared to a current original equipment manufacturer (OEM) cylinder management.
3. In average, DSF improves the fuel economy for up to 20 percent over a combined average CAFE fuel efficiency as shown by Tula Technology Inc.
4. The operation of DSF has not shown any effect on emissions of major pollutants such as CO, THC, and NO_x. The results show that the emissions levels remain at levels of that shown by the engine operating at wide open throttle which are, in general, lower than that of the engine running at idle.
5. DSF reduces the emissions of CO_2 emissions along with the improvement in fuel economy, owing to a more efficiency fuel conversion.
6. The use of CNG improves the brake efficiency of the SI engine compared to gasoline, by extending the knock limits. At 1,500 rpm, it has been shown that the engine operates more efficiently with CNG than with gasoline. At part load, CNG improved brake

efficiency up to one percent compared to gasoline, and this improvement seems to increase along with engine load.

7. For the same load conditions, the use of CNG reduces by 27 percent the amount of CO_2 emitted relative to that of gasoline.
8. For the same engine operating conditions, the use of CNG reduces the power and torque delivered by approximately 25 percent and 10 percent respectively compared to that of gasoline.
9. If turbocharged, the port injected CNG fueled engine can match the power density of its analog gasoline fueled engine, though a relatively small lose in efficiency is seen at the nominal operation range.
10. The influence of DSF on the turbocharge system could not be assessed but it is foreseen to have a strong influence in the performance of the turbo-group.
11. If the turbocharging system is used during full load operation, when DSF is inactive, the performance is not expected to be affected.

As a concluding remark, the results shown above can have huge impact on the transportation sector. The current light duty vehicles reaches 251 million units in the United States of which 39 percent are within the truck category (trucks, pick ups, and vans) with six or more engine cylinder which makes this category susceptible to integration of DSF. This category of vehicle performs to date an average of 20.1 miles/gallon and drive an average of 11.8 thousand miles per year. The vehicle population growth has been rather constant since 2002 at 1.3 percent per year (EPA, 2014).

With the above numbers, if Tula Technology and its DSF technology follows technology integration patterns as introduced in Chapter 1, Section 1.2 we can expect a linear penetration of DSF up to 50 percent in the sector by year 2030. Considering a 20 percent improvement on fuel economy (25 miles/gallon) the introduction of DSF will save the sector from consuming 48 billion gallons of gasoline and consequently the emission of 434 mega tonnes of CO_2 in the coming 15 years. This news is not only good for the environment, but also for the ratepayers who will save an average of four billion dollars per year over the next 15 years.

Under a predicted scenario in which the same penetration of DSF is achieved by CNG vehicles, the transportation market would reduce the oil consumption by three billion gallons per year average increasing the saving of CO_2 emissions from 434 mega tonnes to 910 mega tonnes, an average of 61 mega tonnes per year.

Focusing on the benefits for California alone, all the above represents a reduction of 5.3 billion gallons of gasoline along 15 years, a displacement of 353 million gallons of gasoline to CNG and a total reduction of CO_2 emissions of 100 mega tonnes, an average of 7 mega tonnes per year). These fuel savings represent a reduction of 20 million barrels of crude oil imported average saving per year in the following 15 years, nearly 6 percent of the foreign current oil imports in 2014.

With an average price of crude oil of 60 a barrel, this reduction in oil imports results in a reduction of State expenses of approximately 120 million dollars per year.

Moreover, the above benefits could translate into a significant rate of job creation. If the above state savings are to be reinvested on transportation technologies and easing the penetration of DSF and CNG, 120 million per year of state investment would translate into the creation of 1,300 direct jobs per year and an induced amount of jobs of 730 jobs per year, summing to a total of nearly 2,000 jobs/year. Moreover, if we consider the tax incentive induced from the use of CNG, with a reduction in fuel use tax from 30 cpg on gasoline to 0.008 cpg on CNG, the tax incentive sums up to approximately 300 million dollars per year. As per the state savings, 300 million dollars per year could have significant influence on the job creation rate. Based on the American Recovery and Reinvestment Act, the level of influence on the job market could reach 5,000 jobs per year including induced job creation.

Although the results presented along this report are quite clear and conclusive many issues were left unclear. More detailed analysis must be carried out on the air gas dynamics of turbocharging and DSF. For this purpose, a gasoline direct injection system would be preferred. This research group will continue to research on this engine platform to evaluate:

1. The conversion efficiency of TWC converters running on CNG at different conditions through modeling and validation to predict conversion of pollutants at lean conditions and low temperatures.
2. Possible fuel economy improvement at lean conditions with the use of enhanced fuel ignition systems concretely, the technology developed by transient plasma systems.
3. The capability of operating a wide range of engine loads on natural gas homogeneous charge compression ignition (HCCI)[5] through the use of DSF with assisted injection of dimethyl ether.

DSF is not only a technology that SI engines can benefit from. Other engine types can potentially benefit from this concept as well, especially dual fuel engines and HCCI engines. In general, this research has proven that Dynamic Skip Fire is indeed a technology suitable to reduce the environmental impact of the transportation sector, especially the SI engine and natural gas is a suitable fuel for the present and future of transportation.

[5] Internal combustion method where fuel and air are compressed to the point of auto-ignition.

GLOSSARY

Term	Definition
AC	Alternative Current
ACC	Active Cylinder Control
ACT	Active Cylinder Management Technology
AFR	Air to Fuel Ratio
AIT	After Ignition Timing
APP	Acceleration Pedal Position
ATDC	After Top Dead Center
AVS	Audi Valvelift System
BDC	Bottom Dead Center
BMEP	Brake Energy Mean Effective Pressure
BSCO	Brake Specific Carbon Monoxide Emissions
$BSCO_2$	Brake Specific Carbon Dioxide Emissions
BSFC	Brake Specific Fuel Consumption
BS NO_x	Brake Specific Nitrogen Oxides Emissions
BSO_2	Brake Specific Oxygen Content
BSTHC	Brake Specific Total Hydrocarbons Emissions
BTDC	Before Top Dead Center
CAD	Crank Angle Degree
CAFÉ	Corporate Average Fuel Economy
CAM	Cam Shaft Phasing
CARB	California Air Resources Board
CEC	California Energy Commission
CGA	Compressed Gas Association Standards
CLMEP	Combustion Losses Mean Effective Pressure Equivalent
CNG	Compressed Natural Gas

CO	Carbon Monoxide
CO_2	Carbon Dioxide
DC	Direct Current
DISI	Direct Injection Spark Ignited
DPG	Drive Pulse Generator
DSF	Dynamic Skip Fire
ε-NTU	Effective Number of Transfer Units Method
EC	Eddy Current
ECU	Engine Computer Unit
EGR	Exhaust Gas Recirculation
EIA	U.S. Energy Information Administration
EVC	Exhaust Valve Closing
EVO	Exhaust Valve Opening
FCU	Fire Control Unit
FMEP	Friction Losses Mean Effective Pressure Equivalent
FuelMEP	Fuel Energy Mean Effective Pressure Equivalent
GCHR	Gross Cumulative Heat Release
GDI	Gasoline Direct Injection
GDP	Gross Domestic Product
GHG	Greenhouse Gases
GM	General Motors
HCCI	Homogeneous Charge Combustion Ignition
HE	Heat Exchanger
HHV	High Heating Value
HMI	Human Machine Interface
IC	Internal Combustion Engine
IEA	International Energy Agency

$IMEP_G$	Gross Indicated Mean Effective Pressure
$IMEP_H$	Net Indicated Mean Effective Pressure
IT	Ignition Timing
IVC	Inlet Valve Closing
IVO	Inlet Valve Opening
KIT	Karlsruhe Institute of Technology
LMTD	Logarithmic Mean Temperature Difference Method
LOMA	Litter Oil Manifold Assemly
LPG	Liquefied Petroleum Gas
MABx	Micro Autobox Hardware
MAP	Manifold Air Pressure
MBT	Maximum Brake Torque
MDS	Multi-Displacement System
MEP	Mean Effective Pressure
NI	National Instruments
NMHC	Non-Methane Hydrocarbons
NO_x	Nitrogen Oxides
NTC	Negative Temperature Coefficient
NVH	Noise, Vibration, and Harshness
OEM	Original Equipment Manufacturer
PFR	Primary Fuel Reference
PID	Proportional Integral-Derivative Controller
PMEP	Pumping Losses Mean Effective Pressure Equivalent
PMEPpump	Pumping Work Mean Effective Pressure Equivalent
PMEPvalves	Valve Flow Losses Mean Effective Pressure Equivalent
QLMEP	Heat Losses Mean Effective Pressure Equivalent
QMEP	Heat after Combustion Mean Effective Pressure Equivanet

RON	Research Octane Number
SI	Spark Igntied Engine
TDC	Top Dead Center
THC	Total Hydrocarbons
TU/e	Technische Universiteit Eindhoven
TWC	Three Way Catalyst Converter
US	United States of America
UCB	University of California, Berkeley
UHC	Unburnt Hydrocarbons
V10	V Shape Ten Cylinder Engine
V12	V Shape Twelve Cylinder Engine
VCM	Variable Cylinder Management
VVT	Variable Valve Timing
WOT	Wide Open Throttle
xMEP	Pressure Representation of Energy Flow x

NOMENCLATURE

Term	Definition	Units
γ	Adiabatic Index	-
λ	Lambda	-
μ	Absolute Viscosity	Pa s
ω	Engine Rotational Speed	rad/s
ϕ	Equivalence Ratio	-
ρ	Density	kg/m^3
θ	Crank Angle	rad
a	Crankshaft Radius	mm
A/F	Air to Fuel Ratio	-
A_p	Piston Area	m^2
A_w	Cylinder Wall Area	m^2
B	Piston Bore	Mm
$BS\chi_i$	Brake Specific Emissions for Species i	g/kWh
c	Speed of Sound	m/s
C	Generic Constant	-
$C_{p,mix}$	Mass weighed mean heat capacity at constant pressure	J/kg K
C_p	Heat capacity at constant pressure	J/kg K
C_v	Heat capacity at constant volume	J/kg K
CA_{10}	Crank angle at which 10% heat has been released	CAD
CA_{50}	Crank angle at which 50% heat has been released	CAD
CA_{90}	Crank angle at which 90% heat has been released	CAD
CA_{EOC}	Crank angle at end of combustion	CAD
CA_{SOC}	Crank angle at start of combustion	CAD
F_B	Brake Force	N
F_f	Engine Firing Fraction	-

F_{rf}	Friction Force	N
h	Specific Enthalpy	kJ/kg K
k	Polytropic Index	-
l	Piston Rod Length	mm
m_{bb}	Blowby mass per cycle	kg
$m_{cyl,0}$	Initial mass in the cylinder at time of inlet valve closure	kg
$m_{e,cyl}$	Effective mass in the cylinder	Kg
$\dot{m}_{X,i}$	Mass flow of species i	g/h
$\dot{m}_f$	Fuel mass flow	g/h
M_{exh}	Mean molar mass of exhaust gases	g/mol
M_i	Molar mass of species i	g/mol
η_B	Brake efficiency	-
η_C	Combustion efficiency	-
$\eta_{G.E}$	Gas exchange efficiency	-
η_M	Mechanical efficiency	-
η_T	Thermodynamic efficiency	-
N	Engine frequency	Hz
N	Normal to Surface Force	N
n_θ	Subset of n samples at different θ	-
n_c	Number of crank revolutions per engine cycle	rev/cycle
N_p	Number of different combustion product species	-
p	Thermodynamic state variable pressure	Pa
Δp	Pressure difference	bar
P_B	Brake Power	W
Q	Heat release during combustion	J
$\dot{Q}_w$	Heat power losses through cylinder wall	W
Q_f	Chemical energy contained in the fuel	MJ/kg

Q_G	Combustion heat released	J
$Q_{LHV,i}$	Lower heating value of species i	MJ/kg
Q_{LHV}	Lower heating value	MJkg
Q_{loss}	Combustion heat loss	J
Q_w	Heat losses through the cylinder wall	J
R	Piston rod to radius ratio	-
r	Radius	m
R	Universal gas constant	J/mol K
R_{bs}	Bore to stroke ratio	-
r_c	Compression ratio	-
R_{fluid}	Specific gas constant of the fluid	J/kg K
S	Piston stroke	Mm
S	Sommerfield number	-
s_L	Laminar flame speed	m/s
s_p	Piston mean velocity	m/s
t	Time	s
T	Thermodynamic state variable temperature	K
ΔT	Temperature difference	K
T_B	Brake torque	Nm
U	Internal Energy	J
U	Overall heat transfer coefficient	W/m^2 K
V	Thermodynamic state variable volume	m^3
V_a	Actual volume displacement	m^3
V_c	Combustion chamber volume	m^3
V_d	Cylinder displacement volume	m^3
v_p	Velocity of the moving piston	m^3
V_T	Total cylinder volume	m^3

W_{aux}	Auxilar systems consumed work	J
W_B	Brake work	J
W_{pump}	Pumping work	J
W_{rf}	Rubbing friction work	J
W_T	Work in the thermodynamic cycle	J
$x_{i,dry}$	Dry concentration of species i	-
$x_{i,wet}$	Wet concentration of species i	-
Z	Compressibility factor	-

REFERENCES

Aleiferis, P. G., Serras-Pereira, J., & Richardson, D. (2013). Characterisation of flame development with ethanol, butanol, iso-octane, gasoline and methane in a direct-injection spark-ignition engine. *Fuel*, *109*, 256–278. Retrieved from http://www.sciencedirect.com/science/article/pii/S0016236113000045

Ali, M. F. M., Kodoguchi, Y., Oka, Y., & Kaida, T. (2011). Improvement of Combustion of CNG Engine using CNG Direct Injection and Gas-jet Ignition Method. SAE International. http://doi.org/10.4271/2011-01-1994

Allard, A. (1986). *Turbocharging & supercharging*. Stephens. Retrieved from http://books.google.com/books?id=Y-VQAAAAYAAJ&pgis=1

Arnold, S., Balis, C., Jeckel, D., Larcher, S., Uhl, P., & Shahed, S. M. (2005). Advances in Turbocharging Technology and its Impact on Meeting Proposed California GHG Emission Regulations. SAE International. http://doi.org/10.4271/2005-01-1852

Ayala, F. A., Gerty, M. D., & Heywood, J. B. (2006). Effects of Combustion Phasing, Relative Air-fuel Ratio, Compression Ratio, and Load on SI Engine Efficiency. SAE International. http://doi.org/10.4271/2006-01-0229

Ayala, F. A., & Heywood, J. B. (2007). Lean SI Engines: The role of combustion variability in defining lean limits. Consiglio Nazionale delle Ricerche. http://doi.org/10.4271/2007-24-0030

Bach, C., Lämmle, C., Bill, R., Soltic, P., Dyntar, D., Janner, P., … Baronick, J. D. (2004). Clean Engine Vehicle A Natural Gas Driven Euro-4/SULEV with 30% Reduced CO_2-Emissions. SAE International. http://doi.org/10.4271/2004-01-0645

Badr, O. A., Elsayed, N., & Karim, G. A. (1996). An Investigation of the Lean Operational Limits of Gas-Fueled Spark Ignition Engines. *Journal of Energy Resources Technology*, *118*(2), 159. http://doi.org/10.1115/1.2792708

Bailey, R. (1995). *True State of the Planet*. Free Press. Retrieved from http://www.amazon.com/True-State-Planet-Ronald-Bailey/dp/0028740106

Baratta, M., D'Ambrosio, S., & Misul, D. A. (2013). Performance and Emissions of a Turbocharged Spark Ignition Engine Fuelled with CNG and CNG/Hydrogen Blends. SAE International. http://doi.org/10.4271/2013-01-0866

Bell, S. R., & Gupta, M. (1997). Extension of the Lean Operating Limit for Natural Gas Fueling of a Spark Ignited Engine Using Hydrogen Blending. *Combustion Science and Technology*, *123*(1-6), 23–48. http://doi.org/10.1080/00102209708935620

Blackmore, D. R., Thomas, A., & Affleck, W. S. (1977). *Fuel economy of the gasoline engine: fuel, lubricant, and other effects* (Vol. 1977). Wiley. Retrieved from http://books.google.com/books/about/Fuel_economy_of_the_gasoline_engine.html?id=gt

BSAAAAMAAJ&pgis=1

Blarigan, A. Van, Rimkus, B., Dibble, R., & Chen, J. Y. (2011). Novel Adaptation of a Three-Way Catalyst for NO_x Reduction in Exhaust of Landfill and Biogas Engines. *7th US National Technical Meeting of the Combustion Institute*, 6.

Blasing, T. J. (2009). *Recent Greenhouse Gas Concentrations.* Oak Ridge, TN. Retrieved from http://digital.library.unt.edu/ark:/67531/metadc11963/

Boretti, A., & Scalco, J. (2011). Piston and Valve Deactivation for Improved Part Load Performances of Internal Combustion Engines. SAE International. http://doi.org/10.4271/2011-01-0368

Boye, M., Döring, M., der Staay, F. Van, Raposo, J., Jucker, C., Morales, M., & Hermens, S. (2009). Innovation Trends in the Field of Internal Combustion Engines. *SAE Int. J. Engines*. SAE International. http://doi.org/10.4271/2009-01-1944

British Petroleum (BP). (2013). *BP Statistical Review of World Energy June 2013*. London. Retrieved from http://www.bp.com/content/dam/bp/pdf/statistical-review/statistical_review_of_world_energy_2013.pdf

Brown, K. A., Harmon, J., Manning, A., Skonicki, V., Conlin, L., & Weidner, G. (2011). *IEA-Advanced Motor Fuels Annual Report 2011*. Retrieved from http://www.iea-amf.org/content/publications/annual_reports

California Air Resources Board. (n.d.). Retrieved from http://www.arb.ca.gov/homepage.htm

Callaghan, C. A. (2006). *Kinetics and Catalysis of the Water-Gas-Shift Reaction: A Microkinetic and Graph Theoretic Approach*. WORCESTER POLYTECHNIC INSTITUTE.

Catania, A. E., D'Ambrosio, S., Mittica, A., & Spessa, E. (2001). Experimental Investigation of Fuel Consumption and Exhaust Emissions of a 16V Pent-Roof Engine Fueled by Gasoline and CNG. SAE International. http://doi.org/10.4271/2001-01-1191

Cengel, Y. A. (2002). *Heat Transfer: A Practical Approach*. Mcgraw-Hill (Tx). Retrieved from http://www.amazon.com/Heat-Transfer-A-Practical-Approach/dp/0072458933

Cengel, Y. A., & Boles, M. A. (2001). *Thermodynamics: An Engineering Approach*. Mcgraw-Hill College. Retrieved from http://www.amazon.com/Thermodynamics-Engineering-Approach-Yunus-Cengel/dp/0072383321

Ceper, B. A. (2012). *Hydrogen Energy - Challenges and Perspectives*. InTech. http://doi.org/10.5772/2824

Chien, L.-C., Younkins, M., & Wilcutts, M. (2015). Modeling and Simulation of Airflow Dynamics in a Dynamic Skip Fire Engine. In *SAE Technical Paper*. SAE International. http://doi.org/10.4271/2015-01-1717

Chiodi, M., Berner, H.-J., & Bargende, M. (2006). Investigation on different Injection Strategies in a Direct-Injected Turbocharged CNG-Engine. SAE International.

http://doi.org/10.4271/2006-01-3000

Cho, H. M., & He, B.-Q. (2007). Spark ignition natural gas engines—A review. *Energy Conversion and Management*, *48*(2), 608–618. http://doi.org/10.1016/j.enconman.2006.05.023

Cleary, D., & Silvas, G. (2007). Unthrottled Engine Operation with Variable Intake Valve Lift, Duration, and Timing. SAE International. http://doi.org/10.4271/2007-01-1282

Dale, J. (1997). Application of high energy ignition systems to engines. *Progress in Energy and Combustion Science*, *23*(5-6), 379–398. http://doi.org/10.1016/S0360-1285(97)00011-7

Das, A., & Watson, H. C. (1997). Development of a natural gas spark ignition engine for optimum performance. *Proceedings of the Institution of Mechanical Engineers, Part D: Journal of Automobile Engineering*, *211*(5), 361–378. http://doi.org/10.1243/0954407971526506

Davis, R. S., & Patterson, G. J. (2006). Cylinder Pressure Data Quality Checks and Procedures to Maximize Data Accuracy. SAE International. http://doi.org/10.4271/2006-01-1346

Davis, S. C. (2014). *Transportation Energy Data Book*. Tennessee. Retrieved from http://cta.ornl.gov/data/index.shtml

Davis, S. C., Diegel, S. W., Boundy, R. G., & Moore, S. (2014). *2014 Vehicle Technologies Market Report*. Oak Ridge. Retrieved from http://cta.ornl.gov/vtmarketreport/index.shtml

DeFilippo, A., Saxena, S., Rapp, V., Dibble, R., Chen, J.-Y., Nishiyama, A., & Ikeda, Y. (2011). Extending the Lean Stability Limits of Gasoline Using a Microwave-Assisted Spark Plug. SAE International. http://doi.org/10.4271/2011-01-0663

Dillon, M. C. (2013). New collaborative study at WVU will measure methane emissions associated with natural gas vehicles and fueling stations. *Statler College of Engineering and Mineral Resources*. Morgantown, WV. Retrieved from http://wvutoday.wvu.edu/n/2013/03/04/scemr-release

Douailler, B., Ravet, F., Delpech, V., Soleri, D., Reveille, B., & Kumar, R. (2011). Direct Injection of CNG on High Compression Ratio Spark Ignition Engine: Numerical and Experimental Investigation. SAE International. http://doi.org/10.4271/2011-01-0923

Droste-Franke, B., Paal, B. P., Rehtanz, C., Sauer, D. U., Schneider, J.-P., Schreurs, M., & Ziesemer, T. (2012). *Balancing Renewable Electricity*. Springer Berlin Heidelberg. Retrieved from http://www.springer.com/us/book/9783642251566

Dugdale, P. H., Rademacher, R. J., Price, B. R., Subhedar, J. W., & Duguay, R. L. (2005). Ecotec 2.4L VVT: A Variant of GM's Global 4-Cylinder Engine. SAE International. http://doi.org/10.4271/2005-01-1941

Elkington, J. (1994). Towards the Sustainable Corporation: Win-Win-Win Business Strategies for Sustainable Development. *California Management Review. Winter94*, *36*(2), 90–100. 11p. 1 Diagram.

EPA, U. S. (2014). *Light-Duty Automotive Technology, Carbon Dioxide Emissions, and Fuel Economy Trends: 1975 Through 2014*. Retrieved from http://www.epa.gov/otaq/fetrends.htm

Evans, R. L. (2009). Extending the Lean Limit of Natural-Gas Engines. *Journal of Engineering for Gas Turbines and Power*, *131*(3), 32803. http://doi.org/10.1115/1.3043814

Falkowski, A., McElwee, M., & Bonne, M. (2004). Design and Development of the DaimlerChrysler 5.7L HEMI® Engine Multi-Displacement Cylinder Deactivation System. SAE International. http://doi.org/10.4271/2004-01-2106

Fanelli, I., Camporeale, S. M., & Fortunato, B. (2012). Efficient On-Board Pegging Calculation from Piezo-Electric Sensor Signal for Real Time In-Cylinder Pressure Offset Compensation. *SAE Int. J. Engines*. SAE International. http://doi.org/10.4271/2012-01-0901

Fujiwara, M., Kumagai, K., Segawa, M., Sato, R., & Tamura, Y. (2008). Development of a 6-Cylinder Gasoline Engine with New Variable Cylinder Management Technology. SAE International. http://doi.org/10.4271/2008-01-0610

Gardiner, W. C., & Burcat, A. (1984). *Combustion Chemistry*. London: Springer.

Gautam, A. S., Garrick, R., Lee, J. H., Deminco, C. M., Hannum, P. E., & Villasmil, L. A. (2012). A Comparison of the Emissions from Gasoline vs. Compressed Natural Gas for an Electronic Fuel Injected Two Cylinder, Four-Stroke Engine. SAE International. http://doi.org/10.4271/2012-32-0016

General Motors Corp. (2011). 100 Millionth Chevy Small Block to be built in 2011. *General Motors Powertrain*. Retrieved from http://media.gm.com/media/us/en/gm/news.detail.html/content/Pages/news/us/en/2011/Aug/0818_chevysmallblock.html

General Motors Powertrain. (2013). US Vehicle Engines & Transmissions. Retrieved from http://www.gmpowertrain.com/

Geok, H. H., Mohamad, T. I., Abdullah, S., Ali, Y., & Shamsudeen, A. (2009). Experimental Investigation of Performance and Emissions of a Sequential Port Injection Compressed Natural Gas Converted Engine. Society of Automotive Engineers of Japan.

Hawken, P., Lovins, A., & Lovins, L. H. (2008). *Natural Capitalism: Creating the Next Industrial Revolution*. Back Bay Books. Retrieved from http://www.amazon.com/Natural-Capitalism-Creating-Industrial-Revolution/dp/0316353000

Heywood, J. (1988). *Internal Combustion Engine Fundamentals*. McGraw-Hill Science/Engineering/Math. Retrieved from http://www.amazon.com/Internal-Combustion-Engine-Fundamentals-Heywood/dp/007028637X

Hiereth, H., & Prenninger, P. (2007). *Charging the Internal Combustion Engine*. Vienna: Springer Vienna. http://doi.org/10.1007/978-3-211-47113-5

Hill, P. G., & Zhang, D. (1994). The effects of swirl and tumble on combustion in spark-ignition engines. *Progress in Energy and Combustion Science*, *20*(5), 373–429. http://doi.org/10.1016/0360-1285(94)90010-8

Hong, M., Zhang, J., Li, J., & Ouyang, M. (2008). Potential Fuel Consumption Improvement Analysis for Integrated Starter Generator System Base on the New European Drive-cycle. SAE International. http://doi.org/10.4271/2008-01-1570

Huber, R., Klumpp, P., & Ulbrich, H. (2010). Dynamic Analysis of the Audi Valvelift System. *SAE Int. J. Engines*. SAE International. http://doi.org/10.4271/2010-01-1195

International Energy Agency. (2013). *CO_2 EMISSIONS FROM FUEL COMBUSTION*. Paris. Retrieved from http://www.iea.org/publications/freepublications/publication/CO_2EmissionsFromFuelCombustionHighlights2013.pdf

International Monetary Funds. (2013). World Economic Outlook Database October 2013. Retrieved from http://www.imf.org/external/pubs/ft/weo/2013/02/weodata/index.aspx

Ishii, M., & Engineers, S. of A. (1994). *Experimental Studies on a Natural Gas Vehicle*. SAE International. Retrieved from http://books.google.com/books/about/Experimental_Studies_on_a_Natural_Gas_Ve.html?id=m6aXGwAACAAJ&pgis=1

Isidore, C. (2013). Impact of war on stocks and oil. *Money CNN*. New York. Retrieved from http://money.cnn.com/2013/09/03/investing/war-syria-stocks-oil/

Jahirul, M. I., Masjuki, H. H., Saidur, R., Kalam, M. A., Jayed, M. H., & Wazed, M. A. (2010). Comparative engine performance and emission analysis of CNG and gasoline in a retrofitted car engine. *Applied Thermal Engineering*, *30*(14-15), 2219–2226. http://doi.org/10.1016/j.applthermaleng.2010.05.037

Jerzembeck, S., Peters, N., Pepiot-Desjardins, P., & Pitsch, H. (2009). Laminar burning velocities at high pressure for primary reference fuels and gasoline: Experimental and numerical investigation. *Combustion and Flame*, *156*(2), 292–301. Retrieved from http://www.sciencedirect.com/science/article/pii/S0010218008003489

Johansson, B. (2011). *HCCI according to Lund*. Lund.

Joseph, L. K., Ju, Y., Tsuruoka, R., & Ikeda, Y. (2012). A Studies of Plasma-Assisted Ignition in a Small Internal Combustion Engine (AIAA). *AIAA*. Tenesse: ARC. http://doi.org/10.2514/6.2012-1133

Kubsh, J. (2006). *Advanced three-way catalysts*. Warrendale Pa.: Society of Automotive Engineers. Retrieved from http://www.worldcat.org/title/advanced-three-way-catalysts/oclc/66905973

Kundu, P. K., Cohen, I. M., & of Technology, D. R. D. P. D. A. C. I. (2011). *Fluid Mechanics, Fifth Edition*. Academic Press. Retrieved from http://www.amazon.com/Fluid-Mechanics-

Fifth-Edition-Pijush/dp/0123821002

Kutlar, O. A., Arslan, H., & Calik, A. T. (2005). Methods to improve efficiency of four stroke, spark ignition engines at part load. *Energy Conversion and Management*, *46*(20), 3202–3220. http://doi.org/10.1016/j.enconman.2005.03.008

Lampert, J., Kazi, M., & Farrauto, R. (1997). Palladium catalyst performance for methane emissions abatement from lean burn natural gas vehicles. *Applied Catalysis B: Environmental*, *14*(3-4), 211–223. http://doi.org/10.1016/S0926-3373(97)00024-6

Law, C., Makino, A., & Lu, T. (2006). On the off-stoichiometric peaking of adiabatic flame temperature. *Combustion and Flame*, *145*(4), 808–819. http://doi.org/10.1016/j.combustflame.2006.01.009

Lee, K., Kwon, M., Sunwoo, M., & Yoon, M. (2007). An In-Cylinder Pressure Referencing Method Based on a Variable Polytropic Coefficient. SAE International. http://doi.org/10.4271/2007-01-3535

Li, H., Karim, G. A., & Sohrabi, A. (2009). The Lean Mixture Operational Limits of a Spark Ignition Engine When Operated on Fuel Mixtures. *Journal of Engineering for Gas Turbines and Power*, *131*(1), 12801. http://doi.org/10.1115/1.2978998

MA, F. (2008). Study on the extension of lean operation limit through hydrogen enrichment in a natural gas spark-ignition engine. *International Journal of Hydrogen Energy*, *33*(4), 1416–1424. http://doi.org/10.1016/j.ijhydene.2007.12.040

MacKay, D. J. C. (2009). *Sustainable Energy - Without the Hot Air*. UIT Cambridge Ltd. Retrieved from http://www.amazon.com/Sustainable-Energy-Without-Hot-Air/dp/0954452933

Maji, S., Ranjan, R., & Sharma, P. B. (2000). Comparison of Emissions and Fuel Consumption From CNG and Gasoline Fueled Vehicles - Effect of Ignition Timing. SAE International. http://doi.org/10.4271/2000-01-1432

Malagi, R. R. (2012). Estimation of Blowby in Multi-cylinder Diesel Engine Using Finite Element Approach. SAE International. http://doi.org/10.4271/2012-01-0559

Manivannan, A., Porai, P. T., Chandrasekaran, S., & Ramprabhu, R. (2003). Lean Burn Natural Gas Spark Ignition Engine - An Overview. SAE International. http://doi.org/10.4271/2003-01-0638

Merker, G., Schwarz, C., Stiesch, G., & Otto, F. (2006). *Simulating Combustion*. Berlin/Heidelberg: Springer-Verlag. http://doi.org/10.1007/3-540-30626-9

Mondt, J. R. (2000). *Cleaner Cars: The History and Technology of Emission Control Since the 1960s*. Society of Automotive Engineers Inc. Retrieved from http://www.amazon.com/Cleaner-Cars-History-Technology-Emission/dp/0768002222

Morse® MORFLEX®. (n.d.). Morse MORFLEX Couplings. Retrieved from http://www.emersonindustrial.com/en-US/powertransmissionsolutions/brands/kop-

flex/Pages/kop-flex.aspx

Nakamura, N., Baika, T., & Shibata, Y. (1985). Multipoint Spark Ignition for Lean Combustion. SAE International. http://doi.org/10.4271/852092

Nam, E. K., Jensen, T. E., & Wallington, T. J. (2004). Methane emissions from vehicles. *Environmental Science & Technology*, *38*(7), 2005–2010. Retrieved from http://www.ncbi.nlm.nih.gov/pubmed/15112800

Nanthagopal, K., Subbarao, R., Elango, T., Baskar, P., & Annamalai, K. (2011). Hydrogen enriched compressed natural gas (HCNG): A futuristic fuel for internal combustion engines. *Thermal Science*, *15*(4), 1145–1154. http://doi.org/10.2298/TSCI100730044N

National Institute of Standard and Technology. (n.d.). No Title. Retrieved from http://www.nist.gov/

Nestorides, E. J. (1958). *A Handbook on Torsional Vibration*. Cambridge University Press. Retrieved from http://books.google.com/books?id=LmEBdI7KJfcC&pgis=1

Owen, K., & Coley, T. (1995). *Automotive Fuels Reference Book*. Society of Automotive Engineers, Incorporated. Retrieved from http://books.google.com/books?id=HhmSBV6vDWkC&pgis=1

Parvate-Patil, G. B., Hong, H., & Gordon, B. (2003). An Assessment of Intake and Exhaust Philosophies for Variable Valve Timing. SAE International. http://doi.org/10.4271/2003-32-0078

Pisarski, A. E., & de Terra, N. (1975). American and European transportation responses to the 1973–74 oil embargo. *Transportation*, *4*(3), 291–312. http://doi.org/10.1007/BF00153580

Porritt, J. (2007). *Capitalism as if the World Matters*. Routledge. Retrieved from http://www.amazon.com/Capitalism-as-if-World-Matters/dp/1844071936

Quader, A., & General Motors Corp. (1976). What Limits Lean Operation in Spark Ignition Engines-Flame Initiation or Propagation? *SAE International*. SAE International. http://doi.org/10.4271/760760

Radulescu, A., JR, J. M., & Brownell, S. (2013). Development of a Switching Roller Finger Follower for Cylinder Deactivation in Gasoline Engine Applications. SAE International. http://doi.org/10.4271/2013-01-0589

Ramsey, M., & Rogers, C. (2013). Pickups Steer U.S. Auto Sales. *The Wall Street Journal*. Retrieved from http://online.wsj.com/article/SB10001424127887324766604578456570695755336.html#project%3DWSJ_US_Autosales%26articleTabs%3Darticle

Rapp, V. H., DeFilippo, A., Saxena, S., Chen, J.-Y., Dibble, R. W., Nishiyama, A., … Ikeda, Y. (2012). Extending Lean Operating Limit and Reducing Emissions of Methane Spark-Ignited Engines Using a Microwave-Assisted Spark Plug. *Journal of Combustion*, *2012*(x),

1–8. http://doi.org/10.1155/2012/927081

Sandhu, S. S., Babu, M. K. G., & Das, L. M. (2011). Investigations of emission characteristics and thermal efficiency in a spark-ignition engine fuelled with natural gas-hydrogen blends. *International Journal of Low-Carbon Technologies*, *8*(1), 7–13. http://doi.org/10.1093/ijlct/ctr038

Sileghem, L., Alekseev, V. A., Vancoillie, J., Van Geem, K. M., Nilsson, E. J. K., Verhelst, S., & Konnov, A. A. (2013). Laminar burning velocity of gasoline and the gasoline surrogate components iso-octane, n-heptane and toluene. *Fuel*, *112*, 355–365. Retrieved from http://www.sciencedirect.com/science/article/pii/S0016236113004614

Smutzer, C. (2006). *Application of Hydrogen Assisted Lean Operation to Natural Gas-Fueled Reciprocating Engines (HALO)*.

Sobukawa, H. (2002). Development of Ceria-Zirconia Solid Solutions and Future Trends. *R&D Review of Toyota CRDL*, *37*(4), 1–5. Retrieved from http://www.tytlabs.com/english/review/rev374epdf/e374_001sobukawa.pdf

Stabinsky, M., Albertson, W., Tuttle, J., Kehr, D., Westbrook, J., Karbstein, H., & Kuhl, M. (2007). Active Fuel Management™ Technology: Hardware Development on a 2007 GM 3.9L V-6 OHV SI Engine. SAE International. http://doi.org/10.4271/2007-01-1292

Stone, R. (1999). *Introduction to Internal Combustion Engines*. Society of Automotive Engineers Inc. Retrieved from http://www.amazon.com/Introduction-Internal-Combustion-Engines-Richard/dp/0768004950

Takigawa, A., Matsunami, A., & Arai, N. (2005). Methane emission from automobile equipped with three-way catalytic converter while driving. *Energy*, *30*(2-4), 461–473. http://doi.org/10.1016/j.energy.2004.04.016

The California ENERGY COMMISSION. (n.d.). Gasoline Gallon Equivalent of Alternative Fuels. Retrieved from http://www.energyalmanac.ca.gov/transportation/gge.html

The Shoutheast Missourian. (1980). Cadillac's better idea: V 8-6-4 engine. *The Southeast Missourian*. Cape Girardeau, Mo. Retrieved from http://news.google.com/newspapers?id=e1ofAAAAIBAJ&sjid=1dgEAAAAIBAJ&pg=2262,3959179

Thiem, S. (2013). *Experimental investigation of continuously variable displacement for natural gas spark-ignition engines*.

Thomas, J. F., & Staunton, R. H. (1999). What Fuel Economy Improvement Technologies Could Aid the Competitiveness of Light-Duty Natural Gas Vehicles? SAE International. http://doi.org/10.4271/1999-01-1511

Tripathi, A. S., & Silvestri, C. J. (2012). Internal combustion engine control for improved fuel efficiency. Retrieved from http://www.google.com/patents/US8336521#backward-citations

Tunestål, P., Christensen, M., Einewall, P., Andersson, T., Johansson, B., & Jönsson, O. (2002). Hydrogen Addition For Improved Lean Burn Capability of Slow and Fast Burning Natural Gas Combustion Chambers. SAE International. http://doi.org/10.4271/2002-01-2686

U.S. Department of Transportation. (2014). *State Transportation Statistics 2014*. Washington. Retrieved from http://www.rita.dot.gov/bts/sites/rita.dot.gov.bts/files/STS_2014_revised.pdf

U.S. Energy Information Agency. (2013). International Energy Outlook 2013. *Outlook 2013*. http://doi.org/EIA-0484(2013)

U.S. Environmental Protection Agency. (2015). *Inventory of U.S. Greenhouse Gas Emissions and Sinks: 1990 - 2013*. Retrieved from http://www.epa.gov/climatechange/Downloads/ghgemissions/US-GHG-Inventory-2015-Main-Text.pdf

Unger, D.-I. H., Schwarz, D.-I. C., Schneider, D. J., & Koch, D.-I. K.-F. (2008). The Valvetronic. *MTZ Worldwide*, *69*(7-8), 30–37. http://doi.org/10.1007/BF03227902

Unnasch, S., Pont, J., & TIAX LLC. (2007). *Full Fuel Cycle Assessment Well to Tank Energy Inputs, Emissions, and Water Impacts, TIAX Consultant Report*. *CEC-600-2007-002-D*. Retrieved from http://www.energy.ca.gov/2007publications/CEC-600-2007-002/CEC-600-2007-002-D.PDF

US Department of Transportation. (2007). Table 2.1. - 2.11. Truck Transportation, Messenger Services & Warehousing. US Department of Transportation. Retrieved from http://www.census.gov/svsd/www/services/sas/sas_data/sas48.htm

US Department of Transportation. (2012). Office of Highway Policy information. Retrieved from http://www.google.com/publicdata/explore?ds=gb66jodhlsaab_&ctype=l&strail=false&bcs=d&nselm=h&met_y=Trucks&scale_y=lin&ind_y=false&rdim=state&ifdim=state&tdim=true&ind=false

US, G. M. (2013). 2013 GM Powertrain Product Portfolio. GM Powertrain. Retrieved from http://gmpowertrain.com/VehicleEngines/PowertrainProducts.aspx

Wan, Y., & Du, A. (2013). Reducing Part Load Pumping Loss and Improving Thermal Efficiency through High Compression Ratio Over-Expanded Cycle. SAE International. http://doi.org/10.4271/2013-01-1744

Wang, J., Chen, H., Liu, B., & Huang, Z. (2008). Study of cycle-by-cycle variations of a spark ignition engine fueled with natural gas–hydrogen blends. *International Journal of Hydrogen Energy*, *33*(18), 4876–4883. http://doi.org/10.1016/j.ijhydene.2008.06.062

Wang, X., & Stone, C. R. (2008). A study of combustion, instantaneous heat transfer, and emissions in a spark ignition engine during warm-up. *Proceedings of the Institution of Mechanical Engineers, Part D: Journal of Automobile Engineering*, *222*(4), 607–618.

http://doi.org/10.1243/09544070JAUTO610

Warnatz, J., Maas, U., & Dibble, R. W. (2006a). *Combustion: Physical and Chemical Fundamentals, Modeling and Simulation, Experiments, Pollutant Formation*. Springer. Retrieved from http://books.google.com/books/about/Combustion.html?id=2bgQBg-nOpoC&pgis=1

Warnatz, J., Maas, U., & Dibble, R. W. (2006b). *Combustion: Physical and chemical fundamentals, modeling and simulation, experiments, pollutant formation*. *Combustion: Physical and Chemical Fundamentals, Modeling and Simulation, Experiments, Pollutant Formation*. http://doi.org/10.1007/978-3-540-45363-5

Watson, H. C., & Mehrani, P. (2010). The Performance and Emissions of the Turbocharged Always Lean Burn Spark Ignition (TC-ALSI) Engine. SAE International. http://doi.org/10.4271/2010-01-1235

Watson, H. C., Mehrani, P., & Brear, M. J. (2009). The Always Lean Burn Spark Ignition (ALSI) Engine – Its Performance and Emissions. SAE International. http://doi.org/10.4271/2009-01-0932

Watson, N. A., & Janota, M. S. (1982). *Turbocharging: The Internal Combustion Engine*. Macmillan Publishers Limited. Retrieved from http://books.google.com/books/about/Turbocharging_the_internal_combustion_en.html?id=JsugQgAACAAJ&pgis=1

Wiesenthal, T., Leduc, G., Christidis, P., Schade, B., Pelkmans, L., Govaerts, L., & Georgopoulos, P. (2009). Biofuel support policies in Europe: Lessons learnt for the long way ahead. *Renewable and Sustainable Energy Reviews*, *13*(4), 789–800. http://doi.org/10.1016/j.rser.2008.01.011

Wilcutts, M., Switkes, J., Shost, M., & Tripathi, A. (2013). Design and Benefits of Dynamic Skip Fire Strategies for Cylinder Deactivated Engines. *SAE Int. J. Engines*. SAE International. http://doi.org/10.4271/2013-01-0359

Yang, J., & Anderson, R. W. (1998). Fuel Injection Strategies to Increase Full-Load Torque Output of a Direct-Injection SI Engine. SAE International. http://doi.org/10.4271/980495

Yaws, C. (2001). *Matheson Gas Data Book*. McGraw-Hill Professional. Retrieved from http://www.amazon.com/Matheson-Data-Book-Carl-Yaws/dp/0071358544

Zhang, H. G., Wang, D. J., Sun, X. N., Wang, X., Lei, Y., Bai, X. L., & Yao, B. F. (2012). Effects of Engine Operating Parameters on Lean Combustion Limit of Hydrogen Enhanced Natural Gas Engine. *Advanced Materials Research*, *383-390*, 6116–6121. Retrieved from http://www.scientific.net/AMR.383-390.6116

APPENDIX A:
The Engine Test Facility

For the purpose of testing DSF technology, a new test cell had to be designed and constructed. This work starter in July 2013, however it was not until October 2013 when the different purchase orders were sent. Consequently, the design and construction of this cell, though not considered scientific work, is major part of the work realized along this master report. The test cell became operative November 27th, and we acquired the first set of data the first week of December, 2013. A total period of five months was needed to accomplish the construction of the test cell. In this chapter, the different systems of the cell will be explained in enough detail to understand the logic of the result and ensure that the experiment can be replicated in the future.

A.1 General Overview

The engine test cell is illustrated in Figure A.1. In this scheme, the test cell is divided within six different systems based on the the most relevant processes taking place in the cell. In addition, two more systems are added, the control system and the data acquisition system (DAQ). These two systems are not necessary for the engine operation, but are essential to accomplish scientific work. The control system is in charge of synchronizing all the other systems to successfully operate the cell and the DAQ allow us to perform combustion analysis during and after the realization of the experiments.

The needs of the different systems may be better understood by considering the test cell as a thermodynamic system, where first and second thermodynamic laws apply. Energy enters the system through the fuel supply system. The engine transforms the fuel energy into heat and work through an air-fuel thermodynamic cycle. The heat and work generated is transferred to the cooling system and the dynamometer respectively. Finally, the waste products, such as the exhaust gases, are extracted from the engine through the exhaust system. The energy balance

$$Q_{fuel} = Q_{coolingsystem} + W_{dynamometer} + Q_{exhaustsystem} \tag{A.1}$$

states that the energy entering the cell must be equal to the energy leaving the system. The different system must be designed and build to maintain the mass and energy balance constantly.

The design and working principles behind each of the different systems will be explained further in this chapter. The sensors and devices integrated in the cell will be introduced along with the systems where they are installed.

Figure A.1: General Overview of the Engine Test Cell At UC Berkeley

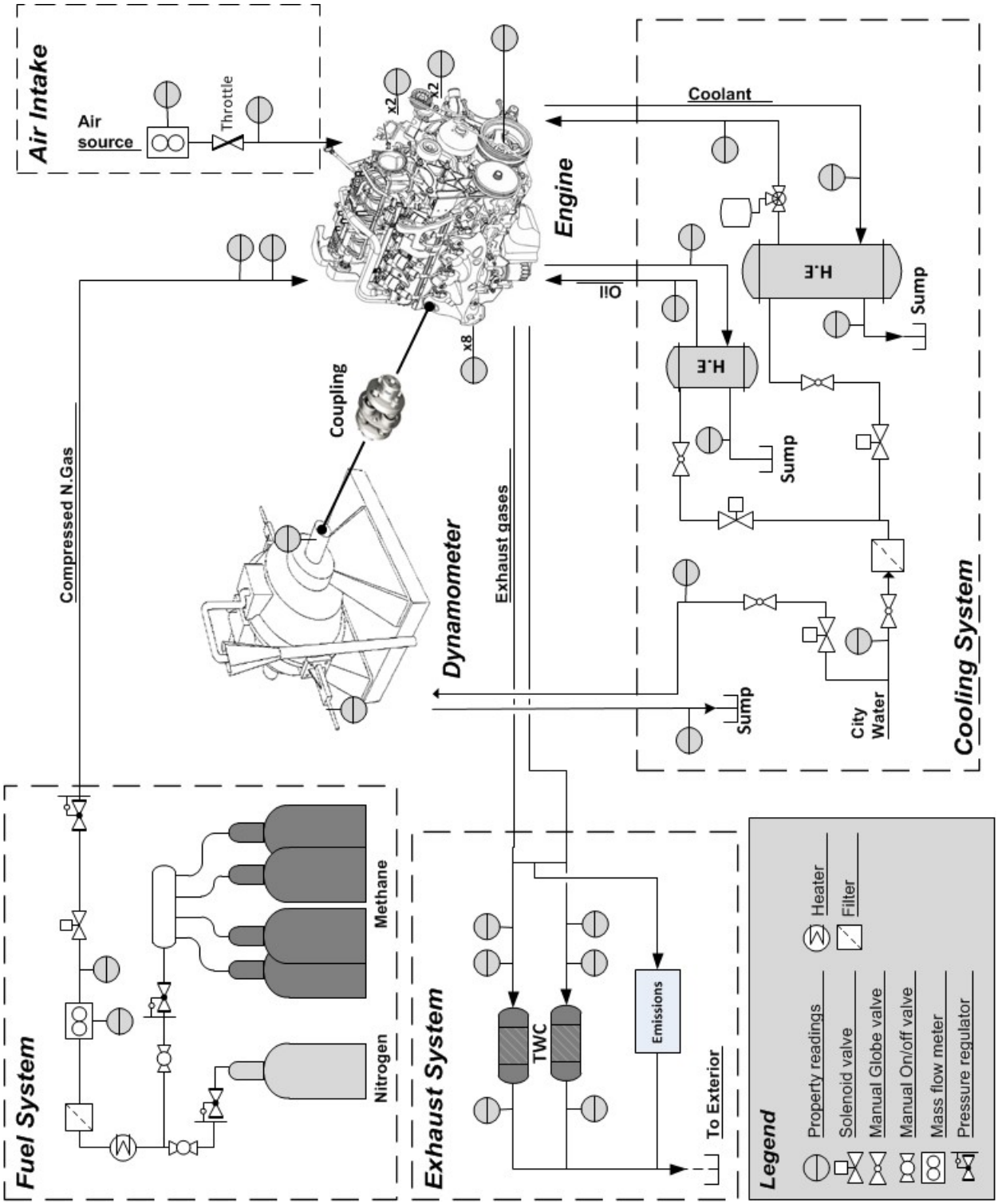

Source: University of California, Berkeley

A.2 Fuel Supply System

The purpose of this report is to evaluate the behavior of DSF in combination with alternative cheap fuel such as natural gas. In that respect, the fuel supply system had to be adapted to supply gaseous fuel. Because the composition of the Natural Gas supplied through the regional pipeline is very irregular, the fuel used in this work is bottled 99 percent methane which specs are introduced in Table C.1. An alternative to bottled fuel is the use of a gas chromatograph which allows us to measure the composition of the pipeline gas and compute its Wobbe index before each experiment. This system was not available at the time, and we opted for bottled methane.

While liquid fuel properties remain nearly constant throughout a wide range of conditions such as temperature and pressure, the use of gaseous fuel represents a challenge because it is a compressible fluid whose properties strongly vary with surrounding conditions. Moreover, the density of gaseous fuels compared to liquid fuels forces the use of highly compressed fuel to increase the autonomy of engine operation. This force the system to be highly pressurized which is an extra challenge on matter of safety and control. A scheme of the fuel system is illustrated on Figure A.2.

Figure A.2: Generic Scheme of the Engine CNG Fuel Supply System at UC Berkeley

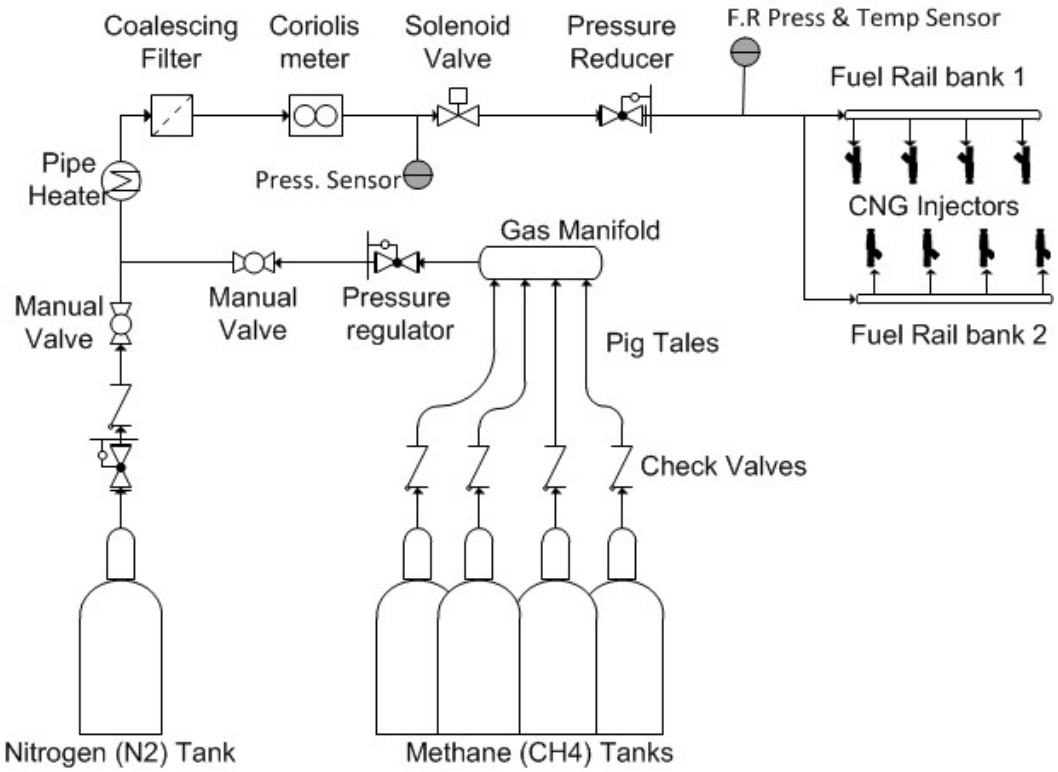

Source: University of California, Berkeley

The fuel used in this project comes in the standard biggest available tank, supplying 9.59 standard m^3 of methane at 165 bar, or in kg, 6.3 kg of methane. This tank has a water capacity of49 kg. The connection to the tank is a CGA 350, characteristic of flamable gases. The composition of the fuel is shown in Table A.1.

Table A.1: Methane Compressed Grade 2.0 composition as Supplied by Praxair. Gas Formula: CH4. Colorless, Odorless, and Flammable Gas. CAS Number: 74-82-8.

Methane	CH_4	99 percent
Oxygen	O_2	50 ppm (max)
Water	H_2O	10 ppm (max)
Nitrogen	N_2	20 ppm (max)
Carbon dioxide	CO_2	100 ppm (max)

Source: University of California, Berkeley

In order to increase the autonomy of the operation, a high pressure brass manifold (200 bar maximum pressure) was used to connect 4 methane tanks in parallel with potential to connect 4 more. Considering stoichiometric conditions, the 6.2 L engine will consume at high speed (3000 rpm, near 0.6 kg of methane per minute). Therefore, four tanks at full load will allow the engine to run for nearly 40 minutes. In the agenda of this project, it is planned to purchase a natural gas compressor which could be connected directly to the engine while running.

At the manifold the pressure is too high for the different components. A pressure regulator was needed to reduce the pressure to an easier working range. Two pressure regulators were used in this project. The first single stage pressure regulator was set up to reduce the pressure from 165 bar to 18 bar. The second regulator, here called pressure reducer, would accurately reducethe pressure from 18 bar to the desired 9.4 bar at the fuel rail. The pressure reduction in both regulators takes place through a diaphragm - poppet valve mechanism. The high pressure fluid flows through a passage until the force exerted over the diaphragm overcomes the spring pressure. Then the poppet valve in between inlet and outlet closes. When the pressure at the outlet falls, the valve opens again and fluid flows through. This process does not consume nor produce any thermodynamic work, and thus it is isenthalpic. Indeed, because the pressure drops across the pressure regulator is done under isoenthalpic conditions, the temperature of the gas drastically decreases freezing the water in the surroundings. This phenomenom is known as the Joule-Thomson effect. Repetitive temperature changes in the pipeline during a prolonged period of time causes the fittings to open loose causing high pressure gas leaks. Therefore, a source of heat is needed to maintain the gas temperature constant. The power needed is proportional to the pressure drop which varies along the operation (the fuel is being consumed) and the fuel flow going through. The energy needed to maintain the fuel at constant temperature can be derived from the equation of the JouleThomson coefficient. This expression relates the change in temperature with the pressure drop across valves.

$$\mu_{JT} = \left(\frac{\partial T}{\partial P}\right)_H = \frac{1}{C_p} * \left(T\left(\frac{\partial V}{\partial T}\right)_P - V\right) \quad \text{(A.2)}$$

By integrating this function from the highest pressure point P_0 to the lowest P_1 the temperature drop experimented by the gas is found as $T_0 - T_1$. The energy required to bring the gas back to its initial temperature T_0 can be computed from the first law of thermodynamics

$$dU = dQ - dW \tag{A.3}$$

Figure A.3: Methane Gas Expansion From 165 Bar to 18 Bar through a Single Stage Regulator Followed by a Heating Process from 230 K to Ambient Temperature 300 K

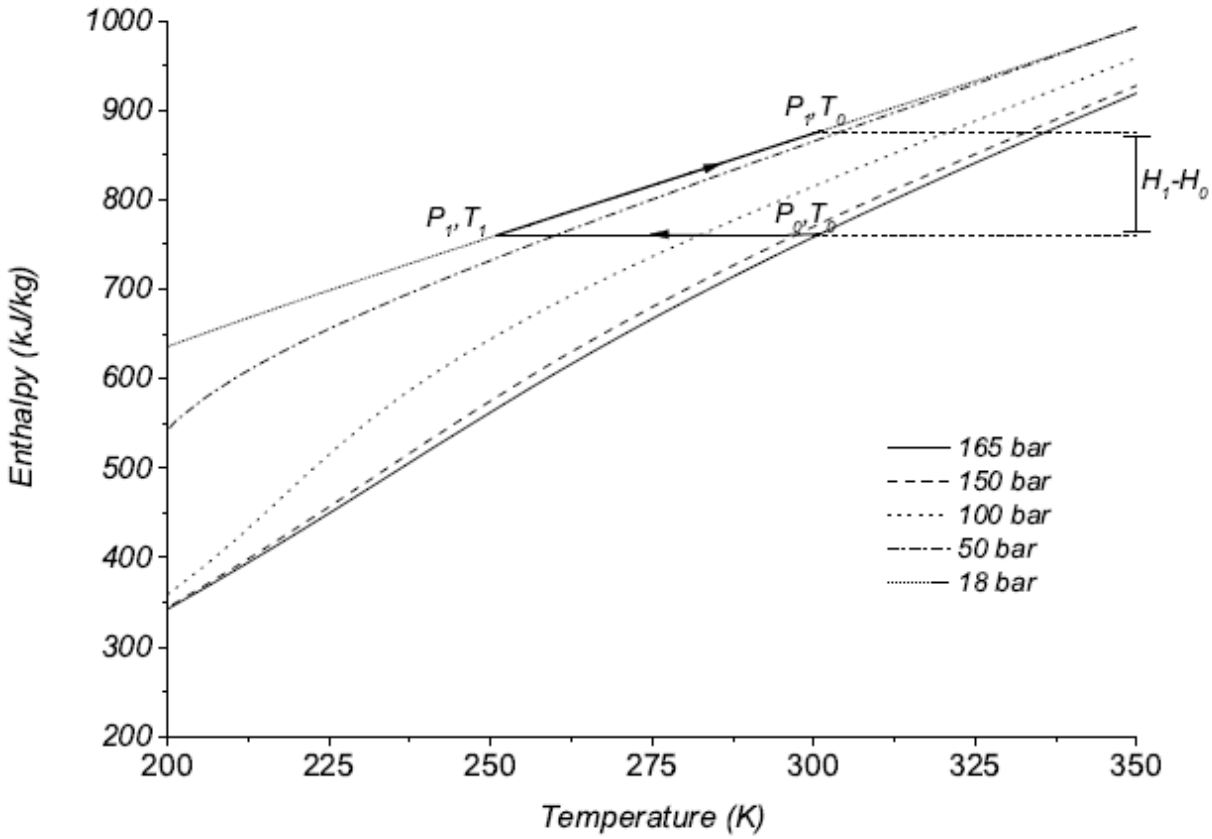

Source: National Institute of Standard and Technology, n.d.

Because no work is realized, the heating process is carried out at constant pressure.

$$dU = dQ = Tds - VdP = T \cdot \left[\left(\frac{\partial S}{\partial T}\right)_p dT - \left(\frac{\partial S}{\partial P}\right)_T dP\right] \tag{A.4}$$

$$dQ = Tds = T \cdot \left(\frac{\partial S}{\partial T}\right)_p dT \tag{A.5}$$

$$Q = \int_{T_1}^{T_0} C_p\,(T) dT \tag{A.6}$$

$$C_p = T \cdot \left(\frac{\partial S}{\partial T}\right)_p \tag{A.7}$$

The relation for $C_p(T)$ can be easily found in the National Institute for Standards and Technology (National Institute of Standard and Technology, n.d.). A scheme of the process is shown in Figure A.3. The maximum temperature drop is 67 degrees Celsius for a pressure drop of 147 bar. The power needed is dependent on the fuel flow, though the maximum specific energy required was found to be 155 kJ/kg. During the experiments, the heaters were tuned to deliver the right amount of power depending on both, the pressure upstream the system and the fuel flow. Constant measurement of the fuel temperature was read by the mass flow meter and the fuel rail temperature sensor.

A coalescing filter was set in the line to retain condensates, oil, and other contaminants in the gas, which could cause the injectors to clog. The principle behind the coalescing filtration is the gravitational draining of a determined size droplet. These droplets are formed by the agglomeration of molecules as they pass through the filter porous element.

To measure the fuel flow, a Coriolis mass flow meter was used. Because the fuel is compressible, average mass flow meters such as those based on heating coils don't guaranty accuracy. A Coriolis meter was used instead to provide an accurate mass flow measurement. The principle behind this device is based on the Coriolis Effect suffered by a fluid in motion. The incoming flow splits into two equal streams which flow through parallel tubes. Both pipes are tight together through a coil, which during operation is energized to infer a constant oscillation motion to both tubes. When fluid is flowing through the device, the inlet tube which drives the fluid far from the center axis has to act to increase the angular momentum of the fluid. By contrast, the part of the tube which bends toward the center axis has to decrease the angular momentum of the fluid. The angular acceleration caused by the flow is proportional to the mass flowing through the tubes as derived from Newton's equation.

$$F_c = m \cdot a_c \tag{A.8}$$

F_C is the Coriolis force, m the mass of the fluid and a_c the Coriolis acceleration. Because the amplitude of the oscillation is a direct measure of the force exerted by the tubes on the coil, and the acceleration is function of the predetermined oscillation pattern, the mass can be computed by comparison with the no flow case. This sensor is essential if the aim of the research is fuel consumption.

In order to prevent the engine from shutting down at last moment notice, a high pressure sensor reads the upstream pressure. When the pressure falls below 9 bar, the fuel rail pressure is no longer adequate and the experiment is over. This sensor is the analog to the fuel gauge in a normal vehicle. Because volumetric measurements do not directly relates to mass flows in the case of compressible fluids, the pressure measurement is a good indicative of the amount of fuel remaining in the tanks. As a matter of safety, a high pressure solenoid valve was set in between the fuel tanks and the engine. In case gas leaks occur or fire originates at the engine, the fuel flow could be terminated intermediately from the engine control desk.

The engine vibrates during operation, and in DSF conditions, such vibrations were expected to be higher. A set of flexible high pressure hoses was installed within the interface between the fuel system and the fuel rail. This measure was taken to prevent the tube fitting from opening

loose and also to not deteriorate the fuel rail which was manufactured in a softer metal than the fuel supply system.

Finally, to achieve well controlled injection, temperature and pressure at the fuel rail must be known. Because CNG is a compressible fluid, density is highly sensitive to changes in pressure and temperature. If fuel temperatures are too high, density may fall and not enough mass flow would reach the cylinder. In the same way, if pressure is too low, not enough pressure difference is built across the injector and the fuel flow will be limited. This sensor is wired to the ECU to indicate the injection system the properties of the fuel at the moment of injection. The fuel system trims the pulse width accordingly to deliver the right amount of fuel.

Finally, as explained in previous section, natural gas requires a different type of injector. For this project the injector used were *Bosch's* NGI2 dedicated natural gas injectors. The reason for these injectors was their dimensions, which fitted perfectly the spaces left by the previous gasoline injectors.

In conclusion, the fuel supply system has been designed to match the injectors demand. Four different sensing devices where installed within the fuel system to ensure good control over the system and perform later consumption and combustion analysis. The sensors are listed in Table A.2.

Table A.2: Fuel System Sensors and Property Measurements

Part.No	Mfr	Sensor type	Symbo	Description
CMF010M DS-HD-KV4 51CP26-01	*MicroMotion* *Bosch* *Sensat* *a*	Coriolis flow meter Pressure sensor Absolute pressure sen- sor	$\dot{m}_{fuel}$ p_f P_{FR}	Fuel mass flow Fuel tank pressure Fuel rail absolute pres- sure
51CP26-01 NGI2	*Sensat* *a* *Bosch*	NTC thermistor CNG injector	T_{FR} Pw	Fuel rail temperature Pulse width

Source: University of California, Berkeley

A.3 Engine and Air Intake System

The engine used in this project was a GM Gen IV L94 V8 VORTEC 6.2 VVT. The reason for its selection was the large portion of the car manufacturing market that this engine hoards. In 2011, the number of V8 small block being produced by the*General Motors* reached 100 million (General Motors Corp., 2011).

With this in mind, Tula aims to develop DSF for an engine which would facilitate the transition of the technology from the research state to production. The engine was modified to operate in Dynamic Skip Fire mode through the addition of the the Lifter Oil Manifold Assembly (LOMA) and the deactivation lifters as explained in Section D.2. Furthermore, the injectors were replaced by *Bosch's* NGI2 dedicated natural gas injectors to enable CNG operation. As for the reliable operation of DSF, Tula Technology integrated proximity sensors at the valve train, concretely, one

sensor per valve to monitor the status of the deactivation. More about this topic will be discussed in Section A.7. A set of different sensor where installed at cylinders 3 and 4 to evaluate the performance of the engine and the combustion process (Figure A.5).

Figure A.4: GM Engine Block with Enumerated Cylinders

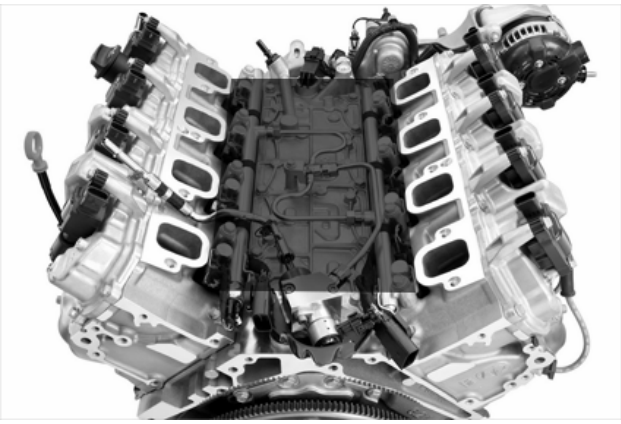

Source: Image adapted from (General Motors Powertrain, 2013)

As presented in Chapter 1, the full potential of CNG is exploited when the compression ratio of the engine is increased. For this project the compression ratio of the engine has not been modified and remained at 10.4:1. The aim of this project is to demonstrate the fuel improvement caused by DSF technology and thus, the comparison will be made between CNG in normal operation mode and CNG on DSF mode regardless of fuel performance. Table A.3 lists all the different devices. A summary of the major characteristics of the engine is shown in Table A.3.

The air intake system seen in Figure A.1 is integrated within the engine. This system is of extreme influence for the performance of the engine on DSF mode. The air inhaled by the engine goes first through a filter to prevent big particles, such as sand and dust, from entering the cylinders. The cross section area of the air box is bigger than the air intake system passages in order to maintain close to laminar flow regimes. The advantage of inhaling through the air box is the possibility to measure mass air flow via a hot wire anemometer.

Figure A.5: Air Intake System Diagram

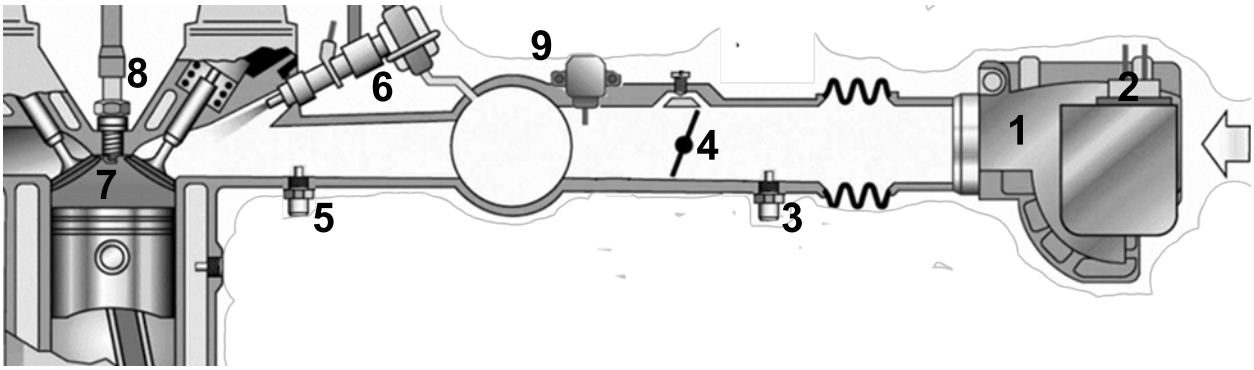

1.Air box; 2.Hot wire anemometer; 3.Thermocouple; 4.Throttle; 5.Thermocouple; 6.Gas injector; 7.Adapted spark plug; 8.Piezoelectric P Sensor; 9.MAP sensor.

Source: Image adapted from (General Motors Powertrain, 2013)

A conductive wire is installed in the middle of the air box, perpendicular to the direction of flow. Because the flow regime is laminar, the flow velocity profile can be computed from:

$$v(r) = v_{max}\left[1 - \left(\frac{r}{R}\right)^2\right] \tag{A.9}$$

r is the position in cylindrical coordinates and R is the radius of the air box cross section. To compute the maximum velocity, the wire acts as a resistance which under electric current or voltage, heats up. The air flows around the wire cooling it down and thus reducing its resistance which can be measured by the change in voltage across the wire. This voltage difference is proportional to the heat loss due to convection and thus v_{max} can be obtained. By integrating Equation A.9 over the air box cross sectional area the average velocity and the total air mass flow are obtained.

Moreover, a barometric pressure sensor is needed to adjust the engine injection look up tables for variation on ambient pressure. Although these adjustments are mainly carried out by the close loop lambda control, the barometric sensor supports this system by measuring the ambient pressure and consequently the relative to temperature fluid density at different heights. The position of this sensor is irrelevant and is normally set under the hood.

Table A.3: Engine Integrated and Installed Sensors for Engine Performance Assessment

Part.No	Mfr	Sensor type	Symbo	Description
H25D-SS-720-	*BEI*	Optical encoder	ω	Engine speed
ABZC-28V/5-				
SM18				
2503679	*GM*	Pressure sensor	MAP	Manifold air pressure
1600683 - - GH13Z-24	*GM* *GM* *GM* *AVL*	Pressure sensor Pressure sensor Hot wire anemometer Piezoelectric pressure transducer	p_{baro} p_{oil} $\dot{m}_{air}$ p_{cy}	Barometric pressure Oil pressure air mass flow Cyl 3,4 In cylinder pressures
TJ-72-CASS-116E-6-SB	*Omega*	Thermocouple (k)	T_{air}	Intake air temperature
TJ-72-CASS-116E-6-SB	*Omega*	Thermocouple (k)	T_{air}	Cyl 3, 4 Intake runner air temperature

Source: University of California, Berkeley

After the air box, a thermocouple is installed to measure ambient air temperature. Because the test cell warms up with the heat released during engine operation, the air supply will vary on density. When the overall system has reached equilibrium the air density will stabilize and the result are then reliable for performance and combustion analysis.

The throttle valve follows. This engine carries an OMG electric throttle valve which facilitates the reading of the throttle position. The throttle position communicates to the ECU in order to smootlhy modify injection and ignition to catch up with the variation on engine load.

Furthermore, a manifold air pressure sensor read the pressure after the throttle. This measurement indicates the ECU the flow conditions previous to the inlet valve and thus the cam phasing is modified accordingly to reduce pumping losses.

Finally, to be able to predict the volumetric efficiency of the engine, thermocouples are installed at the intake runners of selected cylinders 3 and 4. The selection of these two cylinders was based on their position. Peripheral cylinders are more susceptible to surrounding conditions because of their higher are exposed. For that reason inner located cylinders were chosen to reduce measurement variation due to external experimental conditions.

Finally, for combustion analysis, two piezoelectric pressure transducers were allocated in cylinder 3 and 4 respectively. Under DSF conditions many of the cylinders are disabled. For that reason two sensor were needed to prevent from reading deactivated cylinders only.

Table A.4: Modified GM Gen IV L94 V8 VORTEC 6.2 VVT Characteristic for Operation on CNG under DSF Mode

General	
Type	6.2L Gen IV V-8 Small Block
Displacement	6162 [cc]
Engine Orientation	10.4:1
Compression Ratio	1 – 8 – 7 – 2 – 6 – 5 – 4 – 3
Fuel System	Sequential
Emission Control	Three-Way Catalytic Converter
Geometry	
Bore	10.325 [mm]
Stroke	92 [mm]
Bore Center	111.76 [mm]
Total Engine Bore Area	669.82 [cm²]
Connecting Rod Length	154.9 [mm]
Valve Train	
Valve Configuration	Overhead Valves
Valves Per Cylinder	2
Valve Lifters	Hydraulic Roller
IVO	336.514 [CAD ATDC]
IVC	-86.38 [CAD ATDC]
EVO	98.0365 [CAD ATDC]
EVC	385.1 [CAD ATDC]
VVT	0 to 50 [CAD] Retard
Performance	
Maximum Power	403 [hp] /301 [kW] @ 5700 rpm SAE CERTI-FIED
Maximum Torque	565 [Nm] @ 4300 rpm SAE CERTIFIED 6000 [rpm]
Maximum Speed	6000 [rpm]
Modification	
Fuel Injector	NGI2 *Bosch*
Cylinder Management	Dynamic Skip Fire

*Values related to gasoline operation.

Source: (General Motors Powertrain, 2013)

A.4 Cooling System

The engine is not 100 percent efficient and part of the power produced by the engine does not reach the crankshaft. This wasted power must be dissipated through a different path. In a car mounted engine, the heat released by the engine is transported by the cooling systems to a radiator where it is delivered to the atmosphere. In our case, the engine is stationary and no air flow is present to enhance the heat transfer of an automotive radiator. For this reason, heat exchangers of the type Shell and Tube were chosen (Figure A.6). The cooling system was design to cope with a source of heat relative to the maximum power produced by the engine, 301 kW. In average, SI engines are 25 to 35 percent efficient meaning that 65-75 percent of the energy

produced leaves the engine through the cooling system. In the case of our test cell all the power generated by the engine must leave the cell through the cooling system. Because the brake power generated by the engine is being absorbed by an Eddy Current dynamometer, it has to, eventually, transfer the mechanical energy into heat which is later dissipated by the cooling system. In summary, the cooling system must be able to dissipate 1000 kW of power for the safe operation of the test cell. The system is illustrated in Figure A.7.

Figure A.6: An Approximate Scheme of Both Shell-Tube Heat Exchangers with One-Shell Pass and Two-Tube Pass

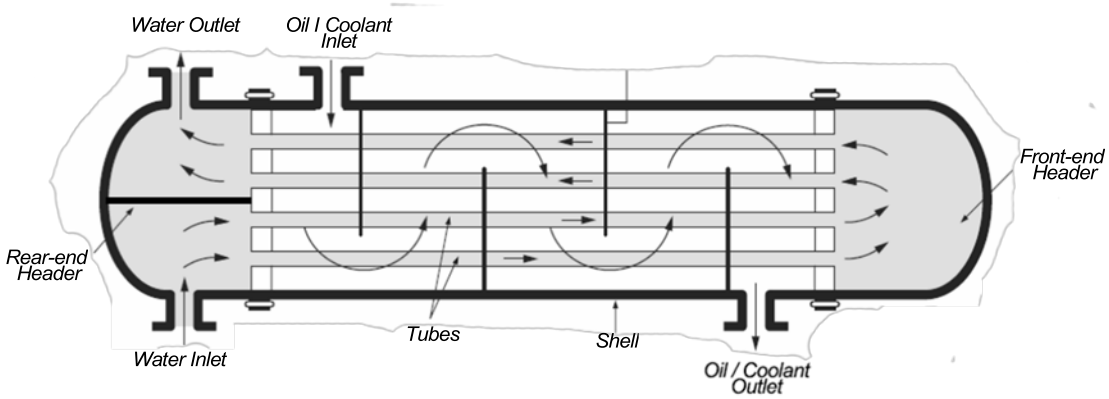

Source: (Cengel, 2002)

The cooling of the engine is normally achieved in two steps. The coolant, a primary fluid composed of water and gycol, flows through different engine passages absorbing the heat that flows outside the cylinder through the walls. In the next step, the hot coolant leaving the engine enters a heat exchanger where it releases the heat to a lesser quality fluid or secondary fluid. The oil circuit work similarly to the coolant. The oil leaves the engine and flows through a heat exchanger to return to the engine once the heat has been released to the secondary fluid.

In the case of the dynamometer, there is not primary and secondary fluid and normal water carries out the heat dissipation. The need for secondary steps is due to fluid quality and purity. In order to avoid the clogging of the conducts and the corrotion of the engine components, clean distillated water and glycol is used. In the case of the Dynamometer, the fluid passages are large and no specific properties are needed. As can be seen in Figure A.7, the cooling system is split into three: the coolant circuit, the oil circuit and the dynamometer.

City water was used as secondary fluid for the oil and coolant system and as primary for the dynamometer. The supply line provided water at 7 bar which after the heat exchangers was discharged to ambient, at a sump channel under the test cell trench. The water inlet temperature was measured at the source. Normal values stand near the 15-25 ^{o}C range. A manual valve and a pressure gauge was installed at the source to manually control the system if the situation required. After the manual valve, a high capacity water filter was installed to prevent big particles from entering the heat exchangers and corrosion. For that purpose, all pipes used in this system were made of galvanized steel.

Figure A.7: Cooling System's Generic Scheme of the Engine Test Cell at UC Berkeley

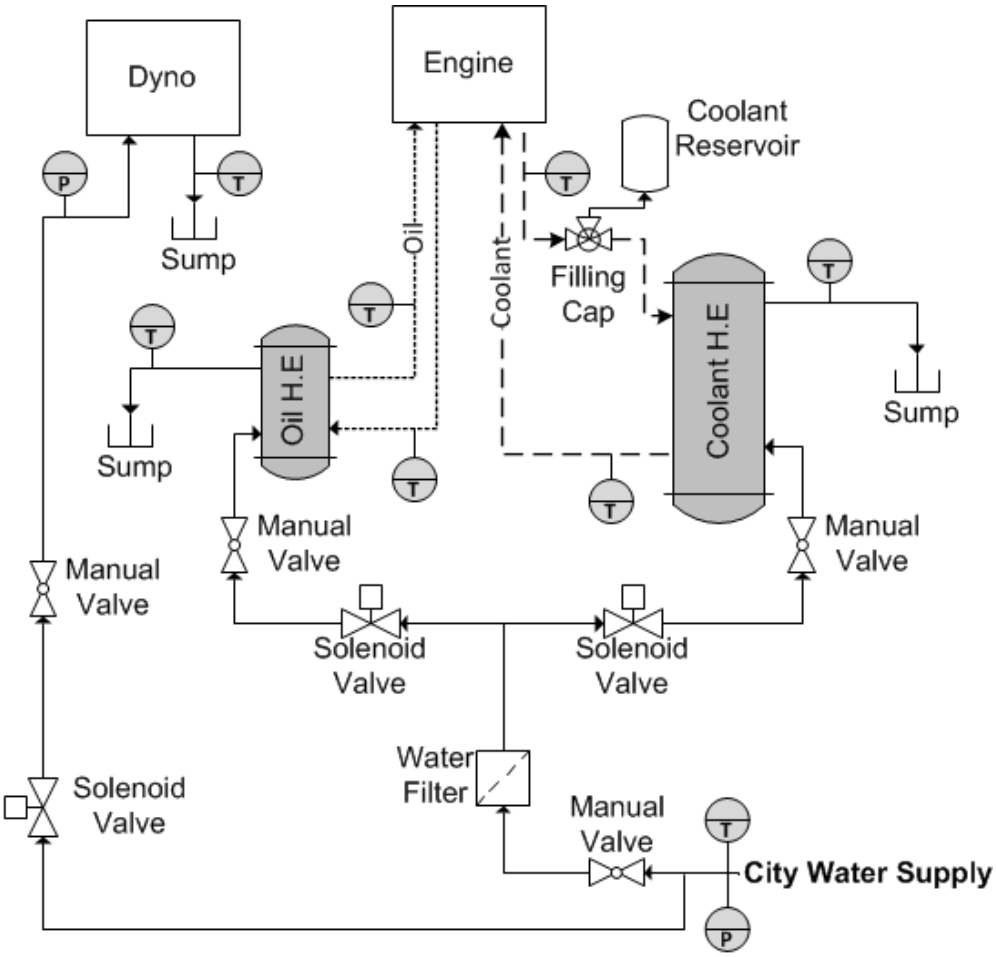

Source: University of California, Berkeley

In order to control the system, three solenoid valves were installed (one per circuit). The solenoid valves were thermostatically controlled to open or close depending on the load. Each of the PID controllers reads the temperature at the outlet side of the primary fluid systems, oil and coolant, to determine how much water is needed to maintain stable temperatures. Normal engine temperature seat around 90 ^{o}C degrees Celsius, and thus desired output coolant and oil temperatures were fixed at this set point.

In the case of the dynamometer, no PDI controller was used. The solenoid valve was actuated to remotely switch on or off the dynamometer cooling. A desired flow was prescribed by the manufacturer. Making use of an installed pressure gauge, the pressure at the inlet was set to 5 bar through the actuation of a manual valve.

A.4.1 Engine Cooling

The engine cooling system is the one absorbing the maximum amount of power. Nearly 35 percent of the power generated leaves the system in the form of heat through the coolant circuit.

A summary of the main properties of the engine's integrated cooling circuit is presented in table A.5.

Table A.5: Engine Coolant Circuit Operating Parameters

Coolant Circuit			**Heat Exchanger**		
Parameter	Unit	Value	Parameter	Unit	Value
Volumetric flow rate	l/min	160	Shell Diameter	cm	15.24
Mass Flow Rate	kg/s	2.68	Material	-	Copper
Temperature In	°C	62	Inner Tube Diameter	mm	9.525
Temperature Out	°C	90	Outer Tube Diameter	mm	12.7
Average Temperature	°C	76	Amount Of Tubes	-	116
Heat Load	kW	298	Tubes Length	m	1.22

Source: University of California, Berkeley

The size of the heat exchanger was predefined because a shell and tube heat exchanger was already in our inventory. However, a study was done to evaluate the heat transfer capabilities of the heat exchanger. The effectiveness-NTU method is preferred for this type of application, however for simplicity, the Logarithmic Mean Temperature Difference method (LMTD) was used. This type of calculation allows a heat exchanger to achieve certain thermodynamic conditions. In order to use this method for evaluating the suitability of a given heat exchanger, the thermodynamic conditions where first approximated. Through iteration the thermodynamic conditions were modified until the solution converges to the prescribed heat exchanger size. The LMTD method is explained in Section A.4.

The result of this calculation showed the heat exchanger was oversized for our application and thus it was more than sufficient for our testing conditions.

A.4.2 Oil Cooling

In small engine blocks such as an inline 4 or smaller, oil cooling is normally not needed and the oil cools itself when it reaches the sump. However for larger size engines, oil may absorb more heat due to the higher lubricating surface area. In the case of our V8 block, the Oil circuit would absorb up to 55 kW of heat. Because the engine is stationary, the sump itself is not able to dissipate that much heat through its walls and an oil cooling circuit is needed. The characteristics of the oil circuit are introduced in Table A.6.

The size of the heat exchanger was calculated through the Logarithmic Mean Temperature Difference method (LMTD). This method is based on the assumption that the enthalpy change over both fluids flowing, across the heat exchanger, is proportional to each other, and thus there is balance between the energy absorbed by one fluid and the energy lost by the other.

$$\delta\dot{Q} = -\dot{m}_h C_{p,h} dT_h \tag{A.10}$$

$$\delta\dot{Q} = \dot{m}_c C_{p,c} dT_c \tag{A.11}$$

Table A.6: Oil Cooling Circuit Operating Parameters

Oil Circuit			**Heat Exchanger**		
Parameter	Unit	Value	Parameter	Unit	Value
Volumetric Flow Rate	l/min	30	Shell Diameter	cm	7.62
Mass Flow Rate	kg/s	0.425	Material	-	Copper
Temperature In	°C	135	Inner Tube Diameter	mm	6.35
Temperature Out	°C	80	Outer Tube Diameter	mm	9.525
Average Temperature	°C	107.5	Amount Of Tubes	-	60
Heat Load	kW	55	Tubes Length	m	0.61

Source: University of California, Berkeley

Therefore a differential temperature difference change across both fluids is then dependent on the thermal inertia $\dot{m}C_p$ of each and the heat transfer rate $\delta\dot{Q}$ in the way:

$$\delta(T_h - T_c) = -\delta\dot{Q}\left(\frac{1}{m_h C_{p,h}} + \frac{1}{m_h C_{p,c}} m_c C_{p,c}\right) \tag{A.12}$$

This formula can be rewritten if $\delta\dot{Q}$ is substituted as:

$$\delta\dot{Q} = U(T_h - T_c)dA \tag{A.13}$$

where U stands for the overall heat transfer coefficient.

$$\frac{d(T_h - T_c)}{T_h - T_c} = -UdA\left(\frac{1}{m_h C_{p,h}} + \frac{1}{m_c C_{p,c}} m_c C_{p,c}\right) \tag{A.14}$$

If the expression is integrated over a desired temperature range, the total heat transfer surface area read:

$$A = \frac{\dot{Q}}{U\Delta T_{lm}} \tag{A.15}$$

$$\Delta T_{lm} = \frac{\Delta T_{in} - \Delta T_{out}}{\ln\left(\frac{\Delta T_{in}}{\Delta T_{out}}\right)} \tag{A.16}$$

where the subscript “in” and “out” stand for the inlet and outlet of either fluid, though the notation must be consistent throughout the problem. The overall heat transfer coefficient must be computed based on the geometry of the heat exchanger chosen and the material properties. It reads:

$$U = \frac{1}{\frac{1}{h_{out}} + \frac{1}{h_{in}}} \tag{A.17}$$

where h_{in} and h_{out} represent the convection coefficient at the outer and inner surface at the fluids interface. These values are obtained from:

$$h = Nu \cdot \frac{k}{D} \tag{A.18}$$

where kis the thermal conductivity of the fluid (in our case Oil SAE 5W30), D is the diameter of the tube regarding the fluid position, outside or inside, and Nu is the Nusselt number. Nusselt

numbers are computed from correlations, based on the Reynolds number (Re) , Prandtl Number (Pr) and other related system conditions.

$$Re = \frac{pV_{max}D}{\mu} \tag{A.19}$$

$$Pr = \frac{C_p\mu}{k} \tag{A.20}$$

With the resulting Reynolds number, a Nusselt number correlation was chosen and Nu was obtained. Consequently, the convection coefficients for both, outer and inner fluid were computed and thus the overall transfer coefficient (aprox 950 W/m^2 K). The surface are required was 0.7 m^2.

In the same way, with a given surface area, the overall heat transfer coefficient was computed for the Engine cooling system(aprox 1700 W/m^2 K). With these results the oil heat exchanger was chosen, and the Engine cooling heat exchanger proved to be sufficient to cope with a maximum load of 310 kW without concerns.

The characteristic of the heat exchanger is shown in Table A.4 for reference. The oil is recirculated by the engine oil pump which supplies up to 3 bar pressure line from the the engine sump, which acts as an expansion tank for the oil lines.

As seen in Figure A.7 many different temperature sensors were installed within the cooling system. No data is collected from the dyno cooling water. Both, the pressure and temperature indication in the figure refer to optical pressure and temperature gauges. For the rest of the systems, thermocouples were set at the inlet and outlet of each heat exchanger, in both the primary and secondary circuits. Althoug this information is not essential for combustion or performance analysis, it is relevant for engine control, safety and if necessary, to perform an energy balance of the cell. A list of the different sensors is presented in Table A.7.

A.4.3 Dynamometer Cooling

The Dynamometer did not need of any external cooling system. A flow of incoming water goes through the eddy current itself, between an outer shell and the inner rotors as can be seen in Figure A.8. A pressure gauge was setup at the inlet to control the internal pressure. For standard conditions, the inlet pressure recommended range was 3 - 7 bar.

A.5 Dynamometer

The dynamometer system is in charge of absorbing and measuring the brake power and torque generated by the engine. For this project an eddy current (EC-Dyno) and a Morse MORFLEX elastomeric coupling were used.

Table A.7: Cooling System Sensors and Property Measurements Summary.

Part.No	Mfr	Sensor type	Symbo	Description
KMQSS-062E-12	*Omega*	Thermocouple (k)	$T_{w,i}$	City water inlet temperature
KMQSS-062E-12	*Omega*	Thermocouple (k)	$T_{w,c,o}$	City water-coolant outlet temperature
KMQSS-062E-12	*Omega*	Thermocouple (k)	$T_{w,o,o}$	City water-oil outlet temperature
KMQSS-062E-12	*Omega*	Thermocouple (k)	$T_{c,i}$	Coolant inlet temperature
KMQSS-062E-12	*Omega*	Thermocouple (k)	$T_{c,o}$	Coolant Outlet temperature
KMQSS-062E-12	*Omega*	Thermocouple (k)	$T_{o,i}$	Oil inlet temperature
KMQSS-062E-12	*Omega*	Thermocouple (k)	$T_{o,o}$	Oil Outlet temperature
KMQSS-062E-12	*Omega*	Thermocouple (k)	$T_{dyno,o}$	City water-dyno Outlet temperature

Source: University of California, Berkeley

The eddy current dynamometer, as illustrated in Figure A.8 consists of a set of coils, a rotor and a stator. When the electromagnetic coils inside are energized, they generate a negative torque in the rotor and a positive torque in the stator. The positive torque is computed by measuring the force exerted over a load cell at the end of torque arm. In addition the velocity at which the dyno is spinning is measured by a magnetic pickup sensor. When the force F, the distance to the center of rotation r and the rotational velocity ω are known, the torque and power are easily obtained by:

$$T = F \cdot r \tag{A.21}$$

$$P = T \cdot \omega \tag{A.22}$$

The characteristics of the dynamometer are shown in Table A.5.

Table A.8: Characteristics of the Eddy Current Dynamometer at UC Berkeley.

Mid-West 1519 EC Dynamometer		
Property	Value	Unit
Maximum Power	310	kW
Maximum Torque	822	Nm
Base speed	3600	rpm
Maximum Speed	7000	rpm

Source: University of California, Berkeley

From the data in Table A.5 and Equations A.21 and A.22 the dynamometer curve can be estimated and the result can be compared with which is expected from the engine. The results in Figure A.9 show that the dyno is perfectly capable of handling the engine and thus its selection was adequate for our purposes.

Figure A.8: Mid-West 1519 EC Dynamometer Cross Section Plane

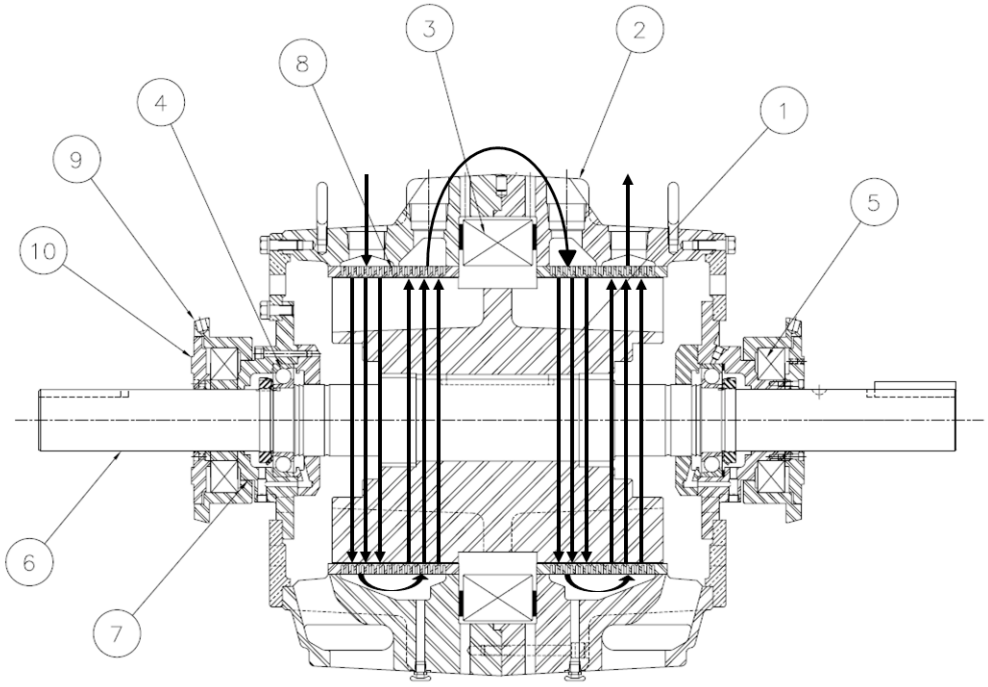

1. Rotor; 2. Stator; 3. Field Coil; 4. Rotor bearings; 6. Shaft; 7. Trunnion; 8. Inductor Rings; 9. Rotators; 10. Trunnion Bearing Cover.

Source: (Dyne Systems; Inc, 2012)

To operate the dyanmometer it must first be synchronized with the engine operation conditions. This way it is possible to accurately absorb the entire power being generated by the engine without letting the engine stall either fly out. Moreover, the control over the engine must be precise. The reason being that the power and torque measured at the dyanmometer should be equivalent to the brake power and brake torque being generated by the engine so that the values stored by the data acquisition system are useful for posterior combustion analysis.

A digital dyno controller Dyn-Loc IV from *DyneSystems* was acquired. This control system allows two modes of control. In the speed mode, the current reaching the coil is controlled to keep the engine at a constant speed thus the torque absorbed will vary on function of the load generated by the engine. On the other hand, the load mode allows to set a desired load, in units of torque, to be produced by the engine. In this project all data have been acquired in speed mode. For safety, the rate of change of setpoints was configured to 50 rpm/s. This value can be modified for driving cycle experiments when more sudden changes in operating points are desired. For the

dynamometer controller to properly correct the current supplied, it needs accurate and fast dyanmometer state feedback. For that reason, the sensor sin Table A.9 were used.

Table A.9: Dynamometer Sensors and Property Measurements Summary.

Part.No	Mfr	Sensor type	Symbo	Description
3030AN	*Shimpo*	Magnetic pickup sensor	ω_{dyno}	Dynamometer speed
-	DyneSystems	Stain gauge load cell	F	Dyno arm force

Source: University of California, Berkeley

For the safe and reliable operation of the Dynamometer system, the power to the coil was directly extracted from the 480 V line via a 480-240 V step transformer. To avoid noise, an isolation transformer was installed in between the step transformer and the dyno controller.

The Morse MORFLEX 1002-R (round flange) was chosen for coupling the engine and dynamometer together. Elastomeric couplings are known by its good behavior under accentuated angular deflection. The reason of this behavior is the neoprene rubber biscuits integrated within the coupling. The rubber compensates for angular deflection, axial displacement, and torsional deflection from torque loads and torsional vibrations. In expect forharsh vibrations under DSF operation, this type of coupling is best suited for the reliable and safe testing of the engine. Furthermore, as a matter of safety, a shaft guard was set on top of the coupling in case of failure. It is important to notice that even though the coupling can handle certain amount of vibration, if resonance frequencies are excited the operation must be quickly terminated or such set point avoided. In our test cell, at engine's regime within the range 1700-1800 rpm resonance frequency were excited and thus these points were avoided.

Figure A.9: Morse MORFLEX 1002-R And Its Properties to Withstand Torsional and Angular Deflection

Torsional deflection

Elastomeric Coupling

Angular Deflector

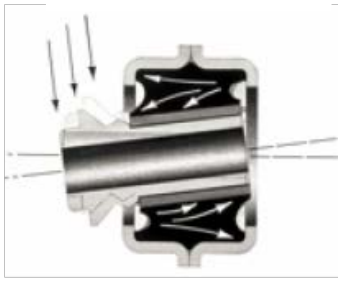

Source: (Morse® MORFLEX®, n.d.)

A.5 Exhaust System

The exhaust system for this engine was set up to emulate that one of a real vehicle. The engine block tested in this project is carried on a Yukon Denali 1500 XL from *General Motors*. With the aim of collecting data closest to on road conditions, the exhaust system was cloned from its analog in the vehicle. Few modifications were needed to adjust the pipes to the available space in the test cell. The exhaust pipes were connected to a vacuum line available at the test cell which carries the exhaust outside the building. In order to avoid the influence of the downstream vacuum on the breathing process of the engine, the original vehicle muffler was installed and the pipes after it were made a little bitlonger.

The emission control system consists of two gasoline three way catalyst converters, one per exhaust bank. Future research will need to add a CNG adapted TWC with higher content in Palladium (Pd). In this project, the performance of the catalyst has not been studied but is scheduled further in the project. A stream of exhaust gas, previous to the catalyst, was redirected through stainless steel piping to a 5-Gas analyzer from *Horiba*. Within this line, a condenser was installed to collect the condensates and prevent water from reaching the gas analyzer. A vacuum pump was set in between to ensure enough flow of exhaust gas to the analyzer.

Different data types were collected at the exhaust. Temperatures were measured with thermocouples at each of the eight cylinder exhaust ports, after each exhaust bank, and after each catalyst converter. Exhaust pressures were measured at the end of each exhaust bank, previous to the catalyst.In addition a wide band oxygen sensor was set at each bank to control the stoichiometry of the operation and achieve accurate injection control.

A.6 Control System

Apart from the physical design of the engine facility, a controls system was also designed and built to ensure total, remote, and continuous management of the engine. The controls were split and synchronized between two different modules.

Figure A.10: Generic Scheme of the Engine Exhaust System at UC Berkeley

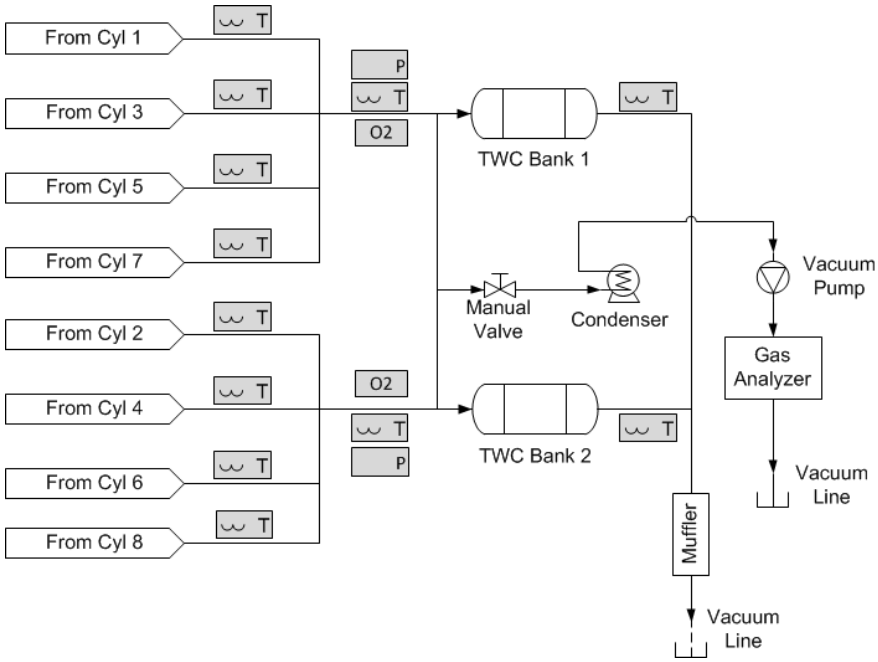

Source: University of California, Berkeley

A.6.1 Engine Control Module

Often in an engine's test cells, the engine control is achieved through the ECU (a real time processor) and a human-machine interface (HMI). For this experiment, *Tula Tech* substituted the OMG ECU by a Micro-Auto Box (MABx), a fast prototyping system manufactured by *dSPACE*. This component enhances the control capabilities to modify the engine behavior on the fly and remotely. Moreover, MABx allows the integration of the ECU and the FCU together within the same component. In order to trigger and collect the different outputs and inputs signals (I/O) a smart Rapid-pro system was used. This component is able to read at fast enough rate to reliably perform DSF patterns without compromising the integrity of the engine. The Human machine interface is integrated in a normal computer through the software *Advanced Control MicroAutobox II* which communicates to the MABx by a fast Ethernet cable. The HMI is illustrated in Figure A.11.

The available features at the HMI are numerous but only few were of main concern for the realization of the experiments. They are listed below.

1. Manual throttle control (acceleration pedal position APP).
2. Manual Valve train control.
3. Closed loop Lambda control.
4. Closed loop MAP control.
5. Manual ignition timing control.

6. Independent cylinder control.
7. DSF firing fraction control.

Table A.10: Exhaust System Sensors and Property Measurements.

Part.No	Mfr	Sensor type	Symbo	Description
LSU 4.9	*ECM*	Wideband Lambda	λ	Bank 1,2 Lambda
FMA-220	*Horiba*	Flame Ionization	*THC*	Hydrocarbons [ppm]
		Detector		
MPA-220	*Horiba*	Magneto-pneumatic Analyzer	O_2	Oxygen [percent]
AIA-220	*Horiba*	Non-dispersive Infrared Analyzer	*CO*	Carbon Monoxide [ppm]
AIA-220	*Horiba*	Non-dispersive Infrared Analyzer	CO_2	Carbon Dioxide [ppm]
CLA-220	*Horiba*	Chemiluminescent Analyzer	NO_x	Oxides of Nitrogen [ppm]
TJ-72-CASS	*Omega*	Thermocouple (K)	T_{exh}	Exhaust Runner Temperatures
TJ-72-CASS	*Omega*	Thermocouple (K)	T_{cat}	Pre- and Post- Catalyst Temperatures
PX209-030A5V	*Omega*	Pressure Transducer	P_{exh}	Bank 1 and 2 Absolute Pressures

Source: University of California, Berkeley

A.6.2 Power Supply Control Module

At the engine room, many devices need to be electrically powered, such as sensors and engine auxiliary systems. Because all the devices don't work at the same voltage level, three different electric systems are utilized.

1. Computer and monitor screen.
2. Coriolis mass flow meter.
3. Oil and engine coolant thermocontrollers.
4. Oil coolant and dynamometer solenoid valves.
5. Dynamometer controller.
6. Isolation transformer.
7. Pressure charge amplifier.
8. National instrument SCXI chassis.
9. Lights and other auxiliaries.

Figure A.11: Illustration of the dSPACE Human Machine Interface (HMI) at the Engine Test Facility

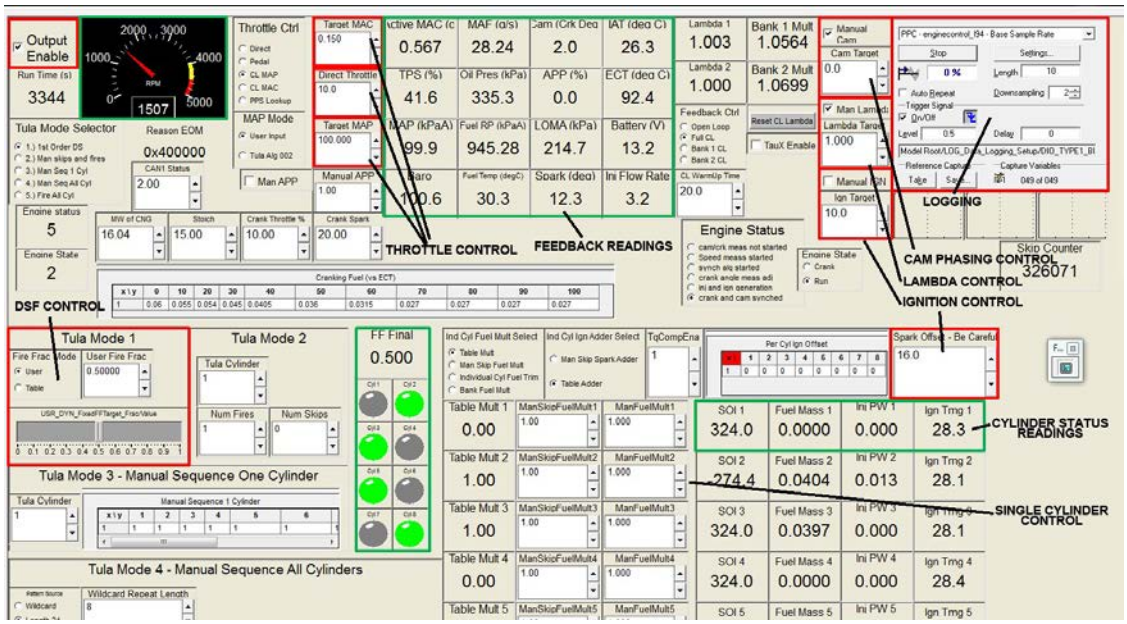

Source: University of California, Berkeley

The 12V DC power line was drawn from a 12V battery and a 60 Amps 12V power supply. The line would be energized via a main toggle switch which would close the circuit at the low side (0 V). The majority of the systems are powered at this voltage level. The different devices are listed below.

1. Ignition coils.
2. Injectors.
3. Exhaust pressure sensor.
4. Starter.
5. Oil pump.
6. Coolant pump.
7. Lambda controller.
8. Shelf cooling fan.
9. Rapid-pro.
10. Fuel supply system solenoid valve.

All the sensors at the test cell use the 5V level as reference to scale their output signal, normally ranging within a scale from 0 to 5V, except for the Coriolis flow meter which reads in a scale of 4 to 20 mA and the exhausyt pressure transducer which are powered by the 12V line. This line is

created through both, stepping down and converting the 120V AC line via National instrument DAQ board and stepping down the 12V line through the Rapid-pro device.

In order to actuate the different devices from the control desk, a main switch panel and a fuse box were set up. In this panel eight different switches and three major push buttons allow to control all the above systems.[6] An overall diagram of the circuitry is shown in Figure A.12.

Figure A.12: Scheme of the Different Control Components at the Control Desk

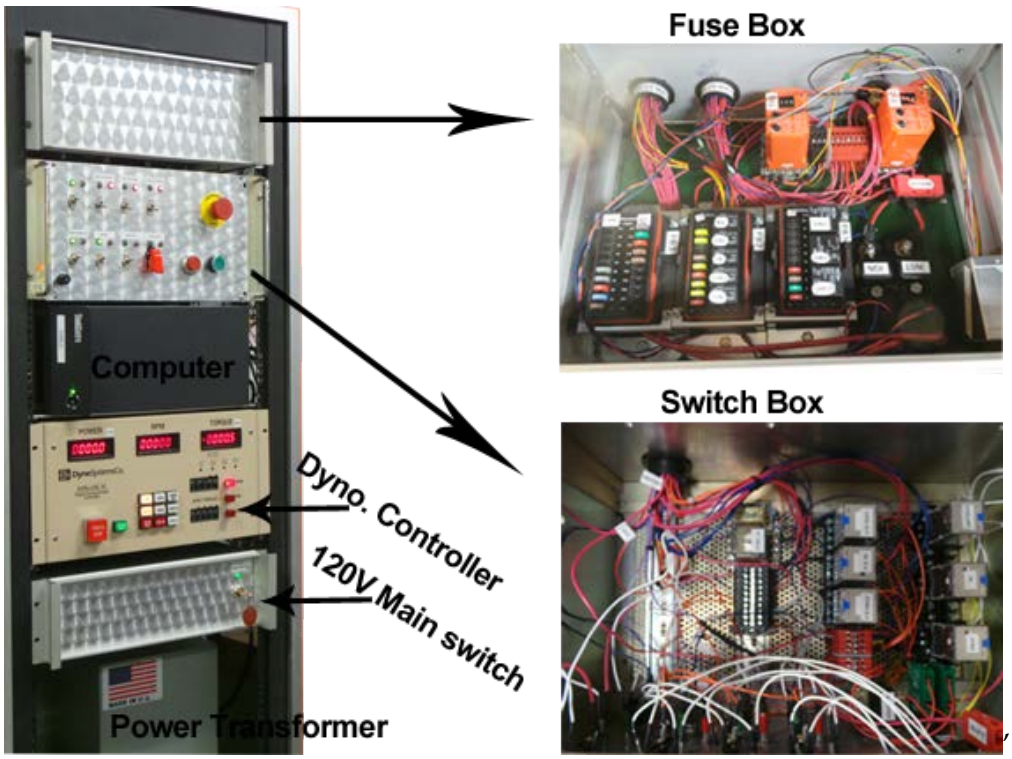

1. Main Power Switch. The main power switch (PWR in the diagram) would be the switch in charge of activating the 12V power supply line. When switched on, all the different terminals will found the common stud and the rest of the panel components will be enabled. If the main power switch is off, no 12V power is supplied and the system is disabled.

2. Dyno, Oil and Coolant switches. The Dyno, Oil and Eng switches main task is to open the dyno cooling solenoid valve and activate the thermo-controllers for the coolant and oil cooling circuit respectively. A green pilot light would indicate if the devices are operative unless the devices are not working propery in which case a red pilot would be active.

   The way in which a system is known to be active is through sensing switches. When all the conditions are fulfilled a series of switches and relays close the circuit and energize the green

[6] The electrical diagrams are too extensive and complex, so they have not been attached to this document.

pilot light. The different conditions are

a. Dynamometer Temperature. Water temperature below maximum limit ($90^{o}C$) indicating good operation conditions.

b. Dynamometer pressure. Water pressure above minimum pressure (4 bar) meaning existence of water flow.

c. Dynamometer s.valve. Solenoid valve open.

d. Coolant temperature. Coolant fluid temperature below maximum limit ($115^{o}C$) indicating good operation conditions.

e. Coolant s.valve. Water circuit solenoid valve open.

f. Oil temperature. Oil temperature below maximum limit ($115^{o}C$) indicating good operation conditions.

g. Oil pressure. Oil pressure above lower limit (1.35 bar).

h. Oil s.valve. Oil-Water circuit solenoid valve open.

3. Instruments. The instrument switch energizes the instruments relay at the fuse box which successively energizes all the auxiliary devices such as: 12V Power supply, Shelf fan, an auxiliary pump and the exhaust pressure transducer.

4. MABX switch. This switch wake sup the MABx from standby together with the power supply, so that the operation settings can be accessed and modified independently, without the need of operating the engine. The power supply is automatically activated to prevent the battery from draining.

5. Ignition switch. The ignition switch enables the ignition coils, activates lambda control, opens the fuel supply line to the engine and turn on MABx and Rapid-pro. it also enables the injection switch.

6. Injection Switch. The injection switch energizes the injectors.

7. Reset Button. Reset the alarms to original state.

8. Starter. Energizes the starter of the engine for cranking.

9. Emergency stop. Pressed in cased of emergency to shut down the entire engine cell.

The circuitry was designed to prevent the engine from running without the essential component activated. The entire cooling system, the ignition switch (which enables MABx and subsidiary systems), the injection switch and the dynamometer controller must be active to operate the engine. Sufficient oil pressure in the circuit is a condition for operation, however, at the start stage no oil pressure has yet been built on the circuit and that conditions should be overridden. To do so, the reset button must be pressed during the cranking event together with the starter

switch. Once the engine starts and the reset and starter buttons are released the engine continues operation unless any of the above conditions fails including oil pressure.

The normal shut down procedure is normally performed from the HMI. Injection and ignition signals are disabled and the engine softly stops. In case of emergency, three different emergency stop buttons are around (at the panel, at the dynamometer controller and inside the cell). When either of these emergency stop buttons is pressed, power to ignition coils and injectors is cut off including the fuel supply. The system is designed to trip when any of the conditions mentioned in the previous section fail. If cooling system is getting too hot, oil pressure too low or dynamometer fails to control the engine the system trips. A maximum speed of operation was set at 4,000 rpm above which, the control system will order the dynamometer to activate braking while simultaneously disabling injection and ignition.

With this configuration, the cell is configured for a single man operation.

A.7 Data Acquisition

The data acquisition system (DAQ) consist of several *National Instruments* (NI) DAQ boards, Rapid-pro, MABx, and all the sensors introduced along the previous section in this chapter.

The data is generated by the sensors, and it is acquired by Rapid-Pro or NI boards depending on whether the data regards engine control or combustion analysis respectively. Therefore, cam position, pulse width and lambda among others, are acquired by Rapid-pro. Signal such as in cylinder pressure, exhaust temperatures and fuel flow are collected by the NI boards. The signal processing is carried out by both, the MABx real time processor and NI DAQ boards. The entire system collects, processes, and compiles the information provided by the sensing devices. The system overview is illustrated in Figure A.13.

Once the data is collected, it is desired to have real time visualization capabilities, logging and analysis. The engine controller processes and logs the following data upon request:

1. In Cylinder Pressure
2. Real mixture polytropic coefficient during compression and expansion strokes.
3. Indicated values power, and efficiency.
4. In cylinder mass
5. In cylinder temperature
6. Heat release rate
7. Combustion timing

Figure A.13: Summary of the Data Acquisition System at UC Berkeley

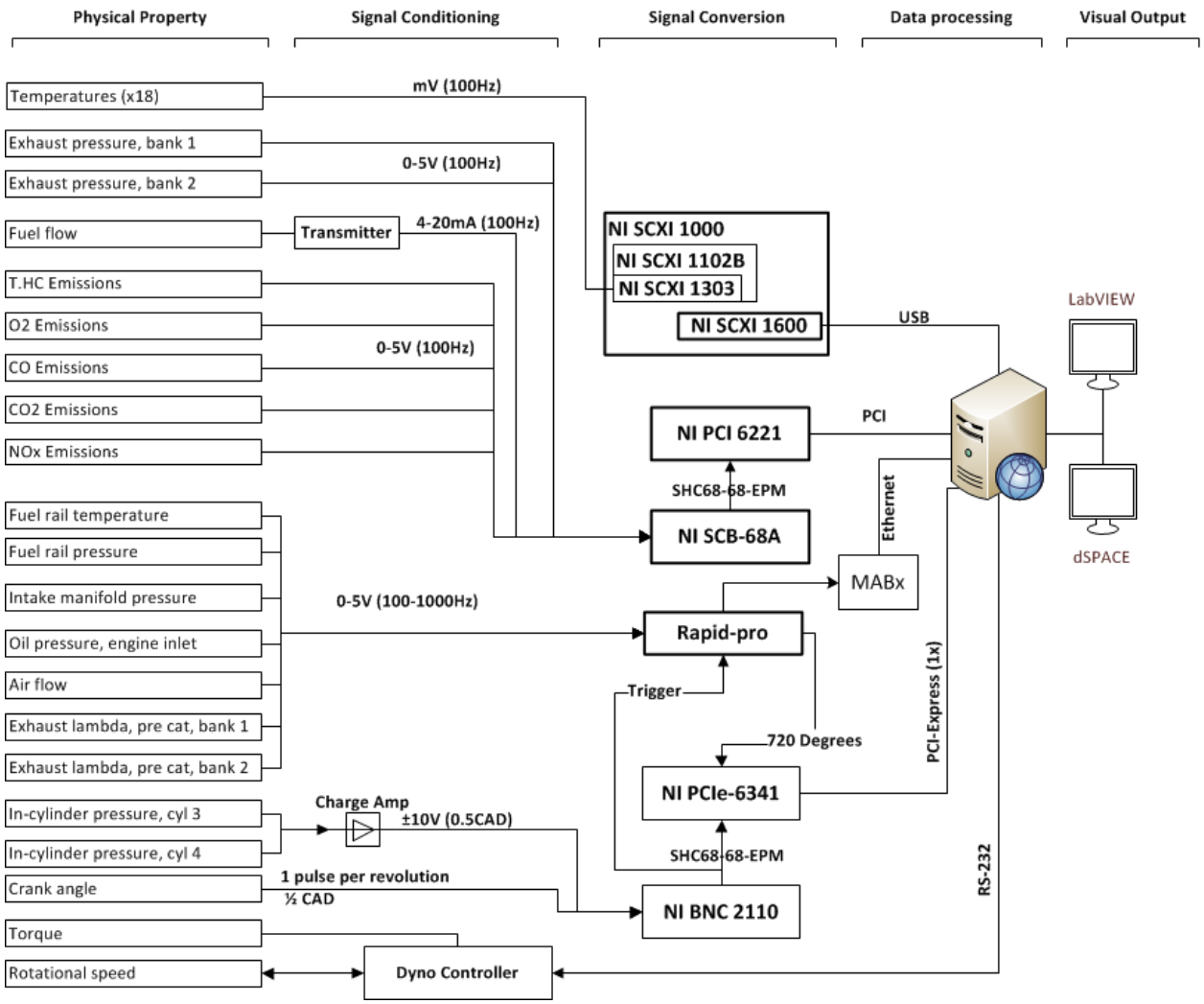

Source: (Thiem, 2013)

APPENDIX B:
IC Engine Fundamentals

B.1 Engine Geometry

Reciprocating internal combustion (IC) engines convert thermal energy into mechanical energy through the linear displacement of a piston. Although the piston, in a four stroke engine, consumes four strokes to complete a power cycle, the thermodynamic cycle is completed within only two of them: the compression stroke and power stroke. In the specific case of the SI engine, the different stages are as follows:

1. Intake stroke. The process starts with the piston at the very top of its travel or top dead center (TDC). The inlet valve opens, and the piston travels down inducing the air-fuel mixture to come inside the cylinder.
2. Compression stroke. When the piston has reached the bottom end of the stroke or bottom dead center (BDC), inlet valve closes and air inside is compressed by the piston traveling upward. When the piston reaches TDC, the combustion event is triggered by a spark.
3. Power stroke. The combustion event had occurred and the sudden pressure raise in the cylinder pushes the piston down delivering work to the crankshaft.
4. Exhaust stroke. When the piston raches BDC, the exhaust valve opens and the piston, on its way up, pushes the burnt gases outside the cylinder.

The most characteristic geometry of a single piston SI engine is the one shown in Figure B.1. The piston transforms linear velocity into rotational speed via a piston rod and crank mechanism.

The piston moves in a reciprocal manner, up and down, drawing a sinusoidal trajectory with an amplitude equivalent to half the stroke (S) determined by the crankshaft radius (a) and piston rod length (l). The frequency (N) is determined by the crankshaft rotational speed (ω)

$$s(\theta) = a \cdot \cos(\theta) + \sqrt{l^2 - a^2 sin^2(\theta)} \tag{B.1}$$

Figure B.1: Example of a Four Stroke SI Engine Cylinder-Pistion Geometry

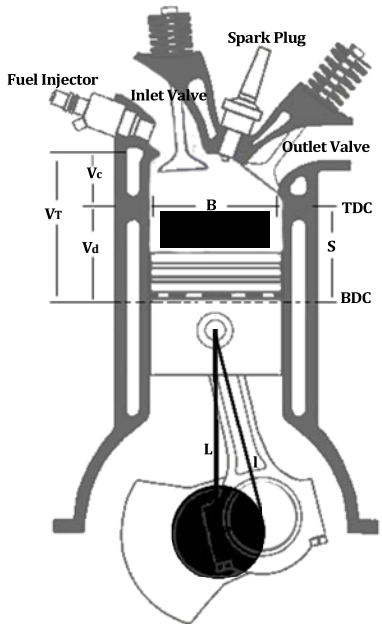

V_c = Combustion chamber volume; V_d = Volume displacement; V_T = Total cylinder volume; TDC = Top Dead Center; BDC = Bottom Dead Center; S = Stroke; B = Bore; L = Rod length.

Source: University of California, Berkeley

$$S = 2 \cdot a \tag{B.2}$$

$$N = \frac{\omega}{2\pi} \tag{B.3}$$

The volume trapped between the cylinder head and the piston ($V(t)$) varies in time from a minimum, when the piston is at the very top, to a maximum, when the piston is at the very bottom. These two maximum and minimum points are normally called top dead center (TDC) and bottom dead center (BDC) and correspond to 0° and $\pm 180^\circ$ crank angle degrees (CAD). The minimum volume, at TDC, is called the combustion chamber volume V_c. The volume generated by the piston in motion is called the displaced volume V_d and varies in time, with the angular position (θ) of the piston rod

$$\theta = \omega \cdot t \tag{B.4}$$

$$V_d(\theta) = \big(a + l - s(\theta)\big) \cdot A_p \tag{B.5}$$

The total capacity of the cylinder V_T is the sum of the combustion chamber volume V_c and the maximum volume displaced by the piston.

$$V_T = V_c + V_d(180°) \tag{B.6}$$

where the surface area A_p is derived from the piston's diameter or bore B as follows

$$A_p = \frac{\pi B^2}{4} \tag{B.7}$$

The mean linear velocity of the piston is used to compare different characteristic stroke engines and is given by

$$\bar{s_p} = 2 \cdot S \cdot \omega \tag{B.8}$$

These set of parameters define the kinetic characteristics of the engine and serve to carry out the combustion analysis from the physical properties measured by the sensors. Three important ratios are derived from the above equations: the compression ratio (r_c), the bore to stroke ratio (R_{bs}) and the piston rod to radius ratio (R) as defined in (Heywood, 1988). The first ratio

$$r_c = \frac{V_d + V_c}{V_c} \tag{B.9}$$

is a direct indicator on how efficient the engine is, as it will be explained in Section B.3.3. Less influential is

$$R_{bs} = \frac{B}{S} \tag{B.10}$$

which characterizes the rotational speed range at which a given engine operates. Large bores to stroke ratios are characteristics of fast spinning engines and vice versa. This allows to optimize an engine on a power versus torque bases as inferred from the power-torque relationship in Equation B.12. The third ratio is an indicator of engine's size.

$$R = \frac{1}{a} \tag{B.11}$$

B.2 Engine Brake Parameters

Regarding engine performance, it is common to use terms such as brake power, brake thermal efficiency among many other brake terms. Brake values are related to the net output of the engine. Outside research environments, an engine is normally defined by what it has to offer to the operator while integral aspects of the machine are overlooked. The different and most relevant terms are introduced below. In this document, brake terms will be identified by a subscript "B" or the prefix "b".

B.2.1 Brake Power and Torque

Brake torque and brake power are the most important values regarding the engine performance. They indicate the potential of the engine to generate work and the rate at which the work is generated, respectively. They are related through

$$P_B = \omega T_B \tag{B.12}$$

where ω is the rotational velocity of the engine in radians per second. The torque is computed through

$$T_B = F_B \cdot r \tag{B.13}$$

where F_B is the brake force generated by the engine's pistons and r the radius of the rotational motion. In general this parameter is read by a dynamometer, with F_B being the force measured at

the dynamometer arm and r the dynamometer arm length. Torque relates to engine brake work W_B through

$$W_B = \int_{\theta_0}^{\theta_i} T_B d\theta \tag{B.14}$$

where $d\theta$ represents a differential of crank angle degree and $\theta_0$and $\theta_i$are the initial and final crank angle positions of the piston rod.

B.2.2 Brake Specific Fuel Consumption

The fuel consumption of an engine is of great relevance. The amount of fuel being consumed is indicated by the fuel mass flow ($\dot{m}_f$). More relevant than the fuel flow is the fuel flow per unit of brake power. In other words, the amount of fuel needed to produce a kWh of brake work. This measurement is defined as the brake specific fuel consumption (BSFC) and it is given by

$$BSFC = \frac{\dot{m}_f}{P_B} \tag{B.15}$$

This term is often used as a measure of engine's efficiency when the comparison is being made between same fuel operated engines.

B.2.3 Brake Specific Emissions

As in the case of fuel consumption, it is useful to normalize emissions values in order to compare different size engines. Brake specific emission BSχi read in g/kWh and is computed for species i as follows

$$BS_{X,i} = \frac{\dot{m}_{X,i}}{P_B} \tag{B.16}$$

where $\dot{m}_{X,i}$ is the total mass flow of species i which is obtained by

$$\dot{m}_{X,i} = \dot{m}_f \left(1 + \frac{A}{F}\right) \frac{M_i}{M_{exh}} \cdot X_{i,wet} \tag{B.17}$$

$$\frac{A}{F} = \frac{\dot{m}_{air}}{\dot{m}_f} \tag{B.18}$$

where A/F is the ratio of air to fuel ratio at which the engine is being operated. M_i and M_{exh} are the molar mass of species i and exhaust respectively, and $x_{i,wet}$ is the wet volumetric concentration of species i[7] given by

$$X_{i,wet} = (1 - X_{H2O}) \cdot X_{i,dry} \tag{B.19}$$

with $x_{i,dry}$ the dry volumetric concentration of specie i normally measured with a gas analyzer device.

The terms introduced above will be widely use along this work. More terms are defined in literature. However, for simplicity, they will be introduced when they are needed.

[7] Wet concentration regards the volumetric concentration of species on a mixture with water content. On the contrary, dry concentration relates to water free mixtures.

B.3 Internal Combustion Engine Efficiency

In this section, the fundamental concepts behind the performance of IC engines are introduced. For the sake of simplicity and clarity of this report, only the four stroke SI engine will be described. Broader and more detailed information on IC engines can be found in (Heywood, 1988)(Stone, 1999).

The basic purpose of an IC engine is to transform chemical energy, stored in the fuel, into mechanical work. This conversion is achieved through a thermodynamic cycle. In general, the engine performance is assessed based on how much work it is able to deliver (W_B) from a given amount of chemical energy (Q_f). The ratio of these two quantities is denominated Brake Efficiency and is given by

$$\eta_B = \frac{W_B}{Q_f} \tag{B.20}$$

$$\eta_B = \eta_C \cdot \eta_T \cdot \eta_{G.E} \cdot \eta_M \tag{B.21}$$

where Q_f represents the energy contained in the consumed fuel (m_f). The brake efficiency term in Equation B.20 describes how great or poorly an engine performs, although it does not tell the reason why. To be able to improve and develop better and more sophisticated engines, it is crucial to know which are the sources of inefficiencies and which other aspects of the engine are already fully developed. To do so, more variables than just the overall efficiency have to be evaluated.

In Johansson's work (Johansson, 2011), he defines the overall engine efficiency

$$\eta_B = \eta_C \cdot \eta_T \cdot \eta_{G.E} \cdot \eta_M \tag{B.22}$$

In this equation, the engine brake efficiency is broken down into four different terms. Each of them represents a different source of irreversibilities in the energy conversion process.

1. Combustion efficiency η_C.
2. Thermodynamic efficiency η_T.
3. Gas exchange efficiency $\eta_{G.E}$.
4. Mechanical efficiency η_M.

These terms follow in order from the very beginning, the energy contained in the fuel through the entire process, until the very end, the work delivered by the engine.

B.3.1 Mean Effective Pressure

Though efficiency is an effective approach to compare the performance between different engines and operation conditions, the evaluation of different type of energy losses such as heat losses or mechanical losses, cannot be directly achieved by assessing their direct values because they are strongly influenced by the size of the engine. For this purpose, it is useful to normalize with size the different parameters resulting from the engine operation.

The mean effective pressure is the result of normalizing energy parameters with the displacement volume of the engine. Because the displaced volume V_d is a predefined and constant parameter of any engine, it serves greatly to this purpose. Thus, any energy quantity x can be expressed in terms of pressure by

$$xMEP = \frac{x}{V_d} \tag{B.23}$$

where xMEP is the representation of the energy flow x in terms of pressure. Size normalized values allow for the comparison of different energy streams from different engines. Thus, Equation B.20 can be also expressed in the form

$$\eta_B = \frac{BMEP}{FuelMEP} \tag{B.24}$$

where BMEP and FuelMEP are the pressure equivalents for the brake work and the energy contained in the fuel, respectively. They are computed as follows

$$BMEP = \frac{P_b n_c}{V_d \omega} \tag{B.25}$$

$$FuelMEP = \frac{Q_f}{V_d} \tag{B.26}$$

where n_c is the number of revolution per engine cycle, and Q_f is the energy contained in the fuel at each cycle.

Along this report, mean effective pressure equivalents will be used to refer to energy flows, and conclusion are drawn based on these values. An easy conversion to the original values is possible by multiplying by the displacement volume V_d of the engine studied.

For the case of variable displacement engines, V_d is not a predefined parameter. The volume displaced by the engine varies on time at different operating conditions. The brake power (P_B) and torque (T_B) generated by the engine is now dependent on the number of cylinders firing, and thus to compare different points of operation, an extra term is needed, BMEP*. This new definition of brake mean effective pressure accounts for the variable volume displacement in the form

$$V_d{}^* = V_d \cdot F_f \tag{B.27}$$

where F_f is the firing fraction at which the engine is being operated. Although this term is necessary, the conventional definition of BMEP is still of use to compare coherently different engines of this kind. Notice that the BMEP will always be a pressure representation of the engine load, independently of the engine's actual displacement.

BMEP values redefine the load scale. If two engines or the engine's conditions need to be compared, BMEP defines the total energy being delivered by each engine no matter of its actual displacement. Thus, for the same power being delivered, different parameters can be compared.

BMEP* is an equivalent to the net indicated mean effective pressure ($IMEP_N$) which will be explained further in this chapter. It is a representation of cylinder load and thus of engine's

efficiency. For a normal engine, BMEP is both, a representation of load and a representation of efficiency. For variable displacement engines, BMEP cannot be used to evaluate theengine's efficiency, because this value does not account for the deactivated cylinders which do not positively contribute to the power output. Instead, BMEP* considers each cylinder behavior, and adds up the friction losses caused by the disabled cylinders.

The concept of BMEP* can be better understood with the aid of an example in which an8 cylinder engine is first working at its maximum capacity ($P_{100\%}$) and later, at exactly half its capacity ($P_{50\%}$). In the case of throttled operation the first conditions is achieved at wide open throttle (WOT) and thus BMEP reads

$$BMEP_{100\%} = \frac{P_{100\%}\eta_c}{V_8\omega} \tag{B.28}$$

which tells the working pressure at which the engine is operating to produce its maximum power. At half load ($P_{50\%}$), BMEP reads

$$BMEP_{50\%} = \frac{P_{50\%}n_c}{V_8\omega} = \frac{BMEP_{100\%}}{2} \tag{B.29}$$

Again, BMEP communicates the power being delivered by the engine, in this case, half of its maximum. In addition, it also tells the load at which the cylinders are working. Let usnow consider the case of variable displacement under half load conditions. At half load, only 4 of the 8 cylinders need to be active. BMEP reads

$$BMEP_{4cyl} = \frac{P_{4cyl}\eta_c}{V_8\omega} \cong \frac{P_{50\%}\eta_c}{V_8\omega} = \frac{BMEP_{100\%}}{2} \tag{B.30}$$

It shows that the engine, is indeed working at half its load, but it misleads in terms of cylinder working conditions, as it indicates that the working pressure is half its real value. Therefore, BMEP is a good indicator of the engines power generation but not of the engine's working conditions. For the same case, BMEP* reads

$$BMEP_{4cyl}{}^{*} = \frac{P_{4cyl}\eta_c}{V_{4cyl}{}^{*}\omega} \cong BMEP_{100\%} \tag{B.31}$$

which indicates that the working cylinders are working nearly as efficiently as the engine does at full load. The power generated by the set of 4 cylinders is expected to be slightly lower than that of the normal engine at half load because the remaining 4 deactivated cylinders will consume power in the form of friction losses. The reason being that under variable displacement mode the engine works continuously at WOT.

B.3.2 Combustion Efficiency

The first term, η_C in Equation B.21 indicates the effectiveness with which the energy from the fuel is extracted. It is strongly dependent on the type of fuel used, combustion chamber geometry, and combustion temperatures among other parameters (Heywood, 1988)(Stone, 1999). It is expressed as the ratio between the energy released by the combustion event and the total energy contained in the fuel.

$$\eta_c = \frac{Q}{Q_f} = \frac{QMEP}{FuelMEP} \tag{B.32}$$

where Q is the energy released during combustion. The energy contained in the fuel Q_f reads

$$Q_f = m_f \cdot Q_{LHV} \tag{B.33}$$

where m_f is the fuel mass and Q_{LHV} is the lower heating value of the fuel. The energy released during the combustion event can be computed through an energy balance. However, this technique requires numerous assumptions which diminish the accuracy of the results.

Nonetheless, if the emissions before the catalyst are known, the energy lost due to uncompleted combustion can be measured. The useful energy could be inferred from the difference between energy contained in the fuel and the energy lost. If the total amounts of remaining reactants and reaction intermediates (THC), such as remaining fuel or other hydrocarbons are known, the chemical energy leaving the system through the exhaust gases can be written as

$$Q_{loss} = m_f \cdot \left(1 + \frac{A}{F}\right) \sum_{i=1}^{N} \frac{M_i}{M_{exh}} \cdot X_{i,wet} \cdot Q_{LHV,i}\,;\, i = 1, \dots, N_p \tag{B.34}$$

where $Q_{\mathrm{LHV},i}$ is the lower heating value of the different N_p hydrocarbons present in the exhaust stream. Therefore, a good approximation of the energy losses due to incomplete combustion can be obtained from the amount of the most energy dense compounds such as total remaining unburnt hydrocarbons (THC), carbon monoxide (CO) and Hydrogen (H_2). The first two terms are obtained through a 5 gas analyzer device. The last is obtained by approximation with the aid of the water gas shift reaction

$$CO + H_2O \leftrightarrow CO_2 + H_2 \tag{B.35}$$

with equilibrium constant given by

$$K = \frac{X_{CO} X_{H_2O}}{X_{CO_2} X_{H_2}} \tag{B.36}$$

which, for temperatures within 600 to 2000 K, can be approximated (Callaghan, 2006) by

$$\log(K) = -2.4198 + 0.0003855T + \frac{2180.6}{T} \tag{B.37}$$

where T is the temperature of the exhaust, normally around 700 to 1000 K. Normal lower heating values for the aforementioned compounds are shown in table B.1. Notice that the concentration of H_2O is not given by the gas analyzer as it dries the samples first. In order to approximate this value, we balance the chemical equation for the combustion reaction. For methane it reads

$$aCH_4 + b(O_2 + 3.727N_2) \rightarrow cCO_2 + dH_2O + 3.727bN_2 \tag{B.38}$$

To obtain the molar concentration of water

$$X_{H_2O} = \frac{d}{c+d+3.727b} \tag{B.39}$$

Table B.1: Lower Geating Value of CO, H2 and CH4

Compound	Formula	Lower Heating Value (*MJ/kg*)
Methane	CH_4	50.01
Carbon monoxide	CO	10.112
Hydrogen	H_2	119.96

Source: (Callaghan, 2006)

Finally, with all the values available we can normalizing the combustion losses by

$$CLMEP = \frac{Q_{loss}}{V_d} \tag{B.40}$$

The energy available in the combustion chamber can be written then in the form

$$QMEP = FuelMEP - CLMEP \tag{B.41}$$

and thus the combustion efficiency can be expressed as

$$\eta_c = 1 - \frac{CLMEP}{FuelMEP} \tag{B.42}$$

B.3.3 Thermodynamic Efficiency

The thermodynamic efficiency represents the effectiveness with which the engine uses the heat from combustion Q to produce work W_T. The thermodynamic efficiency can be written as

$$\eta_T = \frac{W_T}{Q} \tag{B.43}$$

This conversion is achieved, in an SI engine, through an Otto cycle (illustrated in Figure B.2). This cycle consists of four different processes:

- Adiabatic compression (point 1 to 2).
- Isochoric compression (point 2 to 3).
- Adiabatic expansion (point 3 to 4).
- Isochoric expansion (point 4 to 1).

The total work delivered by the engine over the thermodynamic cycle can be calculated by integrating the pressure function from the start to the end of the cycle.

$$W_T = \int_1^4 p \cdot dV \tag{B.44}$$

Making use of the thermodynamic relationships for adiabatic and isochoric processes, the theoretical efficiency for in ideal Otto cycle can be written in the form:

$$\eta_T = 1 - \frac{1}{{r_c}^{\gamma-1}} \tag{B.45}$$

where γ is the adiabatic index or heat capacity ratio of the working fluid

$$\gamma = \frac{C_p}{C_v} \tag{B.46}$$

and r_c is the compression ratio of the engine which is the ratio between the volumetric capacity of the cylinder $V_{total,c}$ and the combustion chamber volume V_c:

$$r_c = \frac{V_{total}}{V_C} = \frac{V_1}{V_2} \tag{B.47}$$

Figure B.2: Comparison of a Theoretical Air and an Air Fuel Otto Cycle with a Real Otto Cycle

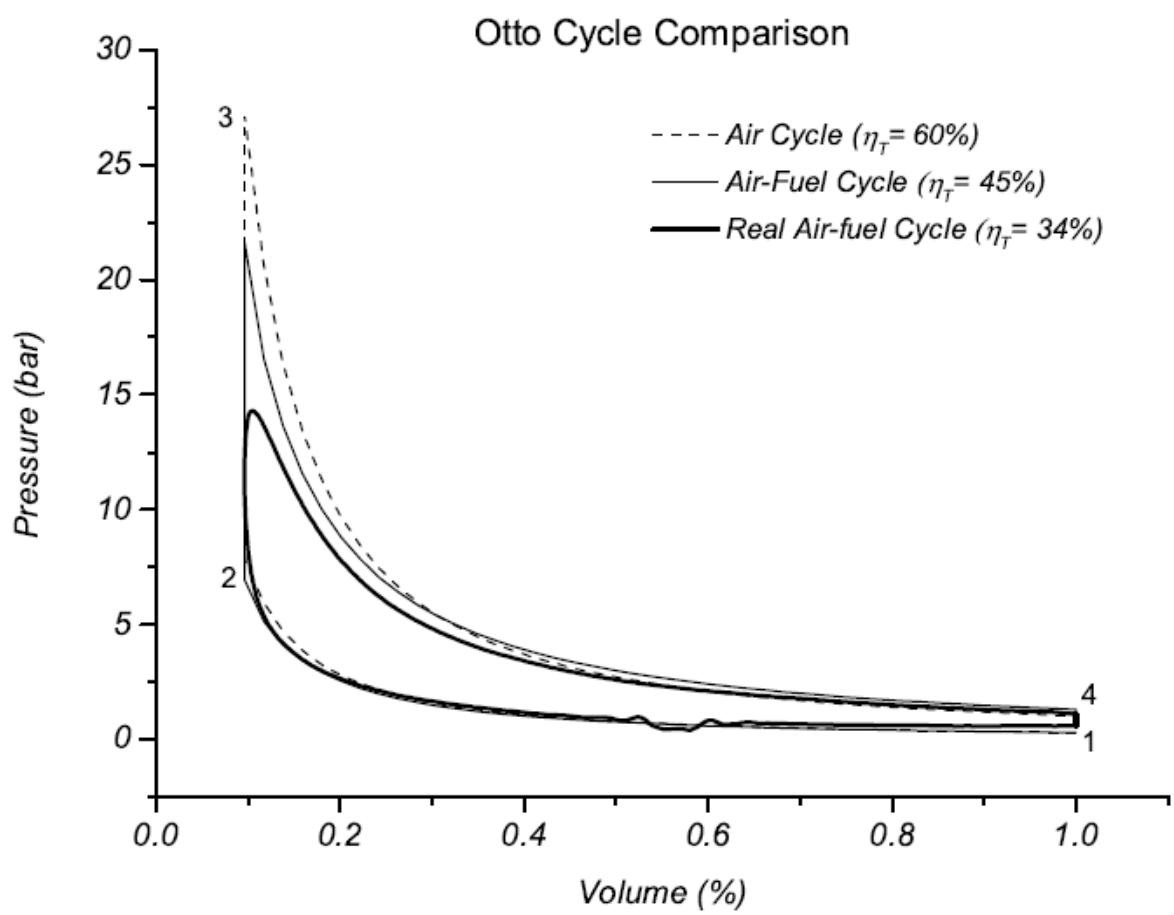

r_c = 10.4:1; A/F = 17; $Q_{2,3}$ = 470 J; $Q_{LHV.CH4}$ = 50 MJ/kg. The real cycle is obtained from an engine operating at 40 kPa intake manifold pressure; 1500 rpm; valve timing advance 40 CAD with respect to standard conditions.

Source: University of California, Berkeley

From Equation B.45 it can be concluded that the thermodynamic efficiency of the engine is only dependent on the working fluid being used ($\gamma_{w.fluid}$) and the compression ratio (r_c) determined by the engine's geometry. A normal SI engine with compression ratio of 10.4 and air (γ_{air} = 1.4) could potentially achieve an efficiency of 60 percent. In reality, such number is not achieved and the engine efficiency falls under the range 25-35 percent. The reasons for such degraded

efficiency are best understood by looking at Figure B.2 where theoretical air and air-fuel cycles are compared with a real engine Otto cycle.

The first source of discrepancy is found in Equation B.45. It assumes the heat capacity at constant pressure C_p to be constant. In reality, C_p varies strongly with temperature and so does γ. If γ is considered temperature independent and constant throughout the process, Equation B.45 holds and the air cycle in Figure B.2 is obtained. Nevertheless if a more accurate approximation is desired, the theoretical model has to account for the variable C_p of the working fluid. Thermodynamic efficiency should then be computed from its original definition

$$\eta_T = \frac{W_T}{Q} = \frac{Q_{2,3} - Q_{4,1}}{Q_{2,3}} \tag{B.48}$$

where $Q_{2,3}$ is the heat added to the cycle at constant volume, and $Q_{4,1}$ is the thermal energy remaining in the fluid after the cycle is completed. These parameters are found through

$$Q_{x,x_0} = m_{fluid}\left(C_{v,x}T_x - C_{v,x_0}T_{x_0}\right);\ C_{v,x} = C_{p,x}(T) - R_{fluid} \tag{B.47}$$

where R_{fluid} is the specific gas constant of the fluid and C_v is the heat capacity of the fluid at constant volume. x and x_0 represent initial and final states of the fluid. Discrepancies also arise from C_p being a property of each gas and therefore changing with the different mixture composition gases. In reality, for a port injected engine, the working fluid is not pure air but a mixture of fuel and oxidizer. Consequently the heat capacity of the working fluid is not one of air but of the mixture air-fuel.

$$C_{p,mix}(T) = \frac{\sum_i C_{p,i}(T) \cdot m_i}{\sum_i m_i} \tag{B.48}$$

Moreover, along the process, the species present in the gases changes owing to the combustion reaction influencing the heat capacity. A more accurate model should account for heat capacity changes with temperature and species. The model for the air-fuel cycle is shown in Figure B.2. The cycle represented by a thin solid line is the result of considering an air-fuel mixture where the γ of the mixture is the result of using the mass weighed average of the air and fuel heat capacity, both temperature dependent. With this new approach, the calculated theoretical efficiency of the cycle is reduced from 60 percent to 45 percent approximately.

a. Because of the high temperatures reached by the gases during combustion, the temperature gradient between the gas and the cylinder wall accentuates, thus enhancing heat flow through the cylinder wall. These type of losses are more noticeable in small engines where the area to volume ratio of the cylinder is bigger and so is the heat transfer.

b. Another source of loss is the heat escaping with the exhaust gas. Because the gases have to be withdrawn from the cylinder, the pressure in the cylinder should no go below atmospheric. Though this measure sacrifices work, it reduces the need for pumping the exhaust gases. The exhaust valve opens (EVO) before bottom dead center (BDC) and full expansion is not achieved. Consequently, hot exhaust escapes the cylinder.

c. A third limitation exists for the real engine cycle. Because the flame speed of common

fuels is not infinitely high, the combustion event takes longers than desired and it is still ongoing when the piston is on its way down, past top dead center (TDC). The addition of heat does not occur completely at constant volume, preventing pressure from reaching its possible maximum.

Similarly to the combustion process, the different energy flows occurring during the thermodynamic cycle can be written in terms of mean effective pressure.

The gross indicated (per cylinder) work generated over the course of the compression and power strokes writes:

$$IMEP_G = \frac{W_T}{V_d} \tag{B.49}$$

The thermodynamic losses are defined by:

$$QLMEP = \frac{Q - W_T}{V_d} \tag{B.50}$$

With all these considered, the thermodynamic efficiency can be written in the form:

$$\eta_T = \frac{QMEP - QLMEP}{QMEP} = \frac{IMEP_G}{QMEP} \tag{B.51}$$

where QMEP is the energy available after combustion.

B.3.4 Gas Exchange Efficiency

While the ideal thermodynamic cycle consists of four processes, a real four stroke (4S) engine cycle follows six. The intake and exhaust strokes carry out the breathing of the engine, while the compression and power stroke realize the Otto Cycle. The two extra strokes consume piston work which otherwise could have reached the crankshaft as occurs in a two stroke engine. Therefore, a difference is made between the total work exerted by the piston ($IMEP_G$), and the work available to spin the crankshaft, the net indicated work $IMEP_N$.

$$IMEP_N = IMEP_G - PMEP \tag{B.54}$$

where PMEP represents the work consumed by the piston to pump fluid in and out of the cylinder.

The meaning of PMEP can be better understood with the aid of Figure B.3. The shadowed area represents the pumping work consumed by the piston and the white area is the real work delivered by the piston. Following Equation B.54 the subtraction of the shadowed area from the white area results in the net work delivered by the cylinder. This difference between gross and net work is accounted in the gas exchange efficiency which indicates how efficiently the breathing is carried out.

$$\eta_{GE} = \frac{IMEP_N}{IMEP_G} \tag{B.55}$$

Figure B.3: Real Engine Operation

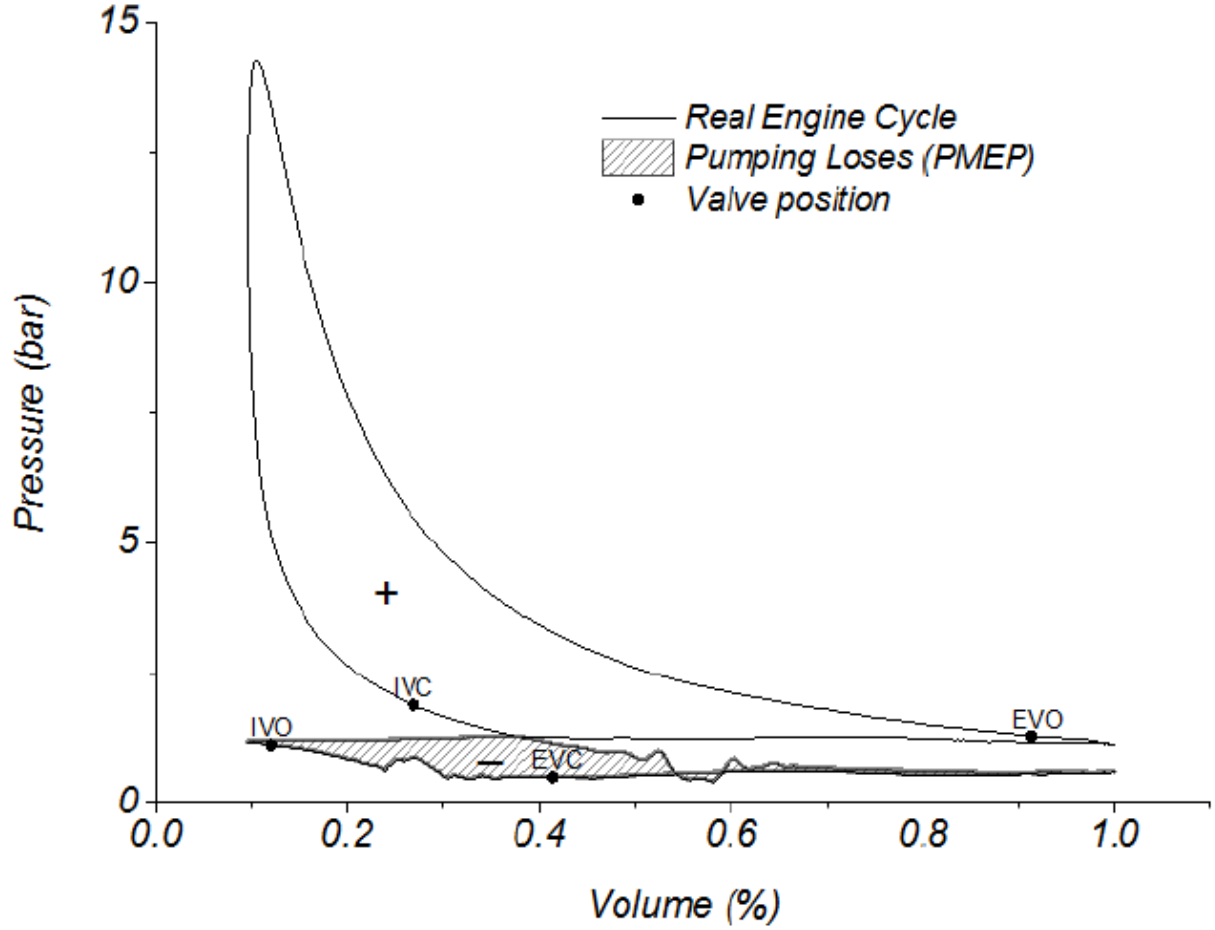

Engine operating at 40 kPa intake manifold pressure with +40 CAD CAM phasing. The shadowed area represents the energy losses due to the breathing process in the engine.

Source: University of California, Berkeley

The overall pumping loss on the cylinder (PMEP) is the combination of the intrinsic pumping work needed ($PMEP_{pump}$) and the pressure drop created across the valves ($PMEP_{valves}$)

$$PMEP = PMEP_{pump} + PMEP_{valves} \tag{B.56}$$

The first term represents the energy consumed by the piston to bring a certain amount of fluid, from an initial state at pinlet to a final state at poutlet. Figure B.4 illustrates the concept. The intake pressure (pinlet) is the pressure at the start of the compression stroke (◎180oCAD); the exhaust pressure is the pressure at which the fluid fronts the exhaust stroke (180oCAD). The pumping work is the rectangular area enclosed by both these asymptotes, from exhaust to intake BDC stroke (V_d):

$$W_{pump} = \int_{180}^{-180} pdV = (p_{exhaust} - p_{intake})V_d \tag{B.57}$$

$$PMEP_{pump} = p_{out} - p_{in} \tag{B.58}$$

Figure B.4: Concept of –MEP Values in Internal Combustion Engines

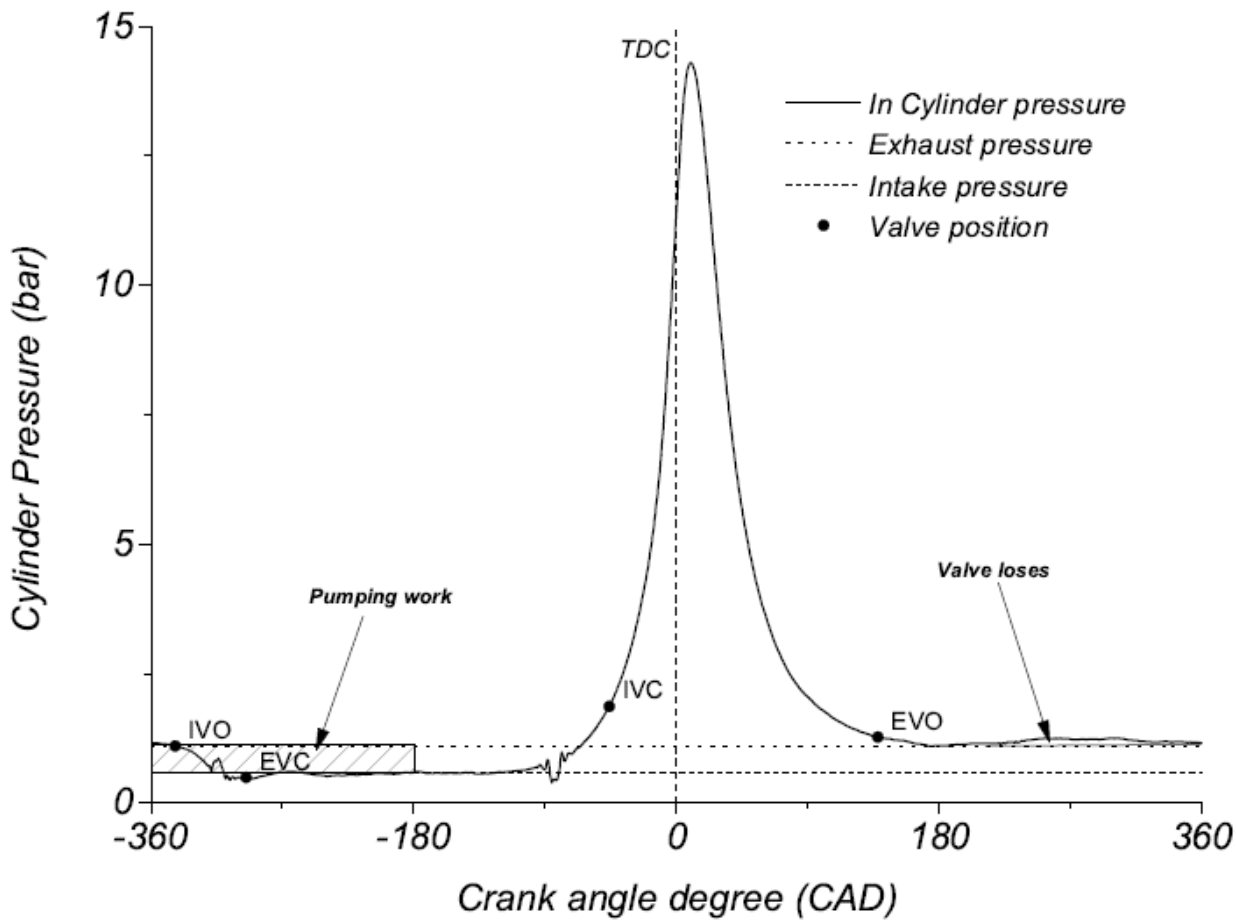

Source: University of California, Berkeley

The second term in Equation B.56 identifies the extra energy needed to overcome the pressure drop that inlet and outlet valves cause across them. This pressure drop is substantially higher at high loads when the mass flow is high, and barely noticeable at low loads. Because the cross sectional area is constant, velocity increases linearly with load thus causing the pressure drop across the valves to increase. Valve pressure losses are minimal in Figure B.4 because of the combination of optimum cam timing and low load (40 kPa manifold pressure). The overall pumping loss in the cylinder PMEP is easy to obtain by integrating the cylinder pressure trace over the intake and exhaust stroke (shadowed area in Figure B.3). The valves losses are then obtained by

$$PMEP_{valves} = PMEP - PMEP_{pump} \tag{B.59}$$

The gas exchange or breathing efficiency can then be written

$$\eta_{GE} = \frac{IMEP_G - PMEP}{IMEP_G} \quad \text{(B.60)}$$

B.3.5 Mechanical Efficiency

The energy produced by the piston is not yet reaching the crankshaft. While the piston is being actuated, shear forces appear between the piston and the cylinder. This shear stress consumes part of the power the piston is producing and therefore the overall efficiency is even lower than expected. Besides the friction caused by the piston-cylinder group, other components also sum to the mechanical work being consumed, i.e. the valve train, consisting of sliding connection rods, camshaft and rockers consume power from the engine to actuate, generating friction forces as well. Also the distribution belt, which transmits power from the shaft to actuate the auxiliaries, such as air conditioning and alternator, consumes power reaching the crankshaft. All this power consumed by the aforementioned activities is included in the term:

$$FMEP = \frac{W_{rf} + W_{aux}}{V_d} \quad \text{(B.61)}$$

where W_{rf} refers to rubbing friction work and W_{aux}, to the work consumed by the auxiliary systems. Although FMEP takes into consideration auxiliary components, friction losses refers to the energy lost owing to shear stresses over the bearing components. Figure B.5 illustrates the main influencing factor on the generation of friction. The coefficient of friction is plotted against the Sommerfeld number:

$$S = \frac{\mu v_p}{p} \quad \text{(B.62)}$$

which relates μ the absolute viscosity of the lubricant fluid, the velocity of the moving piston v_p, and p the pressure over the bearing area.

Friction work should be computed as:

$$W_{rf} = \int F_{rf} dx;\ F_{rf} = f(\mu, v, p) \cdot N \quad \text{(B.63)}$$

where f is the coefficient of friction and N the normal forces to the bearing surface. Because W_{rf} is not easy to measure with experimental devices, the following strategy is followed:

$$FMEP = IMEP_N - BMEP \quad \text{(B.64)}$$

where BMEP, as mentioned in Section B.3.1, refers to the work delivered to the client end of the crankshaft (measured easily with a dynamometer) and $IMEP_N$ refers to the net indicated work.

Figure B.5: Striebeck Diagram

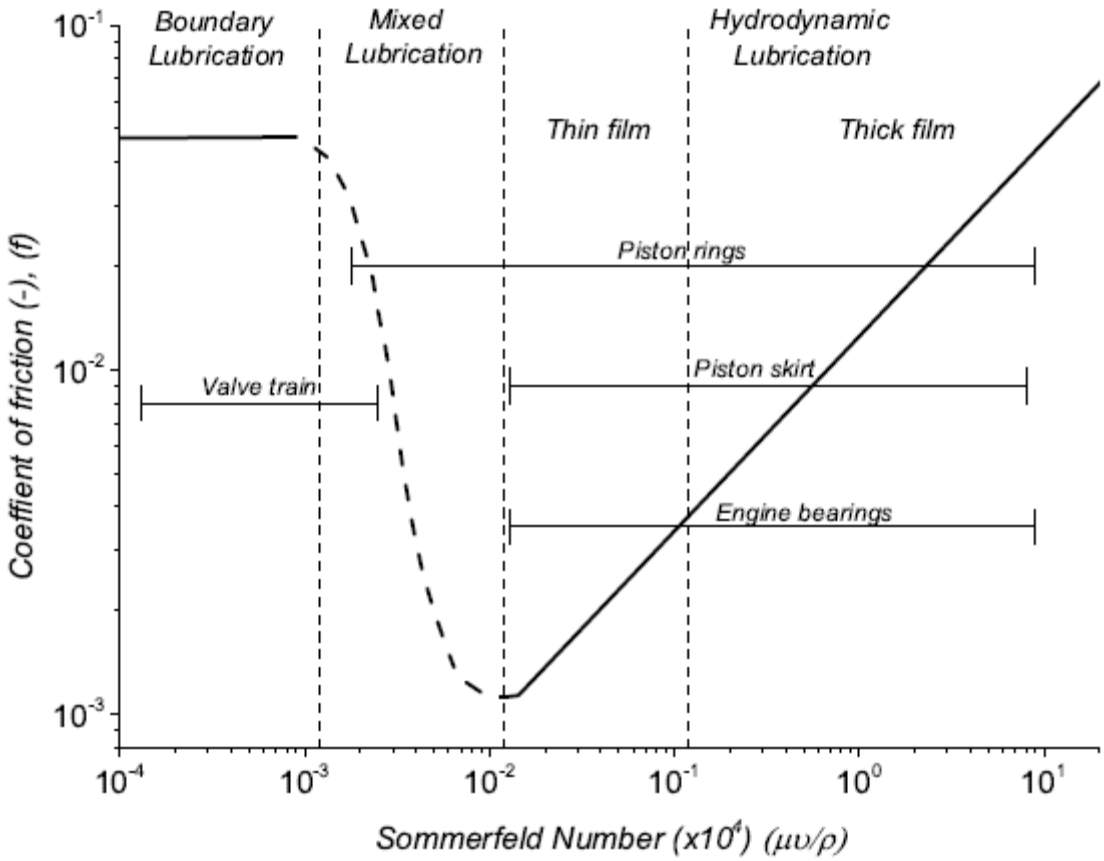

Coefficient of friction is plotted against the Sommerfield number. The overall coefficient of friction results from the sum of hydrodynamic friction and solid friction, projecting different regimes of influence at different engine epeeds. Boundary Regime: mainly solid friction. Mixed Regime: progressive reduction and increment of solid and hydrodynamic solid friction. Hydrodynamic Regime: mainly hydrodynamic friction.

Source: (Stone, 1999)

The mechanical efficiency indicates how well manufactured an engine is, in terms of surface machining. It is defined as:

$$\eta_M = \frac{BMEP}{IMEP_N} = \frac{IMEP_N - FMEP}{IMEP_N} \tag{B.65}$$

Friction losses are normally accentuated with engine load as shown in Figure B.5; i.e an engine at high load will lose more power within the piston-cylinder system than at low load. Similarly, a boosted engine will lose more power through friction than an air aspirated one because the pressure over the bearing surfaces increases. In the same line, higher engine speed (ω) causes an increase in friction losses because of higher linear velocity (υ_p). Even more than velocity and load, the viscosity of the lubricant (μ) influences the friction of the engine. Because this parameter is strongly dependent on temperature and thus on engine operating conditions,

specific lubricants are chosen for different engine conditions. Figure B.6 shows an example of different lubricant behaviors.

Figure B.6: Multi-grade Lubricant Oil Sensitivty with Temperature

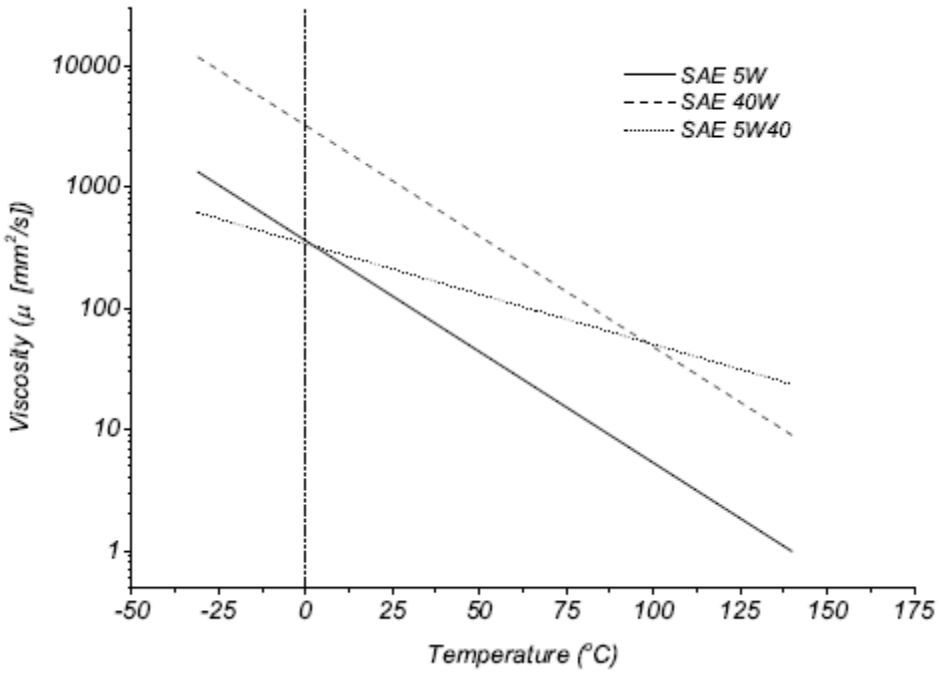

Source: University of California, Berkeley

Multi-grade oil such as 5W40 shown in Figure B.6 helps keep the oil viscosity relatively constant along a wide range of temperatures, thus reducing the influence of environmental conditions on the engine performance. The mechanical efficiency of an engine will normally vary from 0 to a given value, determined by the manufacturing of the components. It is clear that at idle, the mechanical efficiency reaches 0 because the energy generated is exactly the energy needed to overcome the bearing friction. The maximum efficiency is found at the range in which the Sommerfeld number approaches 10^{-2} as can be seen in Figure B.5.

B.3.6 Engine Brake Efficiency

As a result of all the phenomena introduced in previous sections, the end work produced by the engine (*BMEP*) is considerably less than the energy contained in the fuel. Introduced in Section B.3, the overall engine efficiency:

$$\eta_B = \frac{BMEP}{FuelMEP} \tag{B.66}$$

The values for BMEP are obtained by following the example used in Figure B.3. The brake efficiency of the engine is 14 percent at those specific conditions (highly throttled engine, manifold air pressure (MAP): 40 kPa). On average, the IC engine brake efficiency seats around 25

to 35 percent. A summary of the different terms is presented in Figure B.7. Notice that under DSF conditions, the brake efficiency should be computed as follows:

$$\eta_B = \frac{BMEP^*}{FuelMEP} \tag{B.67}$$

where BMEP* is the equivalent of BMEP for variable volume displacement engine conditions.

Figure B.7: Summary of the Different Energy Flows, Losses, and Efficiency Terms

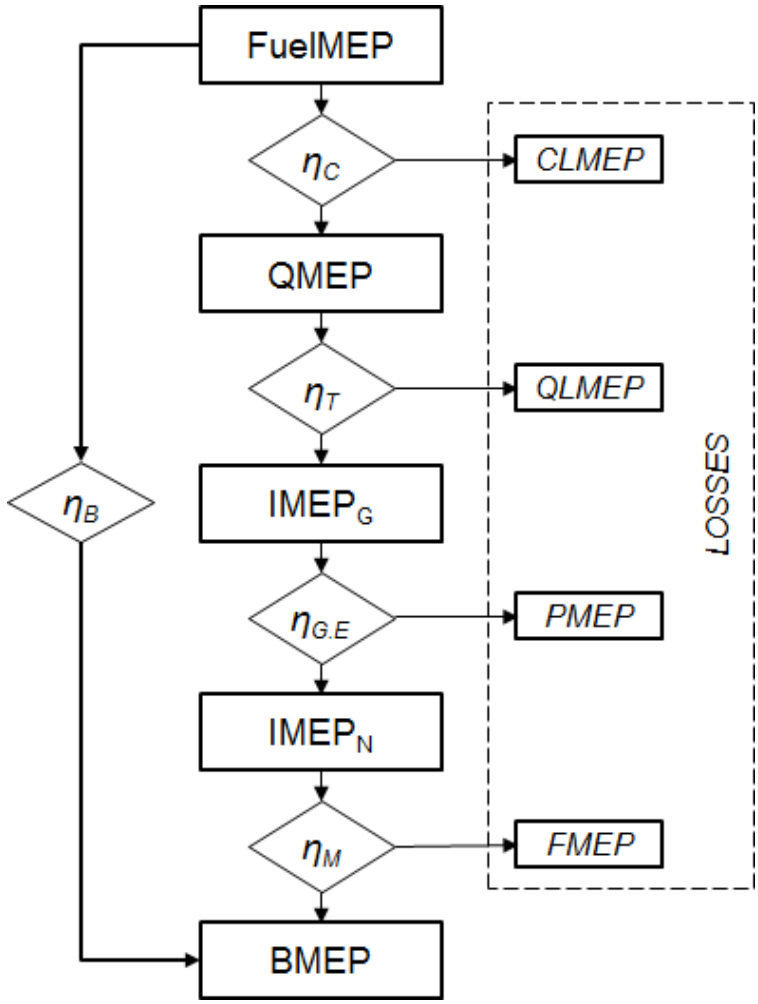

Source: (Johansson, 2011)

In conclusion, for the brake efficiency to improve, each of the inefficiencies of the engine must be reduced. This is achieved through different technological solutions. Nevertheless, there is not yet any technology capable of reducing all inefficiencies simultaneously, and thus a combination of strategies is needed to obtain effective efficiency improvements. In summary, the further development of an engine passes through:

a. Improving the combustion process through reducing reaction quenching, combustion incompleteness, dissociation of products, and combustion speed.

b. Increasing the adiabatic index of the mixture, i.e. through better fuels or working fluids; reduction of heat transfer through the walls, increment on the effective compression ratio.

c. Reduction of pumping work through a better breathing process. Avoid engine's part load regimes. Reduce flow losses across breathing valves.

d. Better machining of the engine block, reduce bearing surface, improve lubricants properties.

This report is focused on the third ($\eta_{G.E}$) of the four different efficiency factors. Nevertheless, each of the different terms is evaluated to understand the side effects that an improvement in gas exchange efficiency can have on the rest of the engine's processes. The technology here presented can well benefit from the company of other known strategies for the reduction of gas exchange inefficiencies. Technologies such as variable valve timing (VVT) (Parvate-Patil et al., 2003) (Unger, Schwarz, Schneider, & Koch, 2008) (Cleary & Silvas, 2007) and lift, turbocharging (Arnold et al., 2005) (Allard, 1986)(N. A. Watson & Janota, 1982), direct injection (DISI) (Yang & Anderson, 1998) and stratified charge are examples of strategies, which could form synergy with dynamic skip fire. Osman Akin Kutlar, in his work (Kutlar et al., 2005), summarizes a few of the major technologies which are in the forefront of engine development for the improvement of mainly, but not only, gas exchange efficiency. Such technologies will be further explained in this work when needed for clarity or discussion.

B.4 The Combustion Analysis System

With the purpose of analyzing the engine performance introduced in Section B.3, integral engine measurement are required to monitor the thermodynamic state of the gas during the engine cycle. The thermodynamic state of the gas trapped in the cylinder can be deduced by the equation of gases

$$Pv = ZRT \quad R = 8.3144 \frac{J}{Kmol} \tag{B.68}$$

where Z is the compressibility factor which reduces to 1 at low ρ_{gas} when the gas can be consider ideal (Cengel & Boles, 2001). Therefore, by means of two state variables (i.e. p, T, ρ, h...) the state of the gas is known. As we have seen in Section B.1, the volume (V) can be deduced from the angular position of the crankshaft[8] (θ) through Equation B.5. Either temperature or pressure within the cylinder would then be sufficient to derive the thermodynamic state of the gas and thus the thermodynamics characteristics of the process such as W_T, Q and ΔU. Nevertheless, the temperature (T) within the cylinder is not homogeneous inside the cylinder, and gradients exist on all three geometric dimensions because it strongly depends on the thermal conductivity, diffusivity and motion of the gas. Unlike the temperature, the pressure (p) propagates at the speed of sound (Kundu, Cohen, & of Technology, 2011).

$$c = \sqrt{\gamma R_s T} \tag{B.69}$$

[8] The crankshaft position is known via an encoder device A.3.

which for the time scale at which the samples are taken[9], it is fast enough to inform on the overall pressure within the cylinder at any time. Therefore, with an in-cylinder pressure transducer this property can be measured. Details on the filtering and processing of this signal can be found in (Thiem, 2013).

B.4.1 In-Cylinder Pressure

The pressure is measured with a piezoelectric sensor whose signal represents a random p_s unreferenced signal. As the pressure measurement is not absolute, an initial state p0 is needed to obtain the absolute pressure value p. The process of coupling the sensor pressure measurement ps to the absolute initial pressure p0 is often referred as pegging of the pressure signal (Lee, Kwon, Sunwoo, & Yoon, 2007) (R. S. Davis & Patterson, 2006)(Fanelli, Camporeale, & Fortunato, 2012).

The initial pressure is normally measured by an atmospheric pressure transducer installed at the intake runner of the cylinder. This method is known as inlet pressure referencing(Lee et al., 2007). However, due to budget limitation these sensors were not available and the pegging was carried outthrough the "three-point polytropic pegging" method. A detailed description on this method is found in Lee's work (Fanelli et al., 2012). A simplified description of the method is given here.

Because the compression and expansion strokes are not adiabatic, as explained in Section B.3.3 the behavior of the cylinder charge is better approximated by a polytropic process which obeys

$$PV^k = P(\theta)V(\theta)^k = C \tag{B.70}$$

with k the polytropic index, which equals γ for an adiabatic process and C represents a constant value. The pressure transducer provides $p_s(\theta)$ which can be written based on absolute pressure

$$p_s(\theta) = m \cdot p(\theta) + \Delta p \tag{B.71}$$

where m and Δp are the gain of the sensor (calibration) and Δp a pressure offset. Discretizing over the sample time in terms of crank angle Equation B.69 reads

$$p(\theta_2)V(\theta_2)^k = p(\theta_1)V(\theta_1)^k \tag{B.72}$$

Considering three different samples at θ_1, θ_2, θ_3 a relation can be obtained by combining Equations B.70 and B.71

$$\Delta p = \frac{p_s(\theta_1) - p_s(\theta_2) \cdot [V(\theta_2)/V(\theta_1)]^k}{1 - [V(\theta_2)/V(\theta_1)]^k} \tag{B.73}$$

$$\frac{p_s(\theta_2) - p_s(\theta_1)}{p_s(\theta_3) - p_s(\theta_1)} = \frac{[V(\theta_1)/V(\theta_2)]^k - 1}{[V(\theta_1)/V(\theta_3)]^k - 1} \tag{B.74}$$

for which k cannot be computed analytically and is obtained through a Taylor series expansion with k_0 being an original approximation.

[9] Measurements are taken every 0.5 crank angle of degrees which at a maximum speed of 3000 rpm, translate to a sampling rate of 36 kHz.

$$k = k_0 + Z_1 \cdot \left[\frac{p_s(\theta_2) - p_s(\theta_1)}{p_s(\theta_3) - p_s(\theta_1)} - Z_2\right] \tag{B.75}$$

with

$$Z_1 = \frac{K^{k_0} - 1}{J^{k_0} \cdot \ln(J) - Z_2 \cdot K^{k_0} \cdot \ln(K)} \tag{B.76}$$

$$Z_2 = \frac{J^{k_0} - 1}{K^{k_0} - 1} \tag{B.77}$$

$$J = \frac{V(\theta_1)}{V(\theta_2)} \tag{B.78}$$

$$K = \frac{V(\theta_1)}{V(\theta_3)} \tag{B.79}$$

The values θ_1, θ_2, θ_3 are points for which the pressure measurement is possible and the polytropic approximation holds. For this reason, the above points must be chosen before combustion is triggered (IT), while the pressure can yet be modeled through the polytropic index k and when the conservation of mass hold, after the inlet valve has closed (IVC). As a consequence, when the IT is advanced, close to IVC, the selection of θ_1, θ_2, θ_3 is restricted to a small arc $\Delta\theta$, so the pressure can no longer be accurately acquired.

Similarly to the compression stroke, the gases trapped in the cylinder after combustion follows a polytropic expansion behavior during the expansion stroke. This is model by Equation B.69.

Applying logarithms on both side of the equation it reads:

$$\log(P) + klog(V) = \log(C) = C' \tag{B.80}$$

$$\log(P) = C' - k\log(V) \tag{B.81}$$

where k is the negative slope of a linear equation. Therefore, by means of a linear fit of the form

$$y = mx + n \tag{B.82}$$

over a subset of pressure ($p(\theta_i)$) and volume ($V(\theta_i)$) samples, C′ is obtained as n and consequently, k = m.

Moreover, the peak pressure ($p_{max}(\theta_{max})$) found during the combustion event is computed through a polynomial fit of order 2 around the a subset of samples (n_θ) chosen around the maximum pressure sample acquired.

$$p_f = c_0 + c_1 x + c_2 x^2 \tag{B.83}$$

where c_0, c_1, c_2 are the polynomial coefficients, obtained through a least square minimization. The location where the maximum pressure occurs (θ_{max})is found where the gradient of Expression 102 is zero.

$$\frac{dp_f(\theta_{\max})}{d\theta} = 0 \tag{B.84}$$

and thus $p_{max}(\theta_{max})$ is obtained by substituting θ_{max} in Equation B.82.

B.4.2 Heat Release and Combustion Timing Characterization

In order to compute the heat release rate $\dot{Q}(\theta)$, first we need to known the mass of fuel and air within the cylinder and the temperature profile along the cycle. The first term, the cylinder mass (m_{cyl}) can be determined by considering the cylinder as the control volume where the conservation of mass holds.

$$\frac{\partial p}{\partial x} + (\nabla \cdot pv) = 0 \tag{B.85}$$

which can be simplified given that the mass balance is realized during the period over which both, inlet and outlet valves remain closed, and so no incoming or outgoing flow is taking place. Nevertheless, a little amount of gas escapes the cylinder through space existing between the cylinder and the piston. This phenomenom is denominated blowby (Merker, Schwarz, Stiesch, & Otto, 2006)(Heywood, 1988). The blowby mass which escapes the cylinder m_{bb} is approximated by the 1 percent to 2 percent of the total mass initially in the cylinder $m_{cyl,0}$. The conservation of mass then reads

$$\frac{\partial m_{cyl}}{\partial x} = -\dot{m}_{bb} \tag{B.86}$$

integrating over the complete cycle, from the closing of the inlet valve (IVC) to the exhaust valve opening (EVO) the effective mass on the cylinder reads

$$m_{e,cyl}(\theta) = m_{cyl,0} - m_{bb}(\theta) \tag{B.87}$$

where $m_{bb}(\theta)$ relates to cylinder pressure (Malagi, 2012) through

$$m_{bb}(\theta) = \int Cp^2(\theta)d(\theta) \tag{B.88}$$

where C is a constant value derived based on a given percentage of blowby effect $m_{bb} = 1$ percent. As $p(\theta)$ is known, the mass on the cylinder ($m_{e,cyl}(\theta)$) can be simply derived by considering

$$m_{e,cyl}(\theta) = m_{cyl,0} - m_{bb}(\theta) = m_{cyl,0} - \int Cp^2(\theta)d(\theta) \tag{B.89}$$

with

$$m_{cyl,0} = \frac{pV}{R_s T} \tag{B.90}$$

where R_s is the specific gas constant of the stoichiometric mixture of methane and air, and p, T, and V are taken at θ_{IVC}.

With the in-cylinder mass profile, the average in-cylinder temperature is given by

$$T(\theta) = \frac{p(\theta)V(\theta)}{m_{e,cyl}(\theta)R_s} \tag{B.91}$$

Finally the heat release rate can be computed through an energy balance over the cylinder as follows

$$\frac{dU}{d\theta} = -p\frac{dV}{d\theta} + \frac{dQ_G}{d\theta} - \frac{dQ_w}{d\theta} - h_{bb}\frac{dm_{bb}}{d\theta} \tag{B.92}$$

where the term $\frac{dQ_G}{d\theta}$ stands for the gross heat release rate, $\frac{dQ_w}{d\theta}$ is the heat loss through the wall, and $h_{bb}\frac{dm_{bb}}{d\theta}$ is the energy escaping within the blowby mass flow $\dot{m}_{bb}$.

The right hand side of Equation B.91 can be solved with the first law of thermodynamics

$$dU = dh - pdV \tag{B.93}$$

where h is the mean specific enthalpy of the fuel-air mixture which is dependent on $T(\theta)$ and $C_p(T(\theta))$. A pragmatic approach to compute the variable mixture's heat capacity is to refer to the molar heat capacities, which can be easily obtained through the NASA polynomial[10] (Gardiner & Burcat, 1984)

$$C_p = \frac{C_{p,mol}}{M} \tag{B.94}$$

where M is the mean molar mass of the fuel-air mixture. With $C_p(T(\theta))$, $p(\theta)$, $V(\theta)$ all therms in Equation B.91 except the heat losses through the wall can be computed.

This last term is normally computed in engine applications through the Modified Woschni heat loss model (Merker et al., 2006). However, because the dynamometer used in our setup is an edddy type dynamometer, the Hohneberg heat loss model was used instead because it does not requires a motorized pressure trace. The general expression for heat transfer

$$\dot{Q}_W = UA_W\Delta T \tag{B.95}$$

where U is the overall heat transfer coefficient, A_W is the cylinder wall area and ΔT is the temperature gradient across the wall. Hohenberg defines U for a reciprocating IC engine as follows

$$U = \frac{C_d {P_c}^{0.8}(\bar{s}_p+1.4)^{0.8}}{{\bar{s}_p}^{0.06}T^{0.4}} \tag{B.96}$$

where C_d is often given the numerical value of 130 (X. Wang & Stone, 2008). Therefore, the heat loss rate is given by

$$\frac{dQ_w}{d\theta} = U(V,T,p)(A_W(\theta)(T(\theta) - T_W) \tag{B.97}$$

With all the terms in Equation B.91, the gross heat released (Q_G) is finally obtained. Known the instantaneous heat release rate, the cumulative heat release can be easily derived by integration.

From the cumulative gross heat release the combustion timing is characterized by the terms CA_{SOC}, CA_{10}, CA_{50}, CA_{90}, and CA_{EOC} which represent the crank angles at which 3 percent, 10 percent, 50 percent, 90 percent and 97 percent of the total heat on the fuel have been released, respectively. A more detailed explanation on the combustion analysis system for this project is found in (Thiem, 2013).

[10] http://www.me.berkeley.edu/gri_mech/data/nasa_plnm.html

APPENDIX C:
Benefits and Drawbacks of CNG for Automobiles

In an effort to both improve fuel economy and meet GHG emissions standards, the automotive industry is looking into new fuels which bring carbon dioxide emissions down while maintaining good engine performance and side NO_x, CO, and UHC emissions low (Gautam et al., 2012). CNG is, thanks to its lower C/H ratio and low cost, a real alternative to compete with gasoline fuel.

Recent studies updated the data and show the effect that different fuels parameters have on the engine efficiency (Ayala, Gerty, & Heywood, 2006). CNG's properties help realize major improvements towards high efficiency engine operation by extending the limits for optimization of factors with significant impact on combustion (Maji et al., 2000) (Ayala & Heywood, 2007).

Figure C.1: Effect of Lambda Ratio and Compression Ratio r_c on Efficiency

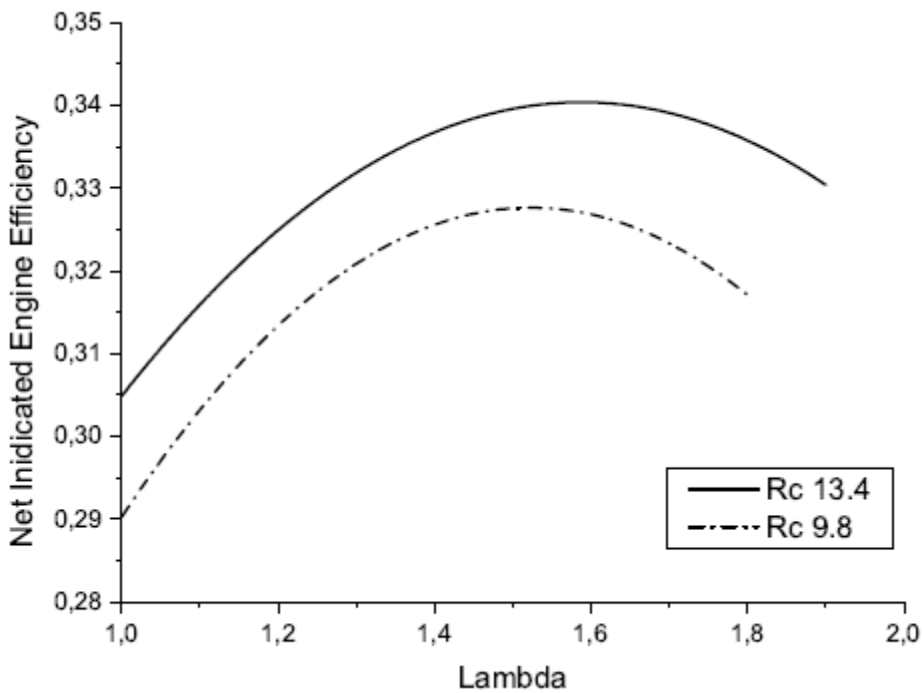

Maximum Brake Torque (MBT) timing = 1500 rpm, Indolene (primary fuel reference PFR)

Source: (Ayala et al., 2006)

A substantial increment on efficiency can be achieved by tuning the engine for optimum air to fuel ratio operation, load, and pressure conditions. The effect that the air to fuel ratio has over the SI engine performance is characterized by a parabolic curve which peaks far lean from stoichiometric ($\lambda = 1$) conditions as shown in Figure C.1. The reasons being the thermodynamic influence that specific heat has on the adiabatic index (γ), which grows with higher air fractions, and the reduction on pumping work owing to reduced throttling. Heat losses to the walls are

also reduced due to lower combustion temperatures which occur for gasoline combustion at leaner than 1.2 equivalence ratio mixtures as can be seen in Figure C.2.

The benefit of running on fuel lean conditions, also known as lean burn conditions, can even be further enhanced by increasing the compression ratio of the engine. This action shifts the efficiency curve to peak at even leaner mixtures as seen previously in Figure D.1 and C.1. This can be attributed to an increase of the mass burning rate which results in faster energy release and reduces heat transfer to the wall. It is important to notice that increasing combustion pressures directly downgrades laminar flame speed as depicted in Figure C.3, but the mass of fuel being burned has increased in a higher proportion, due to the increased density of reactants. Besides, at higher compression ratios, higher temperatures are reached during the compression stroke increasing the reaction rates.

Figure C.2: Effect of Mixture Strength on Laminar Flame Speed and Adiabatic Flame Temperature for Methane and Commercial Gasoline

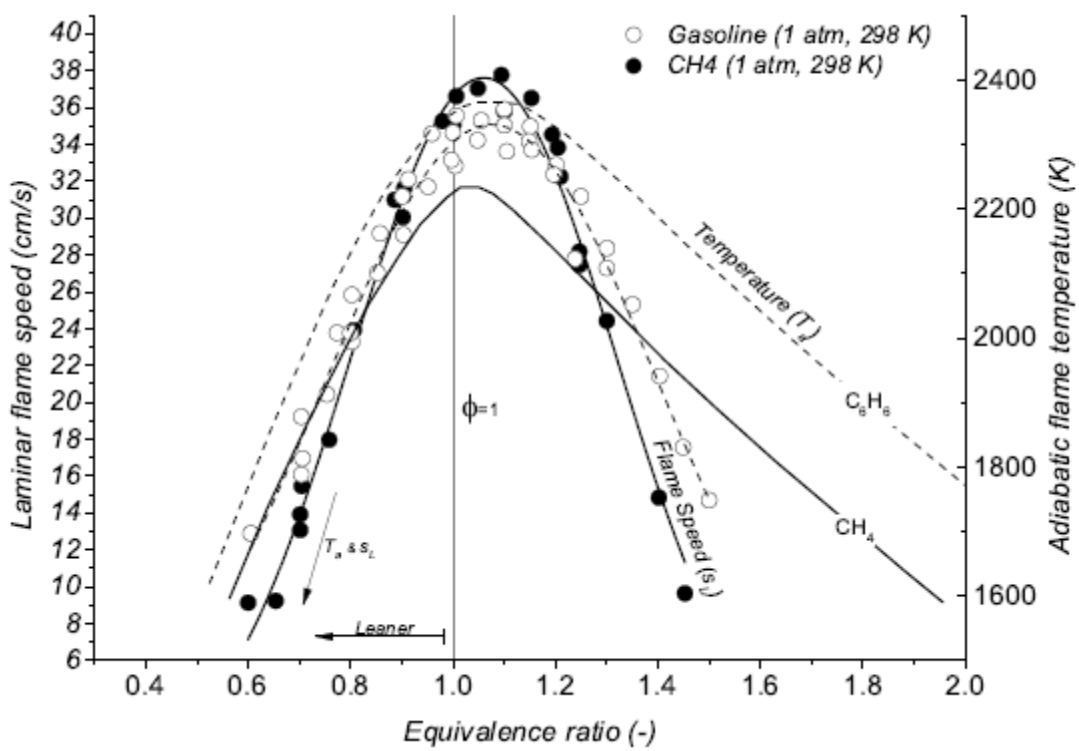

Source: (Jerzembeck, Peters, Pepiot-Desjardins, & Pitsch, 2009; Law, Makino, & Lu, 2006; Sileghem et al., 2013)

Although high compression ratios are desired, often the fuel characteristics present a constraint to the integration of such measure. A too high compression ratio may cause the mixture of fuel-oxidizer to auto or self-ignite before the spark has been fired. This early ignition increases the pressure in the cylinder at an undesired point, increasing work exerted by the piston during the compression stroke. This phenomena is referred as knocking and it limits SI engines' performance. Fuels with higher resistance to auto-ignition are thus desired. This property is defined as the research octane number of the fuel (RON). The scale is built up from n-Heptane (low resistance to self-ignition) to iso-Octane (high resistance to self-ignition). A RON value of 70

means a ignition resistance equivalent to that of a mixture of 70 percent iso-Octane and 30 percent n-Heptane. The RON for various common engine fuels is shown in table C. Today's automotive fuels rank within 80 to 100 in the RON scale. In the same way, Toluene and Methane stand out for their really high RON numbers, and they could potentially extend the knock limit of SI engines.

Figure C.3: Effect of Burning Temperature and Pressure in the Laminar Flame Speed of Methane-Air Mixtures

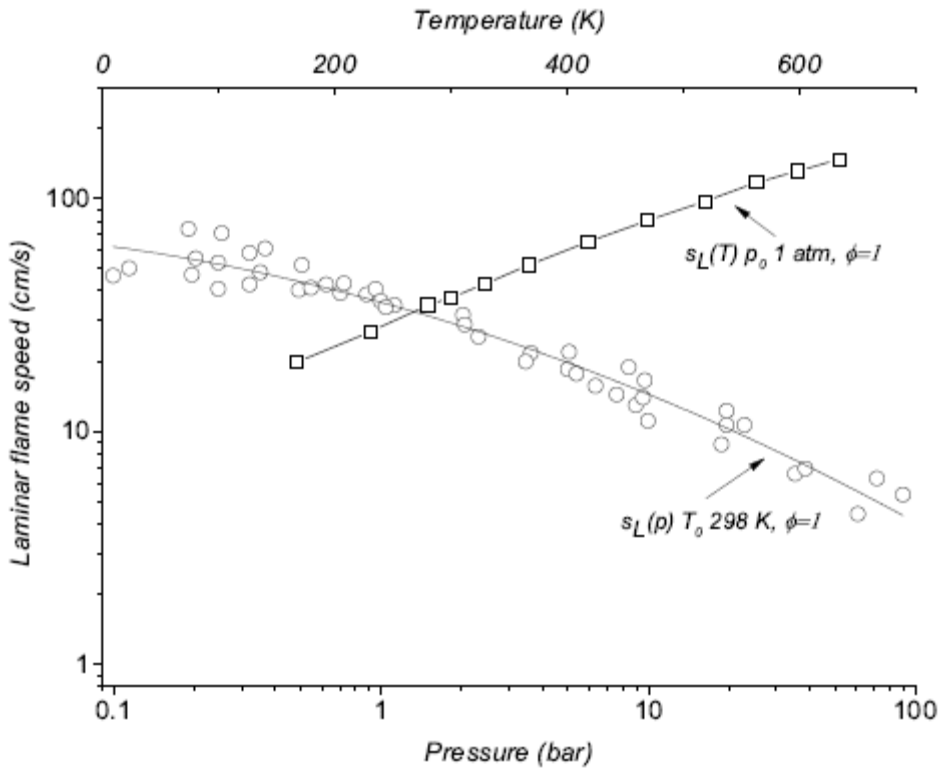

Source: (Warnatz, Maas, & Dibble, 2006b)

In addition, with higher knock resistance capabilities, higher loads can be reached enabling the use of strategies such as turbocharging. A load increase will lead to higher efficiency, as explained in the previous sections, owing to the fact that the ratio of power generated to heat losses substantially increases and therefore, heat losses as percentage of fuel energy is reduced. Notice that pumping losses are also reduced at higher loads and that is indeed the aim of DSF (Wilcutts et al., 2013).

No constraints have yet been described regarding lean combustion. When air-fuel mixtures are too lean, with excess air or heavy exhaust gas recirculation (EGR), the high level of dilution destabilizes combustion, decreasing flame speeds and difficulting ignition (Li, Karim, & Sohrabi, 2009; Quader & General Motors Corp., 1976). To cope with flame speed reduction, modifying fuel blending with hydrogen has proven to enhance flame propagation. (Bell & Gupta, 1997; MA, 2008; Nanthagopal, Subbarao, Elango, Baskar, & Annamalai, 2011; Sandhu, Babu, & Das, 2011; Smutzer, 2006; Tunestål et al., 2002; J. Wang, Chen, Liu, & Huang, 2008; Zhang et al.,

2012). Aiming in the same direction, a reduction on the flame travel and/or the increase of turbulence do also help, but the last could also reduce the ignitability of the

mixture (Hill & Zhang, 1994) (Nakamura, Baika, & Shibata, 1985) (Das & Watson, 1997). Partially stratified charge near the ignition system would enhance ignition but this is restricted to direct injected (DI) engines (Evans, 2009). Conventional spark ignition systems less-reliably ignite the lean fuel-air mixtures under these conditions. The electrical discharge energy across the spark plug electrodes required to generate a flame kernel can be nearly two orders of magnitude higher for lean operation relative to stoichiometric fuel-air ratios (Ayala & Heywood, 2007).

Therefore, to overcome the low ignitability levels the use of more powerful ignition systems is needed (Dale, 1997) (DeFilippo et al., 2011) (Joseph, Ju, Tsuruoka, & Ikeda, 2012) (Rapp et al., 2012)

Table C.1: Experimental Research Octant Numbers (RON) of Some Selected Fuels

Formula	Denominatio	RON
CH_4	Methane	120
C_4H_{10}	n-Butane	94
C_4H_{10}	iso-Butane	102
C_5H_{12}	iso-Pentane	93
C_8H_{18}	iso-Octane	100
C_6H_{12}	Cyclohexane	84
C_6H_6	Benzene	103
C_7H_8	Toluene	120
C_2H_5O	Ethanol	107

Source: University of California, Berkeley

Moreover, the use of high RON fuels , burning near lean limits (higher thermodynamic efficiency), the possible addition of turbocharging (high loads), and the increase of compression ratio lead to extreme thermodynamic conditions within the cylinder. On one hand, the use of turbocharging and high compression ratios enhances ignition to a point where knocking and pre-ignition could occur (Stone, 1999)(Heywood, 1988). On the other hand, the use of high RON and the lean burning conditions reduce the likelihood of self-ignition, but it does also reduce the overall ignitability of the mixture (Owen & Coley, 1995)(Blackmore et al., 1977). The extent to which these four parameters counterbalance each other would determine and justify the need of ignition enhancement measures, such as the previously mentioned, for the integration of lean burn strategies.

C.1 Compressed Natural Gas

The allure of CNG is the level of optimization for all three parameters: load, compression ratios, and air-fuel ratios. Spark ignited engines are knock limited, thus high compression ratios are not permissible since they will lead to pre-ignition and knocking. Low octane number gasolines such as those rich on cyclohexane, iso-Pentane and n-Butene (table C) suffer from this event to a higher extent than natural gas does (Manivannan, Porai, Chandrasekaran, & Ramprabhu, 2003) (Thomas & Staunton, 1999). CNG, because its high RON (120-130) can handle more

extreme conditions without auto-igniting, permitting higher compression ratios by design. Furthermore, the combination of CNG and Direct injection can extend the compression ratio limits, up to 15:1 without incurring knocking (H. C. Watson et al., 2009).

The reason for such improvement resides on the CNG composition which determines its properties as a fuel. CNG is a mixture of different hydrocarbons with Methane being its major component. Because the use of natural gas has gradually extended along the years, regulation has been created to regulate the properties of the commercially available CNG. The California Air Resource Board (CARB) has established minimums and maximum of the different components as shown in Table C.1.

Natural gas (NG) properties vary often due to the influence of underground reservoirs, environmental conditions, and other kinds of events have over the distribution system. Because methane represents a relatively large fraction of the mixture, its properties can help us understand the behavior of natural gas under standard combustion events. Combustion related properties of methane are presented in Table C.1

Table C.2: Specification of Natural Gas used for Emissions Certification and for General Vehicular Use

Constituent	CARB Cert Fuel	CARB In-Use Fuel	EPA Cert Fuel
Methane	90.0 ±1.0	88.0 (min)	89.0 (min)
Ethane	4.0 ±0.5	6.0 (max)	4.5 (max)
C_3 and higher	0.3 ±1.0	3.0 (max)	2.3 (max)
C_6 and higher	0.2 (max)	0.2 (max)	0.2 (max)
Hydrogen	0.1 (max)	0.1 (max)	-
Carbon Monoxide	0.1 (max)	0.1 (max)	-
Oxygen	0.6 (max)	1.0 (max)	0.6 (max)
Inert Gases (COC_2 + N_2)	3.5 ±0.5	1.5 - 4.5	4.0 (max)

Source: ("California Air Resources Board," n.d.; Owen & Coley, 1995)

Table C.3: Methane Physical Properties

Property	value	Unit
Molar mass	16.043	*g/mol*
Boiling point (at 101 kPa)	111.66	*K*
Absolute density (at 101 kPa, 0 ^{o}C)	0.717	*kg/m*$_3$
Viscosity (at 101 kPa , 26.8 ^{o}C)	0.011	*mPasec*
Flammability limits in Air	5.0-15.5	*percent*
Auto-ignition Temperature	810	*K*
Heat of Combustion (HHV)	55.6	*MJ/kg*
Heat of Combustion (LHV)	50	*MJ/kg*
Research Octane Number (RON)	120	–

Source: (Yaws, 2001)

The combustion behavior of methane is compared to gasoline in Figure C.4. At stoichiometric conditions φ 1, gasoline presents a faster burning rate though its laminar flame velocity is lower, as seen in Figure C.2. The reason being the volumetric mass density of the fuel. Despite the higher energy density presented by methane, the stoichiometry of methane is approximately of

17:1 in contrast with that of gasoline, near 15:1. The volume of air added reduces the combustion temperature and thus the reaction rates. However, at lean conditions, burning rates for Methane do not downgrade as much as gasoline does. This property makes it ideal for lean combustion. Besides, because methane is already in gaseous state at engine operating conditions, the temperature of the mixture is higher than with gasoline because no latent heat is lost for evaporation, maintaining higher reaction rates. Notice that burning at leaner conditions, mass burning rates decrease in general forcing the need for advance ignition timing. The limitation for leaner mixtures resides on the time length of the combustion event, the occurrence of knock, and the flammability limits of the mixture.

Further research is looking into the benefits of burning CNG and LPG in diesel engines avoiding the knock limitation and exploring the maximum potential of lean mixtures at high compression ratios (Dale, 1997; Douailler et al., 2011; H. C. Watson & Mehrani, 2010). Moreover, the use of CNG permits a more efficient use of turbocharging because is not knock limited, increasing the load and thus the power to heat loss ratio. Another advantage of CNG SI engines is the easier combustion phasing. By delaying ignition timing, even colder combustion can be achieved and NO_x emissions are further reduced (Baratta, D'Ambrosio, & Misul, 2013).

Nowadays, the biggest reason for the increased interest and acceptance of natural gas vehicles is the advertisement of its environmental benefits and its reduced price compared to other available fuels. CNG engines profit from lower emissions due to several reasons (Owen & Coley, 1995). The most characteristic ones are:

a. Lower emissions of non-methane hydrocarbons (NMHC) as it is mainly composed of methane. Consequently low ozone forming potential in general.

b. Low emissions of benzene and 1,3 butadiene, highly toxic.

c. Low emissions and consumption under Cold-Start and full loads operation as CNGs engines are less susceptible to knocking and mixture enrichment is not needed (Chiodi et al., 2006)(Bach et al., 2004).

Figure C.4: Mass Burnt Fraction Behavior of Methane and Gasoline

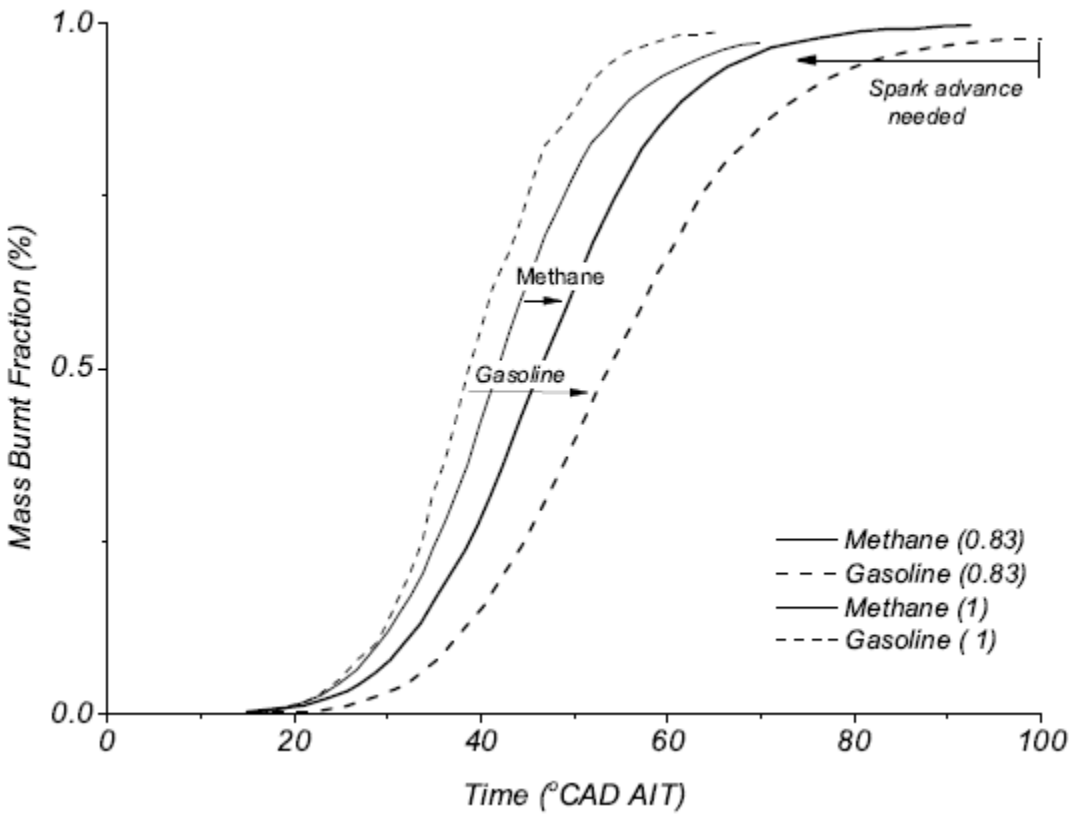

Equivalence ratio φ of 1 and 0.83 at engine speed of 1500 rpm. The time scale is based on crank angle degrees (CAD) after ignition (AIT) are represented.

Source: (Aleiferis, Serras-Pereira, & Richardson, 2013)

Much research has been carried out to assess the performance of CNG adapted SI engines and determine the real benefits of gaseous fuels (Gautam et al., 2012) (Catania, D'Ambrosio, Mittica, & Spessa, 2001)(Geok, Mohamad, Abdullah, Ali, & Shamsudeen, 2009)(Jahirul et al., 2010)(Cho & He, 2007). Results coincide to prove the fuel economy improvement shown under CNG operation. Brake specific fuel consumption (bsfc) increases together with the fuel conversion efficiency (fce). The reason is believed to be the higher calorific value of methane in comparison to gasoline. Nonetheless, a major drawback of CNG operation is the reduction of power and torque output owing to its lower energy density, lower burning rates, and consequently lower heat release rates (Geok et al., 2009)(Jahirul et al., 2010). Another possible drawback regarding the automotive consumption of CNG is the methane leakages. Methane leakages when refueling or within the injection system may cause the opposite outcome: an increased GHG emissions owing to methanes greater potential as GHG than CO_2 (Nam, Jensen, & Wallington, 2004)(Dillon, 2013). Besides those stated above, there are few important aspects regarding the use of CNG in automotives: the injection system for gaseous fuels and the catalytic processes for new fuels.

C.2 Compressed Natural Gas and the Three-Way Catalyst

Compressed Natural Gas (CNG) has been advertised as a cleaner fuel for reasons exposed in Section C.1. However, CNG combustion has been reported, by many researchers, to emit as much nitric oxide as gasoline and even more at high engine speeds (Catania et al., 2001)(Geok et al., 2009)(Jahirul et al., 2010). This occurrence is yet not fully understood. One reason believed to cause this increase in nitric oxide emission is the higher temperature reached at the exhaust when burning CNG. This happens due to a slower combustion speed of natural gas compared to gasoline. Combustion extends in time, finalizing almost at the end of the expansion stroke, keeping exhaust gases from cooling down. Slow combustion has the risk of increasing hydrocarbon emissions, so an advance on the spark timing is required (Gautam et al., 2012). By contrast, it has also been shown a substantial NO_x emissions reduction burning CNG under lean conditions (Cho & He, 2007).

Figure C.5: Different Conversion Levels for Different Air to Fuel Ratios of NO, CO, and HC

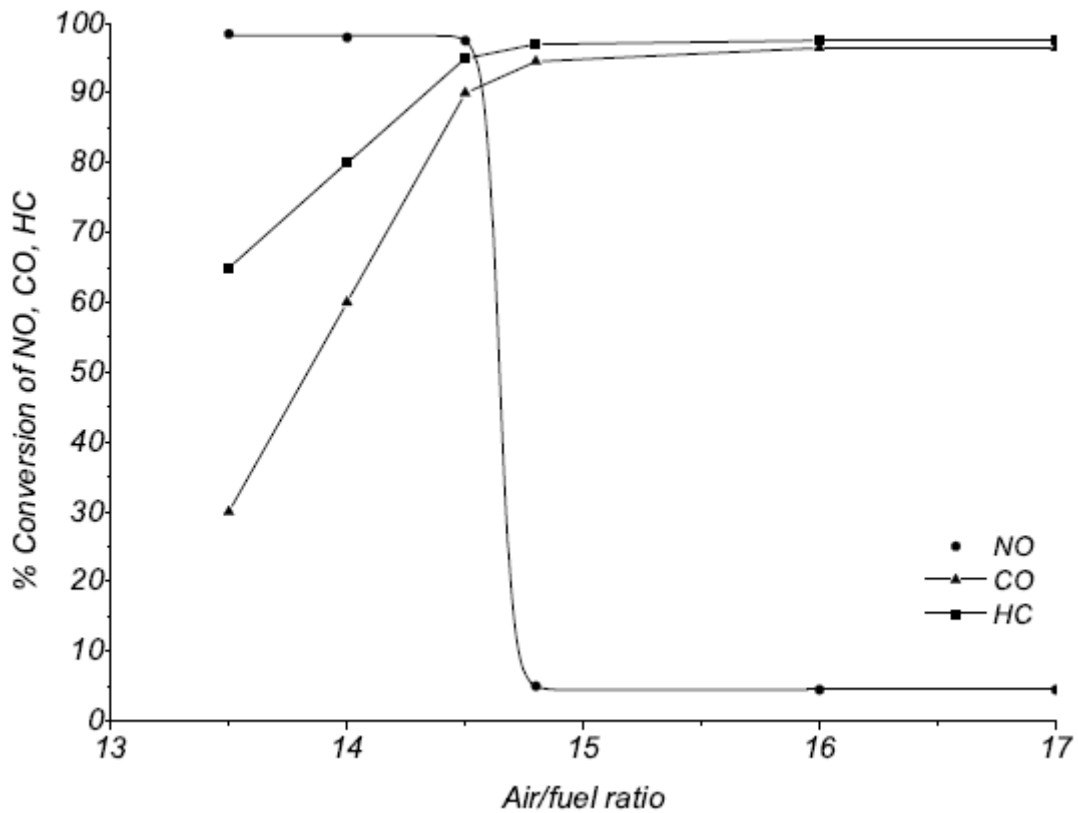

Source: University of California, Berkeley

The three way catalytic converter (TWC) is the preferred method for emission reduction for SI engines. The TWC reduces emission of the three major pollutants of combustion: unburnt hydrocarbons (UHC), carbon monoxide (CO), and nitrogen oxides (NO_x) when the engine operates in a narrow range near stoichiometric air/fuel ratios (Mondt, 2000)(Kubsh, 2006) as depicted by Figure C.5.

The catalytic process taking place in the TWC can be summarized in the oxidation of CO and Hydrocarbons, and the reduction of NO_x. A stream of exhaust gas, mainly constituted of C_xH_{2x+2}, CO, NO_x enters the catalyst and is driven through a series of reactions:

$$2NO + 2CO \rightarrow N_2 + 2CO_2 \tag{C.1}$$

$$2CO + O_2 \rightarrow 2CO_2 \tag{C.2}$$

$$2C_2H_6 + 7O_2 \rightarrow 4CO_2 + H_2O \tag{C.3}$$

The first reaction starts when the NO_x is attracted by the rhodium, present in the magnesium alumina silicate coating the honeycomb ceramic structure. The nitric oxide then, shares the oxygen-nitrogen bond with the rhodium and weakens. Nitrogen atoms combine and desorb from the catalytic surface. Remaining oxygen oxidizes the carbon monoxide around it, resulting in carbon dioxide as illustrated in Figure C.6.

Figure C.6: Catalytic Process Suffered by NO_x and CO Within a Three Way Catalytic Converter

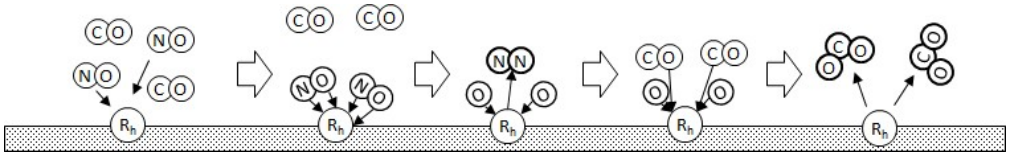

Source: University of California, Berkeley

The CO goes through an oxidation process, but this time triggered by the palladium/platinum catalyst molecules. Oxygen molecules O_2 available in the exhaust stream attach to the Pt/Pd and separate into oxygen atoms, attracting carbon monoxide and oxidizing it. This reaction is illustrated in Figure C.7.

Figure C.7: Catalytic Process Suffered by CO Within a Three Way Catalytic Converter

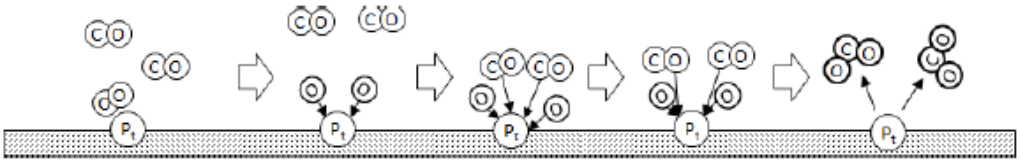

Source: University of California, Berkeley

The two types of reactions are competing between each other, with similar reaction rates. The mass fractions of the reactants are of extreme influence for the TWC. Near stoichiometric conditions, the amount of oxygen reaching the catalyst is enough for oxidizing both the CO and the C_xH_{2x+2} and there is enough reductants (H_2, CO, HCs) available to reduce the nitric oxides. If the exhaust stream reaching the catalyst goes lean, excess of oxygen prevents the reduction reaction from happening and nitric oxides pass through the TWC unaltered. By contrast, fuel rich exhaust will consume oxygen before all conversion reaction have taken place, and thus more CO and C_xH_{2x+2} will more likely not be oxidized while NO_x has found suitable conditions for reduction to occur as can be seen in Figure C.5.

Control over the mixture is needed for efficient use of the catalyst. Commonly used now is the closed loop lambda sensor control. Measuring the composition of the exhaust stream helps the injection system realize when to shift towards leaner or richer mixtures to remain in a range near stoichiometric. Lambda sensor signal is one of the most influential for the ECU to compute the injection pulse width. However, Lambda sensor control relays in upper and lower thresholds, consequently leading to exhaust composition shifting from rich to lean continuously. A solution to such issue has been reported. Doping the magnesium alumina silicate with Ce_2O_3 serves as an oxygen buffer when conditions are rich (Equation C.4), and as storage when conditions are lean (Equation C.5) (Kubsh, 2006)(Blarigan, Rimkus, Dibble, & Chen, 2011). Moreover, further development showed better performance by the addition of zirconium $Ce_{1-x}Zr_x\ O_2$. This measure improved the thermal stability of the cerium oxide (Sobukawa, 2002).

$$2CeO_2 + CO \rightarrow Ce_2O_3 + CO_2 \tag{C.4}$$

$$2Ce_2O_3 + O_2 \rightarrow 4CeO_2 \tag{C.5}$$

In summary, the TWC works more efficiently at stoichiometric conditions. It needs of closed loop lambda control and uses few different catalytic components as Rhodium, Platinum, and Palladium to realize all the reaction necessary. For optimizing, Cerium Oxide is added to obtain better performance of the catalyst out of the stoichiometric conditions. In order to accomplish all the aforementioned conditions, the TWC is designed as a honeycomb structure, optimizing reactive surface while reducing the pressure drop across. The use of ceramic based compounds such as CeO_2/Al_2O_3 is justified for its reduced thermal expansion and high thermal stability at high temperatures.

We have seen in previous paragraphs that the three way catalytic converter works efficiently only under a narrow band around stoichiometric conditions. Engine lean operation has been proven more efficient in terms of brake specific fuel consumption and thermal efficiency but it will not be of utility if pollutants emissions are not reduced simultaneously.

Some experimental work has shown the difference of performance of the TWC with methane in compare to the rest of hydrocarbons. The TWC struggles to achieve good conversion rates for methane. Note that methane is also emitted by gasoline combustion and these emissions increases with engine speed. The aging of the catalyst has been proved to influence the conversion efficiency of methane to a larger extend than other hydrocarbons do. Also, the use of regular gasoline versus premium has important influence owing to the substantial presence of SOx in less purified fuels (Takigawa, Matsunami, & Arai, 2005). Sulfur oxides are known to poison Pd catalyst rather rapidly.

Sulfur oxides inhibit the oxidation of methane as shown in Equation C.6, though, the use of γ-alumina as support helps slow down this process.

$$PdO + SO_x \rightarrow PdO - SO_3 \tag{C.6}$$

Platinum (Pt) based catalysts are more common than palladium (Pd) based due to their resilient performance under SO_x. However their methane conversion performance remains lower than even poisoned Pd catalysts, which are more active to this matter, as seen in Figure C.8 (Lampert, Kazi, & Farrauto, 1997)(Ishii & Engineers, 1994). For that reason, TWC converters rich in Palladium are preferred for CNG dedicated vehicles.

Furthermore, higher temperatures are needed for the light off of the methane conversion which difficult low temperature combustion and thus prevents NO_x formation. Solutions to this problem have been proposed such as the post engine dithering which has proven effective to reduce nitric oxides and hydrocarbon emissions with a well-designed control feedback system (Blarigan et al., 2011).

Figure C.8: Pt based TWC Methane Conversion Efficiency for Gasoline and CNG Combustion

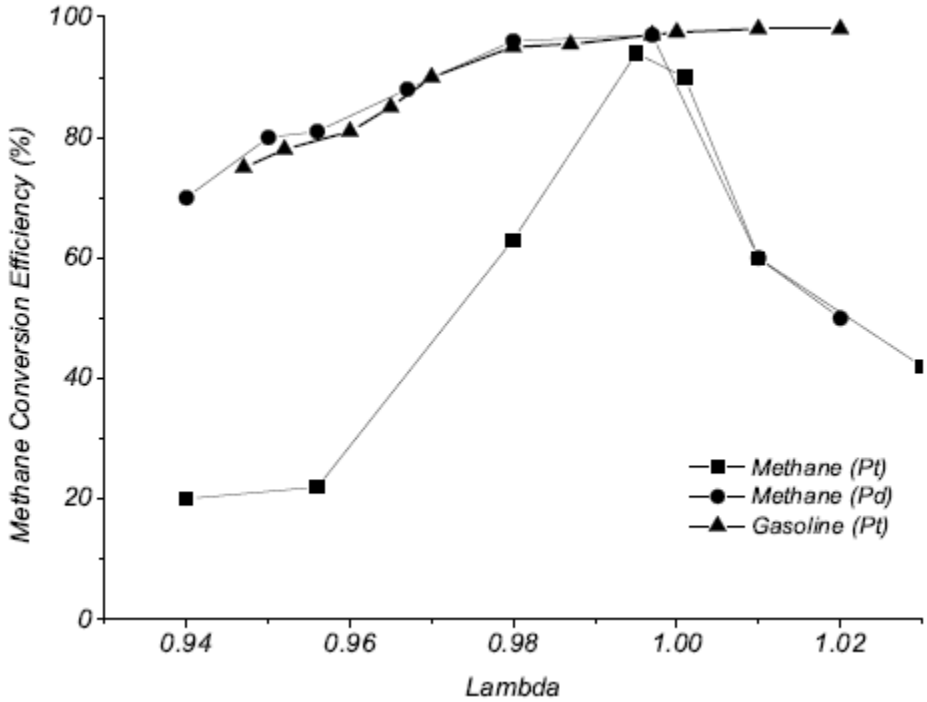

For CNG, two types of catalysts are shown. Palladium shows a better performance converting methane than the platinum based catalyst.

Source: (Lampert et al., 1997)

As a conclusion to this section, the use of CNG for automotives requires good quality fuel to avoid poisoning of the catalyst. CNG dedicated automobiles need a specific catalyst richer in palladium. The desired lean operation is not yet achieved, maintaining NO_x emissions sufficiently down to accomplish with California emissions regulations, though CNG dedicated catalyst is still a hot topic for research and development. For the initial experimental work of this project, stoichiometric conditions are operated to achieve the targets promised in the research proposal.

APPENDIX D:
Dynamic Skip Fire Technology

Dynamic Skip Fire (DSF) is a new technology developed by *Tula Technology Inc*. Tula claims that DSF actuates over the engine to "deliver the best possible fuel efficiency, without compromising the driving experience." The concept behind Dynamic Skip Fire technology is to manage the power delivered by the engine in response to the driver demand by activating or deactivating cylinders rather than by throttling. In the following chapter the details of Dynamic Skip Fire will be discovered to help the reader understand the result shown later in this report. First the concept behind variable displacement is introduced in Section D.1. It is followed by the description of DSF hardware, in Section D.2 and DSF engine control in Section D.3 to ends with an illustrative example on the DSF technological working concept.

D.1 Variable Volume Displacement

Engine load control has been and is still carried out by means of butterfly valves or throttles, mechanically or electronically driven. The idea behind throttling is the active control of power output from combustion by limiting the air flow to the cylinders. Cylinder management is synonymous with variable displacement. Dynamically actuating the inlet and outlet valves, the cylinders can be disabled on demand. Deactivating cylinders reduces the real time displacement of the engine, limiting momentarily its maximum power output. This way the maximum power output of the engine and the actual power demand are matched, so that the engine works continuously at its new full capacity. Cylinder management is, fundamentally, an alternative to throttling for satisfying transient torque demand. Yet it has not been developed to a 100 percent independent functionality, and it is used as a side improvement with throttle operation (Stabinsky et al., 2007).

Dynamic Skip Fire represents a new and innovative approach to cylinder management. This alternative makes the most out of combustion by avoiding part loads. It is known that at part load, low brake mean effective pressure (BMEP) conditions, engines brake efficiency severely decreases (Blackmore et al., 1977) as can be seen in Figure D.1. The reason for this is the notorious increase of pumping losses (PMEP) as explained in Section B.3.4.

Leading automotive manufacturers have already brought to the market products which integrate such technology. Cadillac and Mitsubishi integrated the denominated Modulated Displacement in 1981 and 1982, respectively (The Shoutheast Missourian, 1980). More recently, companies such as DaimlerChrysler (MDS, 2004), Honda (VCM, 2005), GM (AFM, 2005), Mercedes (ACC, 2011), Audi (AVS, 2012) and VW

(ACT, 2013) have integrated cylinder management under different denominations. The most extended approach among them is switching from the entire volume displacement to half the volume displacement of the engine, from V8s to V4s and V6s to L3s (Falkowski, McElwee, & Bonne, 2004)(Fujiwara, Kumagai, Segawa, Sato, & Tamura, 2008)(Huber, Klumpp, & Ulbrich, 2010)(Stabinsky et al., 2007). With these configurations, cylinder deactivation potential is not fully explored, and properly matching the torque demand still needs throttling. The reasons for

such a limited integration results from two major constraints: cost effective mechanical integration and control design.

Figure D.1: Brake Thermodynamic Efficiency (η_T) at Full and Part Throttle Evaluation vs. Compression Ratio (r_c)

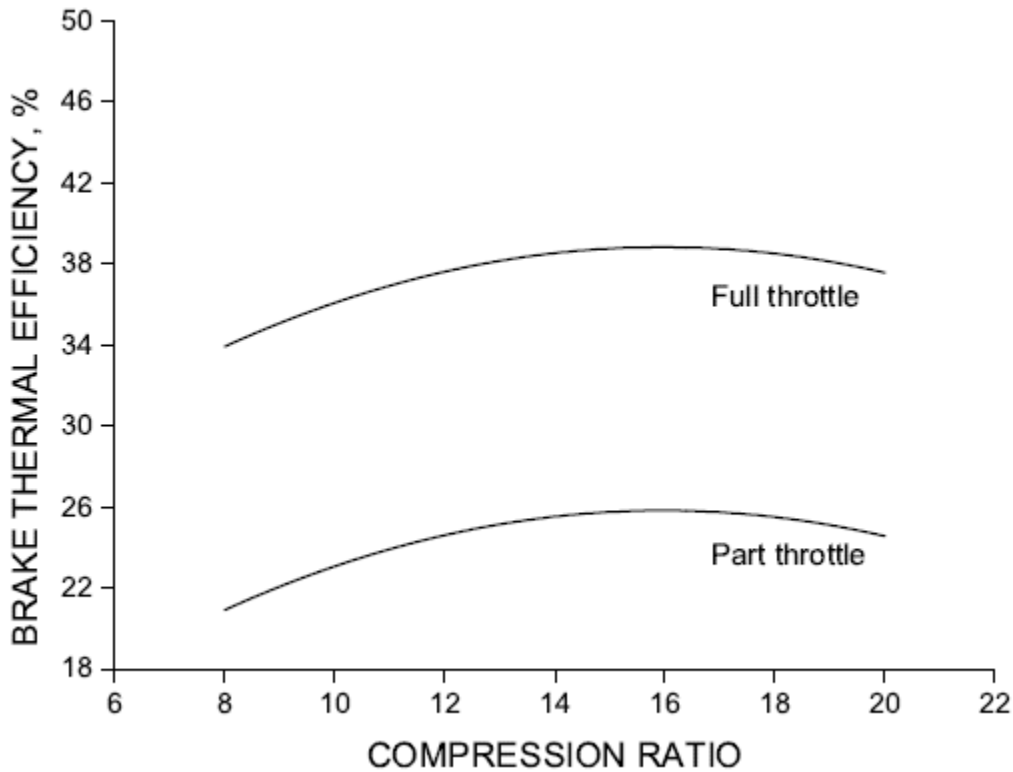

Source: (Blackmore et al., 1977)

D.2 Dynamic Skip Fire Hardware

On the manufacturing side, cylinder deactivation requires reliable valve actuators for complete control of the cylinders. Overhead camshafts are compact arrangements and usual updates represent only a partial valve timing-lift modification for the complete block. For full cylinder control, each valve has to be independently handled, allowing single (random) cylinder deactivation. For a 32-valve V8 engine, it is easy to imagine the manufacturing cost for such demanding modification. However, the aforementioned manufacturers have been capable of implementing multiple cylinder deactivations thanks to hydraulic arrangements. GM (AFM), Honda (VCM), and DaimlerChrysler (MDS) make use of a setup of lifters actuator, operated by oil pressure, activating or deactivating pre-selected cylinders of the engine (Stabinsky et al., 2007)(Falkowski et al., 2004)(Fujiwara et al., 2008)(Radulescu, JR, & Brownell, 2013).

Other approaches, such as Audi's (AVS), are based on electrically driven actuators which shift the camshaft for fronting different cam lobes to the valve push-rods (Huber et al., 2010). In this section, only the system developed by *General Motors* and the posterior update added by *Tula Tech Inc.* will be introduced.

The Active Fuel Management (AFM) system benefits from the actual valve-train architectures and adds only a set of deactivation lifters and a Lifter Oil Manifold Assembly (LOMA) shown in Figure D.2. In contrast with the double overhead camshaft often used in Europe, the actual

valve-train from an American 'V8' block, such as the L94 GM engine, consist of a single 16 lobes camshaft, driven by the crankshaft on a 2:1 spinning ration. This single camshaft configuration obligates the use of push-rods to transmit the lift from the camshaft all the way to the valves at the head of each bank (Figure D.2).

Figure D.2: Example of a Deactivation Lifter and Lifter Oil Manifold Assembly Used in an LT1 GM Engine

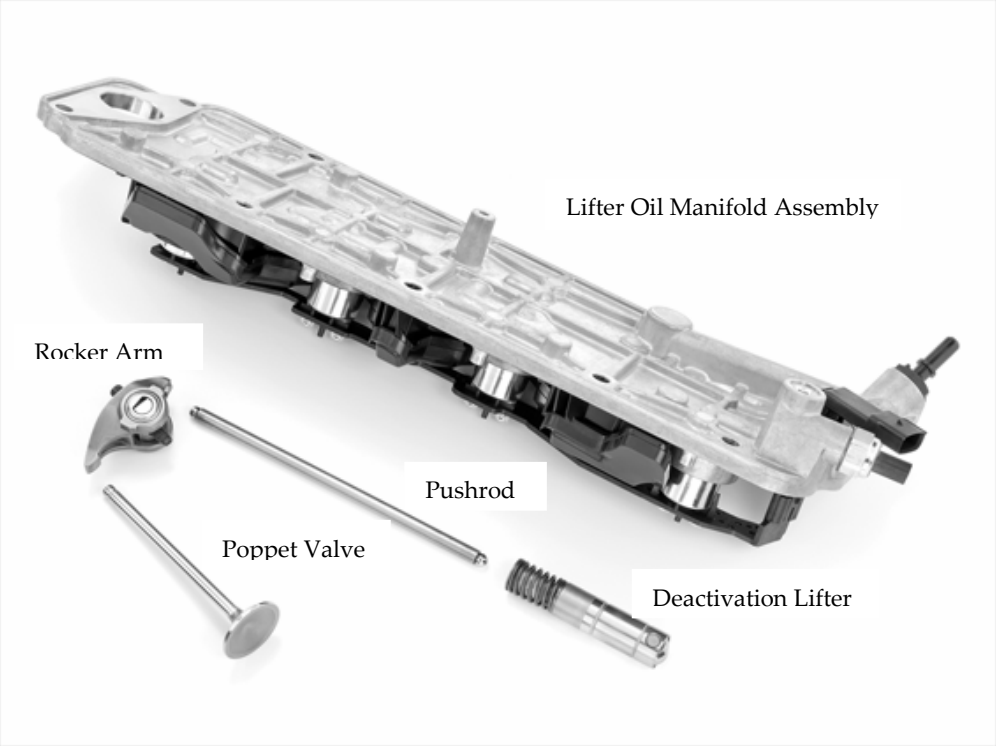

Source: General Motors Powertrains

The Lift Oil Manifold Assembly is a set of oil passages which connect the engine oil circuit to the deactivation lifters. It consists of four solenoid valves which control when the oil should reach the Deactivation Lifters. Each solenoid controls the deactivation of a cylinder through a set of two lifter rollers which simultaneously actuate the inlet and outlet valve of the cylinder. The deactivation lifter is the result of a smart design illustrated in Figure D.3.

In order to disable the valve, the lifter enters a loose mode state which prevents the push-rod from actuating the rocker arm. It splits the interface between the camshaft and the push-rods into two components, an inner and an outer housing. Both housings are connected through a locking pin. When the locking pin is locked within the locking shelf, both housings are attached to each other and the outer house, actuated by the cam lobes, transmits its movement to the inner house. The inner housing then acts over the Pushrod. When valve deactivation is on demand, a solenoid valve at the LOMA opens, allowing pressurized oil to flow through the deactivation lifter

passages. The oil pressure is by design high enough to overcome the pressure exerted by the locking pin compression spring, consequently unlocking the pins from their shelf. When the pins are free, the inner house moves freely within the outer house which prevents it from transmitting the outer house movement to the push-rod. Notice, the camshaft lobes should be in constant contact with the Lifter's rollers so that at no point uncontrolled valve events occur. This is achieved through a lost motion spring which maintains the cam follower's contact with the camshaft. More details on the working principles of the deactivation lifter can be found in (Stabinsky et al., 2007).

Figure D.3: Design of a Deactivation Lifter Used by GM for Their Cylinder Management Strategy AFM

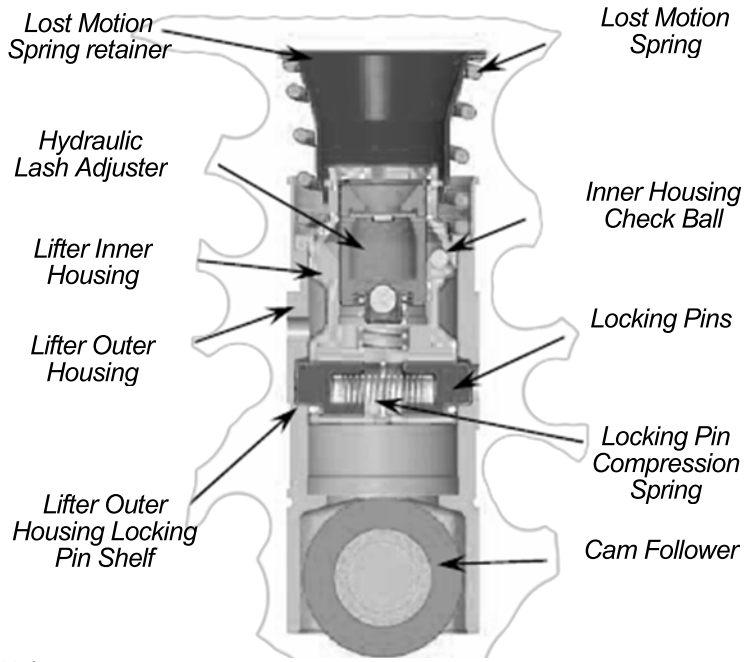

Source: (Stabinsky et al., 2007)

With the goal of fully controlling every single cylinder of the engine, *Tula Tech Inc.* has added an update to the AFM system. The AFM system used the same solenoid for both, inlet and outlet valves, thus activating or deactivating both valves simultaneously. Independent management of each valve opens a wider window of opportunity for the development of variable displacement strategies. With this purpose, *Tula Tech Inc.* modified the oil circuits within the LOMA to add eight extra passages and twelve extra solenoid valves. With this update, each valve can be disabled at any time independently from the rest of the valves. Moreover, the remaining standard Lifter rollers are replaced by deactivation Lifters. This hardware update brings full cylinder deactivation to the L94 GMC engine which increases enormously its potential for improvement in terms of gas exchange efficiency.

Furthermore, the actual variable valve timing technology (VVT) widely found in today's automobiles helps to optimize the operation of DSF. In Figure D.4, it is shown the actual valve timing configuration for the engine tested in this work. This valve timing configuration allows

shifting of the valve timing up to 25 degrees on the camshaft, which represents 50 degrees of the crankshaft. At the engine's extremely low loads (i.e. idle) it may not be optimum to reduce the engine displacement to only one or two cylinders. The reason being the generation of noticeable pulsation stresses over the crankshaft. For instance, demanding 5 percent of the engine maximum power at idle (800 rpm) requires the engine to fire two cylinders every second. This pulsation is quite aggressive for a normal crankshaft and is also easily noticed by the driver. In that respect, firing more cylinders at slightly lower load may be beneficial. Variable valve timing has proven itself a better approach to reduce engine load than it is throttling (Parvate-Patil et al., 2003)(Cleary & Silvas, 2007)(Dugdale, Rademacher, Price, Subhedar, & Duguay, 2005). At a cylinder load of 4 bar IMEP, total pumping loses can be reduced via retarding valve timing. In Figure D.5 it is shown, qualitatively, the effect that valve timing is foreseen to have over the pumping losses. At fully advanced valve timing the pumping losses $PMEP_{pump}$ are expected to be higher than retarded valve timing. On the other hand, valve flow losses $PMEP_{valves}$ are lower. Though valve flow losses increase, throttle losses are reduced to a point at which total pumping losses PMEP are minimized determining the optimal working point.

Figure D.4: Standard Valve Timing for the GM L94 Engine with Variable Valve Timing of up to 25 CAM Angle Degrees Retardation Shift (50 Crank Angle Degrees)

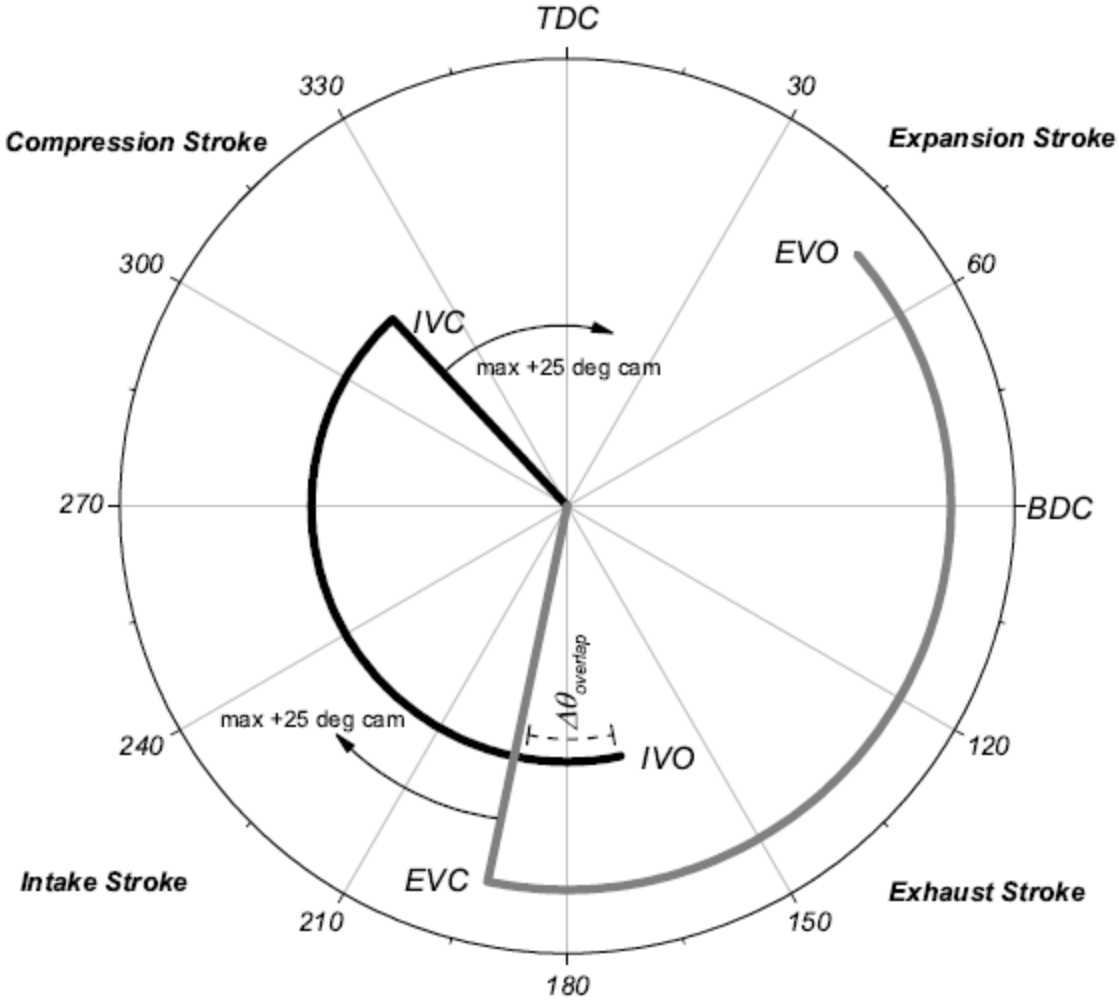

Values are represented in CAM angle degrees. IVO = inlet valve opens; IVC = inlet valve closes; EVC = exhaust valve opens; EVC = exhaust valve closes.

Source: University of California, Berkeley

The L94 GMC engine tested in this work incorporates VVT via an optimized camshaft head. A spring is located inside the camshaft head which forces the cam to remain on its initial position. By means of oil hydraulic pressure, the spring force is overcome causing the rotation of the shaft so many degrees as hydraulic pressure is applied. This system allows up to 50 crank angle degrees retard in respect to the original camshaft position. Notice, this system does not enable modification of the inlet and exhaust valve timing overlap and thus a retard of so many degrees in the inlet valve opening is translated to all other valve events.

Figure D.5: General Illustration on the Effect of Valve Timing on PMEP at Different Cylinder Loads

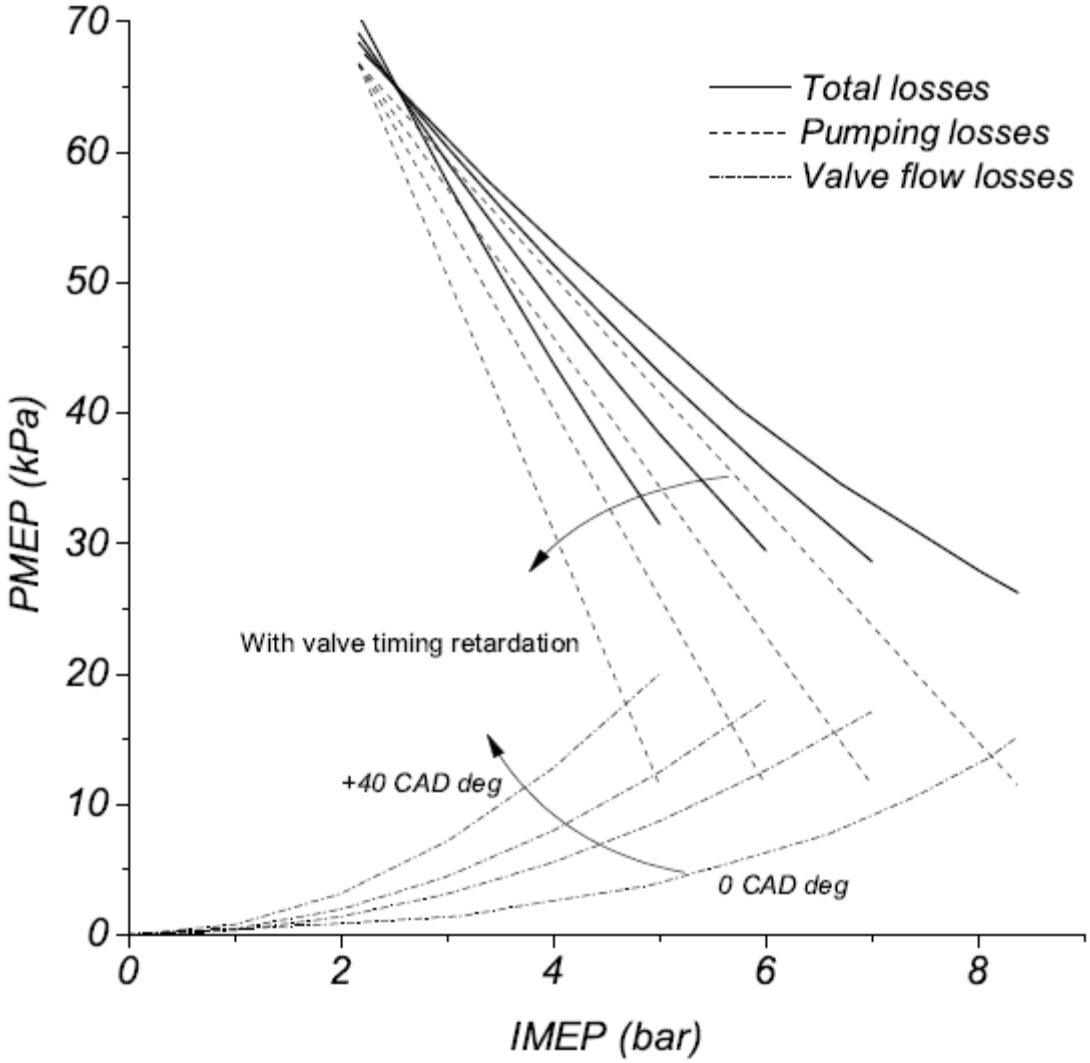

Source: University of California, Berkeley

D.3 Dynamic Skip Fire Control

Even when full independent valve operation is available, deciding the number, timing and selection of cylinders is a challenge. Concerns about noise vibrations and harshness (NVH), smooth matching torque demand, and efficient use of the exhaust catalyst arise.

On one hand, matching continuous transient torque demand with discrete volume displacement uncovers the difficulty of realizing desired loads precisely. As a matter of reliability, torque generation over the crankshaft must be done in such a way that no severe or resonant vibrations occur. Stress over the crankshaft has to be properly handled to avoid excessive wear on localized fragments (Nestorides, 1958)

On the other hand, the cylinder deactivation patterns have to account for the thermal effects on the engine block. A cylinder deactivated for a relatively long period of time may suffer from cold wall effects or cold start up, and thermo dilatation, enhancing the possibility of misfire and wall friction respectively. Furthermore, non homogeneous deactivation patterns may cause higher wear on specific cylinders leading to a reduction of the life expectancy of the engine (Tripathi & Silvestri, 2012).

DSF technology is designed to overcome all above mentioned matters bringing a more effective cylinder management plan. Its main difference with conventional cylinder management is the dynamism of the deactivation patterns. DSF does not rely on prescribed management plans.

Rather, algorithms are built which decide in real time, based on a variety of inputs, which and when a cylinder should be disabled. The algorithms take into account the record of firings to avoid unbalanced stresses, and heterogeneous cylinders operation times. Moreover, the algorithm can be modified to optimize maximum NVH reduction over maximum fuel economy. Notice that the term Dynamic Skip Fire does not refer only to the combustion skip but to the complete cylinder deactivation. If only the spark event is prevented, no cylinder deactivation would be achieved, but a misfire occurred. For the successful deactivation of a cylinder one of the following actions are needed: prevent the injection event or disable inlet valve from opening. In a direct injection engine, only the first will be strictly needed. Dynamic Skip Fire takes advantage of a sequential injection system and full valve train control to both close inlet and exhaust valves and prevent the injection event. This way, not only combustion is avoided but also the pumping work derived from free air flowing through the cylinder. Another option for cylinder management considers detaching the piston from the crankshaft so that friction loses due to piston motion are also reduced (Boretti & Scalco, 2011).

Figure D.6: Example of a General Setup for a Fire Computer Unit

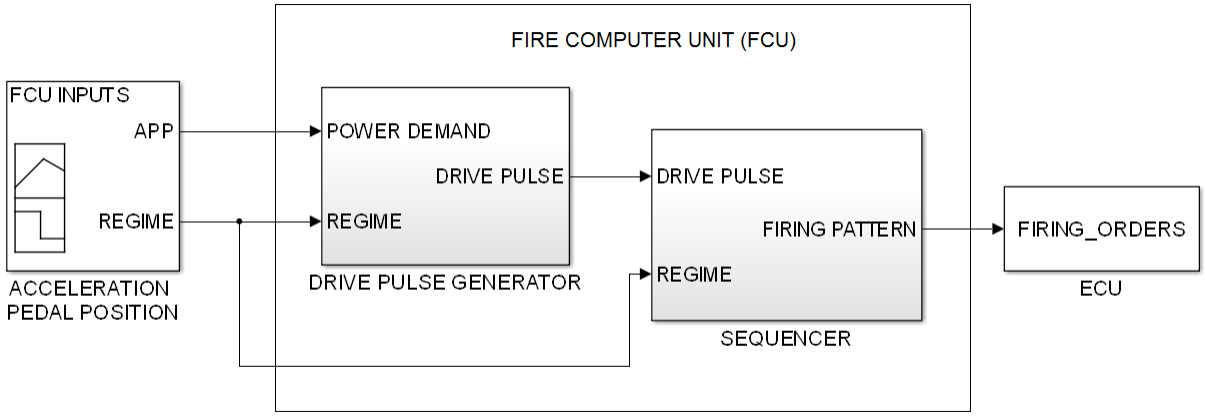

Source: (Tripathi & Silvestri, 2012)

To properly carry out the management of the cylinder, the Engine Computer Unit (ECU) needs a plan of action which tells it which cylinder to deactivate and when. Moreover, this order must be synchronized with the injection and valve events which directly depend on engine speed. In order to do so, *Tula Tech Inc.* integrates a Fire Control Unit (FCU).

Because DSF is developed within and for the private market, the information regarding the FCU is confidential and a non-disclossure agreement has been signed. To that respect, no real information will be shared in this work regarding *Tula Tech Inc.*'s technology. However, for the sake of clarity and without giving any real data, I hereby explain the concept behind DSF control. The following explanation is merely for illustration; it should not be confused with the actual implementation of DSF by *Tula Tech Inc.*

The control system within the FCU consists mainly of two major blocks as depicted in Figure D.6, the Drive Pulse Generator (DPG) and the Sequencer. The major task these two blocks have to carry out is translating the driver's demand for power into a well suited cylinder firing pattern for the engine. The first input required is consequently a representation of drivers demand, i.e. the acceleration pedal position (APP). When the engine operates at wide open throttle (WOT), the FCU will obviously order to fire cylinders at every firing opportunity. All the engine's cylinders are firing and the engine operates as normal. By contrast, when the throttle is loose, the power demand is zero but still the engine must deliver enough power to keep the engine at idle. Therefore some pre-processing of the APP signal is needed to effectively convert it to a real power demand signal.

The second input the FCU requires is the engine's regime. When the APP is at any given position different than 0 percent or 100 percent, the number of cylinders to be fired would be proportional to the percentage of power required. It is important to bear in mind that drivers do not demand energy, but power. For instance, eight cylinders firing after each other will produce nearly double the power at 2000 rpm than the cylinder operating at 1000 rpm. Nevertheless, in both cases the same amount of energy has been delivered per cycle. Therefore, the duty cycle of

the engine varies with engine speed and the FCU has to account for the engine's regime to be able to generate a proper cylinder firing pattern.

The first block in the FCU is the Driver Pulse Generator (DPG). It is responsible for the major part of the duty: creating a firing pattern which obeys the driver's demand while accounting for the engine's operation conditions. The second block is merely a tuning system which processes the signal coming from the previous block and modifies it accordingly to avoid extreme vibration and other problematic issues that may arise during operation. Though the Sequencer operation will produce nothing without the drive pulse generator, this block is the most important block regarding the integration of DSF technology. In this example, the Sequencer will not be discussed, mainly because I lack knowledge of it, and because it is, from a business standpoint, the most precious and valuable component for DSF as a market product.

D.4 Drive Pulse Generator Concept

In this section, the working concept of the Drive Pulse Generator DPG block will be explained with the aid of an example.

Figure D.7: Example of a Sigma-Delta Module

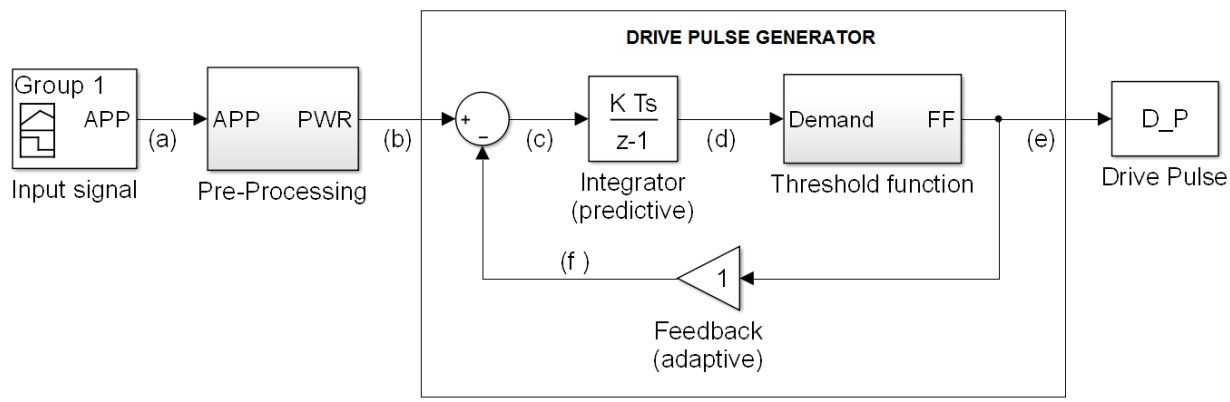

Source: University of California, Berkeley

Let us consider the following situation: An engine is working at full load (WOT) and on a 1000 rpm spinning regime. At a certain time, the driver reduces the pressure on the acceleration pedal down to nearly a third of its total travel, thus activating DSF mode. For this example, a sigma-delta module, as the one shown in Figure D.7, has been chosen to explain the principle of the DPG. The block's behavior is shown in Figure D.8. The development of the signals will be hereby explained from (a) to (f).

a. The first step is to convert the accelerator pedal position into a power demand signal. A possible transfer function would be a linear function where 100 percent and 0 percent throttle are equal to 100 percent and 5 percent power demand, considering that idle operation requires 5 percent of the engine's power generating capacity for this example.

$$P(APP) = 0.95APP + 0.05 \qquad \text{(D.1)}$$

b. This simple function serves as a simple example of a pre-processing function for the APP signal. If the pedal position was nearly 37 percent, the power demand signal reaching the DPG would deliver a signal (b) 0.4.

c. Signal (b) is demanding a firing pattern which delivers 40 percent of the total available power at the actual conditions. Signal (b) enters a sum block where the difference between the input and a feedback signal (f) is computed. The feedback in this case is either one or zero communicating, if in the previous cycle a fire or a skip was ordered. Because the engine was previously working on V8 mode, the last event was a firing event. The (f) signal is then transmitting a 1 at time t_0. Notice that signal (f) is equal to signal (e) because the gain block in between both signals is set to 1.

d. Signal (c) is the result of the sum block. Because (f) signal is present at t_0, the result (c) is -0.6 at t_1. Notice, signal (c) will shape a step function with constant steps at -0.6 and 0.4 unless the pedal position varies its position. For this example, the position is constant for at least a period of 0.3 seconds.

e. The integral block stores each sample along time. Given an initial condition of 0, signal (d) will deliver a value of -0.6 on its next cycle.

f. The threshold function is set to deliver a firing order when the input signal (d) is equal or greater than 0 and a skip order when (d) is negative. Therefor, with (d) equal to -0.6, signal (e) will carry a 0 and so does (f) at t_1.

It easy to see that the complete firing pattern requires over 5 firing opportunities to deliver the right amount of fires. As long as signal (b) is increased the slope of the integral (d) increases, crossing the threshold quicker, thus triggering more fire events. In the same manner, when the throttle position is reduced, the slope of the integral function will decrease, and so the time to trigger the threshold function will increase proportionally.

A quick reasoning will explain why the firing pattern (F-S-S-F-S) is irregular. The input signal reaching the block (b) is ordering the block to fire 60 percent less cylinders. Concretely, it is asking to fire 40 out of 100 cylinders. If both numerator and denominator are factorized, it turns into the firing of 2 cylinders out of 5. Therefore, the time needed for the control system to deliver the demanded pattern is the time period consumed by 5 firing events. This elapsed time (in units of time) varies with the engine regime which explains why the FCU must synchronize its sample rate with the engine speed. Following with the example, two fires out of five fire opportunities can be realized in many ways, although the example used here delivers the closest to a homogeneous pattern because it does not collect any feedback from the engine.

Figure D.8: Simplified Illustration of the Behavior of a Sigma-Delta Control for the Purpose of DSF

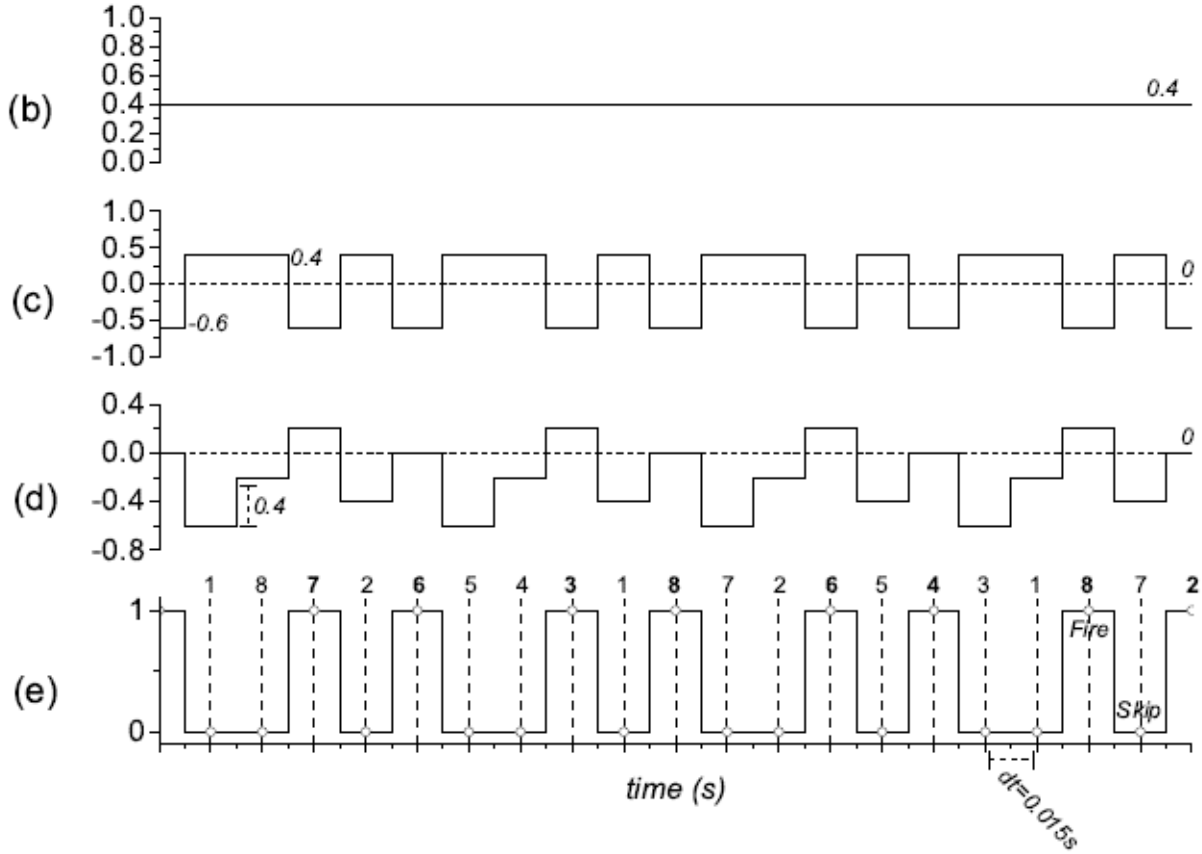

Source: University of California, Berkeley

With

$$Signal(c) = \frac{2}{5} \rightarrow 2\ fire\ events + 3\ skip\ events \rightarrow \frac{skips}{fire} = 1.5 \qquad \text{(D.2)}$$

which dictates that a fire will be in order when 1.5 or more skip events have happened. If at the first opportunity a fire occurs, the following two firing opportunities will lead to skip events leaving a positive residual of 0.5. When the next fire event occurs, the sum of the residual plus the next skip event will deliver a 1.5 for that specific firing event, leading to the pattern 'F-S-S-F-S'. This same reasoning can be realized with any other power fraction and thus the right pattern can be easily obtained. If we put the FCU to the test with a random pedal position function, the result in Figure D.9 shows how the FCU will consequently adapt the number of skips according to high or low load points. It can be seen how at high load no skips are ordered, while at low load the density of deactivated cylinder increases appropriately.

In this section, the DSF technology has been introduced. The fundamentals behind DSF and its potential benefits for further increase on automotive fuel saving have been justified. Information on DSF hardware and control has been briefly introduced. In the coming sections, the use of

compressed natural gas (CNG) is justified. Main concerns and fundamentals on the use of CNG are further explained.

Figure D.9: Approximate Behavior of DSF under Different Engine Loads

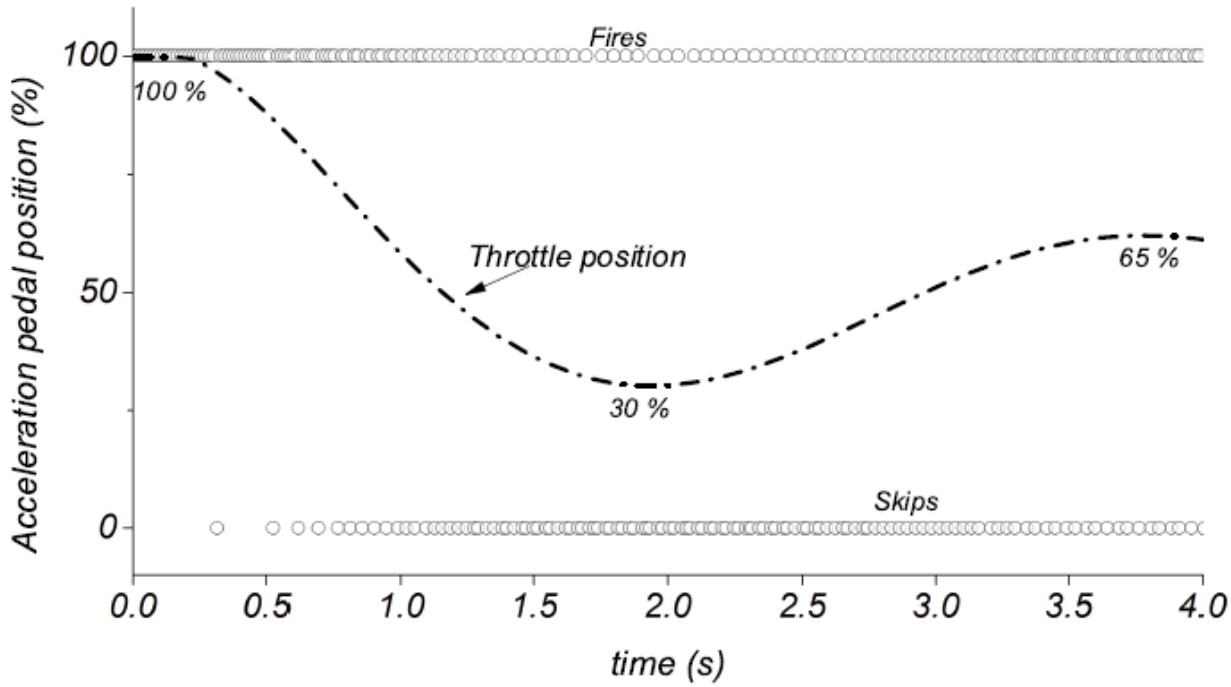

Result obtained from a generic DPG. The regime tested is 1000 rpm, with available fire every 0.015 seconds.

Source: University of California, Berkeley[f]